INDUCTION AND TARGETING OF

THE HEAT SHOCK RESPONSE

IN PROSTATE CANCER

by

Nathan Kade Larson

A dissertation submitted to the faculty of
The University of Utah
in partial fulfillment of the requirements for the degree of

Doctor of Philosophy

Department of Pharmaceutics and Pharmaceutical Chemistry

The University of Utah

May 2013

The University of Utah Graduate School

STATEMENT OF DISSERTATION APPROVAL

The following faculty members served as the supervisory committee chair and members for the dissertation of **Nathan Kade Larson**. Dates at right indicate the members' approval of the dissertation.

Hamidreza Ghandehari, Chair	**28 Jan 2013** Date Approved
Jindrich Kopecek, Member	**28 Jan 2013** Date Approved
Darin Furgeson, Member	**31 Jan 2013** Date Approved
James Herron, Member	**30 Jan 2013** Date Approved
Sunil Sharma, Member	**29 Jan 2013** Date Approved

The dissertation has also been approved by **David Grainger**

Chair of the Department of **Pharmaceutics and Pharmaceutical Chemistry**

and by Donna M. White, Interim Dean of The Graduate School.

ABSTRACT

Specific delivery of chemotherapeutic agents to cancerous tissues can potentially result in increased safety and decreased toxicity. For example, nanomedicines, including polymer-drug conjugates, can potentially accumulate in solid tumors via the "enhanced permeability and retention" (EPR) effect. Further increases in delivery can be achieved via active targeting strategies, wherein cancer-specific targeting moieties enhance cellular binding and internalization. This dissertation describes a strategy which attempts to increase the tumor accumulation and efficiency of active targeting using a combination of tumor hyperthermia and heat shock protein (HSP) targeted *N*-(2-hydroxypropyl)methacrylamide (HPMA) copolymer-drug conjugates. Following exposure to hyperthermia, increases in cellular stress results in initiation of the heat shock response, which includes the synthesis and migration of certain heat shock proteins to the cell surface. It is hypothesized that the induced expression of these HSPs can serve as specific molecular targets for the delivery of anticancer macromolecular chemotherapeutics. HPMA copolymer-drug conjugates bearing peptides targeting cell surface expressed glucose regulated protein 78 kDa (GRP78), a member of the HSP70 family of proteins, were synthesized, characterized, and evaluated for activity in prostate cancer models. Following exposure to hyperthermia, the cell surface expression of GRP78 was also evaluated and correlated to increases in cellular delivery and cytotoxicity of GRP78 targeted HPMA copolymer-

drug conjugates. Combination index analyses indicated that a combination of hyperthermia and HSP targeted drug therapy resulted in combined synergistic effects. *In vivo,* gold nanorod-mediated plasmonic photothermal therapy was utilized to induce tumor hyperthermia in a human prostate cancer animal model to enhance the delivery and efficacy of GRP78 targeted HPMA copolymer-drug conjugates. Results demonstrate that a combination of tumor hyperthermia and HSP targeting can increase tumor accumulation and cellular delivery of macromolecular chemotherapeutics, enabling safer and more effective therapies.

TABLE OF CONTENTS

LIST OF TABLES

LIST OF FIGURES

ABBREVIATIONS

17-AAG	Tanespimycin
ACN	Acetonitrile
AHGDM	Aminohexylgeldanamycin
AIBN	Azobisisobutyronitrile
ANOVA	Analysis of variance
APMA-FITC	5-[3-(methacryloylaminopropyl)thioureidyl] fluorescein
ATF6	Activating transcription factor 6
ATP	Adenosine triphosphate
ATRP	Atom transfer radical polymerization
AUC	Area under the curve
CMC	Critical micelle concentration
CrEL	Cremophor® EL
CT	Computed tomography
DAB	3-3’ diaminobenzidine
DCE-MRI	Dynamic contrast enhanced magnetic resonance imaging
DCM	Dichloromethane

DI	Deionized
DIPC	*N,N'*-dicyclohexylcarbodiimide
DIPEA	*N,N'*-diisopropylethylamine
DLS	Dynamic light scattering
DMAP	4-dimethylamino pyridine
DMF	Dimethylformamide
DMSO	Dimethylsulfoxide
DOC	Docetaxel
DNA	Deoxyribonucleic acid
EDAC	*N*-(3-Dimethylaminopropyl)-*N'*ethylcarbodiimide hydrochloride
EDTA	Ethylenediaminetetraacetic acid
ELP	Elastin-like polypeptides
EM	Electromagnetic
EPR	Enhanced permeability and retention
ER	Endoplasmic reticulum
ESI	Electrospray ionization
FBS	Fetal bovine serum
FDA	Food and Drug Administration
FITC	Fluorescein isothiocyanate
FPLC	Fast Protein Liquid Chromatography

GDM	Geldanamycin
GFLG	Gly-Phe-Leu-Gly
GG	Gly-Gly
GI_{50}	Growth inhibitory concentration (50%)
GNR	Gold nanorod
GRP78	Glucose regulated protein 78 kDa
HEC	Hydroxyethylstarch
HER2	Human epidermal growth factor receptor 2
HIFU	High intensity focused ultrasound
HIPEC	Hyperthermic intraperitoneal chemotherapy
HPLC	High-performance liquid chromatography
HPMA	*N*-(2-hydroxypropyl)methacrylamide
HRP	Horseradish peroxidase
Hrs	Hours
HSC70	Constitutive heat shock protein 70 kDa
HSP	Heat shock protein
HSP70	Heat shock protein 70 kDa
HSP90	Heat shock protein 90 kDa
HUVEC	Human umbilical vein endothelial cell
I	Iodine

IACUC	Institutional Animal Care and Use Committee
IC_{50}	Inhibitory concentration (50%)
ICP-MS	Inductively coupled plasma mass spectrometry
ID	Injected dose
IRE1	Inositol-requiring protein 1
LIMK1	LIM domain kinase 1
LCST	Lower critical solution temperature
MA-GFLG-AHGDM	*N*-methacryloylglycylphenylalanylleucylglycl-17-(6-aminohexylamino)-17-demethoxygeldanamycin
MA-GFLG-DOC	*N*-methacryloylglycylphenylalanylleucylglycl-docetaxel ester
MA-GFLG-NH-Et-NH-Boc	*N*-methacryloyl-glycylphenylalanylleucylglycl-*N*-Boc-1,2-diaminoethane
MA-GFLG-OH	*N*-methacryloylglycylphenylalanylleucylglycine
MA-GG-AHGDM	*N*-methacryloylglycylglycl-17-(6-aminohexylamino)-17-demethoxygeldanamycin
MA-GG-ONp	*N*-methacryloylglycylglycyl-p-nitrophenyl ester
MA-GG-TT	*N*-methacryloylglycylglycyl-2-thiazolidine-2-thione
MA-Tyr-$CONH_2$	*N*-methacryloyl-tyrosinamide
MALLS	Multi-angle laser light scattering
MAPK	Mitogen-activated protein kinase
Min	Minutes
M_n	Number average molecular weight

MRI	Magnetic resonance imaging
MS	Mass spectrometry
MTD	Maximum tolerated dose
M_w	Weight average molecular weight
MW	Microwave
MWCO	Molecular weight cut-off
NCE	New chemical entity
NHS	*N*-hydroxysuccinimide
NIPAAM	*N*-isopropylacrylamide
ONp	*p*-nitrophenol
PAA	Poly(acrylic acid)
PAAm	Poly(acrylamide)
PAK-2	p21-activated kinase-2
PAMAM	Poly(amido amine)
PBS	Phosphate buffered saline
PCL	Poly(ε-caprolactone)
PDMAEMA	Poly(2-dimethylamino)ethyl methacrylate
PEG	Poly(ethylene glycol)
PEI	Poly(ethylene imine)
PERK	Protein kinase-like endoplasmic reticulum kinase

PET	Positron emission tomography
PGA	Poly(glutamic acid)
PI3K	Phosphoinositide 3-kinase
PIC	Poly-ion complex
PK1	*N*-(2-hydroxypropyl)methacrylamide copolymer-doxorubicin
PK2	*N*-(2-hydroxypropyl)methacrylamide copolymer-doxorubicin-galactosamine
PMAA	Poly(methacrylic acid)
PPTT	Plasmonic photothermal therapy
PSA	Prostate specific antigen
Pt	Cisplatin
PVP	Poly(vinyl pyrrolidone)
QELS	Quasi-elastic light scattering
RAFT	Reversible-addition fragmentation chain-transfer
RES	Reticulo-endothelial system
RF	Radiofreqency
RGD	Arg-Gly-Asp
RGDfK	Arg-Gly-Asp-D-Phe-Lys
RI	Refractive index
RNA	Ribonucleic acid

RWLWVADPFLMG	Arg-Trp-Leu-Trp-Val-Ala-Asp-Pro-Phe-Leu-Met-Gly
SD	Standard deviation
SEC	Size exclusion chromatography
SEM	Standard error of the mean
SMA	Poly(styrene-*co*-maleic acid)
SMANCS	Poly(styrene-*co*-maleyl-half-*n*-butylate)-neocarzinostatin
SPECT	Single photon emission computerized tomography
SPR	Surface plasmon resonance
TLC	Thin layer chromatography
UPR	Unfolded protein response
UV	Ultraviolet
VA-044	2,2'-Azobis[2-(2-imidazolin-2-yl)propane]dihydrochloride
VEGF	Vascular endothelial growth factor
WDLAWMFRLPVG	Trp-Asp-Leu-Ala-Trp-Met-Phe-Arg-Leu-Pro-Val-Gly
WIFPWIQL	Trp-Ile-Phe-Pro-Trp-Ile-Gln-Leu
WST-8	2-(2-methoxy-4-nitrophenyl)-3-(4-nitrophenyl)-5-(2,4-disulfophenyl)-2H-tetrazolium monosodium salt

ACKNOWLEDGEMENTS

The work described in this thesis is the product of the efforts of multiple individuals and I have been greatly enriched by our many associations and interactions. It would be difficult to list all of those who have assisted in my development and the work presented herein. However, certain individuals have played a particularly influential role.

Dr. Darin Furgeson, a member of my PhD supervisory committee, has consistently provided feedback on my research, specifically in the areas of tumor hyperthermia and heat shock protein inhibition. In addition to providing insights regarding the current work, I also had the opportunity to work with him as a teaching assistant, where I gained a greater appreciation for those who are devoted to their teaching. I have also appreciated his honest critiques of my work throughout my studies, which have provided me opportunities to grow.

Dr. James Herron, also a member of my PhD supervisory committee, has also played a significant role during the course of my studies. In addition to providing feedback on my research, he has provided constant guidance throughout my studies. He has a tremendous reservoir of knowledge that allows him to provide input across a wide array of disciplines. His comments are always highly valued by me and other students.

I have appreciated his straightforward and honest attitude, and his service to myself and the department as a whole is greatly appreciated.

Dr. Jindrich Kopeček, also a member of my PhD supervisory committee, has also played a significant role during my graduate studies. He carries with him vast experience in the drug delivery field and his genuine love for scientific progress. During the course of my studies, I have had multiple opportunities to interact closely with him, and appreciate his high expectations and cordial nature. To me and my fellow students, he will always be a prime example of a successful scientist.

Dr. Sunil Sharma, also a member of my PhD supervisory committee, provided a unique perspective during my studies. As a clinician, he ensured that I kept in mind the end goal or achieving real, clinical benefits to patients. I appreciate the many opportunities I had to meet with him and receive his honest, candid comments. His wide range of knowledge in oncology, and research focused attitude has made him a great example of successful medical researcher and clinician.

Dr. Abhijit Ray, a great friend and mentor, carefully guided and trained me in the lab, and ensured that I always understood the fundamental chemistry associated with my work. He has always provided honest and sincere scientific guidance, and his efforts are appreciated by me and my fellow students. I have also enjoyed our many "non-scientific" conversations, and admire him for his kindness and friendship.

Dr. Khaled Greish was another individual who provided valuable guidance and training, particularly during our initial animal studies. Khaled also provided the inspiration behind our work using micellar systems. He is also a great friend and

example, and I appreciate his continuous drive and ambitious pursuit for therapies that provide benefits to patients.

Dr. Alexander Malugin also provided valuable guidance and training, particularly during cell culture experiments. His continuous attention to detail and drive for perfection were truly inspiring. On numerous occasions, Sasha provided guidance on methodology and interpretation of data. He was also a great example of integrity in scientific research, for which I am grateful.

Dr. Adam Gormley, a fellow graduate student, played a primary role in the development of the research in this thesis. I was privileged to be able to work collaboratively with him in a complete, mutually beneficial manner. I also appreciate his friendship, honesty, and scientific integrity.

Dr. Hamid Ghandehari, my research advisor and chair of my PhD supervisory committee, provided continuous, unwavering support for me during my graduate studies and during the development of the work presented in this thesis. I appreciate his commitment to fostering an environment in which his students, myself included, can learn and grow. In addition, I greatly appreciate the academic freedom that he has allowed me during the course of my studies. His exemplary work ethic and commitment to excellence have helped my personal development as a scientist.

I would also like to acknowledge the Ghandehari Lab group, as a whole, for taking an active interest in the work of each member and being willing, at any time, to assist in any way. We truly worked together as a team, and the friendships that were gained during my studies will definitely continue throughout our future endeavors.

Mr. Robbie Everett, Mr. Dave Burr, and Mr. Paul Brooks, my high school teachers in biology, chemistry, and mathematics respectively, each took a personal, active interest in me and fostered within me a love for science. Each was a teacher of the highest caliber, and their service to me and other students is forever appreciated.

My parents, Kelly and MaryLynn Larson, have given constant sacrifice, love, and support and encouragement for me during my education from pre-school through my graduate studies.

My dear wife, Maria, provides unwavering support and love at all times. In addition to raising our family, her willingness to serve others and genuine kindness and concern for all is second to none. I appreciate her hard work and perseverance during my graduate studies. I am continually enriched by her and I will always treasure our beautiful relationship.

This research was supported by the National Institutes of Health grant R01 EB007171 and the Utah Science Technology and Research (USTAR) initiative.

CHAPTER 1

INTRODUCTION

1.1 Introduction

1.1.1 Drug delivery

Drug delivery is the method or process by which a pharmaceutically active agent, or drug, is administered. The intended goal is to "deliver" the drug in a manner that allow for its therapeutic effect to be realized by a patient. The field of drug delivery has undergone tremendous evolution over the past few decades.[1] Early drug delivery scientists were primarily focused on technologies to modify drug release kinetics and expand the common routes of drug administration (i.e. transdermal, nasal, pulmonary, etc.). Recent advances, particularly in the field of nanotechnology have provided an array of tools to aid in the successful delivery of drugs.[2] Association of therapeutic compounds with nano-scaled carriers allows new mechanisms by which drug release kinetics can be altered. In addition, modifications in the size and physicochemical properties of these "nanomedicines" offer opportunities to modify their pharmacokinetics and distribution in the body following administration.[3] It is anticipated that these new technologies will allow scientists and clinicians the ability to deliver drugs in a more precise and controlled fashion.

1.1.2 Polymer therapeutics

The use of water-soluble polymeric materials for drug delivery provides several advantages. First, many drugs are natively hydrophobic, and association of such drugs with water soluble polymers via complexation or conjugation can dramatically improve their aqueous solubility.[4] Second, if these carriers are made sufficiently large in size (generally above 7-10 nm in diameter), they can evade renal filtration via the glomeruli, resulting in prolonged systemic circulation.[5] In anticancer applications, such carriers can potentially accumulate in solid tumor tissue via the enhanced permeability and retention (EPR) effect[6], where a combination of increased vascular permeability and reduced lymphatic drainage exist within the tumor microenvironment.[7] Despite these advantages, clinical translation of polymer therapeutics has proven challenging. Anticancer clinical trials to date have demonstrated that while these systems are generally advantageous with respect to safety and tolerability, efficacy has remained marginal due to poor overall tumor delivery.[8] Therefore, strategies to increase specific tumor delivery while minimizing distribution in other organs and tissues are needed.

1.1.3 Active targeting

One way in which a polymer therapeutic may be made more selective towards tumor tissue is via the inclusion of targeting moieties. These targeting moieties are designed to be recognized by and bind to receptors expressed on the surface of cells in target tissues. Antibodies, antibody fragments, peptides, carbohydrates, and other small molecules have been attached to a variety of nanomedicines for this purpose.[9] However, it should be acknowledged that such strategies rely on short-ranged

electrostatic interactions to facilitate binding.[10] Therefore, these strategies are most effective when coupled with other passive targeting strategies (i.e., EPR). Selection of a specific molecular target is critically important. The ideal target is one that is highly expressed on the surface of cells in the tissue of interest with no expression elsewhere. However, this is rarely the case, and the criterion for selection is usually "overexpression" of the target in the region of interest.[11] The difference in the native expression levels between target and nontarget tissues is therefore a fundamental limitation in achieving successful active targeting. The focus of this dissertation is to investigate a strategy to increase total tumor accumulation that does not have this inherent limitation. This approach utilizes tumor hyperthermia and the induced expression of heat shock proteins.

1.1.4 Hyperthermia and the heat shock response

Tumor hyperthermia has been widely investigated as an anti-cancer strategy, wherein the temperature of tumors is elevated to levels high enough to induce cytotoxicity.[12] The alternative approach under evaluation in this dissertation uses moderate hyperthermia to increase the subsequent delivery of polymer therapeutics (Figure 1.1). This occurs through two primary mechanisms: First, moderate tumor hyperthermia can increase the blood flow and vascular permeability of tumor tissue, thereby enhancing passive delivery via the EPR effect.[13] Second, when exposed to moderate hyperthermia, tumor cells respond by inducing the expression of heat shock proteins.[14] While much of this response occurs inside cells, recent observations have indicated that some of these heat shock proteins (i.e. glucose regulated protein 78 kDa,

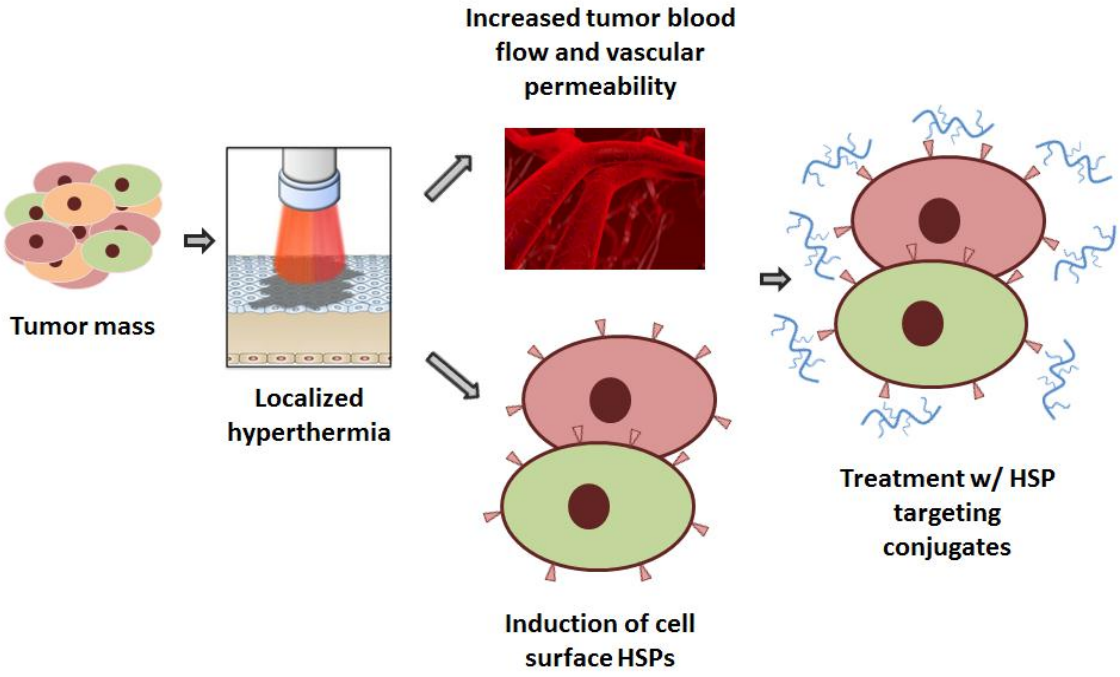

Figure 1.1. Rationale to increase the delivery of macromolecular chemotherapeutics using tumor hyperthermia. The primary focus of this thesis is on the induction of cell surface heat shock proteins (HSPs), and their subsequent targeting using polymer-drug conjugates.

GRP78) also play active roles in signal transduction on the cell surface.[15, 16] Our strategy therefore utilizes these induced cell surface heat shock proteins as specific molecular targets. Through the use of polymer therapeutics targeting this response, we can therefore achieve increased binding and internalization into cancer cells. Increased delivery of polymer therapeutics via these phenomena can translate into better efficacy and safety of cancer chemotherapeutics.

1.2 Specific aims

While the aforementioned phenomena provide rationale for a combination therapy of polymer therapeutics and tumor hyperthermia, the primary focus of this thesis is investigation of the latter, wherein polymer therapeutics are targeted towards the induced expression of the cell surface heat shock protein GRP78. This investigation was carried out by evaluation of the following specific aims:

1. To synthesize and characterize heat shock protein targeted *N*-(2-hydroxypropyl)methacrylamide (HPMA) copolymer-drug conjugates *in vitro* for their ability to bind cell surface expressed GRP78 and induce cytotoxicity in prostate cancer cells.

2. To evaluate the potential for increased delivery of GRP78 targeted HPMA copolymers in combination with hyperthermia.

3. To evaluate the *in vitro* synergism and *in vivo* efficacy of GRP78 targeted HPMA copolymer-drug conjugates with hyperthermia.

1.3 Scope and organization

Chapter 2 provides the necessary background on polymer therapeutics and polymer-drug conjugates, along with a discussion of the challenges facing their utilization in anticancer applications.[17] Background is also provided on the role of tumor hyperthermia in anticancer therapy and the utilization of heat shock proteins as anticancer targets. Specifically, the role of GRP78 and its implications in targeted tumor therapy will be reviewed. As localized tumor hyperthermia in this study was delivered via gold nanorod-mediated plasmonic photothermal therapy, a brief discussion of this technique is also included. In Chapter 3, HPMA copolymers bearing the model anticancer drug aminohexylgeldanamycin (AHGDM) and the GRP78 targeting peptide WIFPWIQL were synthesized.[18] Their ability to bind to cell surface expressed GRP78 and induce cytotoxicity in human prostate cancer cells was then evaluated. In Chapter 4, the expression profile of cell surface expressed GRP78 following hyperthermia was evaluated and its impact on the cellular uptake and cytotoxicity of targeted HPMA copolymers assessed.[19] The *in vivo* tumor accumulation and biodistribution of GRP78 targeted HPMA copolymers were also investigated in prostate tumor bearing mice following localized tumor hyperthermia. In Chapter 5, GRP78 targeted conjugates bearing three different drugs (AHGDM, docetaxel (DOC), and cisplatin (Pt)) were evaluated for their ability to demonstrate synergistic cytotoxic effects in combination with moderate hyperthermia.[20] Based on these results, conjugates bearing DOC were selected and evaluated for *in vivo* efficacy in combination with localized tumor hyperthermia in prostate tumor bearing mice.

Finally, Chapter 6 briefly summarizes the major finding and implications of the dissertation and suggests potential future directions.

In Appendix A, the synthesis and evaluation of HPMA copolymers bearing the chemotherapeutic DOC and the angiogenesis targeting peptide RGDfK is described, wherein the utility of a well characterized active targeting strategy was demonstrated.[21] This study provided a basis for the proposed work.

During the course of the described studies, it was observed that the chemical modification necessary for conjugation of the drug geldanamycin to the HPMA copolymer backbone resulted in a significant decrease in its activity. This prompted work with a non-conjugated micellar system, which is described in Appendix B.[22]

During initial *in vivo* biodistribution studies of HPMA copolymers bearing the WIFPWIQL GRP78 targeting peptide, significant nonspecific uptake in healthy tissues was observed. This prompted an investigation into the use of an alternative, more hydrophilic, GRP78 targeting peptide, namely WDLAWMFRLPVG. A brief comparison of the biodistribution of the two systems is included in Appendix C.

Additional size exclusion data for selected HPMA copolymer-drug conjugates is also included in Appendix D.

1.4 References

1. A.S. Hoffman. The origins and evolution of "controlled" drug delivery systems. J Control Release. 132:153-163 (2008).

2. M. Chakraborty, S. Jain, and V. Rani. Nanotechnology: emerging tool for diagnostics and therapeutics. Appl Biochem Biotechnol. 165:1178-1187 (2011).

3. S. Venkataraman, J.L. Hedrick, Z.Y. Ong, C. Yang, P.L. Ee, P.T. Hammond, and Y.Y. Yang. The effects of polymeric nanostructure shape on drug delivery. Adv Drug Deliv Rev. 63:1228-1246 (2011).

4. L.E. van Vlerken, T.K. Vyas, and M.M. Amiji. Poly(ethylene glycol)-modified nanocarriers for tumor-targeted and intracellular delivery. Pharm Res. 24:1405-1414 (2007).

5. V. Torchilin. Tumor delivery of macromolecular drugs based on the EPR effect. Adv Drug Deliv Rev. 63:131-135 (2011).

6. Y. Matsumura and H. Maeda. A new concept for macromolecular therapeutics in cancer chemotherapy: mechanism of tumoritropic accumulation of proteins and the antitumor agent smancs. Cancer Res. 46:6387-6392 (1986).

7. H. Maeda. Tumor-selective delivery of macromolecular drugs via the EPR effect: background and future prospects. Bioconjug Chem. 21:797-802 (2010).

8. R. Duncan and M.J. Vicent. Do HPMA copolymer conjugates have a future as clinically useful nanomedicines? A critical overview of current status and future opportunities. Adv Drug Deliv Rev. 62:272-282 (2010).

9. V.P. Torchilin. Passive and active drug targeting: drug delivery to tumors as an example. Handb Exp Pharmacol:3-53 (2010).

10. Y.H. Bae and K. Park. Targeted drug delivery to tumors: myths, reality and possibility. J Control Release. 153:198-205 (2011).

11. T.A. Denison and Y.H. Bae. Tumor heterogeneity and its implication for drug delivery. J Control Release (2012).

12. R.L. Manthe, S.P. Foy, N. Krishnamurthy, B. Sharma, and V. Labhasetwar. Tumor ablation and nanotechnology. Mol Pharm. 7:1880-1898 (2010).

13. S.L. Hokland, T. Nielsen, M. Busk, and M.R. Horsman. Imaging tumour physiology and vasculature to predict and assess response to heat. Int J Hyperthermia. 26:264-272 (2010).

14. K. Richter, M. Haslbeck, and J. Buchner. The heat shock response: life on the verge of death. Mol Cell. 40:253-266 (2010).

15. M. Sato, V.J. Yao, W. Arap, and R. Pasqualini. GRP78 signaling hub a receptor for targeted tumor therapy. Adv Genet. 69:97-114 (2010).

16. M. Ni, Y. Zhang, and A.S. Lee. Beyond the endoplasmic reticulum: atypical GRP78 in cell viability, signalling and therapeutic targeting. Biochem J. 434:181-188 (2011).

17. N. Larson and H. Ghandehari. Polymeric conjugates for drug delivery. Chem Mater. 24:840-853 (2012).

18. N. Larson, A. Ray, A. Malugin, D.B. Pike, and H. Ghandehari. HPMA copolymer-aminohexylgeldanamycin conjugates targeting cell surface expressed GRP78 in prostate cancer. Pharm Res. 27:2683-2693 (2010).

19. A.J. Gormley[*], N. Larson[*], S. Sadekar, R. Robinson, A. Ray, and H. Ghandehari. ([*]first co-authors). Guided Delivery of Polymer Therapeutics Using Plasmonic Photothermal Therapy. Nano Today. 7:158-167 (2012).

20. N. Larson, A.J. Gormley, N. Frazier, and H. Ghandehari. In vitro synergism and in vivo efficacy of combination tumor hyperthermia and heat shock protein targeted HPMA copolymer-drug conjugates. (Submitted).

21. A. Ray[*], N. Larson[*], D.B. Pike, M. Gruner, S. Naik, H. Bauer, A. Malugin, K. Greish, and H. Ghandehari. ([*]first co-authors). Comparison of active and passive targeting of docetaxel for prostate cancer therapy by HPMA copolymer-RGDfK conjugates. Mol Pharm. 8:1090-1099 (2011).

22. N. Larson, K. Greish, H. Bauer, H. Maeda, and H. Ghandehari. Synthesis and evaluation of poly(styrene-co-maleic acid) micellar nanocarriers for the delivery of tanespimycin. Int J Pharm. 420:111-117 (2011).

CHAPTER 2

LITERATURE BACKGROUND

2.1 Introduction

Throughout history, the practice of medicine has utilized therapeutic compounds to treat disease. Beginning is 1894, Felix Hoffman, working for the German medical company Bayer began searching for compounds to alleviate the pain of his father, who suffered from arthritis.[1] His work led him to discover the compound salicylic acid, found in willow bark. A slight chemical modification to reduce the inherent gastric stress of the compound was made followed by development of a commercial method to produce it. The result, aspirin, is still widely used today. From that time until the past few decades, pharmaceutical companies have focused their development efforts on low molecular weight, organically synthesized compounds.[2] With the modern advent of combinatorial chemistry,[3] vast numbers of compounds are now routinely synthesized and screened against a variety of potential therapeutic targets. More recently, however, much attention has been directed towards the development of new classes of therapeutics. The utilization of therapeutic proteins and monoclonal antibodies and their commercial success, particularly in anticancer therapies, has reshaped development efforts of the pharmaceutical industry, primarily as a result of an increased

ability to control and manipulate biological processes.[4] In a similar manner, recent advances in multiple scientific fields have increased our ability to control and manipulate chemical structures and materials at the nanometer scale.[5] The emerging fields of nanotechnology and nanomedicine, as it applies to the medical sciences, are providing new opportunities for improvement in the diagnosis and treatment of diseases. From an industrial standpoint, it is anticipated that the impact of these technologies, which are used in advanced drug delivery systems will continue to grow (see Figure 2.1).[6] For the drug delivery scientist, these new materials and structures can be utilized as tools to more effectively administer and deliver therapeutic agents. The use of synthetic polymers, in particular, has been increasingly used to provide advantageous properties to such materials and structures.

The objective of controlled drug delivery is to provide control over both the drug location and concentration as a function of time in order to maximize therapeutic effect and minimize toxicity. This is of particular importance in anticancer applications where the drug to be delivered is usually potently cytotoxic, resulting in a narrow therapeutic index. In this chapter, the overall rationale for using polymeric materials as carriers to enhance the therapeutic index of chemotherapeutics will be introduced, with a particular emphasis on polymeric drug conjugates. Current strategies to "target" these types of carriers to tumor tissues will also be reviewed, along with a discussion of factors currently limiting these targeting strategies. As the strategy under investigation in this thesis involves a combination therapy utilizing tumor hyperthermia to facilitate the delivery of polymer-drug conjugates, the natural response of tumor tissue and tumor cells to hyperthermia will then be reviewed, with emphasis given to the cellular heat

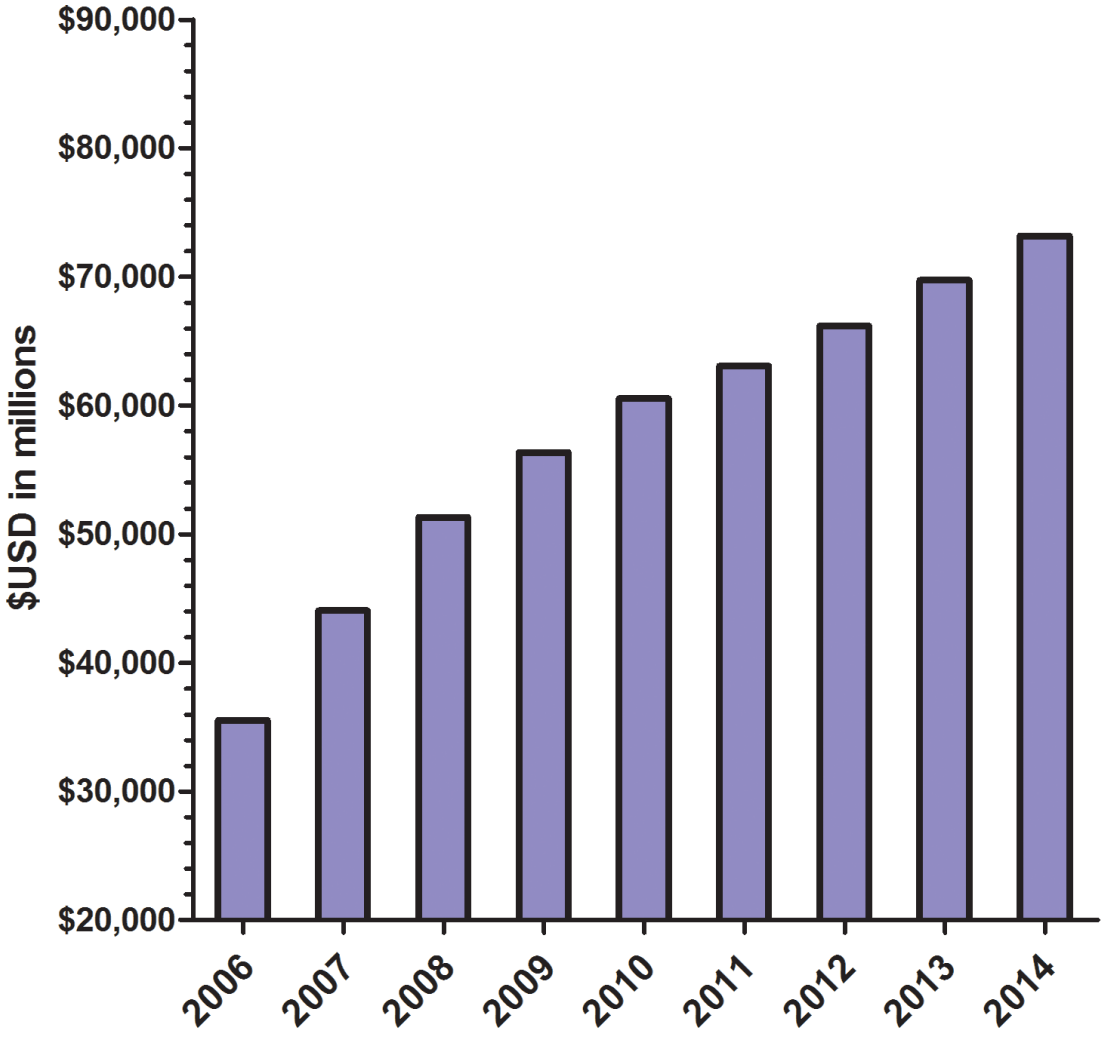

Figure 2.1. Anticipated growth in the global market for advanced drug delivery systems. Data obtained from Kalorama Information.[6]

shock protein response. In particular, the function of glucose regulated protein 78 kDa (GRP78) within and on the surface of tumor cells will be discussed. Studies described in this thesis utilize gold nanorod mediated plasmonic photothermal therapy[7] as a tool to induce localized hyperthermia *in vivo*, so a brief introduction to this method is also included. Finally, challenges in the delivery of chemotherapy for prostate cancer and how this combination strategy can be utilized to improve current treatment options will be presented, along with an introduction to the various anticancer agents utilized herein to test our hypotheses.

2.2 Polymer therapeutics and polymer-drug conjugates

Concepts utilizing polymers in the design of therapeutic agents have been widely investigated for a number of decades. Initial work of the 1960s focused on utilizing polymers as blood plasma expanders, wound dressings, and injectable or implantable depots.[8, 9] In 1975, a rational model for pharmacologically active polymers was first proposed by Helmut Ringsdorf.[10] His concept of covalently bound polymer-drug conjugates still forms the basis for much of the work in this area performed today. The Ringsdorf model (Figure 2.2) primarily consists of a biocompatible polymer backbone bound to three components: 1) a solubilizer, which serves the purpose of imparting hydrophilicity and ensuring water solubility, 2) a drug, usually bound to the polymeric backbone via a linker, and 3) a targeting moiety whose function is to provide transport to a desired physiological destination or bind to a particular biological target. The Ringsdorf model is particularly attractive to drug delivery scientists, whose primary objective is the specific delivery of therapeutic agents to their intended site of

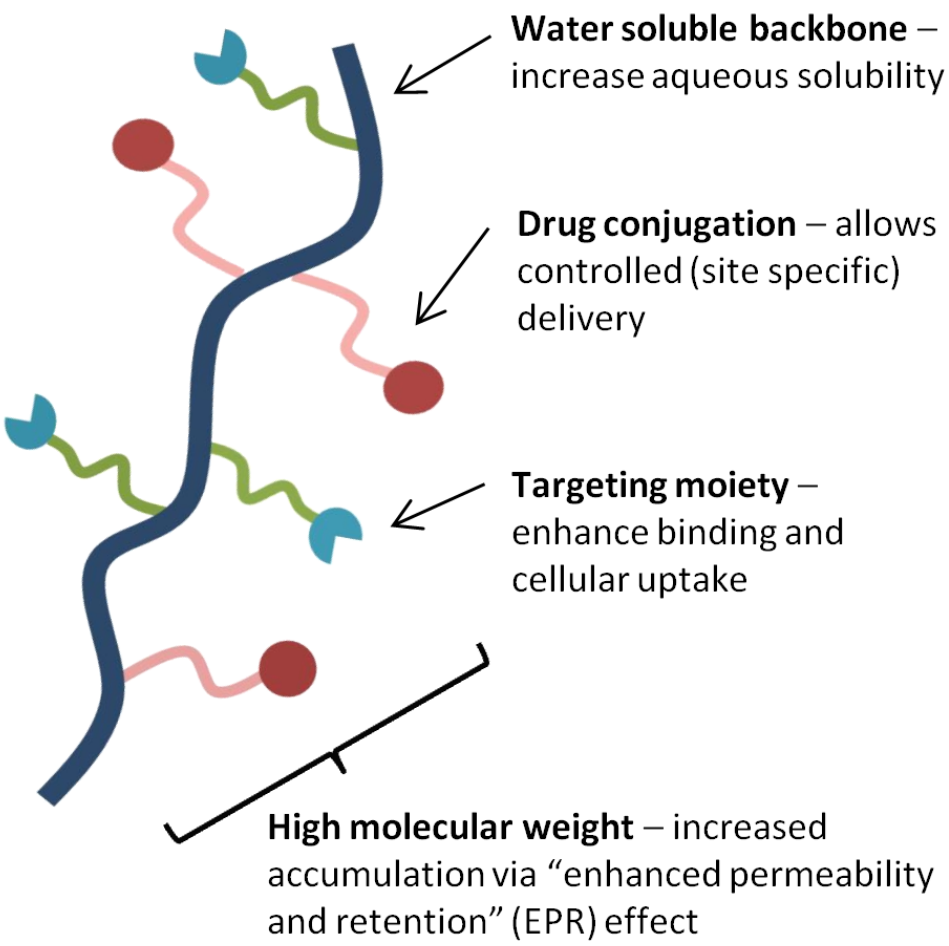

Figure 2.2. Modified Ringsdorf model providing a rationale for drug delivery via polymer drug conjugates. Reprinted with permission.[11]

action in an attempt to improve efficacy and reduce toxicity. These polymer-drug conjugates offer several significant advantages over traditional small molecule therapeutics. First, the aqueous solubility of a drug can be dramatically improved following conjugation to a water soluble polymer.[12, 13] This is of significant relevance as it has been estimated that 40-60% of drugs in development exhibit poor bioavailability due to low aqueous solubility.[14] Next, polymer-drug conjugates offer the potential for a drug to be delivered in a controlled manner, with drug release from the conjugate occurring over a defined time interval. In this way, the rate and duration of delivery can be custom designed to achieve the desired therapeutically effective concentration. Thus it is possible to avoid large fluctuations associated with periodic administration, which can lead to high systemic drug concentrations resulting in undesired side effects, organ damage, or toxicity. Polymer conjugation also provides an opportunity to alter drug pharmacokinetics and biodistribution. This is particularly useful for drugs which exhibit a short blood plasma half-life due to rapid metabolism or clearance or for drugs which exhibit off target toxicities (i.e., anticancer agents). As previously mentioned, another major advantage that can be realized through drug-polymer conjugation is the inclusion of targeting moieties, which function to carry the drug to the site of pharmacological action.

A substantial amount of effort is currently directed toward developing anticancer polymer-drug conjugates. Anticancer agents are often limited by poor water solubility and metabolic instability, and their clinical use is often limited by dose dependent toxicity. The therapeutic index of a given drug is defined as the ratio between its toxic and therapeutic dose. For the clinician, the goal is to deliver an anticancer agent at a

dose high enough to achieve cytotoxicity within tumor tissues. However, the actual dose administered is very often limited by toxicity to other vital organs. Thus, any improvement in the therapeutic index for such drugs which allows the clinician the ability to deliver higher drug concentrations to tumor tissue while maintaining manageable side effects can yield benefits for cancer patients. One of the primary ways in which polymer-drug conjugates can increase the therapeutic index of anticancer agents is via the "enhanced permeability and retention (EPR) effect" first described by Matsumura and Maeda in 1986.[15] They proposed that increased uptake of macromolecules by solid tumors can occur due to a combination of poor lymphatic drainage and increased vascular permeability present within the tumor microenvironment (Figure 2.3). Detailed information about the EPR effect and its implications in cancer chemotherapy has been the subject of several review articles.[16-19]

Despite the vast amount of effort directed toward the development of therapeutic polymer-drug conjugates, success in terms of translation to clinical practice has been slow due to a variety of unique challenges. Many conjugates are, for example, complex multi-component drug delivery systems that must ultimately satisfy the identity and purity regulatory requirements necessary for any new chemical entity (NCE). Validated methods for reproducible synthesis and characterization such as reversible-addition fragmentation chain-transfer (RAFT) polymerization[20-22] or atom transfer radical polymerization (ATRP)[23] need to be further utilized to satisfy drug product quality requirements. In addition to this, regulatory requirements require studies examining the metabolic fate of such conjugates, which can become increasingly difficult to

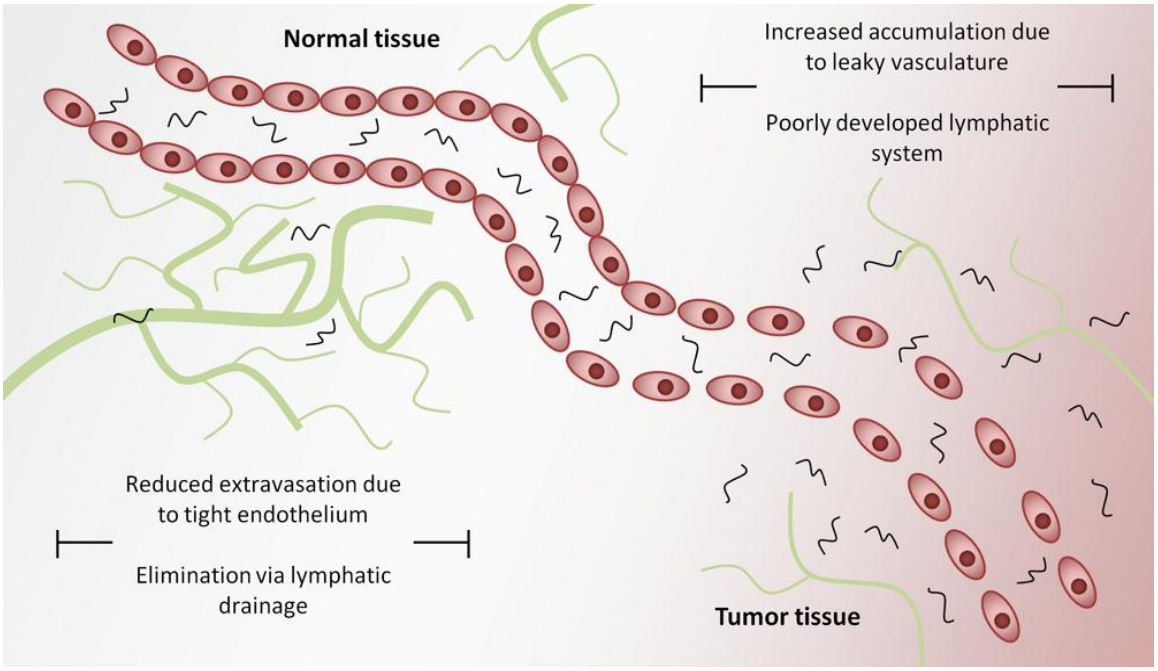

Figure 2.3. The enhanced permeability and retention or "EPR" effect. Increased tumor accumulation of macromolecules occurs via a combination of increased extravasation and reduced lymphatic drainage in tumor tissues. Reprinted with permission.[11]

characterize for multicomponent systems as compared to traditional small molecule therapeutics.

Safety and efficacy of polymer-drug conjugates, as with other more traditional therapeutics, is obviously of the utmost concern during the drug development process. Those conjugates that have progressed to clinical trials have primarily utilized previously approved drugs.[24-30] Although a polymer-drug conjugate is defined as a NCE for regulatory purposes,[31] information pertaining to the safety of the free drug can be utilized as a guide in designing toxicity studies. However, careful consideration must be taken as polymer-drug conjugates frequently show altered biodistribution and pharmacokinetic patterns. A critical parameter directly associated with both safety and efficacy is release of the drug from the polymeric carrier. Generally, drug release from a polymeric carrier is necessary for the drug to elicit its pharmacological effect.[32, 33] This is advantageous as a conjugate will be mostly inactive during systemic transport. If release of the drug from the conjugate occurs prematurely during systemic transport, undesired toxicities may result, and the overall safety profile of the conjugate will be poor.[26, 34] Therefore, the stability of the conjugate is one critical parameter. However, upon reaching the desired target destination, release of the drug is then required to achieve efficacy. There is therefore a critical balance between conjugate stability and drug release that directly impacts safety and efficacy.

The focus of this section is to provide background on the rational design of polymer-drug conjugates and their biological evaluation. Polymer-drug conjugates of various chemistries and architectures will be reviewed with emphasis given on the design of each system and potential applications. Stimuli-sensitive systems and the

emerging field of theranostics based on polymeric systems will also be briefly discussed.

2.2.1 Linear polymers

Many different drug conjugates have been synthesized utilizing water soluble linear polymers. While many polymeric carriers have been described such as poly(vinyl pyrrolidone) (PVP),[35, 36] poly(vinyl alcohol),[37] poly(glutamic acid) (PGA),[38] and poly(malic acid),[39] two of the most widely investigated chemistries are those based on poly(ethylene glycol) (PEG)[29] and *N*-(2-hydroxypropyl)methacrylamide (HPMA) copolymers,[40] which will be reviewed in detail.

2.2.1.1 Poly(ethylene) glycol. Although numerous different polymer compositions have been synthesized and studied, some of the simplest polymers, such as poly(ethylene glycol) (PEG), maintain widespread use and versatility. PEG-protein conjugates have gained particular importance due to the ability of PEG to protect against protein enzymatic degradation and reduce uptake by the reticulo-endothelial system (RES),[41, 42] both properties imparted via simple steric hindrance. Protein PEGylation has led to the development of numerous therapeutics, including the FDA approved products PEG-asparaginase (Oncaspar®),[43] PEG-adensoine deaminase (Adagen®),[44] PEG-interferon α-2a (Pegasys®),[45] PEG-interferon α-2b (PEG-Intron®),[46] PEG-granulocyte colony-stimulating factor (Neulasta®),[47] and PEG-growth hormone receptor antagonist (Somavert®).[48] Most commonly, conjugation to PEG is performed via coupling to the end chains.[49] Functionalities such as *N*-hydroxysuccinimide (NHS) esters or aldehydes allow conjugation to the amine of lysine residues whereas

maleimides react readily with the thiol of cysteine residues. Numerous functionalized PEGs are available to aid in conjugation. Whereas some functionalities allow conjugation to biomolecules such as proteins and antibodies, others can be more generally applied in the synthesis of novel biomaterials.

PEG-drug conjugates have several advantages. First and foremost, the use of PEG as a biocompatible polymer has been established clinically.[50] Due to the widespread use of PEGs in drug conjugation, an array of functional PEGs are now commercially available.[51] In addition, large scale synthesis of PEGs are generally routine, and they can be readily synthesized with narrow molecular weight and molecular weight distribution specifications.[52] These properties make PEG-drug conjugates attractive for pharmaceutical applications.

The use of PEG in conjugation is, however, not without limitations. A fundamental disadvantage of PEG is its nonbiodegradability. As previously mentioned, conjugates with a hydrodynamic radius of approximately 3.5 nm are preferred in many applications due to their ability to avoid renal filtration.[53] However, conjugates of this size have the potential for long term accumulation, resulting in toxic side effects. Another significant disadvantage of traditional PEG-drug conjugates is the low drug loading that is achieved due to conjugation at only the end chains of PEG.[54] In an effort to overcome these limitations, branched[55-57] and multiarm[58, 59] PEGs have been investigated which can be excreted more easily following biodegradation.

2.2.1.2 HPMA copolymers. Copolymers of HPMA, first developed by Kopecek and coworkers, have also been widely investigated as hydrophilic, biocompatible, polymeric drug carriers.[31, 40, 60, 61] Substitution of the α-carbon and the

presence of an amide linkage in the side chain helps ensure hydrolytic stability. In addition, HPMA was selected over other derivatives as the presence of divinyl compounds can be eliminated due to the crystalline nature of the monomer, as compared to 2-hydroxyethyl methacrylate type esters. Various functionalities may be incorporated into HPMA copolymers via functionalized comonomers, allowing control over the composition of these systems. In particular, side chains that include drugs, targeting moieties, imaging agents, or reactive groups can be combined with relative synthetic ease. A major driving force behind the continued development of HPMA copolymers as drug carriers was the development of oligopeptide sequences as drug linkers.[62, 63] These sequences were specifically designed to ensure hydrolytic stability during systemic transport and the ability to be enzymatically cleaved by lysosomal enzymes following cellular internalization.[64] In developing such a system, early studies with model enzymes demonstrated that factors such as peptide sequence structure and length, drug loading, drug structure, and steric hindrance play important roles in stability and drug release kinetics.[65, 66] Studies evaluating release in the presence of the lysosomal enzyme cathepsin B resulted in the isolation of the tetrapeptide sequence glycylphenylalanylleucylglycine (GFLG). Numerous HPMA copolymer-drug conjugates utilizing this lysosomally cleavable linker have been reported to date,[67-70] including several HPMA copolymers used in clinical trials.[25, 71]

PK1 was the first clinically investigated water soluble polymer-drug conjugate for cancer therapy.[72] This agent consists of the anticancer anthracycline antibiotic doxorubicin attached to a HPMA copolymer backbone via the lysosomally degradable sequence GFLG (Figure 2.4). PK1 has a molecular weight of approximately 30 kDa

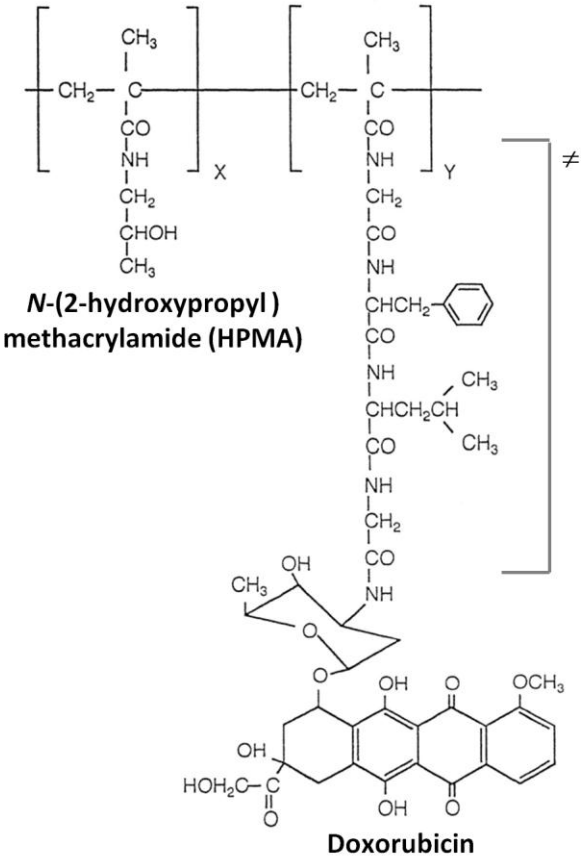

Figure 2.4. Representative structure of PK1 (FCE28068), a HPMA copolymer conjugate bearing the anticancer agent doxorubicin bound via the lysosomally degradable Gly-Phe-Leu-Gly (GFLG) linker (≠). PK1 was the first anticancer polymer-drug conjugate evaluated clinically. Reprinted with permission.[11]

and contains 8.5% doxorubicin by weight.[73] The stability of the GFLG linkage to doxorubicin was demonstrated following intravenous administration, with no release of free doxorubicin and biological inactivity of covalently bound doxorubicin.[73] PK1 in comparison with free doxorubicin also demonstrated decreased cardio- and bone marrow toxicity in animals. In addition, tumor accumulation of doxorubicin was increased 17- to 70-fold as compared to free doxorubicin in melanoma tumor bearing mice.[74] These promising results led to the further clinical development of PK1.[25, 75] PK1 was generally well tolerated with no alopecia until doses greater than 180 mg/m^2, and no anthracycline related cardiotoxicity until doses greater than 1680 mg/m^2. Efficacy was marginal with 2 partial and 2 minor responses out of 36 patients observed during phase I studies, and 6 partial responses out of 56 evaluable patients during phase II studies. Building on the experience gained during the evaluation of PK1, a number of HPMA copolymer-drug conjugates have entered clinical evaluation as anticancer agents.[31, 40, 61]

In the recent decade, strategies to improve on the first generation of HPMA based polymer conjugates have been investigated. For example, HPMA copolymers exhibiting pH dependent drug release have been described (see Section 2.3.6 on pH sensitive systems). The versatility of HPMA copolymer design has also allowed a wide array of conjugates containing a variety of drugs including taxanes,[26, 70, 76] camptothecin,[77, 78] platinates,[27, 28] dexamethasone,[79-81] gemcitabine,[82, 83] and geldanamycin.[68, 84, 85] Conjugates bearing a combination of drugs have also been investigated.[82, 86, 87] A “drug-free” strategy has also been reported, wherein apoptosis of cancer cells is induced via crosslinking of cell surface CD20 using a coiled-coil peptide

approach.[83, 88] More recent attention has also focused on developing backbone degradable HPMA copolymer-drug conjugates.[83, 89]

2.2.2 Dendrimers

Dendrimers are branched polymeric macromolecules forming a star-like structure. Such unique structures allow conjugation of drugs to the surface, thus maximizing the potential for biological interactions. A wide array of chemistries can be employed in the synthesis of dendrimers, where the core, monomer units, and surface functionality determine physiochemical characteristics. However, for use in drug delivery applications, it is necessary to maintain biocompatibility. Physiochemical properties such as solubility, surface group functionality, surface charge density, and stability must therefore be considered. Tomalia et al. first described the synthesis of poly(amido amine) (PAMAM) dendrimers in 1985.[90, 91] Synthesis, which occurs for each "generation" in a stepwise fashion, can result in dendrimers with precisely defined structures. With each synthetic step, the generation increases resulting in a linear increase in radius and an exponential increase in surface groups.[92] For example, PAMAM dendrimers are synthesized from an ethylenediamine core followed by subsequent half-generation addition by reaction with methyl acrylate and complete generation synthesis by reaction with ethylenediamine. A major advantage of dendrimers, as compared to most linear polymers, is their synthetic precision, often yielding structures with polydispersity indices (M_w/M_n) less than 1.05.[93] In addition, the large number and density of functional groups at the dendrimer surface provides opportunities for conjugation of drugs,[94, 95] targeting moieties,[96] imaging agents,[97] etc.

In the field of drug delivery, much of the work with dendrimers has focused on their use in the encapsulation and formulation of drugs.[98] Due to their hyper branched structure, dendrimers often possess open cavities between adjacent branches, thus allowing encapsulation of drugs.[99] This can aid in the solubilization of poorly water soluble drugs. In addition, dendrimers formulated (physically mixed) with drugs have been investigated as both transdermal[100] and oral[101] delivery systems. Dendrimers with positively charged surface functionalities, such as poly(ethyleneimine) and PAMAM dendrimers, have also been investigated as gene carriers,[102] due to their ability to complex with negatively charged DNA.

Despite much progress, clinical translation of dendrimer based drug delivery systems has been limited due to concerns over their biocompatibility and toxicity. Dendrimers have been shown to exhibit high affinity for metal ions, lipids, bile salts, proteins, and nucleic acids, resulting in the disrupting of biological processes and leading to toxicity.[103] The molecular toxicity of dendrimers depends primarily upon their surface functionalization. In particular, dendrimers with a highly positive surface charge have been shown to elicit toxicities *in vitro*[104, 105] and *in vivo.*[106, 107] Therefore, much effort is currently focused towards surface modification of dendrimers to increase biocompatibility. In addition, the difficulty and expense associated with dendrimer synthesis needs to be addressed before clinical translation can be achieved.

2.2.3 Polymeric micelles

Micelles are colloidal particles with a size of about 5-150 nm that consist of self-assembled aggregates of amphiphilic molecules or surfactants. Amphiphiles, at low

concentrations in aqueous media exist as unimers in solution. However, as their concentration is increased, thermodynamic processes drive the formation of aggregates which sequester hydrophobic regions into core like structures surrounded by a hydrophilic corona or shell. The concentration at which aggregation occurs is commonly referred to as the critical micelle concentration (CMC). Traditionally, low molecular weight surfactants (i.e., polysorbates, sodium dodecyl sulfate, etc.) with relatively high CMCs in the range of 10^{-3} to 10^{-4} M have been used extensively in pharmaceutical formulations, primarily as excipients to increase the aqueous solubility of poorly water soluble drugs.[108] Hydrophobic drugs are contained within and associate with the hydrophobic regions of the micelle. However, following administration, dilution of a given pharmaceutical formulation occurs rapidly, and as the micelle concentration drops below its CMC, its stability is compromised.

Early work by Kataoka,[109] Kabanov,[110] and coworkers described the potential use of amphiphilic polymers as drug carriers. These polymeric micelles are primarily composed of block-copolymers with hydrophilic and hydrophobic units that also self-assemble into a hydrophobic core surrounded by a hydrophilic shell (Figure 2.5). Each micellar unimer unit can be assembled in various fashions such as A-B diblock copolymers, A-B-A triblock copolymers, and grafted copolymers. A major advantage of polymeric micelles as compared to traditional low molecular weight surfactant derived systems is their increased stability. Polymeric micelles commonly exhibit CMCs in the 10^{-6} to 10^{-7} M range.[111] The ideal polymeric micelle should demonstrate high drug loading, controlled drug release, and suitable biological compatibility and stability. Physiochemical properties of polymeric micelles are primarily based on the

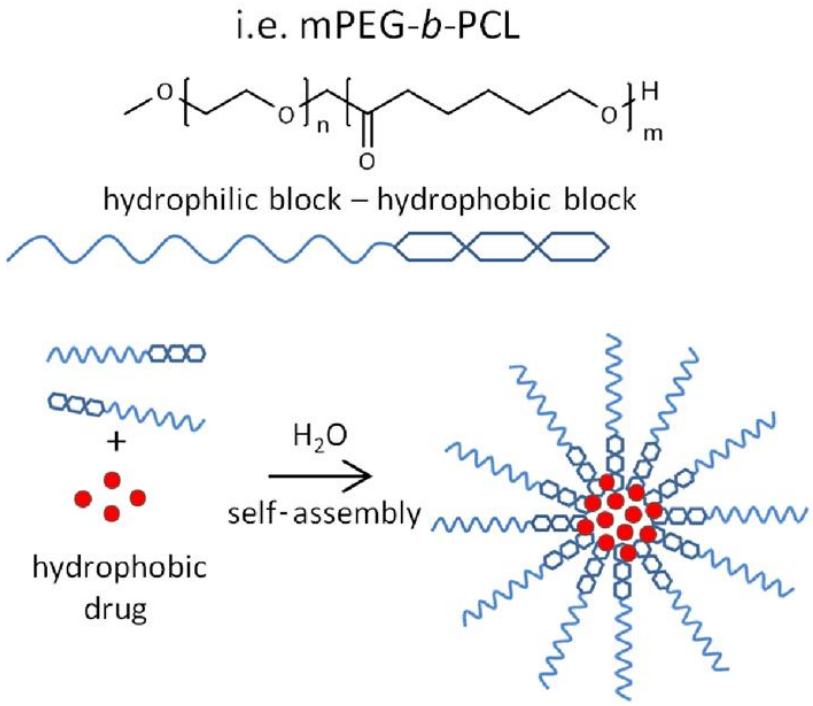

Figure 2.5. An example of a polymeric micelle. A typical example of a polymeric micelle unimer structure composed of both hydrophilic (mPEG) and hydrophobic (PCL) blocks. Hydrophobic drugs associate with hydrophobic domains of the micelle following self-assembly in aqueous conditions. Reprinted with permission.[11]

characteristics and lengths of the hydrophilic and hydrophobic blocks. PEG is the most commonly employed hydrophilic polymer, due to highly hydrated nature and ability to resist uptake by the reticuloendothelial system (RES). However, a number of other hydrophilic polymer chemistries have been applied including poly(*N*-vinyl-2-pyrrolidone) (PVP),[112] poly(vinyl alcohol) (PVA),[113] and poly(ethyleneimine) (PEI).[114] PEG remains the polymer of choice due to its widespread acceptance and availability. A large variety of unimers to form hydrophoblic blocks have been utilized in forming the hydrophobic core of polymeric micelles. Examples include propylene oxide, L-lysine, caprolactone, D,L-lactic acid, styrene, aspartic acid, β-benzoyl-L-aspartate, and spermine among others.[115] More hydrophobic unimers (i.e., styrene) form micelle cores spontaneously, while other less hydrophobic unimers (i.e., lysine) first interact via electrostatic interactions with hydrophobic drug molecules, followed by micelle formation.[116] CMC tends to depend more on the type and length of the hydrophobic block, with lower CMCs associated with greater hydrophobicity and increased hydrophobic block length.[117, 118]

Continued advances are being made in the development of polymeric micelles. Increasingly, there is a trend towards "smart" polymeric micelles in terms of their response to various biological stimuli and their ability to target specific tissues. Another interesting application involves the use of polyion complex (PIC) micelles, wherein the micelle core is composed of a polycation block, for the delivery of negatively charged DNA or small interfering RNA (siRNA).[119, 120] Polymeric micelles based on HPMA copolymers have also been described.[121] PolyHPMA has been used successfully in the generation of polymeric micelles either in the hydrophilic block

comprising the shell,[122-125] or following chemical modification, as the hydrophobic core.[126, 127] A variety of hydrophobic drugs have also been encapsulated in these micelles; however, the majority of the data on the activity of these systems to date have been obtained *in vitro*,[121, 127, 128] and more *in vivo* data are needed to ascertain their potential as carriers.

An advantage of polymeric micelles as compared to other polymeric drug carriers is their relative ease of fabrication, due to their inherent self-assembly properties. This has resulted in a number of polymeric micelles currently under clinical investigation.[129]

2.2.4 Biodegradable polymers

A major advantage of polymer-drug conjugates is their ability to escape filtration via the kidneys, resulting in an increased blood circulation time. For anti-cancer conjugates, an added advantage is increased tumor accumulation via the previously described EPR effect for conjugates at least greater than 3.5 nm.[53] However, eventual elimination from the body is also required to reduce potential long term adverse effects of these carriers. The use of biodegradable systems allows conjugates of a sufficient size to both evade renal filtration and allow subsequent degradation and elimination. Such conjugates should have degradation rates slow enough to allow adequate biodistribution, and such degradation should result in the production of non-toxic degradation products. A number of biologically degradable bonds have been described. Biodegradation generally occurs via hydrolysis, enzymatic cleavage, or reductive degradation. Biodegradable polymers have been described[130, 131] which

include poly(α-amino acids) such as poly(L-lysine),[132] poly(L-glutamic acid),[133] and poly ((*N*-hydroxyalkyl)glutamine)[134] as well as carbohydrate polymers such as dextrins,[135] hydroxyethylstarch (HES),[136] polysialic acid,[137] and the polyacetal Fleximer®.[30]

An example of a biodegradable polymer-drug conjugate currently under phase III clinical development in the United States is OPAXIO™ (formerly branded as XYOTAX), which is a conjugate of poly(L-glutamic acid) and the anticancer agent paclitaxel.[38] Poly(L-glutamic acid) was chosen as its breakdown product L-glutamic acid can enter normal cellular metabolism and is not cleared via the kidneys. Paclitaxel is conjugated via an ester bond to the γ-carboxylic acid side chains. In addition, because conjugation is via the 2' hydroxyl of paclitaxel, the conjugate is unable to bind tubulin and elicit its pharmacological action, thus rendering it inactive. In one example, the poly(L-glutamic acid) conjugate had a molecular weight of 48 kDa, and contained approximately 37% by weight paclitaxel, while maintaining water solubility. During preclinical investigation, this conjugate demonstrated a higher maximum tolerated dose (MTD) and was more efficacious than paclitaxel formulated in Cremophor EL/ethanol. Clinical trials are currently underway[138-142] evaluating OPAXIO™ in prostate, breast, ovarian, colorectal, and lung cancers.

Strategies to produce biodegradable derivatives of more traditional polymers such as PEG and HPMA copolymers have also been investigated. As mentioned previously, biodegradable multiarm PEGs[143] (i.e., ENZ-2208) containing ester bonds between PEG chains have entered clinical trials. Another strategy in which a biodegradable polymer consisting of small molecular weight PEG blocks is linked

together via enzymatically cleavable oligopeptide groups, and bearing the anti-cancer agent doxorubicin, has been described.[144] Work by Ulbrich and coworkers has utilized a variety of approaches to generate biodegradable HPMA copolymer-drug conjugates including graft systems containing oliogopeptide sequences and/or reductive disulfide bonds,[145] as well as the generation of biodegradable star HPMA copolymer-drug conjugates.[146] In the latter, PAMAM dendrimers were modified with polyHPMA grafts via enzymatically cleavable or reducible linkers, thus enabling degradation of the high molecular weight polymer. These star polymer conjugates bearing doxorubicin exhibited prolonged blood circulation, increased tumor accumulation, and anti-tumor efficacy in lymphoma tumor bearing mice.[147] Other recent work by Kopecek and coworkers on the synthesis of biodegradable multiblock poly(HPMA) conjugates generated via a combination of RAFT polymerization and click chemistry has been described.[83, 89, 148] This demonstrates how advances in chemistry (i.e., RAFT polymerization and click chemistry) can be utilized to generate new biodegradable polymer-drug conjugates with well-defined physicochemical properties.

2.2.5 Stimuli-sensitive polymers

So called "smart polymers" have been engineered to contain a vast array of properties, including the ability to respond to changes in environmental stimuli such as pH, ionic strength, temperature or externally applied heat, magnetic or electric fields, or ultrasound.[149] Such polymers commonly respond via conformational and/or electrostatic changes, which can be exploited to help facilitate a particular function (i.e., drug release, endosomal escape, etc.). Carriers which respond to variations in pH and

temperature have found the greatest versatility in drug delivery and will be reviewed in brief below.

2.2.6 pH sensitive systems

Exploiting physiological variations in pH has been widely investigated as a means to obtain site specific delivery. The pH of diseased areas such as tumors, infarcts, and sites of inflammation may drop to around 6.5, almost one full pH unit below that of normal blood (pH 7.4) due to hypoxic conditions and extensive cell death.[150, 151] In addition, following cellular uptake via endocytosis, the pH of late endosomes may reach values as low as 5.0, further providing a gradient over which release may be triggered.[152] The polymer backbone can be made pH sensitive, typically through the inclusion of acidic (i.e., carboxylic and sulfonic acids) or basic (i.e., ammonium salts) groups that undergo protonation or deprotonation in response to changes in pH. Commonly studied chemistries of this nature include poly(acrylamide) (PAAm), poly(methacrylic acid) (PMAA), poly(acrylic acid) (PAA), and poly(2-(dimethylamino)ethyl methacrylate (PDMAEMA).[153] Utility is primarily found in non-conjugated systems such as micelles, liposomes, and other nanocarriers, where conformational changes disrupt the stability of the carrier resulting in drug release.[154]

As for polymer-drug conjugation, pH sensitivity is introduced primarily via pH sensitive chemical bonds, which can result in site specific drug delivery. For example, hydrazone bonds formed via the action of hydrazine on ketones or aldehydes exhibit hydrolysis under mildly acidic conditions (pH 5-6) such as that present in lysosomes while maintaining stability at pH values found in blood (pH 7.4).[155, 156]

A number of pH responsive polymeric micelles have also been described including systems in which doxorubicin was conjugated to the side chains of the micelle core-forming blocks via hydrazone bonds.[157] The micelles demonstrated both time and pH dependent release, with increased release under endosomal low pH conditions (5.0-5.5).[157] Biodistribution studies showed minimal signs of premature drug release, and selective accumulation in tumors and the anti-tumor efficacy of these pH sensitive micelles was significantly higher than that achieved with comparable doses of free doxorubicin.[158]

2.2.7 Temperature-sensitive systems

The concept of using temperature to control drug delivery is in part due to the observation that elevated temperature can be associated with diseased tissues. In addition, the external application of hyperthermia can be utilized as a trigger to induce changes in polymer structure resulting in drug release. Water soluble temperature sensitive polymers such as those based on poly(*N*-isopropylacrylamide) (poly(NIPAAM)) undergo a lower critical solution temperature (LCST) phase transition, wherein polymer chains collapse and aggregate at temperatures above their LCST due to the reversible dehydration of hydrocarbon side chains.[159] The LCST for poly(NIPAAM) is approximately 32°C. However, the LCST of such polymers can be adjusted by changing the *N*-substituted carbon chain or via copolymerization.[160]

Over the past decade, elastin-like polypeptides (ELPs) have been investigated in drug delivery applications. ELPs are recombinant polymers produced using genetic engineering techniques,[161, 162] resulting in monodisperse polymers with precisely

defined molecular weights and compositions.[163] They consist of a repeated peptide sequence based on a motif found in mammalian tropoelastin $(VPGXG)_n$, where X is defined as any residue except proline.[164] ELPs exhibit an LCST above which they become insoluble. This LCST can be varied by modifications in molecular weight and composition. A number of strategies utilizing the thermo sensitive nature of ELPs have been investigated. For example, ELPs with LCST above normal body temperature but below 43°C have been utilized as anticancer drug carriers, in which systemic delivery is combined with localized hyperthermia to tumor tissue, resulting in an increased accumulation of ELP aggregates within the tumor.[165] Other strategies including the use of ELP microparticles, ELP micelles, and ELP block copolymers have also been investigated.[166, 167]

2.2.8 Theranostics

In addition to their application as therapeutics agents, polymer-drug conjugates and other nanomedicines are increasingly being studied for diagnostic purposes. The combination of use of therapeutics and diagnostics has resulted in the term "theranostics" which defines delivery systems bearing both therapeutic and imaging or contrast agents.[168] Such systems allow for a more personalized medicine approach, wherein therapy can be directly monitored and custom tailored. Multiple benefits may be realized from these multifunctional systems. For example, biodistribution and accumulation at the target site of therapy can be monitored in a non-invasive manner. In addition, localization at the target site can be used as an accurate predictor of efficacy, thus relieving a patient from subsequent therapy that might not prove

efficacious. This can be achieved by first administering a tracer version of an imaging agent labeled conjugate. Those patients who demonstrate abnormal or unfavorable biodistribution, pharmacokinetics, or localization at the target site are then disqualified from treatment with a therapeutic version of the conjugate. Imaging modalities such as optical imaging, x-ray computed tomography (CT), dynamic contrast enhanced magnetic resonance imaging (DCE-MRI), single photon emission computerized tomography (SPECT) and positron emission tomography (PET) are well established and provide the necessary tools to allow spatial visualization and quantification of delivery. For example, during the initial clinical evaluation of HPMA copolymer-doxorubicin conjugates (PK1, PK2), localization was visualized in patients following treatment with ^{131}I radiolabeled conjugates, allowing information related to potential toxicities and tumor accumulation to be obtained early in the development process. Details regarding the use of macromolecules in theranostic applications are outside the current scope, but have been the subject of several reviews[168, 169] and it is anticipated that going forward, multifunctional polymer-drug conjugates bearing imaging agents will play a role in the future of image guided drug delivery and personalized medicine.

2.3 Targeted anticancer therapies

The inherent cytotoxicity and resulting dose limiting toxicity of cancer chemotherapeutics has driven the development of targeted anticancer therapies. The first goal of any targeted therapy is to concentrate the effect, or pharmacological action, of a therapeutic agent at the intended site of disease. The second goal is to minimize undesired side effects. For polymer-drug conjugates, this can be achieved passively via

the EPR effect (see Section 2.3). Specificity is also gained through a combination of pharmacologic and/or active targeting strategies. The basis and rationale of these strategies, along with their current limitations, will be discussed in this section.

2.3.1. Pharmacological targeting

In anticancer therapy, the common goal of most chemotherapeutics is to disrupt cellular division, thereby inhibiting proliferation of the cancerous tissue. Therefore, the pharmacologic targets of these chemotherapeutics are often proteins or enzymes associated with cell division. For example, the chemotherapeutic camptothecin, which demonstrates strong anti-tumor activity, strongly inhibits DNA and RNA synthesis via inhibition of topoisomerase I, an enzyme required for nucleic acid coiling and uncoiling.[170] DNA itself is also a potential target as DNA duplication is also required for cell division. For example, the anthracycline antibiotic doxorubicin inhibits cell division by intercalating DNA, thereby inhibiting the progression of topoisomerase II, effectively halting DNA replication.[171] This form of pharmacological targeting, has proven itself very successful, given the current array of chemotherapeutics on the market today. However, since the process being targeted is not fundamentally cancer specific, but is cell division specific, other cells in the body are affected. Primary examples included white blood cells, gastrointestinal epithelial cells, and hair cells. These off-target interactions give rise to adverse effects, many of which are dose limiting and can be life threatening. Therefore, additional strategies have been sought for delivery of drugs to cancer cells in a more selective and efficient manner.

2.3.2 Active targeting

Active targeting strategies seek to exploit inherent differences between cancer cells and cells of healthy, normal, tissues. In particular, differences in the expression of cell surface receptors are an attractive target. For a number of targeted therapeutic agents, such as monoclonal antibodies, receptor binding is intended to result in a pharmacological response, commonly via signal transduction (i.e., receptor tyrosine kinases), or receptor inhibition via competition with native ligands (i.e., vascular endothelial growth factors). For drug delivery systems already carrying therapeutic agents (i.e., antibody-drug conjugates, polymer-drug conjugates, or other nanomedicines), pharmacological action upon binding is not a prerequisite. Instead, interaction and binding with the receptor is intended to facilitate retention and internalization.

A tremendous amount of effort developing therapeutic polymer-drug conjugates and other nanomedicines has focused on the inclusion of targeting moieties. In the majority of cases, physicochemical properties of polymer-drug conjugates such a size, surface charge, conformation, and biocompatibility dictate how absorption, distribution, metabolism, and excretion take place.[172] As previously described, polymer-drug conjugates with a size above renal threshold exhibit longer blood circulation times, thereby increasing the probability for a conjugate to interact with its target. The benefits of so called “active targeting” are realized by increasing binding to and internalization into the cells of target tissues, phenomena which occur over short distances. Targeting can therefore be utilized as a way to maximize the effect of

"passive targeting" mechanisms, by ensuring that physically delivered polymer-drug conjugates remain at their intended site of action.

A number of features characterize an ideal target. The target should be universally and uniquely expressed by the diseased tissue. The vast majority of targeting strategies rely on the over expression of particular cell surface markers in diseased cells as compared to normal cells. Therefore, the probability of binding and cellular uptake of a conjugate with its intended target is increased as compared to normal cells. While it is well understood that expression of a particular target is generally not entirely specific, it is nevertheless anticipated that the large relative differences in expression between diseased and normal cells can still be utilized as an effective targeting strategy. Ideally, the target should also facilitate endocytosis following binding of the conjugate, thereby allowing the agent to exert its pharmacological action within the cell.

Sugars, hormones, growth factors, antibodies, antibody fragments, peptides, or other small molecules can be utilized as targeting moieties.[173-176] The targeting moiety must include the necessary functionality to facilitate conjugation, and should be conjugated in a manner that will ensure its stability during systemic circulation. Different targeting moieties have distinct advantages and disadvantages. Antibodies, for example, provide excellent binding affinity and target selectivity. However, their large size can drastically influence the properties of the carrier. Also, the relative cost associated with antibody production, conjugation, and concerns over their stability and immunogenicity remain important issues. The use of antibody fragments (Fab′, single-chain variable fragments (scFvs)) can partially address these concerns.[177] These

proteins retain the specificity of the original antibody, but are reduced in size, and can often be synthesized in bacterial cultures and thus reduce synthetic cost. Other targeting moieties such as peptides, sugars, and hormones can generally be readily synthesized at low cost, but they typically have reduced binding affinity and specificity as compared to antibodies and antibody fragments. These advantages and disadvantages and the choice of carrier dictate targeting moiety selection. How the binding affinity of the targeting moiety is affected following conjugation must also be evaluated.

Recent work has focused on developing HPMA copolymers containing cyclic Arg-Gly-Asp (RGD) peptides that target $\alpha_v\beta_3$ integrins expressed on angiogenic tumor blood vessels and tumor cells.[70, 84, 178-180] Copolymers containing a derivative of the anticancer and antiangiogenic agent geldanamycin (aminohexylgeldanamycin (AHGDM)) bound to the polymer backbone via the lysosomally degradable GFLG linker were synthesized and characterized. Molecular weight was maintained below 40 kDa to allow eventual renal clearance following administration. The conjugates demonstrated the ability for drug release, binding to $\alpha_v\beta_3$ integrins, and introduced cytotoxicity in endothelial and prostate cancer cells at concentrations similar to the free drug controls. To assess the efficiency of targeting, the biodistribution of ^{125}I-labeled copolymers was evaluated in prostate cancer bearing mice. Significantly higher localization was observed in the tumor following administration of the HPMA copolymer containing cyclic RGD peptides as compared to an untargeted control (Figure 2.6). In addition, the tumor accumulation of released drug was quantified by tumor extraction followed by HPLC analysis. Significantly higher concentrations of AHGDM were observed following administration of the targeted conjugate. *In vivo*

efficacy studies were performed in prostate cancer tumor bearing mice. Percent tumor growth as a function of time was evaluated following a single dose of HPMA copolymer-AHGDM-cyclic RGD, HPMA copolymer-AHGDM (untargeted control), AHGDM (free drug control), or saline (negative control). The study also included a large molecular weight HPMA copolymer-AHGDM conjugate so as to see how efficacy via RGD targeting would compare to conjugates relying solely on "passive" targeting via the EPR effect. Tumor growth was suppressed more for HPMA copolymers bearing cyclic RGD peptides as compared to both untargeted controls (small and large molecular weight) and free drugs (Figure 2.6). The results demonstrate that an appropriately selected targeting strategy can yield increased tumor delivery resulting in the increased efficacy of cancer chemotherapy.

2.3.2.1 Challenges and limitations of active targeting**.** While substantial progress has been made in utilizing active targeting strategies to deliver nanomedicines and polymer-drug conjugates, challenges and fundamental limitations remain.

First, inclusion of targeting moieties is often associated with increased material cost and synthetic complexity. This is of significant concern when dealing with advanced drug delivery systems, where cost is already elevated as compared to traditional therapeutics. Clinical translation of such a system will require significant benefits in measureable patient outcomes, the most significant of which are safety and efficacy. Simply put, the benefit must outweigh the cost. In an attempt to find an alternative, low cost, effective targeting strategy, Torchilin and coworkers have described paclitaxel loaded polymeric micelles modified with a tumor-specific phage protein.[181] The amphiphilic nature of the phage fusion coat protein enabled stable

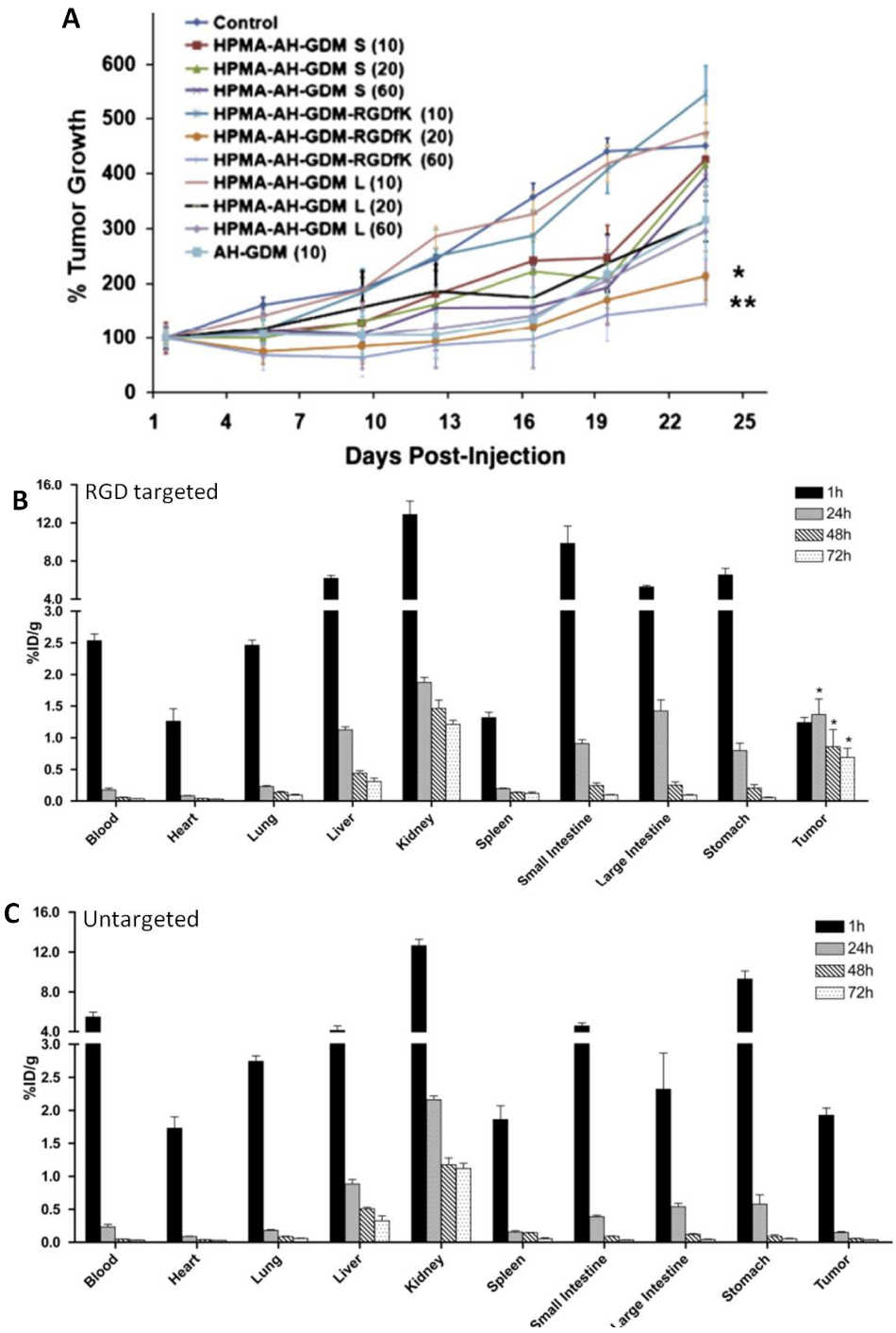

Figure 2.6. Active targeting. (A) Tumor regression as a function of time in DU145 human prostate cancer tumor bearing nu/nu mice. RGD targeted HPMA copolymers demonstrated significant efficacy as compared to untargeted HPMA copolymers and free drug controls. (B) Biodistribution in DU145 bearing mice of ^{125}I-radiolabeled HPMA copolymers bearing AH-GDM and cyclic RGD peptides. Increased accumulation was observed in tumor tissues, as compared to the untargeted conjugate (C). Reprinted with permission.[11]

incorporation into the polymeric micelles without the requirement for specific conjugation chemistry and this approach relied completely on the inherent self-assembly of the phage protein into the micelles, resulting in synthetic ease. *In vitro* evaluation of cellular uptake and cytotoxicity demonstrated enhanced activity as compared to free paclitaxel and nontargeted micelles.[181] However, the clinical utility of such systems remain to be proven.

A more fundamental limitation of active targeting strategies is the inherent difference in cell surface expression of the target receptor in cancer cells as compared to normal cells. Most often, the criteria for target selection is "overexpression" of the receptor on the surface of cells in cancerous tissues. For example, breast cancer tumors are often diagnosed via immunohistochemistry or fluorescence *in situ* hybridization as either positive or negative for human epidermal growth factor receptor 2 (HER2/neu).[182] If diagnosis is positive, treatment with trastuzumab[183] (trade name Herceptin®), a monoclonal antibody that interferes with the action of HER2/neu is often indicated. If the diagnosis is negative, trastuzumab treatment is not considered. While this approach has proven successful, it does not fully consider the heterogeneous nature of tumors. In reality, tumors are comprised of phenotypically distinct cell types, due to high genetic instability.[184, 185] Treatment, which focuses on a particular cell surface target, will therefore elicit its response to a higher degree in cells expressing this target. This process of selection can result in tumor adaptation. The effectiveness of subsequent treatments can then be diminished, due to lack of expression of the required target, eventually resulting in tumor resistance. Therefore, additional strategies, without such fundamental limitations are required.

This thesis proposes and evaluates an additional targeting strategy that can supplement the aforementioned pharmacological, passive, and active targeting strategies. This is achieved through the use of tumor hyperthermia to first induce the expression of cell surface heat shock proteins, followed by subsequent treatment with heat shock protein targeted polymer-drug conjugates.

2.4 Hyperthermia and the heat shock response

Hyperthermia, defined herein as the elevation of tissue temperature, has been investigated for some time due to its inherent ability to induce cell death.[186] In this Section, the potential role of hyperthermia in anticancer therapy will be reviewed, including a discussion regarding currently utilized methods such as radiofrequency (RF) and microwave (MW) radiation and a relatively new option for inducing hyperthermia, high intensity focused ultrasound (HIFU). An introduction to photothermal therapy, generated via laser radiation of plasmonic gold nanorods, will be presented, as this was the method utilized to induce tumor hyperthermia during the *in vivo* studies of this thesis. The biological response to hyperthermia at both the tissue and cellular level will be reviewed, and the rationale and potential for using these responses as a means to increase the delivery of nanomedicines, and polymer-drug conjugates in particular, will then be explained. Specifically, the biological role of glucose regulated protein 78 kDa (GRP78) and its potential as an anticancer target will be discussed.

2.4.1 Anticancer applications of tumor hyperthermia

Application of hyperthermia to tumor tissue has been investigated in anticancer applications for many decades.[186] The term hyperthermia generally refers to the temperatures between 40°C and 45°C, with those exceeding 45°C referred to a thermoablative.[187, 188] A fundamental difference in the response of tumors to heat as compared to normal tissues provides a basis for achieving an anticancer clinical approach. The vasculature of normal tissues responds to heat by dilation, which aids in heat dissipation.[189] This dilation is made possible via autoregulation of the smooth muscle layer. In contrast, the vasculature of tumor tissue, due to its lack of smooth muscle development and proper innervation as a result of rapid growth, is unable to respond in a similar manner to the same extent.[190] These observations have driven the investigation of thermoablative strategies, where the goal is to deliver a thermal dose that is large enough so that the tumor cannot dissipate the heat, resulting in localized cell death. However, these strategies are subject to the following theoretical limitations. First, this phenomena has been primarily investigated in laboratory animal models of cancer, where tumors are growing at a rapid rate.[191] The resulting vasculature of such tumors is therefore less likely to be as maturely developed as that occurring in humans. The observations made in such models may therefore be overestimating this phenomenon. Also, in human tumors, tumor growth often invades normal tissues, where the vasculature will be more developed and able to respond to external stimuli.[189] Therefore, these differences in the ability to dissipate heat may be minimized in these regions. Despite these limitations, tumor hyperthermia has proven effective and is

currently utilized in anticancer applications in countries such as Germany, Italy, and Japan.[192]

2.4.2 Effects of moderate hyperthermia on the tumor microenvironment

In early clinical studies evaluating the efficacy of hyperthermia against various tumors, difficulty in achieving the temperatures necessary to produce cytotoxic effect (greater than 42-43°C) was encountered.[189] However, such therapies nonetheless affected the response of tumors to chemotherapy and radiotherapy wherein increased sensitization was observed in combination with these hyperthermic treatments.[193-195] Over time, it became clear that this added effect was not primarily due to an increase in cellular death elicited by hyperthermia, but due to changes in tumor blood flow.[189]

During conditions of moderate hyperthermia (less than 43°C), increases in tumor blood flow have been observed in numerous studies.[196] For example, one study[197] reported a 2-fold increase in rat carcinoma tumors when heated to 43°C for 20 min. Interestingly, this increase was then followed by a decrease when the heating was further prolonged. Similar observations have been made by others, suggesting the use of shorter periods of hyperthermic treatment where increased tumor blood flow is desired.[198] As previously described, the developing structure of the tumor vasculature is poorly organized, with small gaps present between endothelial cells. The extravasation of polymer-drug conjugates through these gaps is a major factor in driving increased tumor accumulation. During condition of moderate hyperthermia, these gaps potentially can be further opened, resulting in augmentation of the EPR effect. It has also been suggested that during hyperthermic treatment, as the tumor works to dissipate

heat via increases in blood flow, an increase in the average temperature of circulating blood can occur.[199] This can then result in an elevation of cardiac output during the hyperthermic treatment, thereby further increasing blood flow. The resulting increases in tumor blood flow provide an increased opportunity for circulating polymer-drug conjugates to accumulate in tumor tissue via the EPR effect. These phenomena therefore provide additional rationale for a combination therapy of hyperthermia and polymer-drug conjugates.

2.4.3 Methods for inducing tumor hyperthermia

Initially, primitive methods for inducing tumor hyperthermia were limited in their ability to achieve clinically necessary temperature increases in a specific manner.[189] Often these methods resulted in application of significant heat to surrounding tissues. Some of these early methods include heated needles and water baths coupled with peristaltic pumps. For example, one clinical study[200] evaluated a system wherein a heat exchanger and a peristaltic pump were used to circulate a 42-43°C electrolyte solution containing the anticancer agent cisplatin throughout the peritoneal cavity of cancer patients. This method was reported to be successful, in that patients achieved a median survival time of 20 months as compared to the anticipated period of 6 months (control). Similar techniques have also been utilized by other groups to achieve positive results.

2.4.3.1 Radiofrequency and microwave devices. To date, the most commonly used methods of inducing hyperthermia are via RF and MW radiation. These devices generally consist of an applicator (i.e., catheter) which is directed under imaging into

the region of interest, such as a tumor. Localized generation of an electromagnetic (EM) field induces ionic movement resulting in local heat generation from resistive losses.[201] For both RF and MW radiation, the amount of energy absorbed/transduced into heat decreases exponentially in tissues surrounding the applicator.[201] Selection of the appropriate EM wavelength is based upon considerations of tumor size and depth. Lower frequencies (i.e., RF radiation) provide advantages with respect to tissue penetration, but suffer from low resolution due to the large wavelengths involved.[202] Conversely, higher frequencies (i.e., MW radiation) allow focused heat generation, but suffer from higher attenuation which restricts penetration. While these methods are performed in a minimally invasive manner, they can cause significant heating in surrounding fat tissues, and are generally not capable of delivering hyperthermia selectively without damaging adjacent tissues.[188] In addition, the performance of these devices is marginalized when placed next to large vessels that can carry away generated heat.[202] Although these methods and others previously described have demonstrated the clinical utility of hyperthermia, it is acknowledged that such techniques are crude at best in their ability to treat tumors in a specific manner. Therefore, other methods are being developed that allow hyperthermia to be induced with a greater degree over both temperature and temporal distribution.

2.4.3.2 High intensity focused ultrasound (HIFU). HIFU utilizes ultrasound waves generated using a spherical transducer. As these waves travel through tissue, they deposit some of their energy in a kinetic manner. During imaging applications, this amount of energy is generally insignificant. However, by focusing the waves to coincide with constructive interference at a fixed point, a large amount of energy can be

transduced, resulting in localized hyperthermia.[203] HIFU has generally been investigated in anticancer applications as an ablative therapy, where high temperatures are delivered to elicit cellular and vascular damage. Two primary mechanisms are responsible for such damage.[204] First, the thermal effect, due to absorption of the ultrasound energy and its subsequent conversion into heat, elicits damages as previously described. Second, a process termed cavitation occurs at higher energies as a result of the interaction of ultrasound waves and micro-bubbles of water. These microbubbles can grow and oscillate in the ultrasound field, and ultimately collapse, resulting in mechanical damage to tissue. This damage is marginally visible and can generally by visualized by magnetic resonance imaging (MRI), using gadolinium-enhanced T1 mapping.[205] MRI is also being investigated as a means to monitor temperature changes during HIFU, but this technique is not, as of now, widely used in clinical settings.[206] It is probable that the clinical use of HIFU in anticancer therapies will continue to grow, due to its ability to generate high temperatures in a highly specific and minimally invasive manner.

2.4.3.3 Gold nanoparticle-induced hyperthermia. Gold nanoparticles have been utilized in a number of biomedical applications.[207] Traditionally, colloidal gold and gold salts have been found useful as a pharmacologic agent by the medical and holistic health communities for the treatment of conditions ranging from depression, headache, fever, and most predominantly, rheumatoid arthritis.[208] In addition, over time, its widespread use with little observed adverse effects have minimized safety concerns. In one particular study, treatment with gold nanoparticles at doses less than 2 g/year for 10 years has been well tolerated, without any signs of general toxicity.[209] This can be

attributed to the chemically inert nature of gold itself, showing little physical reactivity with biological chemicals and structures.[210] While there have been some concerns raised regarding biocompatibility due to reported activation of the immune complement system,[211, 212] methods intended to enhance their biocompatibility by surface modifications with PEG or dextrans have imparted advantages by way of reducing bio recognition,[213] similar to that observed for PEG-protein conjugates as previously described. Gold nanoparticles can also be synthesized in a controlled manner with relative ease using inexpensive starting materials. The combination of these characteristics has made gold nanoparticles attractive candidates for biomedical applications.

An important characteristic of gold nanoparticles, which is utilized in this thesis, is their ability to absorb light and convert this energy of absorption into localized heat. This light absorption occurs due to the characteristic surface plasmon resonance (SPR) of these particles when they are in the colloidal form.[214] This resonance often occurs in the near infrared region of the electromagnetic spectrum, which is advantageous because light of these wavelengths can penetrate deep (up to 2-3 cm) into tissues.[215] Gold nanorods, utilized in our studies, are advantageous as their characteristics, including size and aspect ratio, can be synthetically controlled, allowing for fine-tuning of the SPR peak. Utilization of these nanoparticles for induction of local hyperthermia can thus be performed via the following. First, the particles must be delivered to the tumor mass. While this can be performed via interstitial injection directly into tumors, a more universal approach is to deliver them in a systemic manner, and allow them to accumulate in the tumor mass passively (i.e., via EPR) or actively using targeting

strategies as previously described. Previous studies in our lab have demonstrated that gold nanorods, surface modified with PEG, can accumulate via the EPR effect in tumors at concentrations exceeding those required for photothermal therapy following systemic administration.[216] This approach is utilized in this thesis to deliver PEGylated gold nanorods to the tumor mass. Second, the tumor is radiated using a laser with a wavelength that matches the corresponding SPR peak of the nanoparticles, resulting in heat generation. This method allows for hyperthermia to be administered in a highly selective manner, without significant disruption of surrounding tissue.

One of the first reports by West et al. to demonstrate the systemic administration of gold nanoparticles and subsequent hyperthermia for thermal ablation utilized gold nanoshells, wherein a solid, silica core is surrounded by a thin gold shell.[217] Following systemic administration of the nanoparticles in tumor bearing mice, tumor accumulation was observed 6 hrs after injection. Near infrared laser treatment at 4 W/cm^3 for a mere 3 min resulted in 90% survival, as compared to 0% for saline administered and non-radiated controls, clearly demonstrating the potential of this type of therapy.[218] Much effort is currently being directed toward utilization of gold nanoparticles in ablative therapies, particularly in anticancer applications.

In this thesis, PEGylated gold nanorods were utilized to deliver moderate hyperthermia. Temperatures for this application were between 42°C and 43°C. This elevation in temperature was used to trigger the heat shock protein response within the tumor, which will now be introduced.

2.4.4 The heat shock protein response

Organisms have adapted the ability to cope with a variety of stressful conditions in their quest for survival, including exposures to sudden increases in temperature. At the cellular level, response to heat involves the expression of heat shock proteins (HSPs), whose primary roles are protective in nature. As molecular chaperones, they serve to assist in folding of proteins into their native structure and under conditions of stress, they act to prevent protein aggregation.[219] More recently, it has been shown that they play a role in signal transduction at the cell surface. This section will summarize key elements of the heat shock protein response and their significance in anticancer therapy.

Proteins are dynamic and flexible and relatively minor changes in conformation often drive various functions and catalysis. Over time, they have adapted to perform these functions efficiently with minimal energy loss. Therefore, they inherently exist in semi-stable states. Thus, it is not surprising that increases in heat can quickly result in loss of protein function. The adverse effects of heat on proteins include unfolding, misfolding, entanglement, and aggregation, with the latter being the most prominent.[220] Aggregation occurs as a result of increased exposure and intermolecular interactions between hydrophobic residues. Molecular chaperones, including heat shock proteins recognize and interact with these exposed hydrophobic amino acids, thereby inhibiting intermolecular interactions and aggregation.[221] This occurs through controlled binding and release of the substrate by the chaperone, and this difference in affinity is usually controlled via ATP binding and hydrolysis.[222] Heat shock proteins can be generally classified as "holdases," which act primarily under stress conditions to prevent

aggregation, or "foldases," which act to stabilize proteins during folding, and can be either stress-induced or constitutively expressed. Structurally similar HSPs can also coexist. For example, the heat induced heat shock protein 70 kDa (HSP70) protein is highly homologous to constitutive heat shock protein 70kDa (HSC70).[219] The prior is expressed in response to stress, while the latter's primary role is in assisting folding of newly synthesized proteins.

In anticancer applications, the goal is to provide therapy specifically in cancer cells, and so only those heat shock proteins which are stress induced are utilized as molecular or pharmacologic targets. A large amount of this effort has been directed towards inhibition of heat shock protein 90 kDa (HSP90) and HSP70, due to their elevated expression in cancer cells where they play a role in stabilizing a number of cancer related proteins, including mutated p53, Bcr-Abl, Raf-1, Akt, ErbB2, and HIF-1 alpha (Figure 2.7).[223, 224] The ability to affect multiple cancer pathways via inhibition of a single HSP has made these proteins attractive anticancer targets, with a number of inhibitors currently under clinical investigation.

The most widely investigated HSP as an anticancer target is HSP90. HSP90 is an ATP-dependent chaperone protein that is involved in the regulation, activation, and stability of a number of so called "client" proteins. Its anticancer potential lies in the fact that many of these client proteins are involved in signal transduction and other major pathways important for cancer progression.[224] Inhibition of HSP90 for cancer therapy was initially viewed with much skepticism, due to the fact that it is expressed constitutively in normal cells, where it plays a role in maintaining protein homeostasis.[223] Initial work in the 1990s was led by the U.S. National Cancer Institute.

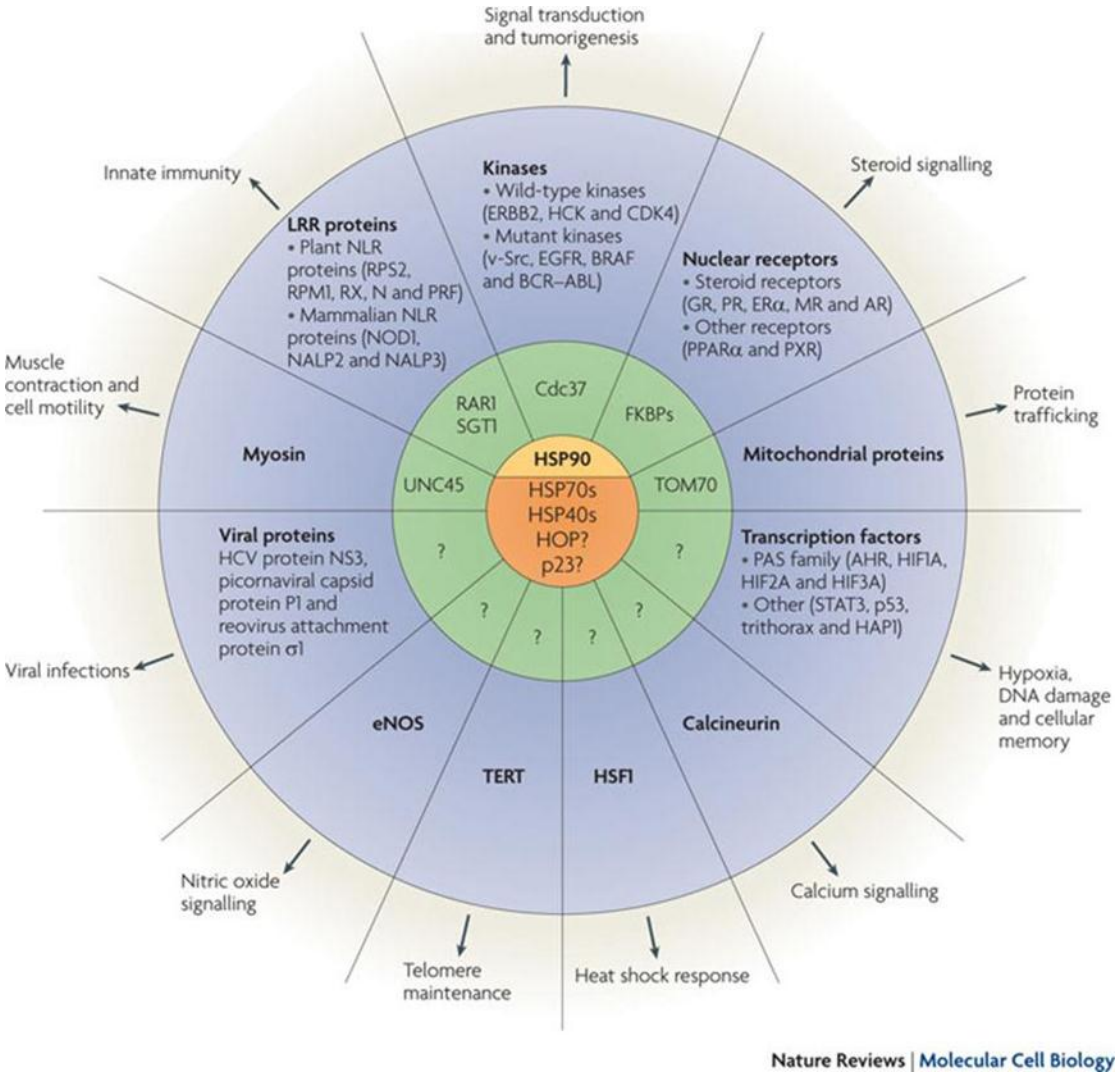

Figure 2.7. Central role of heat shock protein (HSP) chaperones, including HSP90, in the regulation of cancer related proteins. Reprinted with permission.[224]

This work established HSP90 as a viable anticancer target, due to several reasons. First, HSP90 functions by supporting various forms of oncoproteins, including receptor tyrosine kinases and transcription factors that are mutated, incorrectly located, or overexpressed in cancer cells. Second, HSP90 helps to maintain cellular protein function under stress conditions, such as those observed in the tumor microenvironment. Third, HSP90 itself is often overexpressed, and is linked to malignancy and cancer progression. Combined, these results have driven the development of a number of HSP90 inhibitors, with 17 such agents currently under clinical investigation.[225]

The use of HSP90 inhibitors in combination with hyperthermia has also been investigated. As hyperthermia increases protein denaturation and aggregation, it makes logical sense that co-administration of a HSP90 inhibitor would impair the cellular response to this increased stress, resulting in eventual apoptosis. A number of studies have established such synergistic effects using HSP90 inhibitors in combination with hyperthermia.[226-228] For example, one study investigated the use of geldanamycin, a potent inhibitor of HSP90, in combination with hyperthermia in a melanoma model.[226] They demonstrated *in vitro* that treatment with geldanamycin increased susceptibility to hyperthermia and reduced the expression of the HSP90 client protein Akt. They also demonstrated *in vivo* that a combination of geldanamcyin and hyperthermia resulted in a superior anti-tumor effect as compared to either treatment alone, as measured by tumor regression with time. These results led to the decision to utilize geldanamycin as a therapeutic agent in our delivery strategy (see Section 2.6.2).

2.4.5 Glucose regulated protein 78 kDa (GRP78)

In this thesis, the primary goal is to use the cell surface expression of heat shock proteins as a molecular target to increase the delivery of chemotherapeutics. The cell surface expression of heat shock proteins has only been recently established, and the implications and potential applications of such work are currently under investigation. One such protein that is utilized extensively in this thesis is glucose regulated protein 78 kDa (GRP78), which will be reviewed in detail.

Historically, GRP78, also known as BiP or HSPA5, is a chaperone protein of the HSP70 family found in abundance within the endoplasmic reticulum (ER), where it plays a role in protein folding.[229] GRP78 also plays a master regulatory role in initiation of the unfolded protein response (UPR) (Figure 2.8).[230, 231] During normal conditions, GRP78 is primarily bound to the UPR sensor proteins ATF6, PERK, and IRE1. In cancer cells, inherent stress conditions of the tumor microenvironment including glucose deprivation, hypoxia, and acidosis can initiate the UPR. Under these conditions of stress, where aggregated or misfolding proteins accumulate in the ER, GRP78 is released from ATF6, PERK, and IRE1 and binds to exposed hydrophobic residues of malformed proteins, resulting in activation of the UPR sensor proteins. ATF6 is then free to migrate to the nucleus, where is acts eventually as a transcriptional factor for additional ER chaperones. PERK activation results in the eventual attenuation of translational initiation complexes involved in recognition of AUG initiation codons during protein synthesis. This results in reducing the rate of overall protein synthesis, and thereby minimizing the number of potential unfolded proteins within the ER. When IRE1 is activated, it exhibits RNAse activity on mRNA encoding

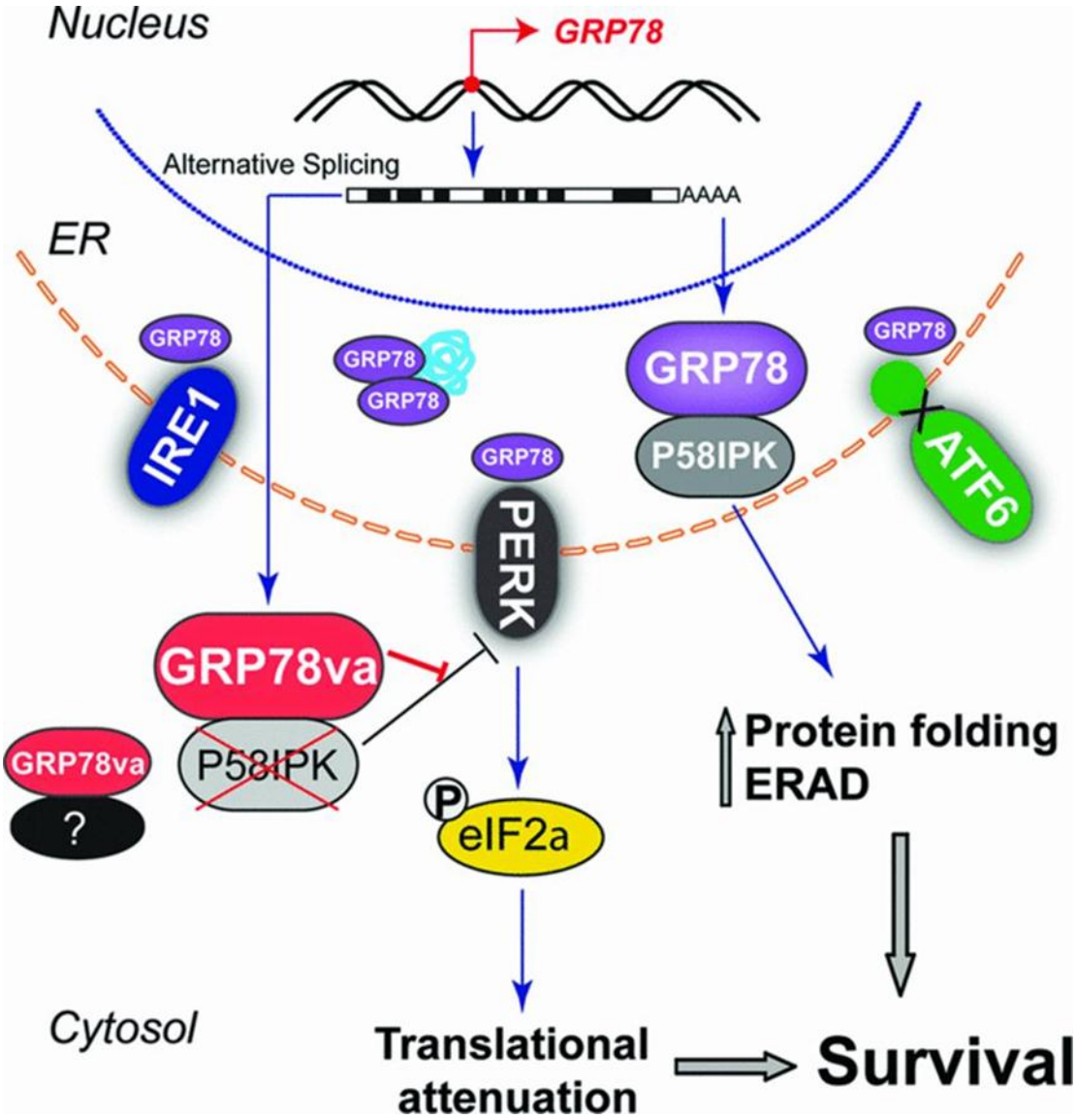

Figure 2.8. Role of GRP78 (and its isoform GRP78va) in regulating the unfolded protein response (UPR) pathway and cell survival via interaction with IRE1, PERK, and ATF6. Reprinted with permission.[231]

for UPR related proteins, eventually leading to increased activation and transcription of UPR target genes. Therefore, by regulating AFT6, PERK, and IRE1, GRP78 acts as a direct mechanism by which the stress conditions of the ER can be sensed and regulated.

In 1997, the cell surface localization of GRP78 was first reported[232], and its existence on the surface of various cancer cell types including melanoma, osteosarcoma, hepatoma, breast, gastric, and pancreatic cancer has since been described.[233-235] Under conditions of elevated stress, localization of GRP78 to the cell surface occurs. Here, it assumes a different function where it acts as a receptor/co-receptor for signal transduction. This occurs through the formation of various complexes with other proteins (Figure 2.9).[231] For example, its interaction with activated α_2-macroglobulin (α_2M*) is probably the best understood.[235-237] In 1-LN metastatic prostate cancer cells, GRP78 on the cell surface acts as a receptor for α_2M*, leading to activation of PAK-2 (p21-activated kinase-2), which works with LIMK1 (LIM domain kinase 1) and cofilin phosphorylation to increase cell motility and facilitate metastasis. In addition, cell surface GRP78 also acts to increase cell proliferation via the activation of ERK1/2 (extracellular-signal-regulated kinase 1/2), p38 MAPK (mitogen-activated protein kinase) and PI3K (phosphoinositide 3-kinase) and acts to increase cell survival via the Akt and NF-κB (nuclear factor κB) signaling cascade.

Recent studies have also described GRP78 expression of the cell surface of proliferating endothelial cells, where it plays a role in the endothelial cell survival and as a signaling receptor.[238] The expression of GRP78 on the cell surface of VEGF (vascular endothelial growth factor)-activated HUVECs (human umbilical vein

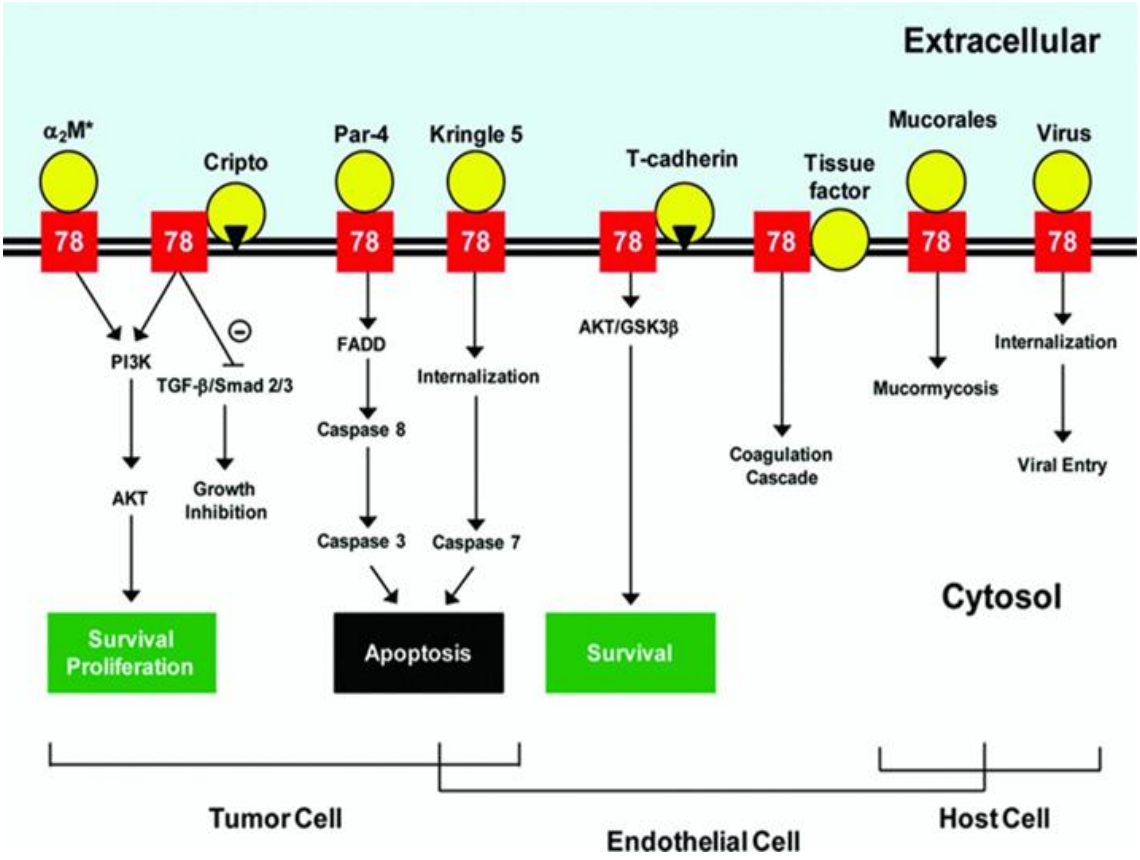

Figure 2.9. Extracellular GRP78. Cell surface expressed glucose regulated protein 78 kDa (GRP78) forms complexes with various extracellular ligands, leading to both pro-survival and pro-apoptotic pathways, thereby serving as a receptor for cell signaling. Reprinted with permission.[231]

endothelial cells) has been studied where it plays a role in cell growth and proliferation.[239]

These combined studies provide the basis for utilizing cell surface expressed GRP78 as a cancer specific target. Beyond its inherent expression in cancer cells, the current study is primarily focused on the induction of cell surface GRP78 following the initiation of cellular stress via hyperthermia. A correlation between cellular stress and GRP78 cell surface expression has been demonstrated via an *in vitro* study wherein thapsigargin, an agent which induces ER stress, was shown to promote cell surface expression.[234] Interestingly, the increase in cell surface expression observed was higher than the intracellular response. The ability of hyperthermia to induce ER stress and the subsequent expression of GRP78 has also been described. In one study,[240] melanoma cells were exposed to hyperthermia (45°C, 60 min) and the expression of GRP78 followed as a function of time. An elevated expression of approximately 7X was observed 3 hrs post hyperthermia, with elevated levels remaining out to 18 hrs. The role of temperature and treatment duration may, however, play a major role in inducing expression. For example, one study[241] clearly demonstrated a decrease in expression of GRP78 following induction of higher temperature, possibly due to a global repression of transcription and translation. However, mild hyperthermia resulted in increased expression of GRP78 along with other HSPs. Therefore, there is most likely a small window of opportunity wherein cell surface expression of GRP78 can be induced, and it was therefore critical in this project that hyperthermia be applied precisely in a controlled manner to avoid such complications.

2.4.5.1 Peptides targeting cell surface expressed GRP78. As previously described, a number of different targeting moieties can be utilized to direct the localization of polymer-drug conjugates. Work by Pasqualini and coworkers[233, 242] has developed a combinatorial strategy to find relevant, specific anticancer targets. In this strategy, they isolated peptides recognized by antibodies from the serum of prostate cancer patients. They were then able to identify a consensus motif that bound to these antibodies preferentially over control antibodies from other blood donors. They then identified the corresponding protein, GRP78, and demonstrated a correlation between GRP78 expression and development of metastatic disease and short overall survival. By such a method of screening libraries of peptides and antibodies using phage display, GRP78 was identified with high specificity for cancerous tissue. This type of approach is advantageous as the selection process occurs *in vivo*, resulting in more relevant targets as compared to traditional *in vitro* assays. Via subsequent phage display, two peptide ligands for GRP78 with amino acid sequences of WIFPWIQL and WDLAWMFRLPVG were identified. It was shown that these sequences were specific for binding to GRP78, and their ability to target prostate cancer tumor cells *in vitro*, *in vivo*, and in human cancer specimens *ex vivo* was verified. Building upon this work, one study[239] demonstrated that liposomes modified with the WIFPWIQL peptide were uptaken to a greater extent by VEGF-activated HUVECs as compared to the non-targeted carriers. The ability of the WIFPWIQL liposomes to accumulate in tumor endothelial cells *in vivo* and suppress tumor growth in a colon carcinoma mouse tumor model was also demonstrated. These results demonstrate that these peptide ligands can

be successfully utilized as targeting moieties in a strategy to target cell surface expressed GRP78.

2.5 Prostate cancer

In the United States, prostate cancer[243] is the second leading cause of cancer death in men, behind only lung cancer. It is estimated that approximately 242,000 new cases will be diagnosed in 2012, and approximately 28,000 men will die of the disease. Approximately 1 out of every 6 men will be diagnosed with prostate cancer at some point during their lifetime. Disease progression generally occurs slowly, resulting in a 5-year survival rate of nearly 100% and even a 15-year survival rate of 91%. There is, however, a clear distinction between localized and metastatic disease. When prostate cancer is no longer localized (Stage IV), the 5-year survival rate drops precipitously to 29%. There is therefore a critical need for treatment while the disease is localized and manageable. In this Section, the current treatment options for prostate cancer will be introduced, including the role of chemotherapy for late stage disease. In addition, the chemotherapeutic agents utilized in this thesis for evaluation against prostate cancer will be briefly discussed.

2.5.1 Current treatment options

In many cases, prostate cancer diagnosis may occur so early in the disease progression process that there is little immediate health threat posed by the cancer. For many of these patients, a strategy of watchful waiting, also known as active surveillance, is used.[244] These patients are monitored routinely for disease progression,

often via PSA tests and digital rectal exams. Treatment may be required at a later stage. However, for some patients, especially those older patients where the risks of treatment outweigh the potential benefits, treatment may not be required.

When prostate cancer is still localized to the prostate gland, other approaches using radiation therapy are widely used. External beam radiation is used to deliver X-rays from outside the body to the diseased area. This can be conducted in a non-invasive manner with very little pain. However, it is often associated with adverse effects which include sexual dysfunction, fatigue, and urinary or rectal bleeding.[245] A somewhat similar strategy delivers radiation via small radioactive metal pellet or seeds. These are implanted in the prostate near the cancerous tissue where they release low doses of radiation over a period of several months. This type of procedure, called brachytherapy[246] is advantageous over external beam radiation in that it can minimize damage to surrounding tissues. However, it has a higher risk of impaired urinary function, and still maintains a risk of sexual dysfunction.

Surgery is also used for the treatment of localized prostate cancer. Prostatectomy,[247] or removal of the prostate gland itself, is the primary goal of a number of surgical procedures. The choice of surgical procedure is generally dependent on the location of the disease, with more invasive procedures required if the cancer has spread to surrounding lymph nodes. As with many surgeries, outlook is dependent on the skill and expertise of the surgeon. While prostatectomy is the most effective way to remove prostate cancer when localized to the prostate gland, a high risk of loss of urinary control and sexual functions remains.

For more advanced disease, hormone therapy is the first line of treatment.[248] The male sex hormones, including testosterone, are required for prostate cancer growth. The goal of hormone therapy is to deprive the cancer of these hormones. Hormone therapy is often used to treat advanced disease, where the cancer has spread from the region surrounding the prostate, but it can also be used as a means to reduce primary tumor size to enhance the effectiveness of other treatments (i.e., after surgery). Hormone therapy is generally effective in reducing tumor burden and slowing tumor growth. However, tumor cells over time often become "androgen independent" and no longer require hormones for survival and proliferation, and hormone therapy becomes ineffective.[249] In addition, hormone therapy is associated with a number of adverse effects due to the loss of androgens which include sexual problems, loss of muscle mass, weight gain, and fatigue.

For patients with advanced or metastatic disease, chemotherapy is indicated. As previously described, the goal of chemotherapy is to kill rapidly dividing cells. However, it often kills other rapidly dividing healthy cells, resulting in adverse effects which include neutropenia, nausea, vomiting, loss of appetite, mouth sores, and hair loss. Because of these side effects, its use in the treatment of advanced, localized disease is generally not warranted. In addition, chemotherapy for those with metastatic disease is primarily beneficial in extending life and decreasing pain. It is not anticipated to provide a cure. However, if chemotherapy could be delivered in a targeted, site-specific manner, the benefit-to-risk ratio could potentially be shifted enough to allow for more aggressive treatment in late-stage disease, and more routine use in localized disease.

Three different chemotherapeutic agents were conjugated to HPMA copolymers in the current thesis. They are aminohexylgeldamycin, docetaxel, and cisplatin, and each will be briefly reviewed hereafter.

2.5.2 Geldanamycin

Geldanamycin (GDM), a benzoquinone ansamycin, is a naturally occurring inhibitor of heat shock protein 90 (Hsp90) and has been widely studied as an anticancer agent.[250] Hsp90 is highly expressed in a variety of cancers including melanoma, leukemia, colon, lung, breast, and prostate cancers,[251] and is thought to play an important role in regulating the folding and activity of its client proteins, which include growth-stimulating proteins involved in malignant transformation.[252] As Hsp90 client proteins have also been implicated in prostate cancer progression,[253] GDM naturally presents itself as an attractive therapeutic agent against this disease. In addition, GDM derivatives have been shown to exert synergistic effects when combined with hyperthermia. For example, one study showed that treatment with GDM resulted in increased susceptibility of melanoma cells to treatment with hyperthermia, which was delivered using thermosensitive ferromagnetic particles.[240] However, the clinical use of GDM has been limited by several factors. It exhibits high hepatotoxicity at therapeutic doses in animal models,[254] is poorly soluble in water, and is metabolically unstable.[251] While GDM derivatives with improved tolerance, metabolic stability, and water solubility are currently under investigation (Table 2.1), clinical response is still limited,[255, 256] and further increases in the therapeutic index for Hsp90 inhibitors is required for full clinical translation.

Table 2.1. Selected clinical trials of geldanamycin analogues as mono- or combination therapy. Data obtained from Hong, D.S., et al.[272]

Drug(s)	Geldanamycin analogue chemical name	Disease type	Clinical development phase	Route	Company / Sponsor
Tanespimycin (17-AAG)	17-allylamino-17-demethoxygeldanamycin	Kidney tumors in Von Hippel-Lindau disease, relapsed or refractory anaplastic large cell lymphoma, mantle cell lymphoma, or Hodgkin's lymphoma	II	i.v.	National Cancer Institute, MD Anderson Cancer Center
IPI-493	17-amino-17-demethoxygeldanamycin	Advanced malignancies (study terminated)	I	oral	Infinity Pharmaceuticals, Inc.
IPI-504	17-allylamino-17-demethoxygeldanamycin hydroquinone hydrochloride	Hormone-resistant prostate cancer	II	i.v.	Infinity Pharmaceuticals, Inc.
IPI-504, docetaxel	17-allylamino-17-demethoxygeldanamycin hydroquinone hydrochloride	Advanced solid tumors	I	i.v.	Infinity Pharmaceuticals, Inc.
IPI-504, everolimus	17-allylamino-17-demethoxygeldanamycin hydroquinone hydrochloride	KRAS mutant NSCLC	I/II	i.v., oral	Infinity Pharmaceuticals, Inc.
IPI-504, trastuzumab	17-allylamino-17-demethoxygeldanamycin hydroquinone hydrochloride	HER2+ breast cancer (study terminated)	II	i.v., i.v.	Infinity Pharmaceuticals, Inc.
Tanespimycin, bortezomib	17-allylamino-17-demethoxygeldanamycin	Advanced solid tumors or lymphoma	I	i.v., i.v.	Mayo Clinic, National Cancer Institute
Tanespimycin, gemcitabine	17-allylamino-17-demethoxygeldanamycin	Recurrent advanced ovarian epithelial or peritoneal cavity cancer	II	i.v., i.v.	Mayo Clinic, National Cancer Institute

2.5.3 Docetaxel

Docetaxel (Taxotere®), is a semi-synthetic anti-mitotic chemotherapeutic of the taxane family that stabilizes microtubules necessary for cell division by binding β-tubulin, resulting in cell-cycle arrest and induction of apoptosis.[257] It is currently approved for marketing in the United States for the treatment of patients with cancers of the breast, lungs, prostate, gastro-intestinal tract, and head and neck. Compared to its taxane predecessor paclitaxel (Taxol®), docetaxel provides superior *in vitro* cytotoxicity[258] and has greater potency with regard to tubulin promotion and inhibition of depolymerization.[259] Docetaxel has proven effective in combination with other traditional chemotherapeutics[260-262] and does not demonstrate complete cross resistance with paclitaxel.[263-265] Docetaxel is also currently under clinical investigation for the treatment of a number of cancers[260, 266-271] and is currently approved as a first line treatment for advanced stage, metastatic prostate cancer. However, the clinically approved formulation for intravenous administration of docetaxel (Taxotere®) contains polysorbate 80 as a solubilizing agent, which has been associated with acute hypersensitivity reactions, and excessive fluid retention resulting in peripheral edema.[273, 274]

2.5.4 Cisplatin

Cisplatin (Platin®) is a platinum containing compound that binds to and crosslinks DNA, eliciting DNA repair mechanisms, followed by eventual apoptosis. Cisplatin, in combination with other chemotherapeutic agents, is a mainstay in the treatment of a variety of cancers, and its use has been approved by the FDA since the

late 1970s. It is currently under clinical investigation as a second-line treatment for prostate cancer in patients whose cancer progressed following docetaxel therapy.[275] In this thesis, cisplatin was chosen for evaluation due to its reported synergism with hyperthermia. For example, in the treatment of ovarian cancer, hyperthermic intraperitoneal chemotherapy (HIPEC) is used to deliver cisplain.[276] While the hyperthermia itself induces some efficacy in this therapy, it has also been shown to increase the sensitivity to chemotherapeutics, including cisplatin, in various *in vitro* and *in vivo* animal models. Although the exact mechanisms are not known, studies have suggested that hyperthermia in combination with cisplatin therapy increases DNA crosslinking and adduct formation.[277] It also can act to deepen penetration into tumor tissues. For the majority of cancer patients, initial response to platinum therapy is high, but a large number eventually relapse with cisplatin resistance. Cisplatin also exhibits marked dose-limiting nephrotoxicity, resulting in a cumulative loss of renal function over time. This is primarily attributed to the accumulation of cisplatin within the proximal tubule as a result of its uptake by basolateral drug transporters.[278] These limitations make cisplatin an excellent candidate for delivery via the proposed targeting system.

2.6 Summary

Drug delivery systems based on polymeric carriers can be utilized in anticancer applications to increase the therapeutic index of chemotherapeutic agents. This can be achieved through either passive or active targeting strategies. However, clinical translation has remained difficult, due to only modest improvements in safety and

efficacy. Therefore, strategies to increase delivery of macromolecular chemotherapeutics are warranted.

Tumor hyperthermia has also been investigated in anticancer applications due to inability of cancerous tissues to effectively dissipate heat, thereby causing significant cellular damage. As a result, most of the work in this area has focused on ablative therapies, where the primary goal of the hyperthermic treatment is direct eradication of the tumor mass. However, moderate hyperthermia has been shown to increase tumor blood flow and vascular permeability, and can therefore be utilized as a tool to increase the passive delivery of macromolecular chemotherapeutics. In addition, part of the cellular response to hyperthermia includes the expression of heat shock proteins, including the expression of particular heat shock proteins (i.e., GRP78) on the cell surface. This induced expression can therefore be utilized to improve the active delivery of targeted drug carriers by enhancing binding and internalization into cancer cells.

It is therefore proposed that a combination of tumor hyperthermia and administration of heat shock targeted polymer-drug conjugates can effectively enhance both passive and active delivery mechanisms. Increases in overall tumor delivery can therefore widen the therapeutic index for chemotherapeutics, resulting in more safe and efficacious therapy.

2.7 References

1. P.A. Mackowiak. Brief history of antipyretic therapy. Clin Infect Dis. 31 Suppl 5:S154-156 (2000).

2. D.J. Newman and G.M. Cragg. Natural products as sources of new drugs over the last 25 years. J Nat Prod. 70:461-477 (2007).

3. J.Y. Ortholand and A. Ganesan. Natural products and combinatorial chemistry: back to the future. Curr Opin Chem Biol. 8:271-280 (2004).

4. M. Berger, V. Shankar, and A. Vafai. Therapeutic applications of monoclonal antibodies. Am J Med Sci. 324:14-30 (2002).

5. M. Ferrari. Cancer nanotechnology: opportunities and challenges. Nat Rev Cancer. 5:161-171 (2005).

6. Mountaintop Medical, LLC. The market for advanced drug delivery systems, *Kalorama Information*, 2010, p. 5.

7. G. von Maltzahn, J.H. Park, A. Agrawal, N.K. Bandaru, S.K. Das, M.J. Sailor, and S.N. Bhatia. Computationally guided photothermal tumor therapy using long-circulating gold nanorod antennas. Cancer Res. 69:3892-3900 (2009).

8. H.A. Shelanski and M.V. Shelanski. PVP-iodine: history, toxicity and therapeutic uses. J Int Coll Surg. 25:727-734 (1956).

9. H.A. Ravin, A.M. Seligman, and J. Fine. Polyvinyl pyrrolidone as a plasma expander. New Eng J Med. 247:921-929 (1952).

10. H. Ringsdorf. Structure and properties of pharmacologically active polymers. Journal of Polymer Science: Polymer Symposia. 51:135-153 (1975).

11. N. Larson and H. Ghandehari. Polymeric conjugates for drug delivery. Chem Mater. 24:840-853 (2012).

12. S. Van, S.K. Das, X. Wang, Z. Feng, Y. Jin, Z. Hou, F. Chen, A. Pham, N. Jiang, S.B. Howell, and L. Yu. Synthesis, characterization, and biological evaluation of poly(L-gamma-glutamyl-glutamine)- paclitaxel nanoconjugate. Int J Nanomedicine. 5:825-837 (2010).

13. P. Zhou, Z. Li, and Y. Chau. Synthesis, characterization, and in vivo evaluation of poly(ethylene oxide-co-glycidol)-platinate conjugate. Eur J Pharm Sci. 41:464-472 (2010).

14. C. Lipinski. Poor aqueous solubility - An industry wide problem in drug discovery. Am Pharm Rev. 5:82-85 (2002).

15. Y. Matsumura and H. Maeda. A new concept for macromolecular therapeutics in cancer chemotherapy: mechanism of tumoritropic accumulation of proteins and the antitumor agent smancs. Cancer Res. 46:6387-6392 (1986).

16. H. Maeda. Tumor-selective delivery of macromolecular drugs via the EPR effect: background and future prospects. Bioconjug Chem. 21:797-802 (2010).

17. H. Maeda, G.Y. Bharate, and J. Daruwalla. Polymeric drugs for efficient tumor-targeted drug delivery based on EPR-effect. Eur J Pharm Biopharm. 71:409-419 (2009).

18. K. Greish. Enhanced permeability and retention of macromolecular drugs in solid tumors: a royal gate for targeted anticancer nanomedicines. J Drug Target. 15:457-464 (2007).

19. A.K. Iyer, G. Khaled, J. Fang, and H. Maeda. Exploiting the enhanced permeability and retention effect for tumor targeting. Drug Discov Today. 11:812-818 (2006).

20. A. Gregory and M.H. Stenzel. The use of reversible addition fragmentation chain transfer polymerization for drug delivery systems. Expert Opin Drug Deliv. 8:237-269 (2011).

21. C. Boyer, V. Bulmus, T.P. Davis, V. Ladmiral, J. Liu, and S. Perrier. Bioapplications of RAFT polymerization. Chem Rev. 109:5402-5436 (2009).

22. A.W. York, S.E. Kirkland, and C.L. McCormick. Advances in the synthesis of amphiphilic block copolymers via RAFT polymerization: stimuli-responsive drug and gene delivery. Adv Drug Deliv Rev. 60:1018-1036 (2008).

23. K. Matyjaszewski and N.V. Tsarevsky. Nanostructured functional materials prepared by atom transfer radical polymerization. Nat Chem. 1:276-288 (2009).

24. V.L. Galic, T.J. Herzog, J.D. Wright, and S.N. Lewin. Paclitaxel poliglumex for ovarian cancer. Expert Opin Investig Drugs. 20:813-821 (2011).

25. L.W. Seymour, D.R. Ferry, D.J. Kerr, D. Rea, M. Whitlock, R. Poyner, C. Boivin, S. Hesslewood, C. Twelves, R. Blackie, A. Schatzlein, D. Jodrell, D. Bissett, H. Calvert, M. Lind, A. Robbins, S. Burtles, R. Duncan, and J. Cassidy. Phase II studies of polymer-doxorubicin (PK1, FCE28068) in the treatment of breast, lung and colorectal cancer. Int J Oncol. 34:1629-1636 (2009).

26. J.M. Meerum Terwogt, W.W. ten Bokkel Huinink, J.H. Schellens, M. Schot, I.A. Mandjes, M.G. Zurlo, M. Rocchetti, H. Rosing, F.J. Koopman, and J.H. Beijnen. Phase I clinical and pharmacokinetic study of PNU166945, a novel water-soluble polymer-conjugated prodrug of paclitaxel. Anticancer Drugs. 12:315-323 (2001).

27. J.M. Rademaker-Lakhai, C. Terret, S.B. Howell, C.M. Baud, R.F. De Boer, D. Pluim, J.H. Beijnen, J.H. Schellens, and J.P. Droz. A Phase I and pharmacological study of the platinum polymer AP5280 given as an intravenous infusion once every 3 weeks in patients with solid tumors. Clin Cancer Res. 10:3386-3395 (2004).

28. M. Campone, J.M. Rademaker-Lakhai, J. Bennouna, S.B. Howell, D.P. Nowotnik, J.H. Beijnen, and J.H. Schellens. Phase I and pharmacokinetic trial of AP5346, a DACH-platinum-polymer conjugate, administered weekly for three out of every 4 weeks to advanced solid tumor patients. Cancer Chemother Pharmacol. 60:523-533 (2007).

29. G. Pasut and F.M. Veronese. PEG conjugates in clinical development or use as anticancer agents: an overview. Adv Drug Deliv Rev. 61:1177-1188 (2009).

30. A.V. Yurkovetskiy and R.J. Fram. XMT-1001, a novel polymeric camptothecin pro-drug in clinical development for patients with advanced cancer. Adv Drug Deliv Rev. 61:1193-1202 (2009).

31. R. Duncan and M.J. Vicent. Do HPMA copolymer conjugates have a future as clinically useful nanomedicines? A critical overview of current status and future opportunities. Adv Drug Deliv Rev. 62:272-282 (2010).

32. A. Malugin, P. Kopeckova, and J. Kopecek. Liberation of doxorubicin from HPMA copolymer conjugate is essential for the induction of cell cycle arrest and nuclear fragmentation in ovarian carcinoma cells. J Control Release. 124:6-10 (2007).

33. N. Larson, A. Ray, A. Malugin, D.B. Pike, and H. Ghandehari. HPMA copolymer-aminohexylgeldanamycin conjugates targeting cell surface expressed GRP78 in prostate cancer. Pharm Res. 27:2683-2693 (2010).

34. F.M. Wachters, H.J. Groen, J.G. Maring, J.A. Gietema, M. Porro, H. Dumez, E.G. de Vries, and A.T. van Oosterom. A phase I study with MAG-camptothecin intravenously administered weekly for 3 weeks in a 4-week cycle in adult patients with solid tumours. Br J Cancer. 90:2261-2267 (2004).

35. Y. Kaneda, Y. Tsutsumi, Y. Yoshioka, H. Kamada, Y. Yamamoto, H. Kodaira, S. Tsunoda, T. Okamoto, Y. Mukai, H. Shibata, S. Nakagawa, and T. Mayumi. The use of PVP as a polymeric carrier to improve the plasma half-life of drugs. Biomaterials. 25:3259-3266 (2004).

36. H. Kamada, Y. Tsutsumi, Y. Yamamoto, T. Kihira, Y. Kaneda, Y. Mu, H. Kodaira, S.I. Tsunoda, S. Nakagawa, and T. Mayumi. Antitumor activity of tumor necrosis factor-alpha conjugated with polyvinylpyrrolidone on solid tumors in mice. Cancer Res. 60:6416-6420 (2000).

37. T. Yasukawa, H. Kimura, Y. Tabata, H. Miyamoto, Y. Honda, Y. Ikada, and Y. Ogura. Targeted delivery of anti-angiogenic agent TNP-470 using water-soluble polymer in the treatment of choroidal neovascularization. Invest Ophthalmol Vis Sci. 40:2690-2696 (1999).

38. S.D. Chipman, F.B. Oldham, G. Pezzoni, and J.W. Singer. Biological and clinical characterization of paclitaxel poliglumex (PPX, CT-2103), a macromolecular polymer-drug conjugate. Int J Nanomedicine. 1:375-383 (2006).

39. J.Y. Ljubimova, M. Fujita, A.V. Ljubimov, V.P. Torchilin, K.L. Black, and E. Holler. Poly(malic acid) nanoconjugates containing various antibodies and oligonucleotides for multitargeting drug delivery. Nanomedicine (Lond). 3:247-265 (2008).

40. J. Kopecek and P. Kopeckova. HPMA copolymers: origins, early developments, present, and future. Adv Drug Deliv Rev. 62:122-149 (2010).

41. G. Pasut, M. Sergi, and F.M. Veronese. Anti-cancer PEG-enzymes: 30 years old, but still a current approach. Adv Drug Deliv Rev. 60:69-78 (2008).

42. F.M. Veronese and J.M. Harris. Theme issue on "Peptide and Protein Pegylation". Adv Drug Deliv Rev. 54:453-606 (2002).

43. M.L. Graham. Pegaspargase: a review of clinical studies. Adv Drug Deliv Rev. 55:1293-1302 (2003).

44. Y. Levy, M.S. Hershfield, C. Fernandez-Mejia, S.H. Polmar, D. Scudiery, M. Berger, and R.U. Sorensen. Adenosine deaminase deficiency with late onset of recurrent infections: response to treatment with polyethylene glycol-modified adenosine deaminase. J Pediatr. 113:312-317 (1988).

45. P. Bailon, A. Palleroni, C.A. Schaffer, C.L. Spence, W.J. Fung, J.E. Porter, G.K. Ehrlich, W. Pan, Z.X. Xu, M.W. Modi, A. Farid, W. Berthold, and M. Graves. Rational design of a potent, long-lasting form of interferon: a 40 kDa branched polyethylene glycol-conjugated interferon alpha-2a for the treatment of hepatitis C. Bioconjug Chem. 12:195-202 (2001).

46. Y.S. Wang, S. Youngster, M. Grace, J. Bausch, R. Bordens, and D.F. Wyss. Structural and biological characterization of pegylated recombinant interferon alpha-2b and its therapeutic implications. Adv Drug Deliv Rev. 54:547-570 (2002).

47. F. Roelfsema, N.R. Biermasz, A.M. Pereira, and J. Romijn. Nanomedicines in the treatment of acromegaly: focus on pegvisomant. Int J Nanomedicine. 1:385-398 (2006).

48. P.J. Trainer, W.M. Drake, L. Katznelson, P.U. Freda, V. Herman-Bonert, A.J. van der Lely, E.V. Dimaraki, P.M. Stewart, K.E. Friend, M.L. Vance, G.M. Besser, J.A. Scarlett, M.O. Thorner, C. Parkinson, A. Klibanski, J.S. Powell, A.L. Barkan, M.C. Sheppard, M. Malsonado, D.R. Rose, D.R. Clemmons, G. Johannsson, B.A. Bengtsson, S. Stavrou, D.L. Kleinberg, D.M. Cook, L.S. Phillips, M. Bidlingmaier, C.J. Strasburger, S. Hackett, K. Zib, W.F. Bennett, and R.J. Davis. Treatment of acromegaly with the growth hormone-receptor antagonist pegvisomant. N Engl J Med. 342:1171-1177 (2000).

49. H. Zhao, C. Lee, P. Sai, Y.H. Choe, M. Boro, A. Pendri, S. Guan, and R.B. Greenwald. 20-O-acylcamptothecin derivatives: evidence for lactone stabilization. J Org Chem. 65:4601-4606 (2000).

50. S. Jevsevar, M. Kunstelj, and V.G. Porekar. PEGylation of therapeutic proteins. Biotechnol J. 5:113-128 (2010).

51. M.J. Joralemon, S. McRae, and T. Emrick. PEGylated polymers for medicine: from conjugation to self-assembled systems. Chem Commun (Camb). 46:1377-1393 (2010).

52. K. Knop, R. Hoogenboom, D. Fischer, and U.S. Schubert. Poly(ethylene glycol) in drug delivery: pros and cons as well as potential alternatives. Angew Chem Int Ed Engl. 49:6288-6308 (2010).

53. J. Fang, H. Nakamura, and H. Maeda. The EPR effect: Unique features of tumor blood vessels for drug delivery, factors involved, and limitations and augmentation of the effect. Adv Drug Deliv Rev. 63:136-151 (2011).

54. E.K. Rowinsky, J. Rizzo, L. Ochoa, C.H. Takimoto, B. Forouzesh, G. Schwartz, L.A. Hammond, A. Patnaik, J. Kwiatek, A. Goetz, L. Denis, J. McGuire, and A.W. Tolcher. A phase I and pharmacokinetic study of pegylated camptothecin as a 1-hour infusion every 3 weeks in patients with advanced solid malignancies. J Clin Oncol. 21:148-157 (2003).

55. Y. Nojima, Y. Suzuki, K. Yoshida, F. Abe, T. Shiga, T. Takeuchi, A. Sugiyama, H. Shimizu, and A. Sato. Lactoferrin conjugated with 40-kDa branched poly(ethylene glycol) has an improved circulating half-life. Pharm Res. 26:2125-2132 (2009).

56. G. Prencipe, S.M. Tabakman, K. Welsher, Z. Liu, A.P. Goodwin, L. Zhang, J. Henry, and H. Dai. PEG branched polymer for functionalization of

nanomaterials with ultralong blood circulation. J Am Chem Soc. 131:4783-4787 (2009).

57. J. Ramon, V. Saez, R. Baez, R. Aldana, and E. Hardy. PEGylated interferon-alpha2b: a branched 40K polyethylene glycol derivative. Pharm Res. 22:1374-1386 (2005).

58. H. Zhao, B. Rubio, P. Sapra, D. Wu, P. Reddy, P. Sai, A. Martinez, Y. Gao, Y. Lozanguiez, C. Longley, L.M. Greenberger, and I.D. Horak. Novel prodrugs of SN38 using multiarm poly(ethylene glycol) linkers. Bioconjug Chem. 19:849-859 (2008).

59. J.Y. Lee, K.H. Bae, J.S. Kim, Y.S. Nam, and T.G. Park. Intracellular delivery of paclitaxel using oil-free, shell cross-linked HSA - Multi-armed PEG nanocapsules. Biomaterials. 32:8635-8644 (2011).

60. T. Lammers. Improving the efficacy of combined modality anticancer therapy using HPMA copolymer-based nanomedicine formulations. Adv Drug Deliv Rev. 62:203-230 (2010).

61. R. Duncan. Development of HPMA copolymer-anticancer conjugates: clinical experience and lessons learnt. Adv Drug Deliv Rev. 61:1131-1148 (2009).

62. V. Subr, J. Kopecek, J. Pohl, M. Baudys, and V. Kostka. Cleavage of oligopeptide side-chains in N-2(hydroxpropyl)meth-acrylamide copolymers by mixtures of lysosomal enzymes. J Control Release. 8:133-140 (1988).

63. D. Putnam and J. Kopeček. Polymer conjugates with anticancer activity. Biopolymers II, Vol. 122, Springer Berlin, 1995, pp. 55-123.

64. P. Rejmanova, J. Kopecek, R. Duncan, and J.B. Lloyd. Stability in rat plasma and serum of lysosomally degradable oligopeptide sequences in N-(2-hydroxypropyl) methacrylamide copolymers. Biomaterials. 6:45-48 (1985).

65. D. Putnam and J. Kopecek. Enantioselective release of 5-fluorouracil from N-(2-hydroxypropyl)methacrylamide-based copolymers via lysosomal enzymes. Bioconjug Chem. 6:483-492 (1995).

66. J. Kopecek. Controlled biodegradability of polymers--a key to drug delivery systems. Biomaterials. 5:19-25 (1984).

67. M.J. Vicent, S. Manzanaro, J.A. de la Fuente, and R. Duncan. HPMA copolymer-1,5-diazaanthraquinone conjugates as novel anticancer therapeutics. J Drug Target. 12:503-515 (2004).

68. Y. Kasuya, Z.R. Lu, P. Kopeckova, T. Minko, S.E. Tabibi, and J. Kopecek. Synthesis and characterization of HPMA copolymer-aminopropylgeldanamycin conjugates. J Control Release. 74:203-211 (2001).

69. J. Hongrapipat, P. Kopeckova, S. Prakongpan, and J. Kopecek. Enhanced antitumor activity of combinations of free and HPMA copolymer-bound drugs. Int J Pharm. 351:259-270 (2008).

70. A. Ray, N. Larson, D.B. Pike, M. Gruner, S. Naik, H. Bauer, A. Malugin, K. Greish, and H. Ghandehari. Comparison of active and passive targeting of docetaxel for prostate cancer therapy by HPMA copolymer-RGDfK conjugates. Mol Pharm. 8:1090-1099 (2011).

71. P.J. Julyan, L.W. Seymour, D.R. Ferry, S. Daryani, C.M. Boivin, J. Doran, M. David, D. Anderson, C. Christodoulou, A.M. Young, S. Hesslewood, and D.J. Kerr. Preliminary clinical study of the distribution of HPMA copolymers bearing doxorubicin and galactosamine. J Control Release. 57:281-290 (1999).

72. P.A. Vasey, S.B. Kaye, R. Morrison, C. Twelves, P. Wilson, R. Duncan, A.H. Thomson, L.S. Murray, T.E. Hilditch, T. Murray, S. Burtles, D. Fraier, E. Frigerio, and J. Cassidy. Phase I clinical and pharmacokinetic study of PK1 [N-(2-hydroxypropyl)methacrylamide copolymer doxorubicin]: first member of a new class of chemotherapeutic agents-drug-polymer conjugates. Cancer Research Campaign Phase I/II Committee. Clin Cancer Res. 5:83-94 (1999).

73. R. Duncan, L.W. Seymour, K.B. O'Hare, P.A. Flanagan, S. Wedge, I.C. Hume, K. Ulbrich, J. Strohalm, V. Subr, F. Spreafico, M. Grandi, M. Ripamonti, M. Farao, and A. Suarato. Preclinical evaluation of polymer-bound doxorubicin. J Control Release. 19:331-346 (1992).

74. L.W. Seymour, K. Ulbrich, P.S. Steyger, M. Brereton, V. Subr, J. Strohalm, and R. Duncan. Tumour tropism and anti-cancer efficacy of polymer-based doxorubicin prodrugs in the treatment of subcutaneous murine B16F10 melanoma. Br J Cancer. 70:636-641 (1994).

75. A.H. Thomson, P.A. Vasey, L.S. Murray, J. Cassidy, D. Fraier, E. Frigerio, and C. Twelves. Population pharmacokinetics in phase I drug development: a phase I study of PK1 in patients with solid tumours. Br J Cancer. 81:99-107 (1999).

76. T. Etrych, M. Sirova, L. Starovoytova, B. Rihova, and K. Ulbrich. HPMA copolymer conjugates of paclitaxel and docetaxel with pH-controlled drug release. Mol Pharm. 7:1015-1026 (2010).

77. V.R. Caiolfa, M. Zamai, A. Fiorino, E. Frigerio, C. Pellizzoni, R. d'Argy, A. Ghiglieri, M.G. Castelli, M. Farao, E. Pesenti, M. Gigli, F. Angelucci, and A.

Suarato. Polymer-bound camptothecin: initial biodistribution and antitumour activity studies. J Control Release. 65:105-119 (2000).

78. S.Q. Gao, Y. Sun, P. Kopeckova, C.M. Peterson, and J. Kopecek. Antitumor efficacy of colon-specific HPMA copolymer/9-aminocamptothecin conjugates in mice bearing human-colon carcinoma xenografts. Macromol Biosci. 9:1135-1142 (2009).

79. L.D. Quan, F. Yuan, X.M. Liu, J.G. Huang, Y. Alnouti, and D. Wang. Pharmacokinetic and biodistribution studies of N-(2-hydroxypropyl)-methacrylamide copolymer-dexamethasone conjugates in adjuvant-induced arthritis rat model. Mol Pharm. 7:1041-1049 (2010).

80. X.M. Liu, L.D. Quan, J. Tian, Y. Alnouti, K. Fu, G.M. Thiele, and D. Wang. Synthesis and evaluation of a well-defined HPMA copolymer-dexamethasone conjugate for effective treatment of rheumatoid arthritis. Pharm Res. 25:2910-2919 (2008).

81. D. Wang, S.C. Miller, X.M. Liu, B. Anderson, X.S. Wang, and S.R. Goldring. Novel dexamethasone-HPMA copolymer conjugate and its potential application in treatment of rheumatoid arthritis. Arthritis Res Ther. 9:R2 (2007).

82. T. Lammers, V. Subr, K. Ulbrich, P. Peschke, P.E. Huber, W.E. Hennink, and G. Storm. Simultaneous delivery of doxorubicin and gemcitabine to tumors in vivo using prototypic polymeric drug carriers. Biomaterials. 30:3466-3475 (2009).

83. J. Yang, K. Luo, H. Pan, P. Kopeckova, and J. Kopecek. Synthesis of biodegradable multiblock copolymers by click coupling of RAFT-generated heterotelechelic polyHPMA conjugates. React Funct Polym. 71:294-302 (2011).

84. K. Greish, A. Ray, H. Bauer, N. Larson, A. Malugin, D. Pike, M. Haider, and H. Ghandehari. Anticancer and antiangiogenic activity of HPMA copolymer-aminohexylgeldanamycin-RGDfK conjugates for prostate cancer therapy. J Control Release. 151:263-270 (2011).

85. M.P. Borgman, A. Ray, R.B. Kolhatkar, E.A. Sausville, A.M. Burger, and H. Ghandehari. Targetable HPMA copolymer-aminohexylgeldanamycin conjugates for prostate cancer therapy. Pharm Res. 26:1407-1418 (2009).

86. K. Miller, A. Eldar-Boock, D. Polyak, E. Segal, L. Benayoun, Y. Shaked, and R. Satchi-Fainaro. Antiangiogenic antitumor activity of HPMA copolymer-paclitaxel-alendronate conjugate on breast cancer bone metastasis mouse model. Mol Pharm. 8:1052-1062 (2011).

87. H. Krakovicova, T. Etrych, and K. Ulbrich. HPMA-based polymer conjugates with drug combination. Eur J Pharm Sci. 37:405-412 (2009).

88. K. Wu, J. Yang, J. Liu, and J. Kopecek. Coiled-coil based drug-free macromolecular therapeutics: In vivo efficacy. J Control Release (2011).

89. H. Pan, J. Yang, P. Kopeckova, and J. Kopecek. Backbone degradable multiblock N-(2-hydroxypropyl)methacrylamide copolymer conjugates via reversible addition-fragmentation chain transfer polymerization and thiol-ene coupling reaction. Biomacromolecules. 12:247-252 (2011).

90. D.A. Tomalia, H. Baker, J. Dewald, M. Hall, G. Kallos, S. Martin, J. Roeck, J. Ryder, and P. Smith. A new class of polymers: starburst-dendritic macromolecules. Polym J. 17:117-132 (1985).

91. D.A. Tomalia, H. Baker, J. Dewald, M. Hall, G. Kallos, S. Martin, J. Roeck, J. Ryder, and P. Smith. Dendritic macromolecules: Synthesis of starburst dendrimers. Macromolecules. 19:2466-2468 (1986).

92. R. Esfand and D.A. Tomalia. Poly(amidoamine) (PAMAM) dendrimers: from biomimicry to drug delivery and biomedical applications. Drug Discov Today. 6:427-436 (2001).

93. S. Svenson and D.A. Tomalia. Dendrimers in biomedical applications--reflections on the field. Adv Drug Deliv Rev. 57:2106-2129 (2005).

94. G. Thiagarajan, A. Ray, A. Malugin, and H. Ghandehari. PAMAM-camptothecin conjugate inhibits proliferation and induces nuclear fragmentation in colorectal carcinoma cells. Pharm Res. 27:2307-2316 (2010).

95. N. Vijayalakshmi, A. Ray, A. Malugin, and H. Ghandehari. Carboxyl-terminated PAMAM-SN38 conjugates: synthesis, characterization, and in vitro evaluation. Bioconjug Chem. 21:1804-1810 (2010).

96. I.J. Majoros, C.R. Williams, A. Becker, and J.R. Baker, Jr. Methotrexate delivery via folate targeted dendrimer-based nanotherapeutic platform. Wiley Interdiscip Rev Nanomed Nanobiotechnol. 1:502-510 (2009).

97. A.R. Menjoge, R.M. Kannan, and D.A. Tomalia. Dendrimer-based drug and imaging conjugates: design considerations for nanomedical applications. Drug Discov Today. 15:171-185 (2010).

98. V. Gajbhiye, V.K. Palanirajan, R.K. Tekade, and N.K. Jain. Dendrimers as therapeutic agents: a systematic review. J Pharm Pharmacol. 61:989-1003 (2009).

99. D. Bhadra, S. Bhadra, S. Jain, and N.K. Jain. A PEGylated dendritic nanoparticulate carrier of fluorouracil. Int J Pharm. 257:111-124 (2003).

100. Y. Cheng, Z. Xu, M. Ma, and T. Xu. Dendrimers as drug carriers: applications in different routes of drug administration. J Pharm Sci. 97:123-143 (2008).

101. D.S. Goldberg, H. Ghandehari, and P.W. Swaan. Cellular entry of G3.5 poly (amido amine) dendrimers by clathrin- and dynamin-dependent endocytosis promotes tight junctional opening in intestinal epithelia. Pharm Res. 27:1547-1557 (2010).

102. Q. Xu, C.H. Wang, and D.W. Pack. Polymeric carriers for gene delivery: chitosan and poly(amidoamine) dendrimers. Curr Pharm Des. 16:2350-2368 (2010).

103. Y. Cheng, L. Zhao, Y. Li, and T. Xu. Design of biocompatible dendrimers for cancer diagnosis and therapy: current status and future perspectives. Chem Soc Rev. 40:2673-2703 (2011).

104. D.S. Goldberg, N. Vijayalakshmi, P.W. Swaan, and H. Ghandehari. G3.5 PAMAM dendrimers enhance transepithelial transport of SN38 while minimizing gastrointestinal toxicity. J Control Release. 150:318-325 (2011).

105. S.P. Mukherjee, F.M. Lyng, A. Garcia, M. Davoren, and H.J. Byrne. Mechanistic studies of in vitro cytotoxicity of poly(amidoamine) dendrimers in mammalian cells. Toxicol Appl Pharmacol. 248:259-268 (2010).

106. K. Greish, G. Thiagarajan, H. Herd, R. Price, H. Bauer, D. Hubbard, A. Burckle, S. Sadekar, T. Yu, A. Anwar, A. Ray, and H. Ghandehari. Size and surface charge significantly influence the toxicity of silica and dendritic nanoparticles. Nanotoxicology (2011).

107. B. Ziemba, A. Janaszewska, K. Ciepluch, M. Krotewicz, W.A. Fogel, D. Appelhans, B. Voit, M. Bryszewska, and B. Klajnert. In vivo toxicity of poly(propyleneimine) dendrimers. J Biomed Mater Res A. 99:261-268 (2011).

108. R.G. Strickley. Solubilizing excipients in oral and injectable formulations. Pharm Res. 21:201-230 (2004).

109. M. Yokoyama, G.S. Kwon, T. Okano, Y. Sakurai, T. Seto, and K. Kataoka. Preparation of micelle-forming polymer-drug conjugates. Bioconjug Chem. 3:295-301 (1992).

110. A.V. Kabanov, S.V. Vinogradov, Y.G. Suzdaltseva, and V. Alakhov. Water-soluble block polycations as carriers for oligonucleotide delivery. Bioconjug Chem. 6:639-643 (1995).

111. V.P. Torchilin. Micellar nanocarriers: pharmaceutical perspectives. Pharm Res. 24:1-16 (2007).

112. Y. Hu, Z. Jiang, R. Chen, W. Wu, and X. Jiang. Degradation and degradation-induced re-assembly of PVP-PCL micelles. Biomacromolecules. 11:481-488 (2010).

113. I. Orienti, G. Zuccari, A. Fini, A.M. Rabasco, R. Carosio, L. Raffaghello, and P.G. Montaldo. Modified doxorubicin for improved encapsulation in PVA polymeric micelles. Drug Deliv. 12:15-20 (2005).

114. D. Mishra, H.C. Kang, and Y.H. Bae. Reconstitutable charged polymeric (PLGA)(2)-b-PEI micelles for gene therapeutics delivery. Biomaterials. 32:3845-3854 (2011).

115. E. Blanco, C.W. Kessinger, B.D. Sumer, and J. Gao. Multifunctional micellar nanomedicine for cancer therapy. Exp Biol Med (Maywood). 234:123-131 (2009).

116. T. Chandran, U. Katragadda, Q. Teng, and C. Tan. Design and evaluation of micellar nanocarriers for 17-allyamino-17-demethoxygeldanamycin (17-AAG). Int J Pharm. 392:170-177 (2010).

117. V.P. Torchilin. Structure and design of polymeric surfactant-based drug delivery systems. J Control Release. 73:137-172 (2001).

118. A.V. Kabanov, E.V. Batrakova, and V.Y. Alakhov. Pluronic block copolymers as novel polymer therapeutics for drug and gene delivery. J Control Release. 82:189-212 (2002).

119. Y. Kakizawa and K. Kataoka. Block copolymer micelles for delivery of gene and related compounds. Adv Drug Deliv Rev. 54:203-222 (2002).

120. A. Lavasanifar, J. Samuel, and G.S. Kwon. Poly(ethylene oxide)-block-poly(L-amino acid) micelles for drug delivery. Adv Drug Deliv Rev. 54:169-190 (2002).

121. M. Talelli, C.J. Rijcken, C.F. van Nostrum, G. Storm, and W.E. Hennink. Micelles based on HPMA copolymers. Adv Drug Deliv Rev. 62:231-239 (2010).

122. P. Chytil, T. Etrych, C. Konak, M. Sirova, T. Mrkvan, J. Boucek, B. Rihova, and K. Ulbrich. New HPMA copolymer-based drug carriers with covalently bound hydrophobic substituents for solid tumour targeting. J Control Release. 127:121-130 (2008).

123. Z. Jia, L. Wong, T.P. Davis, and V. Bulmus. One-pot conversion of RAFT-generated multifunctional block copolymers of HPMA to doxorubicin conjugated acid- and reductant-sensitive crosslinked micelles. Biomacromolecules. 9:3106-3113 (2008).

124. S.S. Chandran, A. Nan, D.M. Rosen, H. Ghandehari, and S.R. Denmeade. A prostate-specific antigen activated N-(2-hydroxypropyl) methacrylamide copolymer prodrug as dual-targeted therapy for prostate cancer. Mol Cancer Ther. 6:2928-2937 (2007).

125. B.S. Lele and J.C. Leroux. Synthesis and micellar characterization of novel amphiphilic A−B−A triblock copolymers of N-(2-hydroxypropyl)-methacrylamide or N-vinyl-2-pyrrolidone with poly(ε-caprolactone). Macromolecules. 35:6714-6723 (2002).

126. D. Neradovic, M.J. van Steenbergen, L. Vansteelant, Y.J. Meijer, C.F. van Nostrum, and W.E. Hennink. Degradation mechanism and kinetics of thermosensitive polyacrylamides containing lactic acid side chains. Macromolecules. 36:7491-7498 (2003).

127. O. Soga, C.F. van Nostrum, M. Fens, C.J. Rijcken, R.M. Schiffelers, G. Storm, and W.E. Hennink. Thermosensitive and biodegradable polymeric micelles for paclitaxel delivery. J Control Release. 103:341-353 (2005).

128. S.G. Krimmer, H. Pan, J. Liu, J. Yang, and J. Kopecek. Synthesis and characterization of poly(epsilon-caprolactone)-block-poly[N-(2-hydroxypropyl)-methacrylamide] micelles for drug delivery. Macromol Biosci. 11:1041-1051 (2011).

129. C. Oerlemans, W. Bult, M. Bos, G. Storm, J.F. Nijsen, and W.E. Hennink. Polymeric micelles in anticancer therapy: targeting, imaging and triggered release. Pharm Res. 27:2569-2589 (2010).

130. H. Sun, F. Meng, A.A. Dias, M. Hendriks, J. Feijen, and Z. Zhong. alpha-Amino acid containing degradable polymers as functional biomaterials: rational design, synthetic pathway, and biomedical applications. Biomacromolecules. 12:1937-1955 (2011).

131. R. De Souza, P. Zahedi, C.J. Allen, and M. Piquette-Miller. Polymeric drug delivery systems for localized cancer chemotherapy. Drug Deliv. 17:365-375 (2010).

132. A.C. Couffin-Hoarau, A.M. Aubertin, M. Boustta, S. Schmidt, J.A. Fehrentz, J. Martinez, and M. Vert. Peptide-poly(L-lysine citramide) conjugates and their in vitro anti-HIV behavior. Biomacromolecules. 10:865-876 (2009).

133. D. Yang, S. Van, J. Liu, J. Wang, X. Jiang, Y. Wang, and L. Yu. Physicochemical properties and biocompatibility of a polymer-paclitaxel conjugate for cancer treatment. Int J Nanomedicine. 6:2557-2566 (2011).

134. J.M. Metselaar, P. Bruin, L.W. de Boer, T. de Vringer, C. Snel, C. Oussoren, M.H. Wauben, D.J. Crommelin, G. Storm, and W.E. Hennink. A novel family of L-amino acid-based biodegradable polymer-lipid conjugates for the development of long-circulating liposomes with effective drug-targeting capacity. Bioconjug Chem. 14:1156-1164 (2003).

135. A.D. Baldwin and K.L. Kiick. Polysaccharide-modified synthetic polymeric biomaterials. Biopolymers. 94:128-140 (2010).

136. J.D. Kemp, T. Cardillo, B.C. Stewart, E. Kehrberg, G. Weiner, B. Hedlund, and P.W. Naumann. Inhibition of lymphoma growth in vivo by combined treatment with hydroxyethyl starch deferoxamine conjugate and IgG monoclonal antibodies against the transferrin receptor. Cancer Res. 55:3817-3824 (1995).

137. D.S. Pisal, M.P. Kosloski, and S.V. Balu-Iyer. Delivery of therapeutic proteins. J Pharm Sci. 99:2557-2575 (2010).

138. T.M. Beer, C. Ryan, J. Alumkal, C.W. Ryan, J. Sun, and K.M. Eilers. A phase II study of paclitaxel poliglumex in combination with transdermal estradiol for the treatment of metastatic castration-resistant prostate cancer after docetaxel chemotherapy. Anticancer Drugs. 21:433-438 (2010).

139. M. Mita, A. Mita, J. Sarantopoulos, C.H. Takimoto, E.K. Rowinsky, O. Romero, P. Angiuli, C. Allievi, A. Eisenfeld, and C.F. Verschraegen. Phase I study of paclitaxel poliglumex administered weekly for patients with advanced solid malignancies. Cancer Chemother Pharmacol. 64:287-295 (2009).

140. P. Sabbatini, M.W. Sill, D. O'Malley, L. Adler, and A.A. Secord. A phase II trial of paclitaxel poliglumex in recurrent or persistent ovarian or primary peritoneal cancer (EOC): a Gynecologic Oncology Group Study. Gynecol Oncol. 111:455-460 (2008).

141. M.E. O'Brien, M.A. Socinski, A.Y. Popovich, I.N. Bondarenko, A. Tomova, B.T. Bilynsky, Y.S. Hotko, V.L. Ganul, I.Y. Kostinsky, A.J. Eisenfeld, L. Sandalic, F.B. Oldham, B. Bandstra, A.B. Sandler, and J.W. Singer. Randomized phase III trial comparing single-agent paclitaxel Poliglumex (CT-2103, PPX) with single-agent gemcitabine or vinorelbine for the treatment of PS 2 patients with chemotherapy-naive advanced non-small cell lung cancer. J Thorac Oncol. 3:728-734 (2008).

142. M. Man and H. Rugo. Paclitaxel poliglumex. Cell Therapeutics/Chugai Pharmaceutical. IDrugs. 8:739-754 (2005).

143. P. Sapra, H. Zhao, M. Mehlig, J. Malaby, P. Kraft, C. Longley, L.M. Greenberger, and I.D. Horak. Novel delivery of SN38 markedly inhibits tumor growth in xenografts, including a camptothecin-11-refractory model. Clin Cancer Res. 14:1888-1896 (2008).

144. M. Pechar, K. Ulbrich, V. Subr, L.W. Seymour, and E.H. Schacht. Poly(ethylene glycol) multiblock copolymer as a carrier of anti-cancer drug doxorubicin. Bioconjug Chem. 11:131-139 (2000).

145. T. Etrych, P. Chytil, T. Mrkvan, M. Sirova, B. Rihova, and K. Ulbrich. Conjugates of doxorubicin with graft HPMA copolymers for passive tumor targeting. J Control Release. 132:184-192 (2008).

146. T. Etrych, J. Strohalm, P. Chytil, P. Cernoch, L. Starovoytova, M. Pechar, and K. Ulbrich. Biodegradable star HPMA polymer conjugates of doxorubicin for passive tumor targeting. Eur J Pharm Sci. 42:527-539 (2011).

147. T. Etrych, L. Kovar, J. Strohalm, P. Chytil, B. Rihova, and K. Ulbrich. Biodegradable star HPMA polymer-drug conjugates: Biodegradability, distribution and anti-tumor efficacy. J Control Release. 154:241-248 (2011).

148. K. Luo, J. Yang, P. Kopeckova, and J. Kopecek. Biodegradable Multiblock Poly[N-(2-hydroxypropyl)methacrylamide] via Reversible Addition-Fragmentation Chain Transfer Polymerization and Click Chemistry. Macromolecules. 44:2481-2488 (2011).

149. V. Torchilin. Multifunctional and stimuli-sensitive pharmaceutical nanocarriers. Eur J Pharm Biopharm. 71:431-444 (2009).

150. P. Vaupel, F. Kallinowski, and P. Okunieff. Blood flow, oxygen and nutrient supply, and metabolic microenvironment of human tumors: a review. Cancer Res. 49:6449-6465 (1989).

151. J.L. Wike-Hooley, J. Haveman, and H.S. Reinhold. The relevance of tumour pH to the treatment of malignant disease. Radiother Oncol. 2:343-366 (1984).

152. L.E. Gerweck and K. Seetharaman. Cellular pH gradient in tumor versus normal tissue: potential exploitation for the treatment of cancer. Cancer Res. 56:1194-1198 (1996).

153. P. Bawa, V. Pillay, Y.E. Choonara, and L.C. du Toit. Stimuli-responsive polymers and their applications in drug delivery. Biomed Mater. 4:022001 (2009).

154. F. Meng, W.E. Hennink, and Z. Zhong. Reduction-sensitive polymers and bioconjugates for biomedical applications. Biomaterials. 30:2180-2198 (2009).

155. M.D. Howard, A. Ponta, A. Eckman, M. Jay, and Y. Bae. Polymer micelles with hydrazone-ester dual linkers for tunable release of dexamethasone. Pharm Res. 28:2435-2446 (2011).

156. L. Zhou, R. Cheng, H. Tao, S. Ma, W. Guo, F. Meng, H. Liu, Z. Liu, and Z. Zhong. Endosomal pH-activatable poly(ethylene oxide)-graft-doxorubicin prodrugs: synthesis, drug release, and biodistribution in tumor-bearing mice. Biomacromolecules. 12:1460-1467 (2011).

157. Y. Bae, S. Fukushima, A. Harada, and K. Kataoka. Design of environment-sensitive supramolecular assemblies for intracellular drug delivery: polymeric micelles that are responsive to intracellular pH change. Angew Chem Int Ed Engl. 42:4640-4643 (2003).

158. Y. Bae, N. Nishiyama, S. Fukushima, H. Koyama, M. Yasuhiro, and K. Kataoka. Preparation and biological characterization of polymeric micelle drug carriers with intracellular pH-triggered drug release property: tumor permeability, controlled subcellular drug distribution, and enhanced in vivo antitumor efficacy. Bioconjug Chem. 16:122-130 (2005).

159. A. Chilkoti, M.R. Dreher, D.E. Meyer, and D. Raucher. Targeted drug delivery by thermally responsive polymers. Adv Drug Deliv Rev. 54:613-630 (2002).

160. X. Yin, A.S. Hoffman, and P.S. Stayton. Poly(N-isopropylacrylamide-co-propylacrylic acid) copolymers that respond sharply to temperature and pH. Biomacromolecules. 7:1381-1385 (2006).

161. D.E. Meyer and A. Chilkoti. Purification of recombinant proteins by fusion with thermally-responsive polypeptides. Nat Biotechnol. 17:1112-1115 (1999).

162. K. Trabbic-Carlson, L. Liu, B. Kim, and A. Chilkoti. Expression and purification of recombinant proteins from Escherichia coli: Comparison of an elastin-like polypeptide fusion with an oligohistidine fusion. Protein Sci. 13:3274-3284 (2004).

163. J.R. McDaniel, D.J. Callahan, and A. Chilkoti. Drug delivery to solid tumors by elastin-like polypeptides. Adv Drug Deliv Rev. 62:1456-1467 (2010).

164. A.S. Tatham and P.R. Shewry. Elastomeric proteins: biological roles, structures and mechanisms. Trends Biochem Sci. 25:567-571 (2000).

165. M.R. Dreher, W. Liu, C.R. Michelich, M.W. Dewhirst, and A. Chilkoti. Thermal cycling enhances the accumulation of a temperature-sensitive biopolymer in solid tumors. Cancer Res. 67:4418-4424 (2007).

166. M.R. Dreher, A.J. Simnick, K. Fischer, R.J. Smith, A. Patel, M. Schmidt, and A. Chilkoti. Temperature triggered self-assembly of polypeptides into multivalent spherical micelles. J Am Chem Soc. 130:687-694 (2008).

167. J.A. Mackay and A. Chilkoti. Temperature sensitive peptides: engineering hyperthermia-directed therapeutics. Int J Hyperthermia. 24:483-495 (2008).

168. S.M. Janib, A.S. Moses, and J.A. MacKay. Imaging and drug delivery using theranostic nanoparticles. Adv Drug Deliv Rev. 62:1052-1063 (2010).

169. R. Huis In 't Veld, G. Storm, W.E. Hennink, F. Kiessling, and T. Lammers. Macromolecular nanotheranostics for multimodal anticancer therapy. Nanoscale. 3:4022-4034 (2011).

170. V.J. Venditto and E.E. Simanek. Cancer therapies utilizing the camptothecins: a review of the in vivo literature. Mol Pharm. 7:307-349 (2010).

171. R. Palchaudhuri and P.J. Hergenrother. DNA as a target for anticancer compounds: methods to determine the mode of binding and the mechanism of action. Curr Opin Biotechnol. 18:497-503 (2007).

172. Y.H. Bae and K. Park. Targeted drug delivery to tumors: myths, reality and possibility. J Control Release. 153:198-205 (2011).

173. B. Yu, H.C. Tai, W. Xue, L.J. Lee, and R.J. Lee. Receptor-targeted nanocarriers for therapeutic delivery to cancer. Mol Membr Biol. 27:286-298 (2010).

174. F. Danhier, O. Feron, and V. Preat. To exploit the tumor microenvironment: Passive and active tumor targeting of nanocarriers for anti-cancer drug delivery. J Control Release. 148:135-146 (2010).

175. V.P. Torchilin. Passive and active drug targeting: drug delivery to tumors as an example. Handb Exp Pharmacol:3-53 (2010).

176. P. Debbage. Targeted drugs and nanomedicine: present and future. Curr Pharm Des. 15:153-172 (2009).

177. P. Holliger and P.J. Hudson. Engineered antibody fragments and the rise of single domains. Nat Biotechnol. 23:1126-1136 (2005).

178. A. Mitra, J. Mulholland, A. Nan, E. McNeill, H. Ghandehari, and B.R. Line. Targeting tumor angiogenic vasculature using polymer-RGD conjugates. J Control Release. 102:191-201 (2005).

179. M.P. Borgman, O. Aras, S. Geyser-Stoops, E.A. Sausville, and H. Ghandehari. Biodistribution of HPMA copolymer-aminohexylgeldanamycin-RGDfK conjugates for prostate cancer drug delivery. Mol Pharm. 6:1836-1847 (2009).

180. D.B. Pike and H. Ghandehari. HPMA copolymer-cyclic RGD conjugates for tumor targeting. Adv Drug Deliv Rev. 62:167-183 (2010).

181. T. Wang, V.A. Petrenko, and V.P. Torchilin. Paclitaxel-loaded polymeric micelles modified with MCF-7 cell-specific phage protein: enhanced binding to target cancer cells and increased cytotoxicity. Mol Pharm. 7:1007-1014 (2010).

182. A.S. Leong and Z. Zhuang. The changing role of pathology in breast cancer diagnosis and treatment. Pathobiology. 78:99-114 (2011).

183. R. Dienstmann, B. Markman, and J. Tabernero. Application of monoclonal antibodies as cancer therapy in solid tumors. Curr Clin Pharmacol. 7:137-145 (2012).

184. J.M. Adams and A. Strasser. Is tumor growth sustained by rare cancer stem cells or dominant clones? Cancer Res. 68:4018-4021 (2008).

185. M. Shackleton, E. Quintana, E.R. Fearon, and S.J. Morrison. Heterogeneity in cancer: cancer stem cells versus clonal evolution. Cell. 138:822-829 (2009).

186. H.D. Suit and M. Shwayder. Hyperthermia: potential as an anti-tumor agent. Cancer. 34:122-129 (1974).

187. R.W. Habash, R. Bansal, D. Krewski, and H.T. Alhafid. Thermal therapy, part 2: hyperthermia techniques. Crit Rev Biomed Eng. 34:491-542 (2006).

188. R.W. Habash, R. Bansal, D. Krewski, and H.T. Alhafid. Thermal therapy, Part III: ablation techniques. Crit Rev Biomed Eng. 35:37-121 (2007).

189. C.W. Song, M.S. Kang, J.G. Rhee, and S.H. Levitt. Effect of hyperthermia on vascular function in normal and neoplastic tissues. Ann N Y Acad Sci. 335:35-47 (1980).

190. T.E. Dudar and R.K. Jain. Differential response of normal and tumor microcirculation to hyperthermia. Cancer Res. 44:605-612 (1984).

191. E.A. Sausville and A.M. Burger. Contributions of human tumor xenografts to anticancer drug development. Cancer Res. 66:3351-3354, discussion 3354 (2006).

192. H.W. Head and G.D. Dodd, 3rd. Thermal ablation for hepatocellular carcinoma. Gastroenterology. 127:S167-178 (2004).

193. J.M. Bull. An update on the anticancer effects of a combination of chemotherapy and hyperthermia. Cancer Res. 44:4853s-4856s (1984).

194. R. Issels. Hyperthermia combined with chemotherapy–biological rationale, clinical application, and treatment results. Onkologie. 22:374-381 (2000).

195. P. Wust, B. Hildebrandt, G. Sreenivasa, B. Rau, J. Gellermann, H. Riess, R. Felix, and P.M. Schlag. Hyperthermia in combined treatment of cancer. Lancet Oncol. 3:487-497 (2002).

196. C.W. Song. Effect of local hyperthermia on blood flow and microenvironment: a review. Cancer Res. 44:4721s-4730s (1984).

197. H.I. Bicher, F.W. Hetzel, T.S. Sandhu, S. Frinak, P. Vaupel, M.D. O'Hara, and T. O'Brien. Effects of hyperthermia on normal and tumor microenvironment. Radiology. 137:523-530 (1980).

198. P.W. Vaupel and D.K. Kelleher. Pathophysiological and vascular characteristics of tumours and their importance for hyperthermia: heterogeneity is the key issue. Int J Hyperthermia. 26:211-223 (2010).

199. C.W. Song. Effect of local hyperthermia on blood flow and microenvironment: a review. Cancer Res. 44:4721s-4730s (1984).

200. Y. Matsuzaki, K. Shibata, M. Yoshioka, M. Inoue, R. Sekiya, T. Onitsuka, I. Iwamoto, and Y. Koga. Intrapleural perfusion hyperthermo-chemotherapy for malignant pleural dissemination and effusion. Ann Thorac Surg. 59:127-131 (1995).

201. C.J. Diederich. Thermal ablation and high-temperature thermal therapy: overview of technology and clinical implementation. Int J Hyperthermia. 21:745-753 (2005).

202. D. Haemmerich and P.F. Laeseke. Thermal tumour ablation: devices, clinical applications and future directions. Int J Hyperthermia. 21:755-760 (2005).

203. H.P. Beerlage, G.J. van Leenders, G.O. Oosterhof, J.A. Witjes, E.T. Ruijter, C.A. van de Kaa, F.M. Debruyne, and J.J. de la Rosette. High-intensity focused

ultrasound (HIFU) followed after one to two weeks by radical retropubic prostatectomy: results of a prospective study. Prostate. 39:41-46 (1999).

204. J.E. Kennedy, G.R. Ter Haar, and D. Cranston. High intensity focused ultrasound: surgery of the future? Br J Radiol. 76:590-599 (2003).

205. O. Rouviere, D. Lyonnet, A. Raudrant, C. Colin-Pangaud, J.Y. Chapelon, R. Bouvier, J.M. Dubernard, and A. Gelet. MRI appearance of prostate following transrectal HIFU ablation of localized cancer. Eur Urol. 40:265-274 (2001).

206. S. Crouzet, F.J. Murat, G. Pasticier, P. Cassier, J.Y. Chapelon, and A. Gelet. High intensity focused ultrasound (HIFU) for prostate cancer: current clinical status, outcomes and future perspectives. Int J Hyperthermia. 26:796-803 (2010).

207. L. Dykman and N. Khlebtsov. Gold nanoparticles in biomedical applications: recent advances and perspectives. Chem Soc Rev. 41:2256-2282 (2012).

208. G.F. Paciotti, D.G.I. Kingston, and L. Tamarkin. Colloidal gold nanoparticles: a novel nanoparticle platform for developing multifunctional tumor-targeted drug delivery vectors. Drug Develop Res. 67:47-54 (2006).

209. Q. Le, T.A. Larson, D.K. Smith, E. Vitkin, Z. Songhua, M.D. Modell, I. Itzkan, E.B. Hanlon, B.A. Korgel, K.V. Sokolov, and L.T. Perelman. Single Gold Nanorod Detection Using Confocal Light Absorption and Scattering Spectroscopy. IEEE J Sel Top Quant Electon. 13:1730-1738 (2007).

210. A.M. Alkilany and C.J. Murphy. Toxicity and cellular uptake of gold nanoparticles: what we have learned so far? J Nanopart Res. 12:2313-2333 (2010).

211. C. Villiers, H. Freitas, R. Couderc, M.B. Villiers, and P. Marche. Analysis of the toxicity of gold nano particles on the immune system: effect on dendritic cell functions. J Nanopart Res. 12:55-60 (2010).

212. M. Hulander, A. Lundgren, M. Berglin, M. Ohrlander, J. Lausmaa, and H. Elwing. Immune complement activation is attenuated by surface nanotopography. Int J Nanomedicine. 6:2653-2666 (2011).

213. X.D. Zhang, D. Wu, X. Shen, P.X. Liu, N. Yang, B. Zhao, H. Zhang, Y.M. Sun, L.A. Zhang, and F.Y. Fan. Size-dependent in vivo toxicity of PEG-coated gold nanoparticles. Int J Nanomedicine. 6:2071-2081 (2011).

214. S. Link and M.A. El-Sayed. Shape and size dependence of radiative, non-radiative and photothermal properties of gold nanocrystals. Int Rev Phys Chem. 19:409-453 (2000).

215. R. Weissleder. A clearer vision for in vivo imaging. Nat Biotechnol. 19:316-317 (2001).

216. A.J. Gormley, A. Malugin, A. Ray, R. Robinson, and H. Ghandehari. Biological evaluation of RGDfK-gold nanorod conjugates for prostate cancer treatment. J Drug Target. 19:915-924 (2011).

217. L.R. Hirsch, R.J. Stafford, J.A. Bankson, S.R. Sershen, B. Rivera, R.E. Price, J.D. Hazle, N.J. Halas, and J.L. West. Nanoshell-mediated near-infrared thermal therapy of tumors under magnetic resonance guidance. Proc Natl Acad Sci U S A. 100:13549-13554 (2003).

218. D.P. O'Neal, L.R. Hirsch, N.J. Halas, J.D. Payne, and J.L. West. Photo-thermal tumor ablation in mice using near infrared-absorbing nanoparticles. Cancer Lett. 209:171-176 (2004).

219. K. Richter, M. Haslbeck, and J. Buchner. The heat shock response: life on the verge of death. Mol Cell. 40:253-266 (2010).

220. R.M. Vabulas, S. Raychaudhuri, M. Hayer-Hartl, and F.U. Hartl. Protein folding in the cytoplasm and the heat shock response. Cold Spring Harb Perspect Biol. 2:a004390 (2010).

221. J.P. Hendrick and F.U. Hartl. Molecular chaperone functions of heat-shock proteins. Annu Rev Biochem. 62:349-384 (1993).

222. J.P. Grenert, W.P. Sullivan, P. Fadden, T.A. Haystead, J. Clark, E. Mimnaugh, H. Krutzsch, H.J. Ochel, T.W. Schulte, E. Sausville, L.M. Neckers, and D.O. Toft. The amino-terminal domain of heat shock protein 90 (hsp90) that binds geldanamycin is an ATP/ADP switch domain that regulates hsp90 conformation. J Biol Chem. 272:23843-23850 (1997).

223. L. Neckers. Hsp90 inhibitors as novel cancer chemotherapeutic agents. Trends Mol Med. 8:S55-61 (2002).

224. M. Taipale, D.F. Jarosz, and S. Lindquist. HSP90 at the hub of protein homeostasis: emerging mechanistic insights. Nat Rev Mol Cell Biol. 11:515-528 (2010).

225. Y.S. Kim, S.V. Alarcon, S. Lee, M.J. Lee, G. Giaccone, L. Neckers, and J.B. Trepel. Update on Hsp90 inhibitors in clinical trial. Curr Top Med Chem. 9:1479-1492 (2009).

226. A. Ito, H. Saito, K. Mitobe, Y. Minamiya, N. Takahashi, K. Maruyama, S. Motoyama, Y. Katayose, and J. Ogawa. Inhibition of heat shock protein 90

sensitizes melanoma cells to thermosensitive ferromagnetic particle-mediated hyperthermia with low Curie temperature. Cancer Sci. 100:558-564 (2009).

227. Y. Bae, R.A. Buresh, T.P. Williamson, T.H. Chen, and D.Y. Furgeson. Intelligent biosynthetic nanobiomaterials for hyperthermic combination chemotherapy and thermal drug targeting of HSP90 inhibitor geldanamycin. J Control Release. 122:16-23 (2007).

228. V. Yavelsky, O. Vais, B. Piura, M. Wolfson, A. Rabinovich, and V. Fraifeld. The role of Hsp90 in cell response to hyperthermia. J Therm Biol. 29:509-514 (2004).

229. K.T. Pfaffenbach and A.S. Lee. The critical role of GRP78 in physiologic and pathologic stress. Curr Opin Cell Biol. 23:150-156 (2011).

230. G. de Ridder, R. Ray, U.K. Misra, and S.V. Pizzo. Chapter Fourteen - Modulation of the Unfolded Protein Response by GRP78 in Prostate Cancer. In P.M. Conn (ed.), Methods in Enzymology, Vol. Volume 489, Academic Press, 2011, pp. 245-257.

231. M. Ni, Y. Zhang, and A.S. Lee. Beyond the endoplasmic reticulum: atypical GRP78 in cell viability, signalling and therapeutic targeting. Biochem J. 434:181-188 (2011).

232. C.L. Berger, Z. Dong, D. Hanlon, E. Bisaccia, and R.L. Edelson. A lymphocyte cell surface heat shock protein homologous to the endoplasmic reticulum chaperone, immunoglobulin heavy chain binding protein BIP. Int J Cancer. 71:1077-1085 (1997).

233. M.A. Arap, J. Lahdenranta, P.J. Mintz, A. Hajitou, A.S. Sarkis, W. Arap, and R. Pasqualini. Cell surface expression of the stress response chaperone GRP78 enables tumor targeting by circulating ligands. Cancer Cell. 6:275-284 (2004).

234. Y. Zhang, R. Liu, M. Ni, P. Gill, and A.S. Lee. Cell surface relocalization of the endoplasmic reticulum chaperone and unfolded protein response regulator GRP78/BiP. J Biol Chem. 285:15065-15075 (2010).

235. U.K. Misra, R. Deedwania, and S.V. Pizzo. Activation and cross-talk between Akt, NF-kappaB, and unfolded protein response signaling in 1-LN prostate cancer cells consequent to ligation of cell surface-associated GRP78. J Biol Chem. 281:13694-13707 (2006).

236. U.K. Misra, R. Deedwania, and S.V. Pizzo. Binding of activated alpha2-macroglobulin to its cell surface receptor GRP78 in 1-LN prostate cancer cells regulates PAK-2-dependent activation of LIMK. J Biol Chem. 280:26278-26286 (2005).

237. U.K. Misra, M. Gonzalez-Gronow, G. Gawdi, F. Wang, and S.V. Pizzo. A novel receptor function for the heat shock protein Grp78: silencing of Grp78 gene expression attenuates alpha2M*-induced signalling. Cell Signal. 16:929-938 (2004).

238. D.J. Davidson, C. Haskell, S. Majest, A. Kherzai, D.A. Egan, K.A. Walter, A. Schneider, E.F. Gubbins, L. Solomon, Z. Chen, R. Lesniewski, and J. Henkin. Kringle 5 of human plasminogen induces apoptosis of endothelial and tumor cells through surface-expressed glucose-regulated protein 78. Cancer Res. 65:4663-4672 (2005).

239. Y. Katanasaka, T. Ishii, T. Asai, H. Naitou, N. Maeda, F. Koizumi, S. Miyagawa, N. Ohashi, and N. Oku. Cancer antineovascular therapy with liposome drug delivery systems targeted to BiP/GRP78. Int J Cancer. 127:2685-2698 (2010).

240. Y.G. Shellman, W.R. Howe, L.A. Miller, N.B. Goldstein, T.R. Pacheco, R.L. Mahajan, S.M. LaRue, and D.A. Norris. Hyperthermia induces endoplasmic reticulum-mediated apoptosis in melanoma and non-melanoma skin cancer cells. J Invest Dermatol. 128:949-956 (2008).

241. X. Xu, S. Gupta, W. Hu, B.C. McGrath, and D.R. Cavener. Hyperthermia induces the ER stress pathway. PLoS One. 6:e23740 (2011).

242. P.J. Mintz, J. Kim, K.A. Do, X. Wang, R.G. Zinner, M. Cristofanilli, M.A. Arap, W.K. Hong, P. Troncoso, C.J. Logothetis, R. Pasqualini, and W. Arap. Fingerprinting the circulating repertoire of antibodies from cancer patients. Nat Biotechnol. 21:57-63 (2003).

243. R. Siegel, C. DeSantis, K. Virgo, K. Stein, A. Mariotto, T. Smith, D. Cooper, T. Gansler, C. Lerro, S. Fedewa, C. Lin, C. Leach, R.S. Cannady, H. Cho, S. Scoppa, M. Hachey, R. Kirch, A. Jemal, and E. Ward. Cancer treatment and survivorship statistics, 2012. CA Cancer J Clin. 62:220-241 (2012).

244. E.A. Singer, A. Kaushal, B. Turkbey, A. Couvillon, P.A. Pinto, and H.L. Parnes. Active surveillance for prostate cancer: past, present and future. Curr Opin Oncol. 24:243-250 (2012).

245. A.R. Kagan and R.J. Schulz. Proton-beam therapy for prostate cancer. Cancer J. 16:405-409 (2010).

246. J. Crook. The role of brachytherapy in the definitive management of prostate cancer. Cancer Radiother. 15:230-237 (2011).

247. A. Ingels, A. de la Taille, and G. Ploussard. Radical prostatectomy as primary treatment of high-risk prostate cancer. Curr Urol Rep. 13:179-186 (2012).

248. F. Schroder, E.D. Crawford, K. Axcrona, H. Payne, and T.E. Keane. Androgen deprivation therapy: past, present and future. BJU Int. 109 Suppl 6:1-12 (2012).

249. K. Lassi and N.A. Dawson. Emerging therapies in castrate-resistant prostate cancer. Curr Opin Oncol. 21:260-265 (2009).

250. J.R. Porter, J. Ge, J. Lee, E. Normant, and K. West. Ansamycin inhibitors of Hsp90: nature's prototype for anti-chaperone therapy. Curr Top Med Chem. 9:1386-1418 (2009).

251. Y. Fukuyo, C.R. Hunt, and N. Horikoshi. Geldanamycin and its anti-cancer activities. Cancer Lett. 290:24-35 (2010).

252. S. Sharp and P. Workman. Inhibitors of the HSP90 molecular chaperone: current status. Adv Cancer Res. 95:323-348 (2006).

253. U. Banerji. Heat shock protein 90 as a drug target: some like it hot. Clin Cancer Res. 15:9-14 (2009).

254. J.G. Supko, R.L. Hickman, M.R. Grever, and L. Malspeis. Preclinical pharmacologic evaulation of geldanamycin as an antitumor agent. Cancer Chemother Pharmacol. 36:305-315 (1994).

255. E.A. Ronnen, G.V. Kondagunta, N. Ishill, S.M. Sweeney, J.K. Deluca, L. Schwartz, J. Bacik, and R.J. Motzer. A phase II trial of 17-(Allylamino)-17-demethoxygeldanamycin in patients with papillary and clear cell renal cell carcinoma. Invest New Drugs. 24:543-546 (2006).

256. U. Banerji, A. O'Donnell, M. Scurr, S. Pacey, S. Stapleton, Y. Asad, L. Simmons, A. Maloney, F. Raynaud, M. Campbell, M. Walton, S. Lakhani, S. Kaye, P. Workman, and I. Judson. Phase I pharmacokinetic and pharmacodynamic study of 17-allylamino, 17-demethoxygeldanamycin in patients with advanced malignancies. J Clin Oncol. 23:4152-4161 (2005).

257. Y. Fu, S. Li, Y. Zu, G. Yang, Z. Yang, M. Luo, S. Jiang, M. Wink, and T. Efferth. Medicinal chemistry of paclitaxel and its analogues. Curr Med Chem. 16:3966-3985 (2009).

258. A. Montero, F. Fossella, G. Hortobagyi, and V. Valero. Docetaxel for treatment of solid tumours: a systematic review of clinical data. Lancet Oncol. 6:229-239 (2005).

259. I. Ringel and S.B. Horwitz. Studies with RP 56976 (taxotere): a semisynthetic analogue of taxol. J Natl Cancer Inst. 83:288-291 (1991).

260. M. Belfiglio, C. Fanizza, N. Tinari, C. Ficorella, S. Iacobelli, and C. Natoli. Meta-analysis of phase III trials of docetaxel alone or in combination with chemotherapy in metastatic breast cancer. J Cancer Res Clin Oncol. 138:221-229 (2012).

261. K. Amarantidis, N. Xenidis, L. Chelis, E. Chamalidou, P. Dimopoulos, P. Michailidis, A. Tentes, S. Deftereos, M. Karanikas, A. Karayiannakis, and S. Kakolyris. Docetaxel plus oxaliplatin in combination with capecitabine as first-line treatment for advanced gastric cancer. Oncology. 80:359-365 (2011).

262. A.G. Pallis, S. Agelaki, A. Agelidou, I. Varthalitis, K. Syrigos, N. Kentepozidis, G. Pavlakou, A. Kotsakis, E. Kontopodis, and V. Georgoulias. A randomized phase III study of the docetaxel/carboplatin combination versus docetaxel single-agent as second line treatment for patients with advanced/metastatic non-small cell lung cancer. BMC Cancer. 10:633 (2010).

263. M. Markman, K. Zanotti, K. Webster, G. Peterson, B. Kulp, and J. Belinson. Phase 2 trial of single agent docetaxel in platinum and paclitaxel-refractory ovarian cancer, fallopian tube cancer, and primary carcinoma of the peritoneum. Gynecol Oncol. 91:573-576 (2003).

264. M. Benjapibal, A.P. Kudelka, A. Vasuratna, C.L. Edwards, C.F. Verschraegen, V. Valero, S. Vadhan-Raj, and J.J. Kavanagh. Docetaxel and cyclophosphamide induced remission in platinum and paclitaxel refractory ovarian cancer. Anticancer Drugs. 9:577-579 (1998).

265. S. Sato, J. Kigawa, Y. Kanamori, H. Itamochi, T. Oishi, M. Shimada, T. Iba, J. Naniwa, K. Uegaki, and N. Terakawa. Activity of docetaxel in paclitaxel-resistant ovarian cancer cells. Cancer Chemother Pharmacol. 53:247-252 (2004).

266. Z. Kafri, L.K. Heilbrun, A. Sukari, G. Yoo, J. Jacobs, H.S. Lin, H. Mulrenan, D. Smith, and O. Kucuk. Phase II Study of Gemcitabine and Docetaxel Combination in Patients with Previously Treated Recurrent or Metastatic Squamous Cell Carcinoma of the Head and Neck. ISRN Oncol. 2012:159568 (2012).

267. S. Tamura, M. Imano, H. Takiuchi, K. Kobayashi, H. Imamoto, H. Miki, Y. Goto, T. Aoki, Y.F. Peng, T. Tsujinaka, and H. Furukawa. Phase II study of docetaxel, cisplatin and 5-fluorouracil (DCF) for metastatic esophageal cancer (OGSG 0403). Anticancer Res. 32:1403-1408 (2012).

268. S. Fu, B.T. Hennessy, C.S. Ng, Z. Ju, K.R. Coombes, J.K. Wolf, A.K. Sood, C.F. Levenback, R.L. Coleman, J.J. Kavanagh, D.M. Gershenson, M. Markman,

K. Dice, A. Howard, J. Li, Y. Li, K. Stemke-Hale, M. Dyer, E. Atkinson, E. Jackson, V. Kundra, R. Kurzrock, R.C. Bast, Jr., and G.B. Mills. Perifosine plus docetaxel in patients with platinum and taxane resistant or refractory high-grade epithelial ovarian cancer. Gynecol Oncol. 126:47-53 (2012).

269. A.A. Garcia, A. Yessaian, H. Pham, G. Facio, L. Muderspach, and L. Roman. Phase II study of gemcitabine and docetaxel in recurrent platinum resistant ovarian cancer. Cancer Invest. 30:295-299 (2012).

270. B. Sorbe, M. Graflund, G. Horvath, M. Swahn, K. Boman, R. Bangshoj, M. Lood, and H. Malmstrom. Phase II study of docetaxel weekly in combination with carboplatin every 3 weeks as first-line chemotherapy in stage IIB to stage IV epithelial ovarian cancer. Int J Gynecol Cancer. 22:47-53 (2012).

271. K. Ushijima, T. Kamura, K. Tamura, K. Kuzuya, T. Sugiyama, K. Noda, and K. Ochiai. Docetaxel/irinotecan combination chemotherapy in platinum/taxane-refractory and -resistant ovarian cancer: JGOG/WJGOG Intergroup Study. Int J Clin Oncol:[Epub ahead of print] (2011).

272. D.S. Hong, U. Banerji, B. Tavana, G.C. George, J. Aaron, and R. Kurzrock. Targeting the molecular chaperone heat shock protein 90 (HSP90): Lessons learned and future directions. Cancer Treat Rev (2012).

273. Q. Tan, X. Liu, X. Fu, Q. Li, J. Dou, and G. Zhai. Current development in nanoformulations of docetaxel. Expert Opin Drug Deliv. 9:975-990 (2012).

274. F.K. Engels, R.A. Mathot, and J. Verweij. Alternative drug formulations of docetaxel: a review. Anticancer Drugs. 18:95-103 (2007).

275. C. Buonerba, P. Federico, C. D'Aniello, P. Rescigno, C. Cavaliere, L. Puglia, M. Ferro, V. Altieri, S. Perdona, S. De Placido, and G. Di Lorenzo. Phase II trial of cisplatin plus prednisone in docetaxel-refractory castration-resistant prostate cancer patients. Cancer Chemother Pharmacol. 67:1455-1461 (2011).

276. E. Dovern, I.H. de Hingh, V.J. Verwaal, W.J. van Driel, and S.W. Nienhuijs. Hyperthermic intraperitoneal chemotherapy added to the treatment of ovarian cancer. A review of achieved results and complications. Eur J Gynaecol Oncol. 31:256-261 (2010).

277. S. Ohno, Z.H. Siddik, Y. Kido, L.A. Zwelling, and J.M. Bull. Thermal enhancement of drug uptake and DNA adducts as a possible mechanism for the effect of sequencing hyperthermia on cisplatin-induced cytotoxicity in L1210 cells. Cancer Chemother Pharmacol. 34:302-306 (1994).

278. N. Pabla and Z. Dong. Cisplatin nephrotoxicity: mechanisms and renoprotective strategies. Kidney Int. 73:994-1007 (2008).

CHAPTER 3

HPMA COPOLYMER-AMINOHEXYLGELDANAMYCIN CONJUGATES TARGETING CELL SURFACE EXPRESSED GRP78 IN PROSTATE CANCER

3.1 Introduction

As previously described in Chapter 2, prostate cancer remains a significant health challenge and a significant cause of cancer related deaths. Geldanamycin (GDM), a benzoquinone ansamycin, is a naturally occurring inhibitor of heat shock protein 90 (Hsp90) and has been widely studied as an anticancer agent.[1] Hsp90 is highly expressed in a variety of cancers including melanoma, leukemia, colon, lung, breast, and prostate cancers,[2] and is thought to play an important role in regulating the folding and activity of its client proteins, which include growth-stimulating proteins involved in malignant transformation.[3] As Hsp90 client proteins have also been implicated in prostate cancer progression,[4] GDM naturally presents itself as an attractive therapeutic agent against this disease. However, the clinical use of GDM has been limited by several factors. It exhibits high hepatotoxicity at therapeutic doses in animal models,[5] is poorly soluble in water, and is metabolically unstable.[2] While GDM

derivatives with improved tolerance, metabolic stability, and water solubility are currently under investigation, clinical response is still limited.[6, 7]

As described in Chapter 2, the use of drug conjugates with water soluble polymers such as poly ethylene glycol (PEG) and *N*-(2-hydroxypropyl)methacrylamide (HPMA) copolymers are well suited to overcome these limitations.[8, 9] First, polymeric carriers can increase the water solubility of poorly water soluble drugs.[10] Second, the use of polymeric conjugates can significantly alter drug pharmacokinetics and biodistribution.[11, 12] This can result in a significant increase in the blood plasma half-life of the drug, which in turn results in an increased total drug exposure. Third, these polymeric conjugates accumulate in solid tumors by the passive "enhanced permeability and retention" (EPR) effect due to the leaky tumor vasculature and reduced lymphatic drainage within the tumor microenvironment.[13] This translates to a higher maximum tolerated dose (MTD) of a given chemotherapeutic agent.[14] The advantage of HPMA copolymers over other water-soluble polymers is that simple chemical modifications can be used to alter drug loading, targeting moiety content, and molecular weight.[15, 16] Drug molecules can be attached to the polymer backbone via the lysosomally degradable peptide sequence Gly-Phe-Leu-Gly (GFLG) allowing intracellular release by lysosomal proteases[17] while remaining stable during systemic circulation.[18] Several HPMA copolymer-drug conjugates have progressed to clinical trials for the treatment of a variety of solid tumor cancers.[19, 20] However, clinical success has remained marginal.[21] The inclusion of targeting moieties bound to the polymer backbone can further enhance accumulation in the target site while minimizing systemic exposure. For example, previous work has described anti-angiogenic HPMA copolymer

conjugates bearing RGD (Arg-Gly-Lys) peptides as targeting moieties toward endothelial cells in the neovasculature of solid tumors (also see Appendix A).[22-24] The success of anti-angiogenic therapy however is limited as angiogenesis inhibitors can inhibit tumor growth in areas of neovascularization but have no direct effect on the survival of tumor cells in the regions of mature, nonproliferating vessels and do not exert cytotoxicity directly to tumor cells.[25] An alternative strategy is to use a combination treatment of targeted drug delivery to both the tumor vasculature and tumor cells.

Glucose regulated protein 78 (GRP78), also known as immunoglobulin heavy-chain binding protein (BiP) was first discovered following glucose starvation in chicken embryo fibroblasts.[26] GRP78 is a member of the Hsp70 protein family and is primarily found in the endoplasmic reticulum (ER) where it acts by facilitating protein folding and functions as a regulator of ER stress signaling.[27] In the tumor microenvironment characterized by glucose deprivation, acidosis, and hypoxia, the accumulation of misfolded and underglycosylated proteins trigger the unfolded protein response, inducing the expression of GRP78 and migration of GRP78 to the cell surface. This presents an attractive molecular target with specific expression occurring presumably in cancer cells. In mouse models, GRP78 expression is selectively induced in cancer cells and cancer associated macrophages but not in major adult organs.[28] GRP78 is also detected on the surface of human prostate cancer cells and may play a role in promoting cell proliferation, survival, and metastasis.[29, 30]

The octopeptide WIFPWIQL, selected by phage display, specifically binds to GRP78 and has shown binding to cell surface expressed GRP78 in human prostate

cancer cells.[31] Recent results demonstrate the ability of WIFPWIQL peptide bearing liposomes to target DU145 prostate cancer cells as well as vascular endothelial growth factor (VEGF)-activated human umbilical vein endothelial cells (HUVECs),[32] an attractive target for anti-angiogenic therapy which may also be utilized by the conjugates described in this report as GDM exhibits both antiangiogenic[33] and antitumor activity.

In this Chapter, the synthesis and in vitro characterization of HPMA copolymer-aminohexylgeldanamycin (AHGDM) conjugates is described. AHGDM was attached to the HPMA copolymer backbone via the lysosomally degradable GFLG linker as well as a non-degradable Gly-Gly (GG) linker for comparison in growth inhibition studies. Conjugates were further modified to incorporate the WIFPWIQL peptide to facilitate binding to cell surface expressed GRP78 in human prostate cancer cells lines.

3.2 Materials and methods

3.2.1 Materials

Geldanamycin (NSC 122750) was supplied by the National Cancer Institute Developmental Therapeutics Program (NCI DTP). The GRP78 targeting peptide WIFPWIQL was supplied and characterized by Anaspec, Inc. (San Jose, CA). *N*-(2-hydroxypropyl)methacrylamide (HPMA)[34]; *N*-methacryloylglycylglycyl-p-nitrophenyl ester (MA-GG-ONp)[35]; *N*-methacryloyl-glycylphenylalanylleucylglycine (MA-GFLG-OH)[36]; *N*-methacryloyl-glycylphenylalanylleucylglycine-p-nitrophenyl ester (MA-GFLG-ONp)[36]; and *N*-methacryloyl-tyrosinamide (MA-Tyr)[37] were synthesized and characterized according to previously described methods. Anti-GRP78 polyclonal

antibody was obtained from Assay Designs, Inc. (Ann Arbor, MI). Na-^{125}I was obtained from American Radiolabeled Chemicals, Inc. (St. Louis, MO). Iodogen reagent, 1,3,4,6-tetrachloro-3α,6α-diphenylglycoluril, was obtained from Thermo Fisher Scientific (Rockford, IL).

3.2.2 Synthesis and characterization of drug-containing monomers

17-(6-aminohexylamino)-17-demethoxygeldanamycin (AHGDM) and N-methacryloylglycylphenylalanylleucylglycl-17-(6-aminohexylamino)-17-demethoxy-geldanamycin (MA-GFLG-AHGDM) were synthesized according to previously described procedures with minor modifications.[14, 38] Briefly, GDM (200 mg, 0.357 mmol) and 1,6-Diaminohexane (1.24 g, 10.7 mmol) were dissolved in anhydrous chloroform (30 mL) and stirred under N_2 gas for 2 hrs at room temperature. Product formation was monitored by thin layer chromatography (TLC) on silica gel with chloroform: methanol [9:1] as the mobile phase. Following product formation, the reaction mixture in chloroform was combined and washed 15X with 30 mL aqueous saturated sodium chloride to ensure removal of excess 1,6-diaminohexane. Complete removal of 1,6-diaminohexane was confirmed by its absence on silica gel eluted with chloroform: methanol [75: 25]. Organic layer was then dried over sodium sulfate, and solvent removed by rotary evaporation. Resulting dark purple solid AHGDM was verified by mass spectrometry (MS). MA-GFLG-AHGDM comonomer was synthesized by adding AHGDM (223 mg, 0.346 mmol) to MA-GFLG-ONp (201 mg, 0.415 mmol) in 3 mL anhydrous dimethylsulfoxide (DMSO). N,N-Diisopropylethylamine (181 μL, 1.04 mmol) was added and the reaction mixture

protected from light and stirred overnight at room temperature. Product formation was monitored by TLC on silica gel with chloroform: methanol [9: 1] and purified by silica gel column with ethyl acetate: methanol [9: 1] as the mobile phase. Solvent was removed and resulting product MA-GFLG-AHGDM was identified by MS. N-methacryloylglycylglycl-17-(6-aminohexylamino)-17-demethoxygeldanamycin (MA-GG-AHGDM) comonomer was synthesized in a manner similar to MA-GFLG-AHGDM utilizing MA-GG-ONp comonomer as a starting material instead of MA-GFLG-ONp. MA-GG-AHGDM comonomer was similarly purified by silica gel column and the resulting product was identified by mass spectrometry.

3.2.3 Synthesis and characterization of HPMA copolymer conjugates

HPMA copolymers were synthesized via free radical precipitation copolymerization of comonomers in acetone: DMSO [9: 1] using N, N'-azobisisobutyronitrile (AIBN) as initiator. The concentrations of monomers and AIBN in solution were maintained at 12.5% and 0.6% (w/v) respectively. The feed composition of comonomers for all copolymers is given in Table 3.1 and a resulting HPMA copolymer structure is graphically represented in Figure 3.1. The comonomer mixtures were sealed in a glass ampoule under N_2 gas and stirred at 50°C for 24 hrs. Following polymerization, product was obtained by precipitation into diethyl ether. p-Nitrophenol (ONp) content in the polymeric precursors was assessed by release of ONp from the copolymer in 1.0 N sodium hydroxide and quantification of released ONp by UV spectrophotometry at 400 nm. To obtain the final untargeted conjugates, ONp was similarly released from polymeric precursors and dialyzed against distilled water for 72

Table 3.1. Characteristics of HPMA copolymer conjugates

Polymer	Description	*-------- Feed composition (mol %) -------*					Apparent M_w[a] (kDa)	M_w/M_n	AH-GDM content[b] (mol %)	WIFPWIQL content[c] (mol %)
		HPMA	MA-GG-ONp	MA-GFLG-AH-GDM	MA-GG-AH-GDM	MA-Tyr				
HPMA-(GFLG-AH-GDM)	AHGDM conjugate utilizing lysosomally degradable GFLG linker	73	20	5	-	2	23.7	1.7	5.1	-
HPMA-(GG-AH-GDM)	AHGDM conjugate having non-degradable GG linker	73	20	-	5	2	26.4	1.5	6.3	-
HPMA-(GFLG-AH-GDM)-WIFPWIQL	AHGDM conjugate utilizing GFLG linker + WIFPWIQL peptide	73	20	5	-	2	23.7[d]	1.7[d]	5.1[d]	6.2

[a] Estimated by size exclusion chromatography.

[b] Determined by UV spectroscopy.

[c] Determined by amino acid analysis.

[d] Values reported are for precursor polymer.

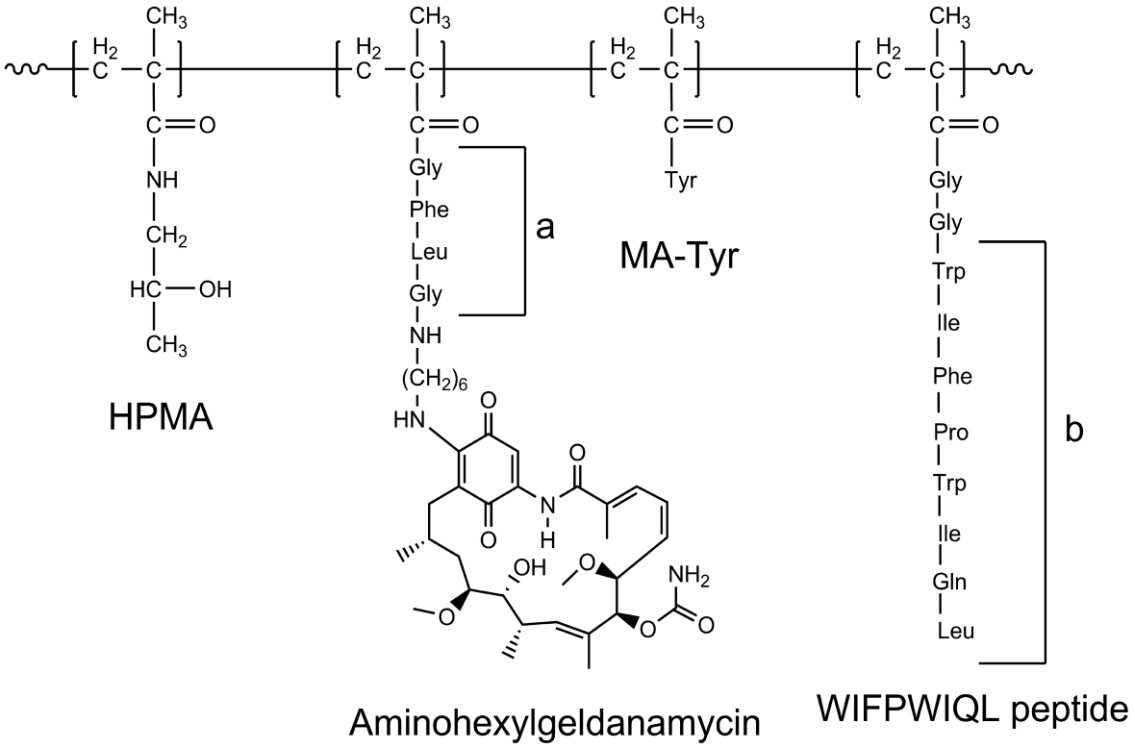

Figure 3.1. Schematics of HPMA copolymer–AHGDM-WIFPWIQL conjugates.

[a] Lysosomally degradable GFLG linker represented as found in HPMA-(GFLG-AHGDM) copolymer. HPMA-(GG-AHGDM) polymer contains non-degradable GG linker.

[b] WIFPWIQL peptide attached to HPMA copolymer backbone via non-degradable GG linker as shown. Untargeted HPMA-(GFLG-AHGDM) copolymer does not contain WIFPWIQL peptide.

hrs in a 3.5 KDa molecular weight cut-off (MWCO) regenerated cellulose dialysis membrane (Spectrum Laboratories, Inc., Rancho Dominguez, CA). Apparent weight average molecular weight (M_w) and polydispersity (M_w/ M_n) were estimated by size exclusion chromatography (SEC) on a Superose 12 column (10 mm x 30 cm) (GE Healthcare, Piscataway, NJ) using a Fast Protein Liquid Chromatography (FPLC) system (GE Healthcare). The Superose 12 column was previously calibrated with fractions of known molecular weight HPMA homopolymers.

HPMA copolymer-WIFPWIQL conjugate was synthesized via ONp ester aminolysis of polymeric precursors. HPMA copolymer precursor was reacted with WIFPWIQL peptide in anhydrous DMSO in the presence of pyridine for 24 hrs. The reaction was terminated and unreacted ONp was released by slow addition of 0.1 N NaOH. Conjugates were dialyzed against distilled water in a 3.5 KDa MWCO regenerated cellulose dialysis membrane to remove low molecular weight compounds. Targeting peptide content of the conjugate was determined by amino acid analysis (University of Utah Core Research Facilities, Salt Lake City, UT). AHGDM content of conjugates was determined spectrophotometrically at 340 nm.

3.2.4 Synthesis of AHGDM hydrochloride salt (AHGDM·HCl)

The water soluble hydrochloride salt of AHGDM was synthesized for use as a control in stability studies. AHGDM was dissolved in freshly prepared methanol hydrochloric acid and stirred overnight. The solvent was removed by rotary evaporation and the resulting material was dissolved in deionized water, filtered through

a 0.22 μm filter to remove insoluble AHGDM, frozen and lyophilized. The resulting product was freely soluble upon reconstitution with deionized water.

3.2.5 Stability of HPMA copolymer conjugates

The release of free AHGDM from the conjugates was assessed in 50 mM NaH_2PO_4 pH 7.4 buffer, 50 mM $NaH_2C_3O_2$ pH 5.0 buffer, complete DU145 cell culture media containing 10% FBS, and 100% FBS. AHGDM equivalent concentrations were maintained below the aqueous solubility of free AHGDM (< 300 ug /mL) in all test solutions to prevent saturation. Quantitative amounts of conjugates or AHGDM·HCl control were dissolved in 1.5 mL of each test solution. One-hundred μL was removed at 0.5, 1, 2, 4, 8, 24, 48 and 72 hrs time points, extracted 3X with 100 uL dichloromethane and transferred to an HPLC vial. Solvent was removed by evaporation, and the resulting residue was reconstituted in HPLC mobile phase, and 20 μL injected for analysis by HPLC. HPLC analyses were performed with an Agilent 1100 HPLC system (Agilent Technologies, Santa Clara, CA, USA) equipped with a photo diode array detector set at 350 nm for quantification using a Waters XBridge column (C18, 4.6 x 250mm, 5μm) and an isocratic mobile phase of 50 mM $NH_4C_2H_3O_2$: Acetonitrile [65: 35 v/v]. A calibration curve was generated by extracting and processing AHGDM·HCl as noted above. An extraction efficiency of 99.4 ± 0.6 % was obtained using this method. The cumulative percent AHGDM released was calculated and plotted as a function of time. Conjugates dissolved in mobile phase alone were analyzed to determine concentrations at time zero.

3.2.6 Cell culture

DU145 and PC3 human prostate cancer cell lines were obtained from ATCC (Manassas, VA). DU145 cell lines were cultured in Eagle's Minimum Essential Medium with Earle's Balanced Salt Solution (ATCC) supplemented with 10 % (v/v) fetal bovine serum (FBS) (Thermo Scientific HyClone, Logan, UT). PC3 cell lines were cultured in F-12K Medium (ATCC) supplemented with 10% (v/v) FBS. Cell lines were cultured at 37°C in a humidified atmosphere of 5% CO_2. For all procedures, cells were harvested using TrypLE^{TM} Express (Invitrogen, Carlsbad, CA) and cell lines were maintained in a logarithmic growth phase during the studies.

3.2.7 Radiolabeling of anti-GRP78 antibody

Anti-GRP78 antibody was radiolabeled with ^{125}Iodine using the Iodogen method with slight modification.[39] Briefly, 20 μL of a 1 mg / mL solution of iodogen reagent in dichloromethane was added to a 1 cm x 7.5 cm glass tube and evaporated to dryness under N_2 gas. Ten μg of anti-GRP78 antibody and 1.0 mCi of Na-^{125}Iodine were combined in the glass tube and allowed to react at room temperature for 10 min with gentle mixing. The solution was transferred to another tube and diluted to 650 μL with phosphate buffered saline (PBS) at pH 7.4. Radiolabeled anti-GRP78 antibody was purified using a Zeba Spin Desalting Column (Thermo Fisher Scientific) with a MWCO of 7 kDa.

3.2.8 Competitive cell receptor binding assay and comparative expression of cell surface expressed GRP78

The comparative affinities of free WIFPWIQL peptide and HPMA copolymer conjugates were assessed using a competitive binding assay to cell surface expressed GRP78 on DU145 and PC3 cells. DU145 and PC3 cells were harvested, washed with PBS, and re-suspended in binding buffer (20 mmol/L tromethamine, pH 7.4, 150 mmol/L NaCl, 2 mmol/L $CaCl_2$, 1 mmol/L $MgCl_2$, 1 mmol/L $MnCl_2$, 0.1% bovine serum albumin). Cell suspension was added in 1.2 μm pore size 96-well Multiscreen HV filter plates (Millipore, Billerica, MA) at 50,000 cells per well. They were then co-incubated at 4°C with 2 ng ^{125}I-anti-GRP78 antibody and increasing targeting peptide equivalent concentrations of copolymer conjugates or free WIFPWIQL peptide between 0 and 500 μM. Following 1 hr incubation, media was removed from cells using a Multiscreen vacuum manifold (Millipore) and cells were washed 3X with binding buffer. Filters were collected and radioactivity determined using a Cobra Auto-Gamma-counter (Canberra Industries, Inc., Meriden, CT). Binding percentage relative to control wells containing only ^{125}I-anti-GRP78 antibody was calculated and nonlinear regression analysis and determination of IC_{50} values was carried out using GraphPad Prism (GraphPad Software, Inc., La Jolla, CA).

The relative cell surface expression of GRP78 in DU145 and PC3 cell lines was estimated by calculating the absolute radioactivity recovered in wells incubated with 2 nm ^{125}I-anti-GRP78 antibody in binding buffer at 4°C for 1 hr (control wells) from the preceding binding experiment.

3.2.9 Cell growth inhibition studies

The ability of the conjugates to inhibit growth of DU145 and PC3 human prostate cancer cell lines was evaluated in vitro using a 2-(2-methoxy-4-nitrophenyl)-3-(4-nitrophenyl)-5-(2,4-disulfophenyl)-2H-tetrazolium monosodium salt (WST-8) cell viability assay (Dojindo Molecular Technologies, Inc., Rockville, MD). Due to the poor water solubility of the free drugs GDM and AHGDM, stock solutions of conjugates, free drugs, and controls were prepared in DMSO and subsequently diluted, resulting in a final concentration of 0.5 % (v/v) DMSO in complete growth medium. No significant toxicities were observed for DU145 or PC3 cells when exposed to 0.5% DMSO concentrations for 72 hrs. DU145 or PC3 cells (3,000 or 7,500 cells per well respectively) were plated in 96-well plates for 24 hrs. Cell culture medium was then replaced with media containing conjugates, free drugs, or controls, and cells were treated for 72 hrs. Following treatment, medium was removed and wells were washed with 200 μL PBS. WST-8 reagent in complete growth medium (100 μL as 10% v/v) was added to each well and cells were incubated at 37°C / 5% CO_2 for 120 min and absorbance at 450 nm minus 630 nm was determined by UV spectrophotometry using a SpectraMax M2 microplate reader (Molecular Devices, Sunnyvale, CA). Relative viability was calculated by normalization of the absorbance of untreated cells. Nonlinear least-squares regression analysis was performed using GraphPad Prism.

3.2.10 Statistical analysis

Differences in relative cell binding affinity and *in vitro* growth inhibition IC_{50} values were determined by one-way ANOVA. Where differences were detected, a

Bonferroni test was used to test for significance between groups. Differences in relative cell surface expression between DU145 and PC3 cells were evaluated using two-sided Student's T-test. The significance level was set at α=0.05 for all statistical tests.

3.3 Results

3.3.1 Synthesis and characterization of the conjugates

Characteristics of HPMA copolymers synthesized are summarized in Table 3.1. AHGDM containing copolymers with the degradable peptide linker GFLG, i.e., HPMA copolymer-(GFLG-AHGDM) and HPMA copolymer-(GFLG-AHGDM)-WIFPWIQL had an apparent weight average molecular weight of 23.7 KDa, a polydispersity index of 1.67, and an AHGDM drug content of 5.1 mol% (16.2%, wt/wt) based on evaluation of the polymeric precursor. The ONp content of the polymeric precursor was 0.639 mmol / g. Following attachment of WIFPWIQL peptide to the polymeric precursor, HPMA copolymer-(GFLG-AHGDM)-WIFPWIQL had a peptide content of 6.2 mol% (0.147 mmol / g). The AHGDM containing copolymer utilizing the nondegradable peptide linker GG had an apparent weight average molecular weight of 26.4 kDa, a polydispersity index of 1.50 and an AHGDM drug content of 6.3 mol% (24.6%, wt/wt). No targeting peptide was attached to the AHGDM containing copolymer utilizing the non-degradable linker.

3.3.2 Stability of the conjugates

The release of AHGDM as a function of time from copolymer conjugates was assessed in 50 mM NaH_2PO_4 pH 7.4 buffer, 50 mM $NaH_2C_3O_2$ pH 5.0 buffer, complete

DU145 cell culture media containing 10% FBS, and in 100% FBS (Figure 3.2). FBS was used to evaluate the potential for enzymatic release during *in vivo* systemic circulation.[40, 41] Release was minimal at pH 7.4 and pH 5.0 and in complete DU145 cell culture medium containing 10% FBS with less than approximately 1% release over 72 hrs and no difference was observed for conjugates with and without WIFPWIQL peptide. In 100% FBS, release from conjugates was increased, with 6.6% and 11.3% released after 72 hrs from conjugates with and without WIFPWIQL peptide. The release from the conjugate with WIFPWIQL was less than the untargeted conjugate at 72 hrs ($p < 0.05$). Overall, the conjugates were stable and exhibited less than 5% release over 24 hrs in test solutions.

3.3.3 Comparative cell surface expression and competitive binding

Competitive binding studies with DU145 and PC3 cells showed binding of copolymer-peptide conjugates to cell-surface expressed GRP78 with IC_{50} values of 1.2 ± 0.3 μM and 4 ± 1 μM respectively as shown in Figure 3.3. Untargeted conjugates showed no competitive binding. At equivalent peptide concentrations, free peptide showed greater binding affinity ($p < 0.05$) as compared to polymer conjugates with IC_{50} values of 0.29 ± 0.07 μM and 1.1 ± 0.1 μM for both DU145 and PC3 cell lines. Comparative cell surface expressions of GRP78 as determined by ^{125}I-anti-GRP78 antibody binding and gamma counting were 2900 ± 300 and 1200 ± 200 cpm for DU145 and PC3 cell lines respectively, indicating statistically significantly higher cell surface expression of GRP78 in DU145 versus PC3 cell lines ($p < 0.0001$) (Figure 3.4).

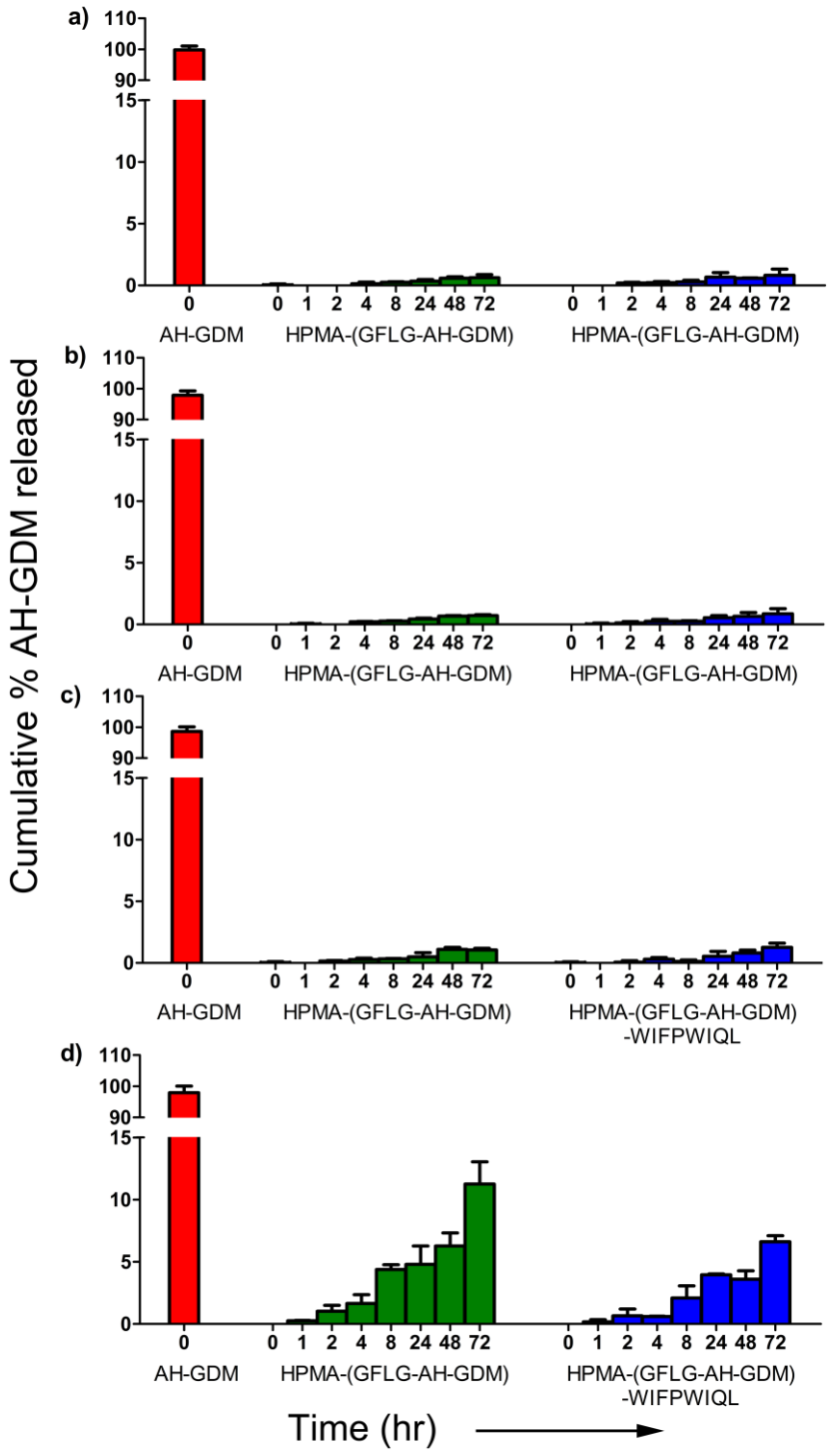

Figure 3.2. Stability of HPMA copolymer–AHGDM-WIFPWIQL conjugates in aqueous media. Release of free AHGDM from HPMA copolymer-(GFLG-AHGDM) (green bars) and HPMA copolymer-(GFLG-AHGDM)-WIFPWIQL (blue bars) was assessed in: a) 50 mM NaH_2PO_4 pH 7.4 buffer, b) 50 mM $NaH_2C_3O_2$ pH 5.0 buffer, c) complete DU145 cell culture media containing 10% FBS, and d) 100% FBS. AHGDM·HCl salt (red bars) was included in each case as control. Data expressed as mean ± SD.

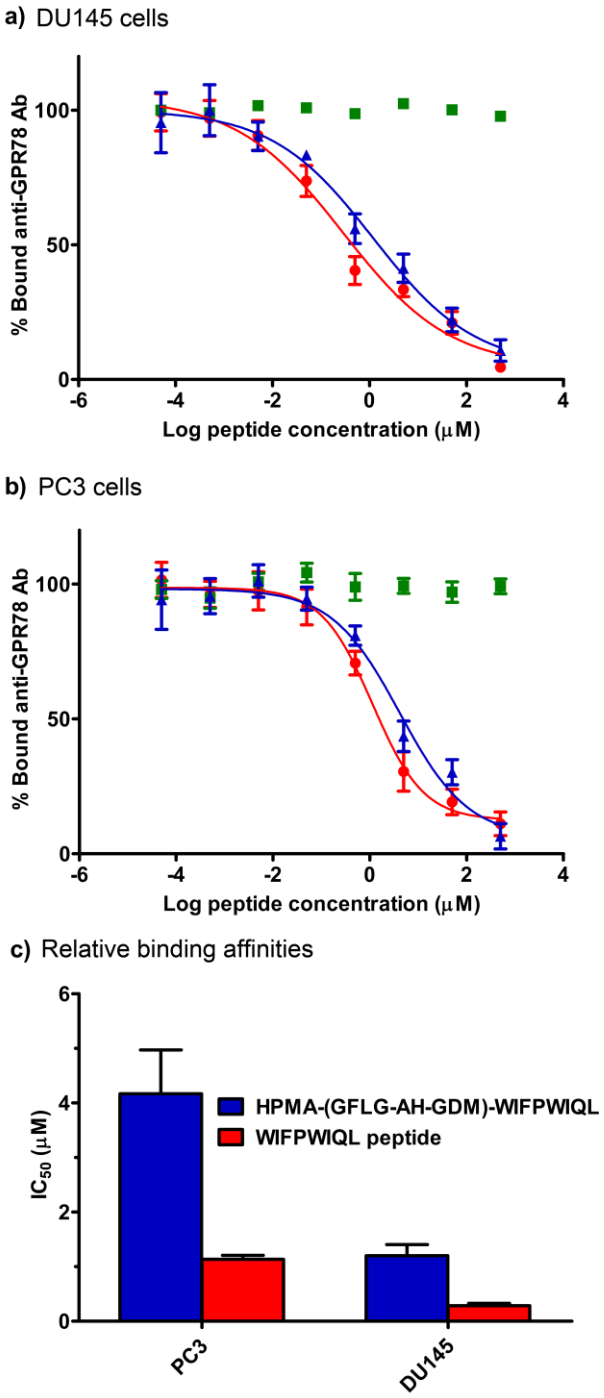

Figure 3.3. Competitive binding of HPMA copolymer – AHGDM WIFPWIQL conjugates to DU145 and PC3 cells lines. a) DU145 or b) PC3 cells were seeded in filter plates and co-incubated at 4°C with ^{125}I-anti-GRP78 antibody and increasing targeting peptide equivalent concentrations of HPMA copolymer-(GFLG-AHGDM) (green squares), HPMA copolymer-(GFLG-AHGDM)-WIFPWIQL (blue triangles), or free WIFPWIQL peptide (red circles). Following 1 hr incubation, media was removed and cells washed. Filters were collected and radioactivity determined by γ-counting.

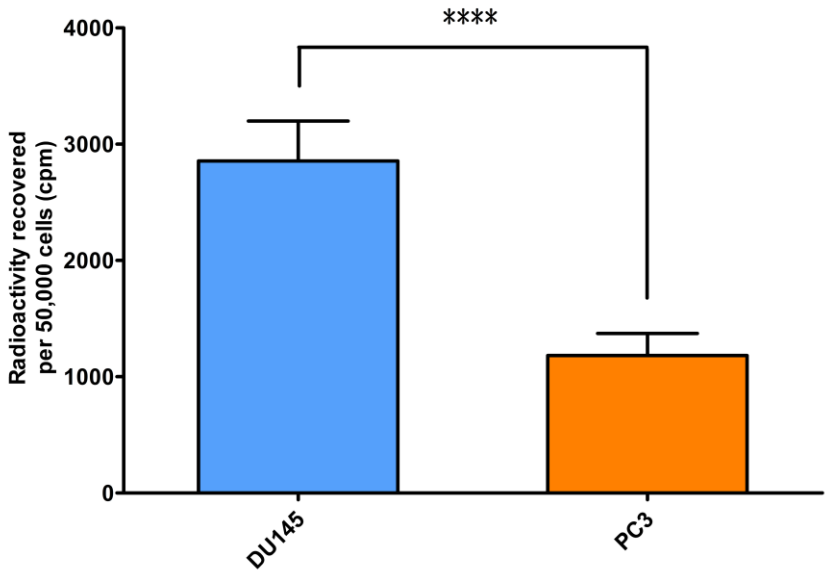

Figure 3.4. Relative GRP78 cell surface expression in DU145 and PC3 cell lines.
a) DU145 or b) PC3 cells were seeded in filter plates and incubated with 2 nM ^{125}I-anti-GRP78 antibody in binding buffer at 4°C for 1 hr. Following 1 hr incubation, media was removed and cells were washed. Filters were collected and radioactivity determined by γ-counting. Data expressed as mean ± SD. **** Indicates significance at $p < 0.0001$

3.3.4 Cell growth inhibition studies

Cell growth inhibition activity of conjugates in DU145 and PC3 cell lines is shown in Figure 3.5. Results demonstrate that modification of geldanamycin at position 17 with 1,6-diaminohexane reduced its ability to inhibit cell growth. All conjugates containing AHGDM were capable of inhibiting cell growth. Conjugation of AHGDM to HPMA copolymers did not have any statistically significant effect on growth inhibition ($p > 0.05$), and attachment of WIFPWIQL peptide statistically significantly reduced growth inhibition in both cell lines with GI_{50} values of 1.7 ± 0.1 μM and 1.8 ± 0.1 μM as compared to 2.6 ± 0.2 μM and 2.8 ± 0.3 μM for untargeted conjugates in DU145 and PC3 cell lines respectively ($p < 0.05$) (Table 3.2, Figure 3.5). Attachment of AHGDM to the HPMA backbone via the nondegradable GG linker resulted in a statistically significant loss of growth inhibition with GI_{50} values of 19 ± 2 μM and 15 ± 1 μM respectively for DU145 and PC3 cell lines as compared to AHGDM attached via the lysosomally cleavable GFLG linker ($p < 0.001$). HPMA homopolymer and free WIFPWIQL peptide controls showed no statistically significant reduction in cell viability over equivalent concentration ranges (data not shown).

3.4 Discussion

The synthesis and in vitro characterization of HPMA copolymer-AHGDM conjugates bearing prostate cancer targeting WIFPWIQL peptide is described in this chapter. It is anticipated that the therapeutic index of AHGDM can be improved by selectively targeting these conjugates to the cell surface expressed GRP78 of metastatic prostate cancer cells. HPMA copolymers containing the geldanamycin derivative

Table 3.2. Cell growth inhibition GI_{50} values of HPMA copolymer conjugates in comparison with geldanamycin compounds

Compound	*Description*	*DU145*		*PC3*	
		Mean GI_{50} (μM)	*SD GI_{50} (μM)*	*Mean GI_{50} (μM)*	*SD GI_{50} (μM)*
GDM	Geldanamycin	0.026	0.003	0.028	0.004
AHGDM	Aminohexylgeldanamycin	2.7	0.2	3.2	0.2
HPMA-(GFLG-AHGDM)	AHGDM conjugate utilizing lysosomally degradable GFLG linker	2.6	0.2	2.8	0.3
HPMA-(GG-AHGDM)	AHGDM conjugate having nondegradable GG linker	19	2	15	1
HPMA-(GFLG-AHGDM)-WIFPWIQL	AHGDM conjugate utilizing GFLG linker + WIFPWIQL peptide	1.7	0.1	1.8	0.1

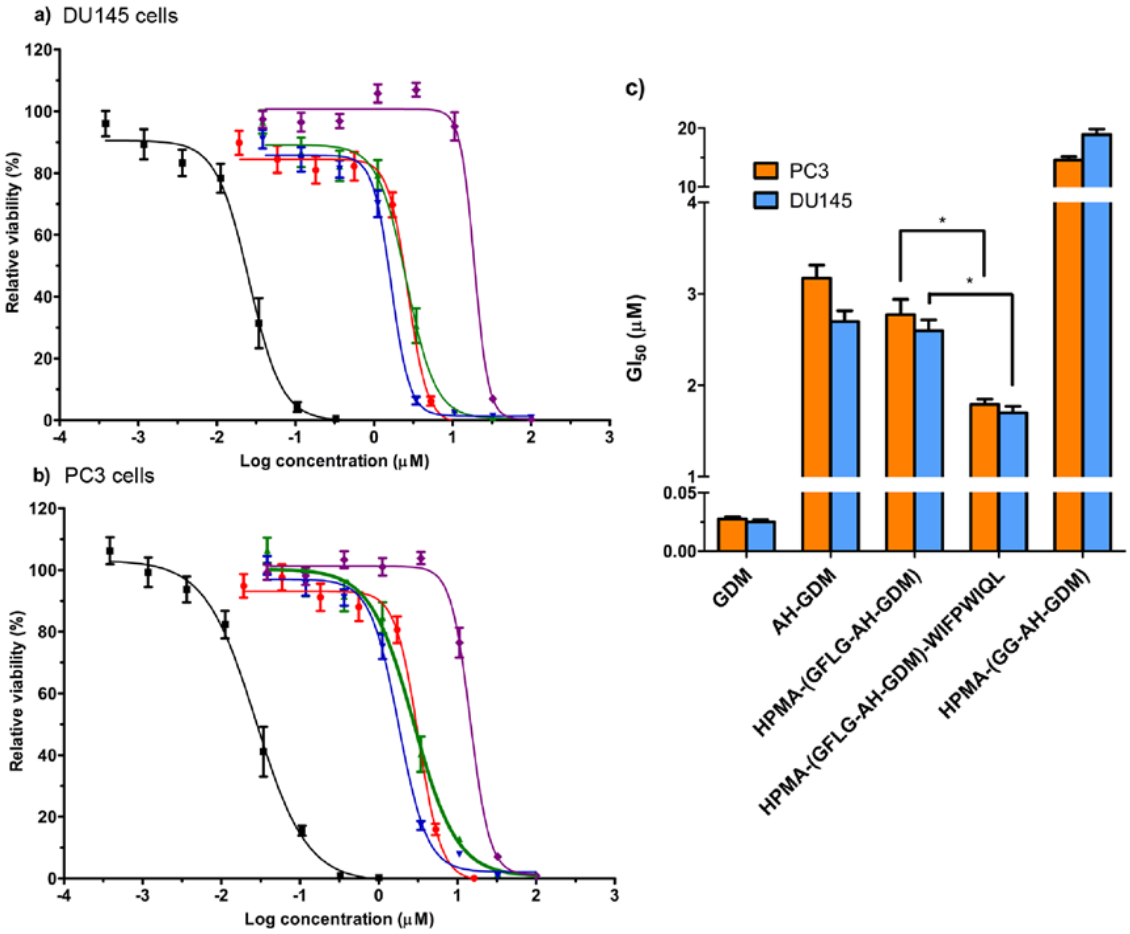

Figure 3.5. Growth inhibition of HPMA copolymer–AHGDM-WIFPWIQL conjugates. a) DU145 or b) PC3 cells were treated for 72 hrs with increasing drug equivalent concentrations of GDM (black squares), AHGDM (red circles), HPMA copolymer-(GFLG-AHGDM) (green triangles), HPMA copolymer-(GFLG-AHGDM)-WIFPWIQL (blue reverse triangles), or HPMA copolymer-(GG-AHGDM) (purple diamonds). Following treatment, cell viability was assessed by WST-8 assay. c) GI_{50} values were determined in DU145 (blue bars) and PC3 (orange bars) by analysis using GraphPad Prism.

* Statistical difference detected ($p < 0.05$) between untargeted and targeted conjugates. Other statistical differences exist between other groups and are not

AHGDM and bearing WIFPWIQL peptide were successfully synthesized. Modification of native GDM to AHGDM is necessary to generate a reactive free amine, thus enabling conjugation to the HPMA copolymer backbone. AHGDM was chosen over other amine geldanamycin derivatives since, when conjugated to HPMA copolymers, they have previously demonstrated favorable stability and cleavage by the lysosomal enzyme cathepsin B.[42] HPMA copolymers achieved an AHGDM drug loading ranging from 5.1 to 6.3 mol% and were water soluble. To generate the targetable HPMA copolymer, WIFPWIQL peptide was successfully conjugated to the HPMA backbone via the non-degradable GG linker, and conjugation was verified and quantified by amino acid analysis. The molecular weight and molecular weight distribution of the conjugates was estimated by SEC and were comparable to similar conjugates previously reported.[14, 23]

Competitive binding studies demonstrated binding of WIFPWIQL peptide bearing conjugates to cell surface expressed GRP78 in DU145 and PC3 cell lines, and untargeted conjugates showed no evidence of competitive binding in either cell line as demonstrated in Figure 3.3. Although a statistical difference in the binding affinity of free peptide in comparison with the targeted conjugate at equivalent peptide concentrations was detected, the binding affinities were similar and demonstrate that attachment of WIFPWIQL peptide to the HPMA copolymer backbone has little effect on the ability of WIFPWIQL peptide to actively bind GRP78. Cell surface expression of GRP78 was observed in both DU145 and PC3 cell lines and agrees with previous studies.[31, 43]

Growth inhibition studies demonstrated the ability of all conjugates bearing AHGDM to limit the proliferation of both DU145 and PC3 cells in vitro. The modification of geldanamycin at position 17 with 1,6-diaminohexane reduced its ability to inhibit growth *in vitro* and is consistent with previous reports. It is possible that alternative geldanamycin analogues having functionality allowing conjugation to polymeric backbones may need to be further investigated. However, previous animal studies[14] have demonstrated that HPMA copolymers bearing AHGDM are tolerated at much higher doses than free AHGDM, suggesting that efficacious levels can be delivered. It is interesting to note that conjugation of AHGDM to the HPMA copolymer backbone did not result in a significant decrease in its ability to inhibit growth of DU145 and PC3 cell lines (Table 3.2, Figure 3.5). An additional HPMA-copolymer bearing AHGDM was synthesized to investigate whether release of AHGDM from the HPMA copolymer backbone was critical for growth inhibition. In this case, the AHGDM was attached to the copolymer backbone via the nondegradable GG linker, as compared to the lysosomally degradable GFLG linker. The ability of the HPMA copolymer containing the nondegradable GG linker to inhibit growth was reduced approximately 7-fold and 5-fold for DU145 and PC3 cell lines, suggesting the necessity of release of free AHGDM via lysosomal degradation as well as increased activity and binding to HSP90 of free AHGDM as compared to HPMA copolymer bound AHGDM. The ability of the nondegradable system to inhibit cell proliferation is however maintained, with a GI_{50} of 19 μM and 15 μM observed for DU145 and PC3 cell lines (Table 3.2). A similar result has been reported for HPMA copolymer conjugates bearing adriamycin bound to the polymer backbone via GFLG and GG

linkages.[44] However, the exact mechanism of action for the nondegradable system requires further investigation.

The ability to target malignant tumors such as prostate cancer is a long-standing goal in oncology. Unfortunately tumor targeting approaches tend to suffer from lack of specificity and incomplete tissue penetration. By screening combinatorial libraries of peptides and antibodies using phage display, unique targeting ligands have been identified. This approach directly selects, *in vivo*, for circulating probes capable of preferential homing into tumors. As a result, new markers have been uncovered, providing a means for selective targeting of therapies and new insights into normal prostate and prostate cancer vasculature and tumor cell specificities.

Application of this technology has led to isolation of GRP78. This is a chaperone heat-shock protein which has been isolated by fingerprinting the circulating repertoire of antibodies from cancer patients[45] and has emerged as an excellent cancer target. GRP78 receptors (i) are abundant and functional on the tumor cell surface, (ii) can confer tumor selectivity on specific inhibitors, and (iii) regulate multiple signaling pathways related to apoptosis, immune response, and drug resistance. Given the promising therapeutic data in tumor models and the presence of the receptor in patient-derived samples, this system provides an ideal platform for targeted drug development. Studies on several ligand-receptor systems based on the tumor cell membrane expression of GRP78 has resulted in identification of a lead peptide motif namely WIFPWIQL[31] which was used in this study. This peptide has been shown to specifically target tumor cells *in vitro*, *in vivo*, and in human cancer specimens *ex vivo*. Moreover, synthetic chimeric peptides composed of GRP78-binding motif WIFPWIQL,

fused to a programmed cell death inducing sequence promoted tumor suppression in xenograft and isogenic mouse models of prostate and breast cancer.[31] Collectively, these preclinical data validate GRP78 on the tumor cell surface as a functional molecular target and WIFPWIQL as a useful targeting peptide that show potential for translation into clinical applications.

In this study the attachment of the WIFPWIQL peptide to the side chains of biocompatible HPMA copolymers containing AHGDM increased the ability of the conjugate to inhibit the growth of both DU145 and PC3 cell lines. Combined with the results from the competitive binding studies which show active binding of the targeted conjugate to both cell lines, this increased potency is possibly due to a combination of both increased binding and cellular uptake. This result coupled with our previous observations that HPMA copolymer-AHGDM conjugates terminated in cyclic RGD peptides substantially increase the localization of drug in solid tumors and improve safety[14, 23] (also see Appendix A) bode well for combination delivery of AHGDM to both angiogenic and tumor cells for a more effective and less toxic treatment of prostate cancer.

3.5 Conclusion

In this chapter, HPMA copolymer conjugates containing the geldanamycin analogue AHGDM and WIFPWIQL peptide for targeting cell surface expressed GRP78 were synthesized and characterized. Conjugates were stable under physiological conditions. The HPMA copolymer conjugate containing AHGDM and WIFPWIQL peptide showed binding affinity to cell surface expressed GRP78 in both DU145 and

PC3 prostate cancer cell lines as compared to the untargeted conjugate. The targeted conjugate also exhibited greater ability to inhibit the growth of prostate cancer cell in vitro as compared to the untargeted conjugate. This conjugate shows promise as a therapeutic agent in combination strategies for delivery of aminohexylgeldanamycin to solid tumors.

3.6 References

1. J.R. Porter, J. Ge, J. Lee, E. Normant, and K. West. Ansamycin inhibitors of Hsp90: nature's prototype for anti-chaperone therapy. Curr Top Med Chem. 9:1386-1418 (2009).

2. Y. Fukuyo, C.R. Hunt, and N. Horikoshi. Geldanamycin and its anti-cancer activities. Cancer Lett. 290:24-35 (2010).

3. S. Sharp and P. Workman. Inhibitors of the HSP90 molecular chaperone: current status. Adv Cancer Res. 95:323-348 (2006).

4. U. Banerji. Heat shock protein 90 as a drug target: some like it hot. Clin Cancer Res. 15:9-14 (2009).

5. J.G. Supko, R.L. Hickman, M.R. Grever, and L. Malspeis. Preclinical pharmacologic evaulation of geldanamycin as an antitumor agent. Cancer Chemother Pharmacol. 36:305-315 (1994).

6. E.A. Ronnen, G.V. Kondagunta, N. Ishill, S.M. Sweeney, J.K. Deluca, L. Schwartz, J. Bacik, and R.J. Motzer. A phase II trial of 17-(Allylamino)-17-demethoxygeldanamycin in patients with papillary and clear cell renal cell carcinoma. Invest New Drugs. 24:543-546 (2006).

7. U. Banerji, A. O'Donnell, M. Scurr, S. Pacey, S. Stapleton, Y. Asad, L. Simmons, A. Maloney, F. Raynaud, M. Campbell, M. Walton, S. Lakhani, S. Kaye, P. Workman, and I. Judson. Phase I pharmacokinetic and pharmacodynamic study of 17-allylamino, 17-demethoxygeldanamycin in patients with advanced malignancies. J Clin Oncol. 23:4152-4161 (2005).

8. J. Kopecek and P. Kopeckova. HPMA copolymers: origins, early developments, present, and future. Adv Drug Deliv Rev. 62:122-149 (2010).

9. F.F. Davis. The origin of pegnology. Adv Drug Deliv Rev. 54:457-458 (2002).

10. M.J. Vicent, S. Manzanaro, J.A. de la Fuente, and R. Duncan. HPMA copolymer-1,5-diazaanthraquinone conjugates as novel anticancer therapeutics. J Drug Target. 12:503-515 (2004).

11. L.W. Seymour, R. Duncan, J. Strohalm, and J. Kopecek. Effect of molecular weight (Mw) of N-(2-hydroxypropyl)methacrylamide copolymers on body distribution and rate of excretion after subcutaneous, intraperitoneal, and intravenous administration to rats. J Biomed Mater Res. 21:1341-1358 (1987).

12. A. Mitra, A. Nan, H. Ghandehari, E. McNeill, J. Mulholland, and B.R. Line. Technetium-99m-labeled N-(2-hydroxypropyl) methacrylamide copolymers: synthesis, characterization, and in vivo biodistribution. Pharm Res. 21:1153-1159 (2005).

13. H. Maeda, J. Wu, T. Sawa, Y. Matsumura, and K. Hori. Tumor vascular permeability and the EPR effect in macromolecular therapeutics: a review. J Control Release. 65:271-284 (2000).

14. M.P. Borgman, A. Ray, R.B. Kolhatkar, E.A. Sausville, A.M. Burger, and H. Ghandehari. Targetable HPMA copolymer-aminohexylgeldanamycin conjugates for prostate cancer therapy. Pharm Res. 26:1407-1418 (2009).

15. A. Nan, N.P. Nanayakkara, L.A. Walker, V. Yardley, S.L. Croft, and H. Ghandehari. N-(2-hydroxypropyl)methacrylamide (HPMA) copolymers for targeted delivery of 8-aminoquinoline antileishmanial drugs. J Control Release. 77:233-243 (2001).

16. A. Nan, S.L. Croft, V. Yardley, and H. Ghandehari. Targetable water-soluble polymer-drug conjugates for the treatment of visceral leishmaniasis. J Control Release. 94:115-127 (2004).

17. V. Subr, J. Kopecek, J. Pohl, M. Baudys, and V. Kostka. Cleavage of oligopeptide side-chains in N-2(hydroxpropyl)meth-acrylamide copolymers by mixtures of lysosomal enzymes. J Control Release. 8:133-140 (1988).

18. D. Putnam and J. Kopeček. Polymer conjugates with anticancer activity. Biopolymers II, Vol. 122, Springer Berlin, 1995, pp. 55-123.

19. L.W. Seymour, D.R. Ferry, D.J. Kerr, D. Rea, M. Whitlock, R. Poyner, C. Boivin, S. Hesslewood, C. Twelves, R. Blackie, A. Schatzlein, D. Jodrell, D. Bissett, H. Calvert, M. Lind, A. Robbins, S. Burtles, R. Duncan, and J. Cassidy. Phase II studies of polymer-doxorubicin (PK1, FCE28068) in the treatment of breast, lung and colorectal cancer. Int J Oncol. 34:1629-1636 (2009).

20. R. Duncan. Development of HPMA copolymer-anticancer conjugates: clinical experience and lessons learnt. Adv Drug Deliv Rev. 61:1131-1148 (2009).

21. R. Duncan and M.J. Vicent. Do HPMA copolymer conjugates have a future as clinically useful nanomedicines? A critical overview of current status and future opportunities. Adv Drug Deliv Rev. 62:272-282 (2010).

22. A. Mitra, T. Coleman, M. Borgman, A. Nan, H. Ghandehari, and B.R. Line. Polymeric conjugates of mono- and bi-cyclic alphaVbeta3 binding peptides for tumor targeting. J Control Release. 114:175-183 (2006).

23. M.P. Borgman, A. Ray, R.B. Kolhatkar, E.A. Sausville, A.M. Burger, and H. Ghandehari. Targetable HPMA copolymer-aminohexylgeldanamycin conjugates for prostate cancer therapy. Pharmaceutical Research. 26:1407-1418 (2009).

24. N. Larson, A. Ray, A. Malugin, D.B. Pike, and H. Ghandehari. HPMA copolymer-aminohexylgeldanamycin conjugates targeting cell surface expressed GRP78 in prostate cancer. Pharm Res. 27:2683-2693 (2010).

25. L.E. Benjamin and E. Keshet. Conditional switching of vascular endothelial growth factor (VEGF) expression in tumors: induction of endothelial cell shedding and regression of hemangioblastoma-like vessels by VEGF withdrawal. Proc Natl Acad Sci U S A. 94:8761-8766 (1997).

26. R.P. Shiu, J. Pouyssegur, and I. Pastan. Glucose depletion accounts for the induction of two transformation-sensitive membrane proteinsin Rous sarcoma virus-transformed chick embryo fibroblasts. Proc Natl Acad Sci U S A. 74:3840-3844 (1977).

27. L.M. Hendershot. The ER function BiP is a master regulator of ER function. Mt Sinai J Med. 71:289-297 (2004).

28. D. Dong, L. Dubeau, J. Bading, K. Nguyen, M. Luna, H. Yu, G. Gazit-Bornstein, E.M. Gordon, C. Gomer, F.L. Hall, S.S. Gambhir, and A.S. Lee. Spontaneous and controllable activation of suicide gene expression driven by the stress-inducible GRP 78 promoter resulting in eradication of sizable human tumors. Hum Gene Ther. 15:553-561 (2004).

29. U.K. Misra, R. Deedwania, and S.V. Pizzo. Activation and cross-talk between Akt, NF-kappaB, and unfolded protein response signaling in 1-LN prostate cancer cells consequent to ligation of cell surface-associated GRP78. J Biol Chem. 281:13694-13707 (2006).

30. Y. Zhang, R. Liu, M. Ni, P. Gill, and A.S. Lee. Cell surface relocalization of the endoplasmic reticulum chaperone and unfolded protein response regulator GRP78/BiP. J Biol Chem. 285:15065-15075 (2010).

31. M.A. Arap, J. Lahdenranta, P.J. Mintz, A. Hajitou, A.S. Sarkis, W. Arap, and R. Pasqualini. Cell surface expression of the stress response chaperone GRP78 enables tumor targeting by circulating ligands. Cancer Cell. 6:275-284 (2004).

32. Y. Katanasaka, T. Ishii, T. Asai, H. Naitou, N. Maeda, F. Koizumi, S. Miyagawa, N. Ohashi, and N. Oku. Cancer antineovascular therapy with liposome drug delivery systems targeted to BiP/GRP78. Int J Cancer. 127:2685-2698 (2010).

33. W.C. Wu, Y.H. Kao, P.S. Hu, and J.H. Chen. Geldanamycin, a HSP90 inhibitor, attenuates the hypoxia-induced vascular endothelial growth factor expression in retinal pigment epithelium cells in vitro. Exp Eye Res. 85:721-731 (2007).

34. J. Strohalm and J. Kopecek. Poly N-(2-hydroxypropyl) methacrylamide: 4. Heterogenous polymerization. Angew Makromol Chem. 70:109-118 (1978).

35. P. Rejmanova, J. Labsky, and J. Kopecek. Aminolyses of monomeric and polymeric p-nitrophenyl esters of methacryloylated amino acids. Makromol Chem. 178:2159-2168 (1977).

36. K. Ulbrich, V. Subr, J. Strohalm, D. Plocova, M. Jelinkova, and B. Rihova. Polymeric drugs based on conjugates of synthetic and natural macromolecules. I. Synthesis and physico-chemical characterisation. J Control Release. 64:63-79 (2000).

37. J.H. Lee, P. Kopeckova, J. Kopecek, and J.D. Andrade. Surface properties of copolymers of alkyl methacrylates with methoxy (polyethylene oxide) methacrylates and their application as protein-resistant coatings. Biomaterials. 11:455-464 (1990).

38. Y. Kasuya, Z.R. Lu, P. Kopeckova, T. Minko, S.E. Tabibi, and J. Kopecek. Synthesis and characterization of HPMA copolymer-aminopropylgeldanamycin conjugates. J Control Release. 74:203-211 (2001).

39. J.M. Walker. The protein protocols handbook, Humana Press, Towota, N.J., 1996.

40. S.H. Kim, J.H. Jeong, S.H. Lee, S.W. Kim, and T.G. Park. PEG conjugated VEGF siRNA for anti-angiogenic gene therapy. J Control Release. 116:123-129 (2006).

41. S. Sugahara, M. Kajiki, H. Kuriyama, and T.R. Kobayashi. Complete regression of xenografted human carcinomas by a paclitaxel-carboxymethyl dextran conjugate (AZ10992). J Control Release. 117:40-50 (2007).

42. Y. Kasuya, Z.R. Lu, P. Kopeckova, S.E. Tabibi, and J. Kopecek. Influence of the structure of drug moieties on the in vitro efficacy of HPMA copolymer-geldanamycin derivative conjugates. Pharm Res. 19:115-123 (2002).

43. U.K. Misra, R. Deedwania, and S.V. Pizzo. Binding of activated alpha2-macroglobulin to its cell surface receptor GRP78 in 1-LN prostate cancer cells regulates PAK-2-dependent activation of LIMK. J Biol Chem. 280:26278-26286 (2005).

44. A. Malugin, P. Kopeckova, and J. Kopecek. Liberation of doxorubicin from HPMA copolymer conjugate is essential for the induction of cell cycle arrest and nuclear fragmentation in ovarian carcinoma cells. J Control Release. 124:6-10 (2007).

45. R. Guerriero, U. Testa, M. Gabbianelli, G. Mattia, E. Montesoro, G. Macioce, A. Pace, B. Ziegler, H.J. Hassan, and C. Peschle. Unilineage megakaryocytic proliferation and differentiation of purified hematopoietic progenitors in serum-free liquid culture. Blood. 86:3725-3736 (1995).

CHAPTER 4

GUIDED DELIVERY OF POLYMER THERAPEUTICS USING PLASMONIC PHOTOTHERMAL THERAPY[≠]

4.1 Introduction[¥]

As described in Chapter 2, incorporation of anticancer agents within nanocarriers represents an effective way of delivering hydrophobic drugs in the blood as well as altering their organ distribution in the body.[2] These nanomedicines have been designed to target sites of disease and enhance delivery to solid tumors. Despite substantial progress, clinical translation has been slow due to limited accumulation in the target site.[3]

The delivery of targeted nanomedicines to solid tumors utilizes a two-pronged approach.[2] First, their nanoscale size (~5-500 nm) is leveraged to reduce the accumulation in healthy organs while maximizing extravasation into the tumor mass. While the junctions between vascular endothelial cells in healthy tissues are too small (~2-6 nm) to allow permeation, larger gaps (up to 1.2 μm), which are present in the tumor's poorly developed and leaky vasculature, allow them to partition out of the blood and into the tumor mass.[4] Described as the enhanced permeability and retention (EPR) effect,[5] this passive targeting approach has been applied ubiquitously in the

[≠] Co-authored (equal contribution) manuscript with A.J. Gormley.[1]
[¥] Indicates section completed in collaboration.

delivery of nanomedicines.[6] Second, once in the tumor interstitial space, contact with receptors expressed on the cancer cell surface immobilizes them and triggers their internalization via endocytosis followed by drug release.[7] This binding and uptake can be further increased through active targeting by conjugating receptor specific ligands to the nanocarriers.[8]

Polymer-based nanomedicines have the advantage of solubilizing hydrophobic drugs and exhibiting stealth-like characteristics thereby evading immune recognition.[9] In such systems drugs can be covalently linked to the polymer backbone and specifically released by enzymatic degradation or hydrolysis.[10] These polymer-drug conjugates are typically 5-15 nm in hydrodynamic diameter and can therefore be cleared by urinary excretion.[11] This is advantageous due to rising safety concerns of nanomedicines which are not eliminated from the body.[12-15] The small size, however, comes with a cost as rapid renal elimination reduces the availability of the conjugates to accumulate in tumors by the EPR effect.[16] With these advantages and limitations in mind, there is therefore a need to develop a strategy which maximizes the delivery of polymer therapeutics within the window of opportunity before renal clearance.

This need is particularly apparent considering conjugates, which aim to maximize tumor delivery, have to date demonstrated only moderate clinical benefit. For example, early generation polymer-drug conjugates such as *N*-(2-hydroxypropyl)methacrylamide (HPMA) copolymer-doxorubicin and poly(ethylene glycol) (PEG)-camptothecin have not obtained the same success in the clinic as other nanomedicines such as Doxil® (liposome-doxorubicin) and Abraxane® (albumin-paclitaxel).[9] While much of this may be related to other variables such as drug release

kinetics, the lack of sufficient delivery to the tumor (<<15% of the injected dose) represents the primary barrier to success. Recent efforts to improve this delivery such as using high molecular weight biodegradable polymers that exhibit prolonged blood circulation as well as using polymers with different architectures (i.e., dendrimers and branched polymers) have achieved some success. However, greater control over both passive and active targeting strategies is desirable.[17]

One method which has been described as a temporary means of enhancing the delivery of macromolecules such as albumin, liposomes and other nanomedicines is by inducing tumor hyperthermia.[18-23] Under conditions of elevated temperatures and increased blood perfusion, it has been found that the tumor microvascular permeability and therefore EPR effect is significantly increased.[24] This is believed to be a result of cytoskeletal disaggregation in endothelial cells leading to further expansion of the fenestrae that already surround them.[25-28] Unfortunately, current techniques for inducing tumor hyperthermia such as radiofrequency ablation or hyperthermic intraperitoneal perfusion are restrictive in their capacity to selectively deliver heat towards cancerous tissue.[29]

More recently several laboratories have initiated hyperthermia by taking advantage of unique nanoscale events that occur when light is absorbed by plasmonic gold nanostructures. In brief, when light with a wavelength that matches the tunable surface plasmon resonance (SPR) of gold nanostructures interacts with these particles, coherent oscillations of electrons in the conduction band allow the light to be absorbed and photothermal conversion to occur.[30] When such particles are delivered to cancerous tissue by EPR, this phenomenon can be used as a tool to selectively induce

hyperthermia.[31] Such plasmonic photothermal therapy has been used to achieve tumor selective temperatures varying from 50°C to over 70°C, well above the threshold required for vascular damage.[32-36] Previously, it has been shown that this heat delivery technique at reduced temperatures (42-45°C) can be applied to selectively increase the perfusion and permeability of the tumor vasculature and hence the delivery of nanomedicines during laser radiation.[37-41] In this way, the delivery of nanoworms, liposomes and micelles have shown to be recruited to the treatment site and sensitized for targeting and drug release.[39-41]

In this chapter, the aim is to remotely modify the tumor microenvironment with laser mediated plasmonic photothermal therapy to increase both passive and active polymeric drug targeting. This technique is used immediately following injection of HPMA copolymers to augment EPR at the treatment site and drive their delivery into the tumor interstitial space while the copolymer is at its peak concentration in the blood. Once at the tumor site, the natural response of tissue to heat shock is taken advantage of by conjugation of a targeting ligand which binds to heat shock proteins (HSPs). This is because the expression of HSPs is significantly increased following exposure to heat shock.[27] In this way, the targetability of these cancer cells can be elevated so that the copolymer is retained in the tumor and taken up by cells to a higher extent.

A technique is introduced wherein a laser can be used to direct the localization and retention of polymer therapeutics in solid tumors. With this technique, it is believed that polymer-drug conjugates can be administered to patients by clinicians and efficiently guided towards the location of disease to maximize treatment efficacy, while minimizing toxicity.

4.2 Materials and methods

4.2.1 Synthesis and characterization of HPMA copolymer-drug conjugates

The comonomers were synthesized as described previously.[42, 43] (See also Chapter 3) Precursor copolymer conjugates containing reactive carboxyl groups (thiazolidine-2-thione) were prepared by free radical copolymerization in methanol using azobisisobutryonitrile (AIBN) as initiator (Figure 4.1). The concentrations of monomers and AIBN during polymerization were maintained at 17.5% and 0.5% (w/v) to control molecular weight. For the conjugates containing drug, aminohexylgeldanamycin (AHGDM) was conjugated to the *N*-methacryloyl-glycylphenylalanylleucylglycine (MA-GFLG-OH) lysosomally cleavable linker prior to copolymerization. Finally, copolymerization with the monomer *N*-methacryloyl-tyrosinamide (MA-Tyr-$CONH_2$) allows for radiolabeling of the conjugates or 5-[3-(methacryloyl-aminopropyl)thioureidyl] fluorescein (APMA-FITC) for fluorescent tracking of cellular uptake in cells. Heat shock targeted conjugates were obtained by aminolysis of precursor copolymers with the GRP78 targeting peptide (WIFPWIQL), synthesized by solid phase. Untargeted conjugates were obtained by hydrolysis of precursor copolymers in the presence of aqueous sodium hydroxide. Copolymer conjugates were purified by dialysis against deionized water, lyophilized, and stored at -20°C. Weight average molecular weight (M_w), number average molecular weight (M_n), and polydispersity (M_w/M_n) were estimated by size exclusion chromatography (SEC) using HPMA homopolymer fractions of known molecular weight. The amount of the anticancer agent AHGDM present was quantified by UV spectrometry, and the amount of the GRP78 targeting peptide was quantified by amino acid analysis (HPLC method).

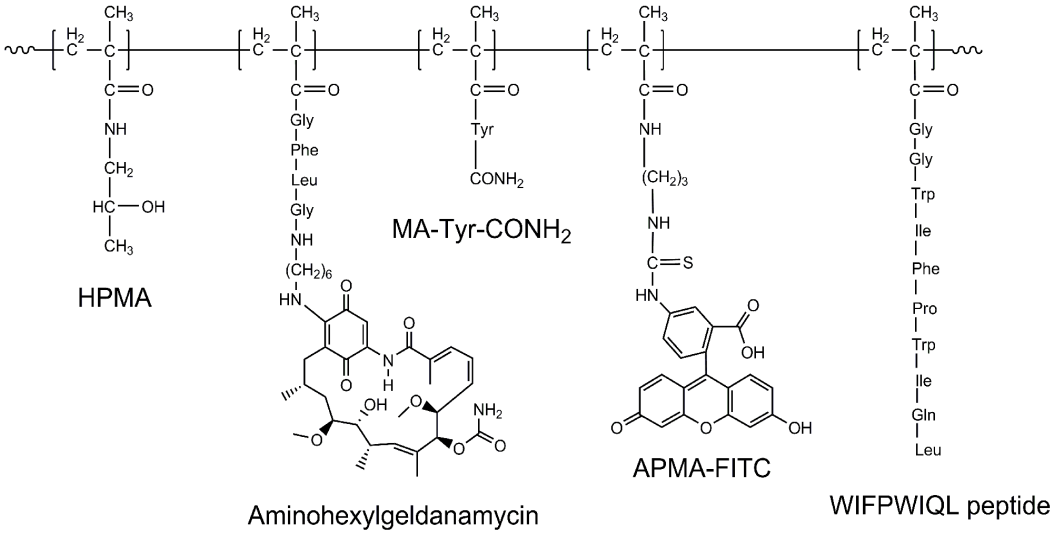

Figure 4.1. HPMA copolymer schematic. Representative HPMA copolymer with all monomers used in the study listed.

^{125}Iodine was conjugated to tyrosine residues to obtain radiolabeled copolymers using the Iodogen method with slight modification.[44] Each copolymer (2 mg) and 0.5 mCi Na-^{125}I were dissolved in 0.5M NaH_2PO_4 pH 7.0 and incubated at room temperature in Iodogen tubes for 10 min. Free radiolabel was removed by dialysis against saline and verified by SEC.

4.2.2 *In vitro* cell surface GRP78 expression

For all *in vitro* experiments, DU145 cells were cultured at 37°C in a humidified atmosphere of 5% CO_2 in Eagle's Minimum Essential Medium with Earle's Balanced Salt Solution (ATCC) supplemented with 10 % (v/v) fetal bovine serum (FBS) (Thermo Scientific HyClone, Logan, UT). Cell surface GRP78 expression was evaluated as a function of time by flow cytometry. Human prostate cancer DU145 cells were subjected to heat shock (43°C / 30 min incubation) or control (37°C, continuous incubation). At each time point, cells were removed and incubated with an anti-GRP78 rabbit polyclonal antibody (Enzo Life Sciences, Farmingdale, NY) followed by incubation with a goat anti-rabbit phycoerythrin (PE) conjugated secondary antibody (Santa Cruz Biotechnology, Santa Cruz, CA). Cells were then fixed in 1% formaldehyde in phosphate buffered saline (PBS) and analyzed by flow cytometry. Incubation with secondary antibody alone served as an additional control for non-specific binding.

4.2.3 Cellular uptake of FITC-labeled conjugates

Cellular uptake as a function of time was quantified by flow cytometry. DU145 cells were exposed to heat shock (43°C / 30 min incubation) or control (37°C, continuous incubation). Eight hrs post heat shock, cells were incubated with 0.1 mg/mL of heat shock targeted or untargeted FITC labeled conjugates. At each time point, cells were washed, harvested, fixed in 1% formaldehyde in PBS, and analyzed by flow cytometry using FACScan flow cytometer (Becton Dickinson, Franklin Lakes, NJ).

4.2.4 *In vitro* cytotoxicity

DU145 cells in 96 well plates (3×10^3 cells per well) were exposed to heat shock (43°C / 30 min incubation) or control (37°C, continuous incubation). Eight hours post heat shock, cells were treated for 4 hrs with increasing concentrations of heat shock targeted or untargeted conjugates or AHGDM free drug controls. Following treatments, cells were washed with PBS and growth media replaced. After 72 hrs total incubation, cell viability was assessed using a 2-(2-methoxy-4-nitrophenyl)-3-(4-nitrophenyl)-5-(2,4-disulfophenyl)-2H-tetrazolium monosodium salt (WST-8) cell viability assay (Dojindo Molecular Technologies, Rockville, MD). IC_{50} values were calculated by nonlinear regression and thermal enhancement defined as IC_{50} observed for control / IC_{50} observed following heat shock.

4.2.5 *In vivo* induction of heat shock via photothermal therapy[¥]

Anesthetized 6- to 12-week old athymic nu/nu mice were subcutaneously injected with 10^7 DU145 cells on each flank and tumors were allowed to grow until

approximately 5-7 mm in diameter. Animals were then administered PEGylated gold nanorods, synthesized as previously described,[38] (9.6 mg/kg) via tail vein injection. After 48 hrs, mice were anesthetized, and tumors were swabbed with 50% propylene glycol to enhance laser penetration depth.[45] Tumors on the right flank only were then radiated for 10 min using an 808 nm fiber coupled laser diode (Oclaro Inc., San Jose, CA) with collimating lens (Thorlabs, Newton, NJ). Intratumoral temperature was monitored using a 33 gauge needle thermocouple (Omega, Stamford, CT) and tumor temperature was maintained between 42°C and 43°C. Tumors on the left flank served as internal controls.

4.2.6 *In vivo* GRP78 expression in tumors following photothermal therapy[¥]

Eight hours following induction of heat shock, mice were euthanized and tumors on the right (laser) and left (control) flanks were removed and snap frozen in liquid nitrogen. Immunohistochemical analysis of GRP78 expression was then performed on 4-micron thick sections of formalin-fixed, paraffin-embedded tissues using a goat polyclonal anti-GRP78 antibody (Santa Cruz Biotechnology, Santa Cruz, CA) and a polyclonal rabbit anti-goat biotinylated antibody. Positive signal was visualized using a streptavidin-HRP system, utilizing DAB (3-3' diaminobenzidine) as the chromogen. The sections were counterstained with hematoxylin. The sections were placed in iodine to remove any precipitates, and then dipped in sodium thiosulfate to clear the iodine. The sections were dehydrated in graded alcohols (70%, 95% x2 and 100% x2), cleared in xylene, coverslipped and imaged.

4.2.7 Tumor accumulation and biodistribution[¥]

Prior to induction of heat shock via photothermal therapy, mice were intravenously administered via the tail vein a single bolus dose of 50 mg/kg ^{125}I radiolabeled conjugates (untargeted or heat shock targeted). At each time point, mice were euthanized, blood immediately collected, followed by blood perfusion with saline. Tumors and major organs were then collected and analyzed by gamma counting. Tumor volumes were estimated as length × width × $\pi/6$. Percent injected dose per gram of blood/tissue (% ID / g) was calculated and expressed as a function of time.

4.3 Results and discussion[¥]

To begin, the HPMA copolymers were synthesized via free radical polymerization and characterized (Figure 4.1, Table 4.1). Molecular weight for the conjugates varied from 60 – 80 kDa, and was maintained slightly above renal threshold to take advantage of the EPR effect. For drug containing conjugates, AHGDM content was approximately 15% by weight. To generate a targetable HPMA copolymer, the WIFPWIQL peptide was conjugated to the HPMA backbone via aminolysis of thiazolidine-2-thione side chains, resulting in copolymers with approximately 20% peptide content by weight. This peptide was chosen due to its known affinity to glucose-regulated protein-78 (GRP78), a member of the HSP70 family of proteins.[46] Previously, we have shown that this receptor-ligand approach can be used to effectively deliver HPMA copolymer-drug conjugates to prostate cancer cells.[42] Full details regarding the feed compositions and resulting polymer characteristics are given in Table 4.1.

Table 4.1. Physicochemical characteristics of HPMA copolymers.

Polymer	*Feed composition (mol %)*					*Polymer Characteristics*			
	HPMA	MA-GG-TT	MA-GFLG-AHGDM	MA-Tyr-$CONH_2$	APMA-FITC	Apparent Mw (kDa)	M_w/M_n	AHGDM content mol% (wt%)	WIFPWIQL content mol% (wt%)
HPMA-(GFLG-AHGDM)	88	5	5	2	0	72.6	1.6	4.9 (16.1)	-
HPMA-(GFLG-AHGDM)-WIFPWIQL	88	5	5	2	0	75.8	1.3	5.6 (14.5)	4.5 (19.9)
HPMA	93	5	0	2	0	83.9	1.6	-	-
HPMA-WIFPWIQL	93	5	0	2	0	72.4	1.6	-	3.8 (20.9)
HPMA-FITC	93	5	0	0	2	62.4	1.4	-	-
HPMA-FITC-WIFPWIQL	93	5	0	0	2	64.4	1.4	-	3.4 (18.0)

Weight average molecular weight (M_w) and polydispersity (M_w/M_n) were estimated by size exclusion chromatography (SEC). The amount of the anticancer agent AHGDM present was quantified by UV spectrometry, and the amount of the GRP78 targeting peptide was quantified by amino acid analysis (HPLC method).

To determine if heat shock could be used to regulate the targetability of these conjugates, the prostate cancer cell surface expression of GRP78 was measured as a function of time after heat shock (43°C, 30 min). This was done by incubation with an anti-GRP78 rabbit polyclonal antibody followed by evaluation of expression by flow cytometry. Indeed, it was observed that the receptor's expression increases after heat shock with maximum expression between 8-12 hrs after heat shock (Figure 4.2).

Next, fluorescently labeled HPMA copolymers with and without the heat shock targeting peptide were introduced to cells eight hours postheat shock (43°C, 30 min) or control (37°C, continuous incubation). Quantification by flow cytometry (selected time points, Figure 4.3) of uptake in cells indicates significantly increased binding and uptake of heat shock targeted conjugates which is in agreement with our previous results.[42] This observation was much more pronounced (3-fold increase), when the cells were first treated with heat shock due to increased receptor expression (Figure 4.3).

New conjugates containing the anticancer drug derivative AHGDM via a degradable linker were then prepared to determine if this increased uptake can be correlated with increased activity. Cells were heat shock treated as before, then exposed to the HPMA copolymer-AHGDM conjugates for 4 hrs and evaluated for growth inhibition. A short period of incubation (4 hrs) was chosen during the period of maximum GRP78 expression (8-12 hrs after hyperthermia, see Figure 4.2) to explicitly determine the effect of increased GRP78 expression on cytotoxicity. In all groups (free

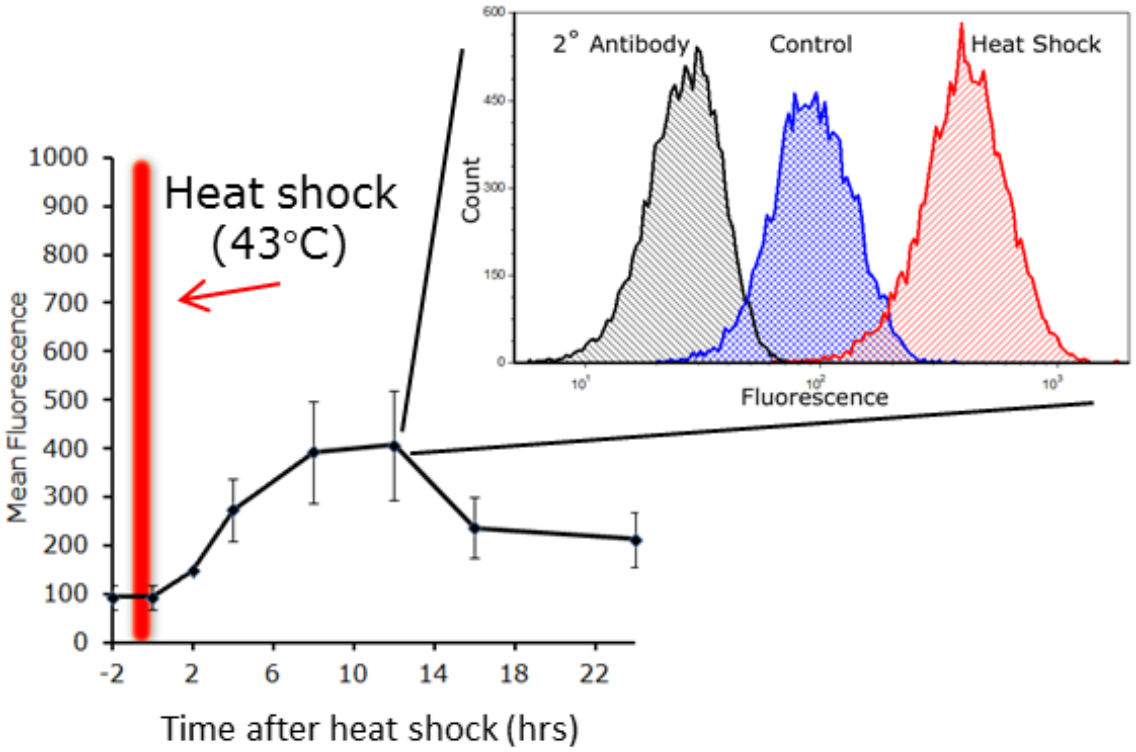

Figure 4.2. Induction of cell surface expressed GRP78 in DU145 cells following exposure to heat shock. After induction of heat shock (43°C, 30 min incubation), the cell surface expression of the heat shock protein GRP78 in DU145 prostate cancer cells was quantified by flow cytometry with peak expression observed at 12 hrs.

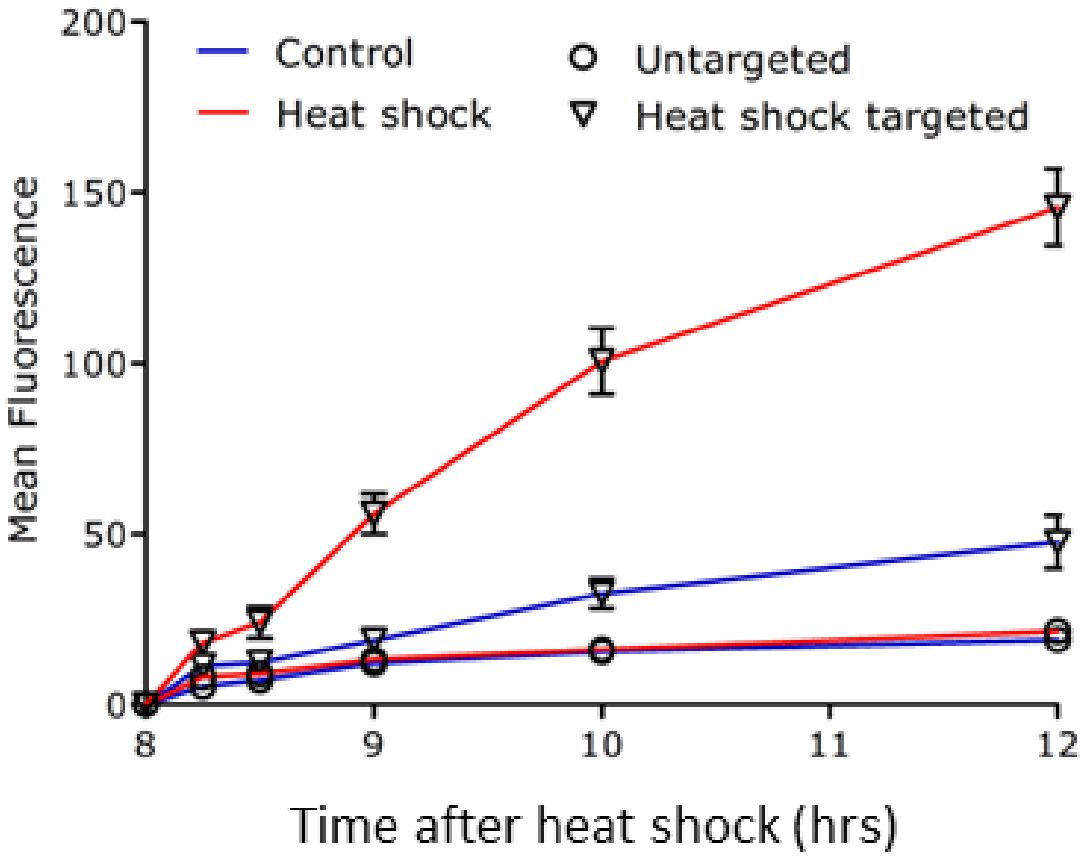

Figure 4.3. Cellular uptake kinetics of FITC labeled HPMA copolymers in DU145 cells following exposure to heat shock. Cells were exposed to FITC labeled HPMA copolymers between 8 and 12 hrs after heat shock (43°C, 30 min incubation). Quantification of cell association was performed by flow cytometry. Prior treatment with heat shock resulted in significantly increased uptake of heat shock targeted conjugates.

drug, untargeted, and heat shock targeted), treatment with heat shock resulted in greater activity (Figure 4.4). While this effect was only slight for free drug and untargeted conjugates, a 4-fold thermal enhancement in conjugate activity was observed for those which were heat shock targeted (Figure 4.4).

Next, the overall hypothesis of enhancing the delivery of these conjugates to laser radiated tissue was tested in mice bearing prostate tumors. Mice bearing two tumors, one on each flank, were intravenously (i.v.) administered PEG coated gold nanorods and allowed 48 hrs for the particles to accumulate in the tumors via EPR (Figure 4.5).[47] Radiolabeled conjugates (heat shock targeted and untargeted) were then administered i.v. followed immediately by laser radiation of the right tumor only for 10 min. During laser radiation the temperature in the right tumor was maintained between 42-43°C by controlling laser power such that only moderate hyperthermia was induced to avoid vascular collapse at higher temperatures.[48] It is important to note here that by directing the laser at the right tumor only, it is possible to directly compare the delivery of polymeric conjugates to tumors in the presence and absence of laser radiation in the same animal.

While the increased HSP expression profile of prostate cancer cells following heat shock was confirmed *in vitro*, it was necessary to confirm this phenomenon *in vivo*. The left (control) and right (laser treated) tumors were evaluated for GRP78 expression by immunohistochemistry. Heat shock treatment of the right tumors by laser resulted in increased HSP expression compared to the untreated tumors (Figure 4.6).

Quantification of the concentrations in tumors and major organs of ^{125}I-radiolabeled polymeric conjugates was evaluated *in vivo* in combination with PPTT, to

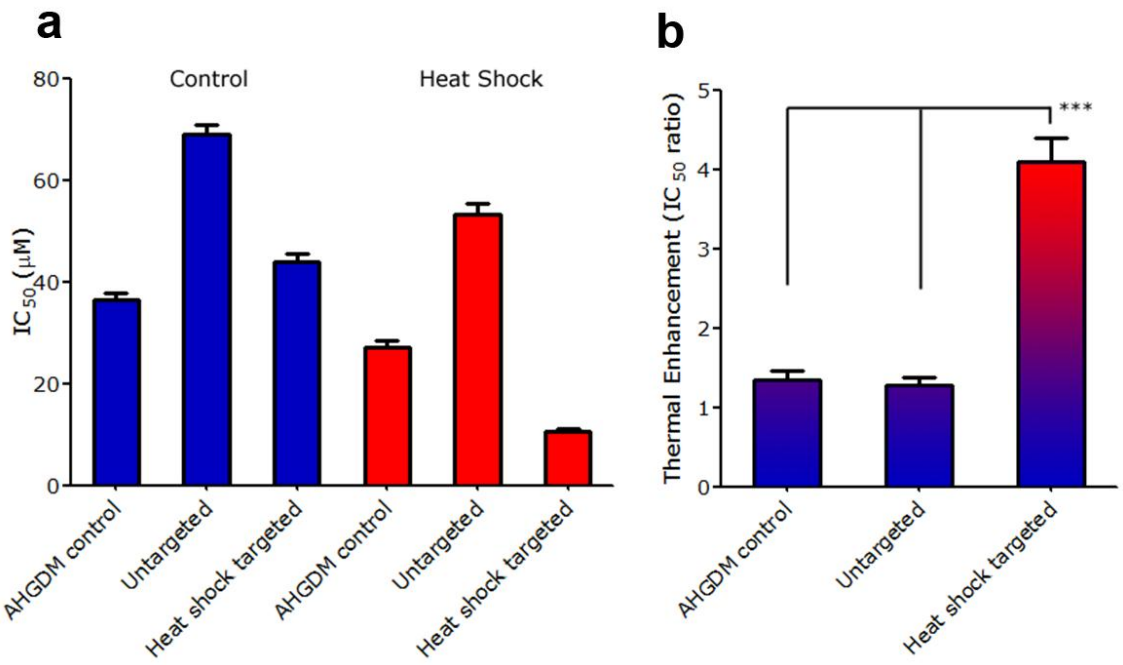

Figure 4.4. Cytotoxicity of AHGDM bearing copolymers following exposure to heat shock. Polymer-drug conjugates anti-cancer activities (a) and related thermal enhancements of toxicity with DU145 human prostate cancer cells (b). Cell were exposed to treatments for 4 hrs during the period of maximum heat shock protein expression (8-12 hrs after heat shock). Treatment with heat shock caused increased toxicity to cells (lowered IC_{50}, greater thermal enhancement), particularly for those which are heat shock targeted.

***Indicates a statistically significant difference ($p < 0.001$) by one-way analysis of variance (ANOVA). Error bars represented as ± standard deviation.

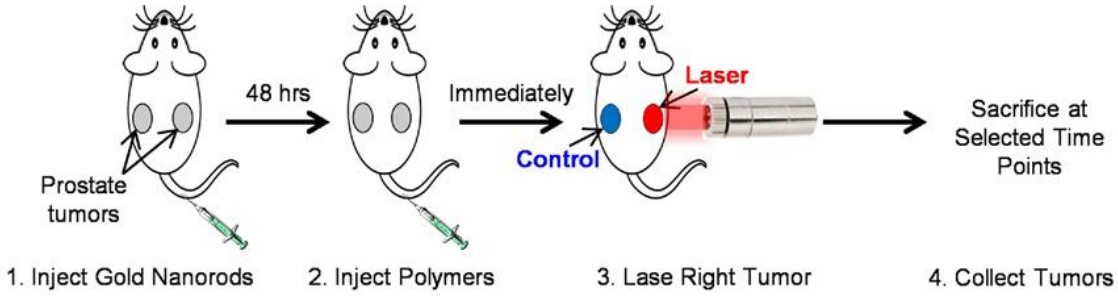

Figure 4.5. Schematic of laser guided delivery of polymeric conjugates in mice. Nu/nu mice bearing subcutaneous DU145 tumor xenografts were intravenously administered PEGylated GNRs. After 48 hrs, ^{125}I radiolabeled HPMA copolymers were intravenously administered, directly followed by laser radiation to the right tumor only (left tumor served as internal control). Tumor accumulation at selected time points was then quantified by gamma counting.

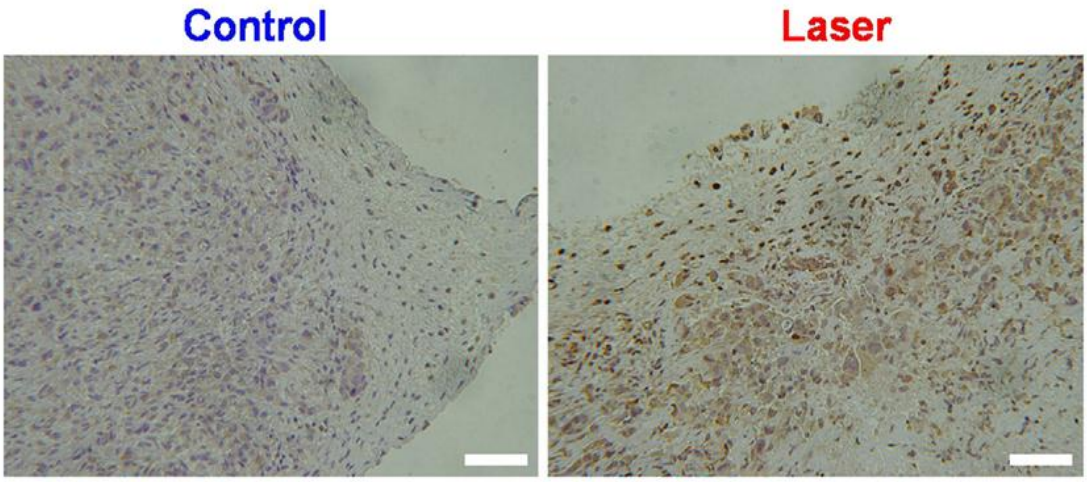

Figure 4.6. ***In vivo*** **expression of GRP78 following PPTT.** Cell expression of heat shock protein GRP78 (red color) in prostate tumors with or without laser treatment. Scale bar, 50 μm. Tumors that have been laser radiated have higher expression of GRP78.

determine the localization of the drug carriers as a function of time (Figures 4.7 and 4.8). Following administration of the conjugates, a comparison of the laser radiated and control tumors 15 min and 4 hrs following laser treatment indicates that a 2-to-3 fold increased burst accumulation occurred in the laser radiated tumors (Figure 4.7). This observation indicates that the treatment of tumors with heat causes increased tumor blood flow and augments the EPR effect by increasing vascular pore size.[20, 21, 38] This burst accumulation was not maintained after 4 hrs for the untargeted conjugates. As intended in the treatment design, the heat shock targeted conjugates were retained in the radiated tumor up to 12 hrs after which elimination began to occur. This observation is supported by GRP78 expression data (Figure 4.2), which shows that HSP expression is reduced after 12 hrs. When this data is expressed as the total area under the tumor concentration vs. time curve (AUC), a 4-fold increase in exposure is observed for tumors which have been laser radiated (Figure 4.7).

The biodistribution of the radiolabeled conjugates in major organs was also evaluated (Figure 4.8). Similar concentrations in the blood were observed over 72 hrs for untargeted and heat shock targeted conjugates. However, significant accumulation was observed for the heat shock targeted conjugate in the liver, spleen, and kidneys. It is speculated that this nonspecific accumulation is most likely due to the increased hydrophobic nature of the heat shock targeted conjugate due to the presence of the hydrophobic WIFPWIQL peptide (cLogP = 3.9). This increased hydrophobicity can potentiate interactions with biological tissues and increase uptake in reticuloendothelial system (RES) organs.[49] It is anticipated that such nonspecific interactions can be minimized by reducing the hydrophobic nature of the conjugates by either reducing the

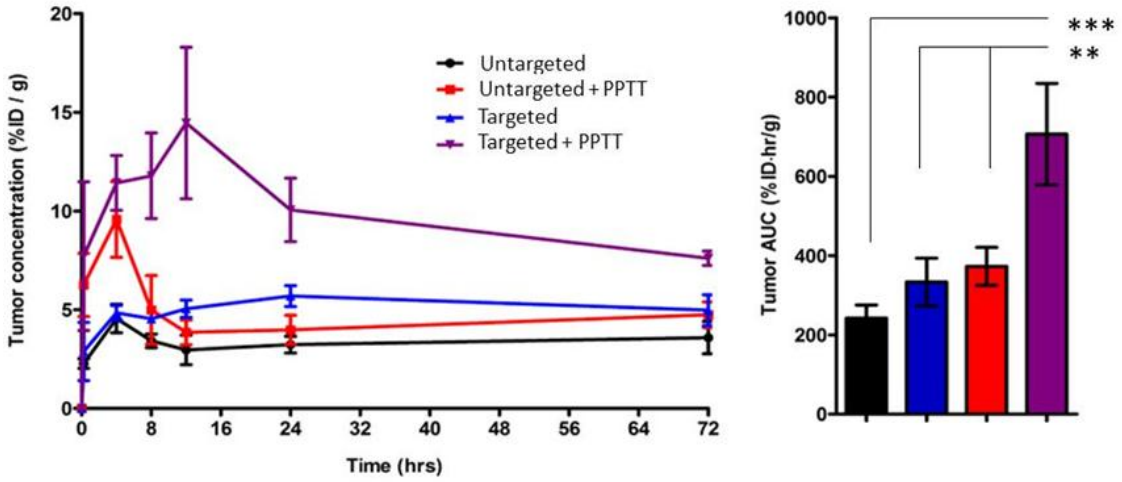

Figure 4.7. Tumor accumulation of HPMA copolymers following PPTT. Tumor accumulation of radiolabeled polymers (untargeted and heat shock targeted) with or without laser treatment (left). Laser radiation results in a burst accumulation (0—4 hrs), which is only maintained (> 24 hrs) for the heat shock targeted polymers due to increased GRP78 expression. Total area under the tumor concentration vs. time curve (AUC) indicates a 4-fold increase in exposure to polymers (right).

** and *** indicates a statistically significant difference ($p < 0.01$ and $p < 0.001$ respectively) by one-way analysis of variance (ANOVA).

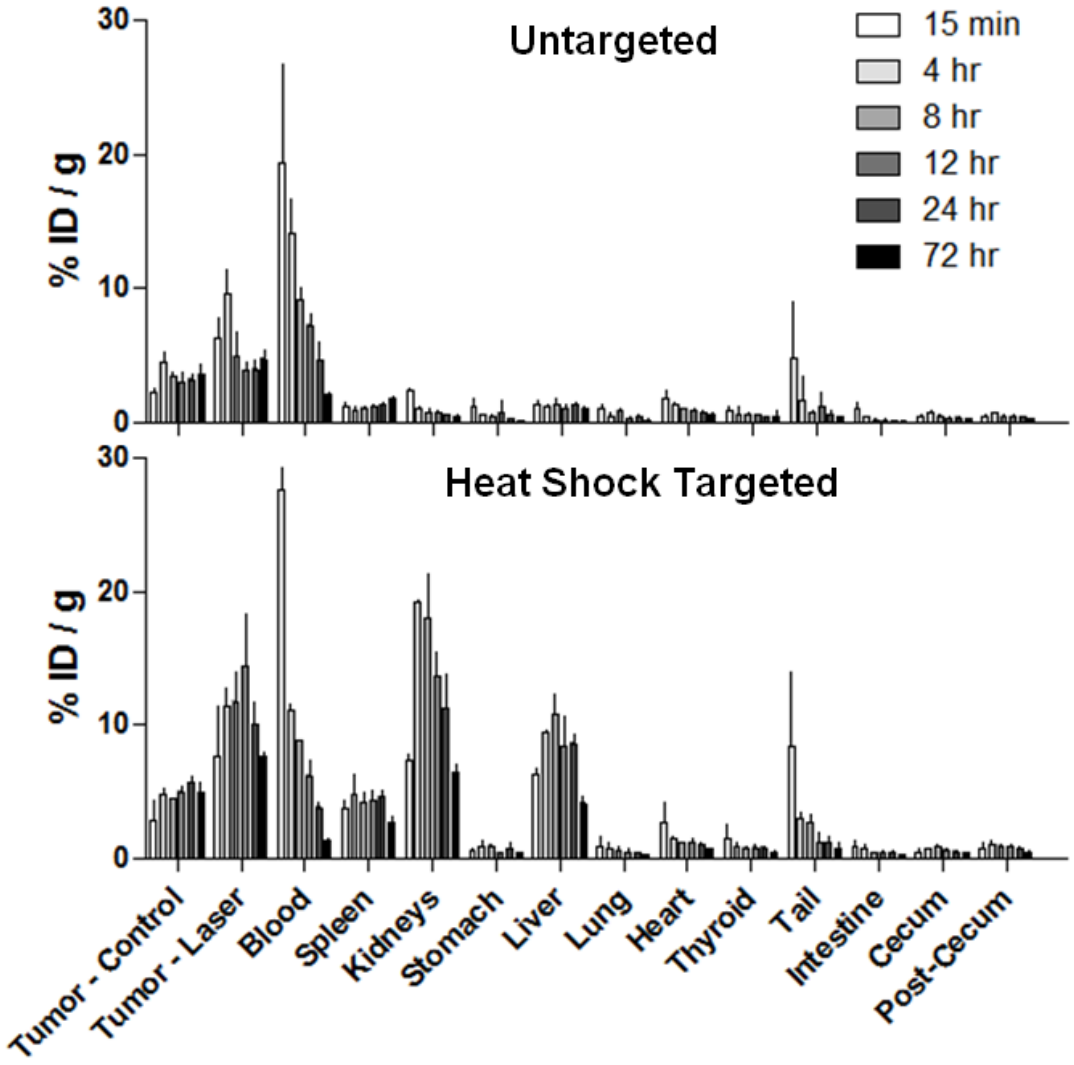

Figure 4.8. Biodistribution of radiolabeled (^{125}I) HPMA copolymers. Data expressed as mean ± standard deviation.

targeting peptide content or utilizing more hydrophilic targeting moieties. Based on these observations, subsequent studies (see Chapter 5) utilized untargeted conjugates bearing scrambled targeting peptide sequences to minimize differences in physicochemical properties and reduce these confounding effects.

In this study, there were some additional controls whose results are not shown due to limited space. For example, some animals did not receive gold nanorods but received laser treatment to see if the laser alone would enhance conjugate delivery. During laser radiation minimal tumor heating and no delivery enhancement was observed. These results corroborate with our previous findings.[38] Also, HPMA copolymers were administered with and without prior administration of gold nanorods to determine if the presence of gold nanorods would impact the delivery of HPMA copolymers. As expected, the presence or absence of gold nanorods did not influence the tumor accumulation of the polymer conjugates.

After sacrifice of the animals at selected time points following laser radiation, the entire biodistribution of the radiolabeled HPMA copolymers was evaluated (Figure 4.8). The size of the conjugates (~70-80 kDa) was chosen for this study so that the polymers would circulate for an extended period of time.[50] When evaluating the blood clearance and biodistribution for the untargeted and heat shock targeted conjugates, a few interesting observations are made. First, while both conjugates have a very similar blood clearance rate, the ultimate fate of the polymers was very different. Though the untargeted conjugates were above renal clearance threshold (~45 kDa), the majority of the radioactivity was not recovered in the animals. After gamma counting the cage bedding material (data not shown), it was determined that the majority of the conjugates

were excreted in the urine. This is in contrast to the heat shock targeted conjugates which showed nonspecific accumulation in the kidneys, spleen and liver in addition to urinary excretion. The difference between these two groups (untargeted vs. heat shock targeted) may be explained in two ways. First, an inherent, baseline expression of GRP78 in various cell types may exist which promotes cellular binding and uptake in these organs. Second, presence of the hydrophobic peptide WIFPWIQL in the heat shock targeted conjugates increases their hydrophobicity which can lead to a greater degree of interaction with biological membranes. These elevated interactions can therefore result in nonspecific accumulation in these organs. In either case, the presence of the peptide resulted in undesirable biodistribution. In Appendix C, the biodistribution of a more hydrophilic GRP78 targeted peptide (WDLAWMFRLPVG) is compared with the peptide utilized in this Chapter (WIFPWIQL). Use of the more hydrophilic peptide reduced this undesired distribution to healthy organs while maintaining enhanced delivery to tumors (see Appendix C). This peptide was therefore utilized in subsequent studies (Chapter 5).

4.4 Conclusion[¥]

In summary, it is demonstrated that it is possible to direct the delivery of targeted polymer therapeutics using plasmonic photothermal therapy by exploiting the physiologic response of tumors to heat. These findings help overcome one of the limitations of polymer therapeutics which is poor tumor accumulation. By using laser directed application of heat via gold nanorods, a burst accumulation of the therapeutics in the region of interest is possible while they are at their highest concentration in the

blood. By incorporation of a heat shock targeting ligand in the copolymer design, high concentration can be maintained as the targeting receptors become increasingly available following heat induction. Ultimately, in a clinical setting, it is anticipated that clinicians will value this additional tool to help guide drug delivery to solid tumors.

4.5 References[¥]

1. A.J. Gormley[*], N. Larson[*], S. Sadekar, R. Robinson, A. Ray, and H. Ghandehari. ([*]first co-authors). Guided delivery of polymer therapeutics using plasmonic photothermal therapy. Nano Today. 7:158-167 (2012).

2. D. Peer, J.M. Karp, S. Hong, O.C. Farokhzad, R. Margalit, and R. Langer. Nanocarriers as an emerging platform for cancer therapy. Nat Nanotechnol. 2:751-760 (2007).

3. M.J. Vicent, H. Ringsdorf, and R. Duncan. Polymer therapeutics: Clinical applications and challenges for development. Adv Drug Deliv Rev. 61:1117-1120 (2009).

4. S.K. Hobbs, W.L. Monsky, F. Yuan, W.G. Roberts, L. Griffith, V.P. Torchilin, and R.K. Jain. Regulation of transport pathways in tumor vessels: role of tumor type and microenvironment. Proc Natl Acad Sci USA. 95:4607-4612 (1998).

5. Y. Matsumura and H. Maeda. A new concept for macromolecular therapeutics in cancer chemotherapy: mechanism of tumoritropic accumulation of proteins and the antitumor agent smancs. Cancer Res. 46:6387-6392 (1986).

6. H. Maeda, J. Wu, T. Sawa, Y. Matsumura, and K. Hori. Tumor vascular permeability and the EPR effect in macromolecular therapeutics: a review. J Control Release. 65:271-284 (2000).

7. T. Lammers, W. Hennink, and G. Storm. Tumour-targeted nanomedicines: principles and practice. Br J Cancer. 99:392-397 (2008).

8. D.B. Pike and H. Ghandehari. HPMA copolymer-cyclic RGD conjugates for tumor targeting. Adv Drug Deliv Rev. 62:167-183 (2009).

9. R. Duncan. The dawning era of polymer therapeutics. Nat Rev Drug Discov. 2:347-360 (2003).

10. J. Kopecek and P. Kopecková. HPMA copolymers: origins, early developments, present, and future. Adv Drug Deliv Rev. 62:122-149 (2010).

11. R. Duncan. Polymer conjugates as anticancer nanomedicines. Nat Rev Cancer. 6:688-701 (2006).

12. G. Oberdörster, E. Oberdörster, and J. Oberdörster. Nanotoxicology: an emerging discipline evolving from studies of ultrafine particles. Environ Health Perspect. 113:823-839 (2005).

13. D.W. Grainger. Nanotoxicity assessment: all small talk? Adv Drug Deliv Rev. 61:419 (2009).

14. G. Oberdörster. Safety assessment for nanotechnology and nanomedicine: concepts of nanotoxicology. J Intern Med. 267:89-105 (2010).

15. W.R. Sanhai, J.H. Sakamoto, R. Canady, and M. Ferrari. Seven challenges for nanomedicine. Nat Nanotechnol. 3:242-244 (2008).

16. L. Seymour, Y. Miyamoto, H. Maeda, M. Brereton, J. Strohalm, K. Ulbrich, and R. Duncan. Influence of molecular weight on passive tumour accumulation of a soluble macromolecular drug carrier. Eur J Cancer. 31:766-770 (1995).

17. R. Duncan and R. Gaspar. Nanomedicine (s) under the microscope. Mol Pharm. 8:2101-2141 (2011).

18. Q. Chen, A. Krol, A. Wright, D. Needham, M. Dewhirst, and F. Yuan. Tumor microvascular permeability is a key determinant for antivascular effects of doxorubicin encapsulated in a temperature sensitive liposome. Int J Hyperthermia. 24:475-482 (2008).

19. M. Gnant, L. Noll, R. Terrill, P. Wu, A. Berger, H. Nguyen, T. Lans, B. Flynn, S. Libutti, and D. Bartlett. Isolated hepatic perfusion for lapine liver metastases: impact of hyperthermia on permeability of tumor neovasculature. Surgery. 126:890-899 (1999).

20. G. Kong, R.D. Braun, and M.W. Dewhirst. Hyperthermia enables tumor-specific nanoparticle delivery: effect of particle size. Cancer Res. 60:4440-4445 (2000).

21. G. Kong, R.D. Braun, and M.W. Dewhirst. Characterization of the effect of hyperthermia on nanoparticle extravasation from tumor vasculature. Cancer Res. 61:3027-3032 (2001).

22. A.T. Lefor, S. Makohon, and N.B. Ackerman. The effects of hyperthermia on vascular permeability in experimental liver metastasis. J Surg Oncol. 28:297-300 (1985).

23. M.L. Matteucci, G. Anyarambhatla, G. Rosner, C. Azuma, P.E. Fisher, M.W. Dewhirst, D. Needham, and D.E. Thrall. Hyperthermia increases accumulation of technetium-99m-labeled liposomes in feline sarcomas. Clin Cancer Res. 6:3748-3755 (2000).

24. K. Fujiwara and T. Watanabe. Effects of hyperthermia, radiotherapy and thermoradiotherapy on tumor microvascular permeability. Pathol Int. 40:79-84 (2008).

25. B. Chen, M. Zhou, and L. Xu. Study of vascular endothelial cell morphology during hyperthermia. J Therm Biol. 30:111-117 (2005).

26. L. Fajardo, A. Schreiber, N. Kelly, and G. Hahn. Thermal sensitivity of endothelial cells. Radiat Res. 103:276-285 (1985).

27. B. Hildebrandt, P. Wust, O. Ahlers, A. Dieing, G. Sreenivasa, T. Kerner, R. Felix, and H. Riess. The cellular and molecular basis of hyperthermia. Crit Rev Oncol Hematol. 43:33-56 (2002).

28. L. Xu, B. Chen, and M. Zhou. Change of individual vascular endothelial calcium during hyperthermia. J Therm Biol. 31:302-306 (2006).

29. P. Wust, B. Hildebrandt, G. Sreenivasa, B. Rau, J. Gellermann, H. Riess, R. Felix, and P.M. Schlag. Hyperthermia in combined treatment of cancer. Lancet Oncol. 3:487-497 (2002).

30. S. Link and M.A. El-Sayed. Shape and size dependence of radiative, non-radiative and photothermal properties of gold nanocrystals. Int Rev Phys Chem. 19:409-453 (2000).

31. X. Huang, P.K. Jain, I.H. El-Sayed, and M.A. El-Sayed. Plasmonic photothermal therapy (PPTT) using gold nanoparticles. Lasers Med Sci. 23:217-228 (2008).

32. E.B. Dickerson, E.C. Dreaden, X. Huang, I.H. El-Sayed, H. Chu, S. Pushpanketh, J.F. McDonald, and M.A. El-Sayed. Gold nanorod assisted near-infrared plasmonic photothermal therapy (PPTT) of squamous cell carcinoma in mice. Cancer Lett. 269:57-66 (2008).

33. L.R. Hirsch, R.J. Stafford, J.A. Bankson, S.R. Sershen, B. Rivera, R.E. Price, J.D. Hazle, N.J. Halas, and J.L. West. Nanoshell-mediated near-infrared thermal therapy of tumors under magnetic resonance guidance. Proc Natl Acad Sci USA. 100:13549-13554 (2003).

34. D.P. O'Neal, L.R. Hirsch, N.J. Halas, J.D. Payne, and J.L. West. Photo-thermal tumor ablation in mice using near infrared-absorbing nanoparticles. Cancer Lett. 209:171-176 (2004).

35. J.M. Stern, J. Stanfield, W. Kabbani, J.T. Hsieh, and J.A. Cadeddu. Selective prostate cancer thermal ablation with laser activated gold nanoshells. J Urol. 179:748-753 (2008).

36. G. von Maltzahn, J.H. Park, A. Agrawal, N.K. Bandaru, S.K. Das, M.J. Sailor, and S.N. Bhatia. Computationally guided photothermal tumor therapy using long-circulating gold nanorod antennas. Cancer Res. 69:3892-3900 (2009).

37. P. Diagaradjane, A. Shetty, J.C. Wang, A.M. Elliott, J. Schwartz, S. Shentu, H.C. Park, A. Deorukhkar, R.J. Stafford, and S.H. Cho. Modulation of in vivo tumor radiation response via gold nanoshell-mediated vascular-focused hyperthermia: characterizing an integrated antihypoxic and localized vascular disrupting targeting strategy. Nano Lett. 8:1492-1500 (2008).

38. A.J. Gormley, K. Greish, A. Ray, R. Robinson, J.A. Gustafson, and H. Ghandehari. Gold nanorod mediated plasmonic photothermal therapy: A tool to enhance macromolecular delivery. Int J Pharm. 415:315-318 (2011).

39. J.H. Park, G.v. Maltzahn, L.L. Ong, A. Centrone, T.A. Hatton, E. Ruoslahti, S.N. Bhatia, and M.J. Sailor. Cooperative nanoparticles for tumor detection and photothermally triggered drug delivery. Adv Mater. 22:880-885 (2010).

40. J.H. Park, G. von Maltzahn, M.J. Xu, V. Fogal, V.R. Kotamraju, E. Ruoslahti, S.N. Bhatia, and M.J. Sailor. Cooperative nanomaterial system to sensitize, target, and treat tumors. Proc Natl Acad Sci USA. 107:981-986 (2010).

41. G. Von Maltzahn, J.H. Park, K.Y. Lin, N. Singh, C. Schwöppe, R. Mesters, W.E. Berdel, E. Ruoslahti, M.J. Sailor, and S.N. Bhatia. Nanoparticles that communicate in vivo to amplify tumour targeting. Nat Mater. 10:545-552 (2011).

42. N. Larson, A. Ray, A. Malugin, D.B. Pike, and H. Ghandehari. HPMA copolymer-aminohexylgeldanamycin conjugates targeting cell surface expressed GRP78 in prostate cancer. Pharm Res. 27:2683-2693 (2010).

43. V. Omelyanenko, P. Kopecková, C. Gentry, and J. Kopecek. Targetable HPMA copolymer-adriamycin conjugates. Recognition, internalization, and subcellular fate. J Control Release. 53:25-37 (1998).

44. J.M. Walker. The protein protocols handbook, Humana Press Inc, Totowa, New Jersey, 1996.

45. R.K. Wang and V.V. Tuchin. Enhance light penetration in tissue for high resolution optical imaging techniques by the use of biocompatible chemical agents. J X Ray Sci Tech. 10:167-176 (2002).

46. M.A. Arap, J. Lahdenranta, P.J. Mintz, A. Hajitou, Á. Sarkis, W. Arap, and R. Pasqualini. Cell surface expression of the stress response chaperone GRP78 enables tumor targeting by circulating ligands. Cancer Cell. 6:275-284 (2004).

47. A.J. Gormley, A. Malugin, A. Ray, R. Robinson, and H. Ghandehari. Biological evaluation of RGDfK-gold nanorod conjugates for prostate cancer treatment. J Drug Target. 19:915-924 (2011).

48. T.E. Dudar and R.K. Jain. Differential response of normal and tumor microcirculation to hyperthermia. Cancer Res. 44:605-612 (1984).

49. D. Owens 3rd and N. Peppas. Opsonization, biodistribution, and pharmacokinetics of polymeric nanoparticles. Int J Pharm. 307:93-102 (2006).

50. L.W. Seymour, R. Duncan, J. Strohalm, and J. Kopecek. Effect of molecular weight (Mw) of N-(2-hydroxypropyl) methacrylamide copolymers on body distribution and rate of excretion after subcutaneous, intraperitoneal, and intravenous administration to rats. J Biomed Mater Res. 21:1341-1358 (1987).

CHAPTER 5

IN VITRO SYNERGISM AND *IN VIVO* EFFICACY OF COMBINATION TUMOR HYPERTHERMIA AND HEAT SHOCK PROTEIN TARGETED HPMA COPOLYMER-DRUG CONJUGATES

5.1 Introduction

In the continual fight against cancer, chemotherapy remains a powerful tool for clinicians, particularly for patients with advanced or metastatic disease. Chemotherapeutics are often categorized into different classes such as alkylating agents, anti-metabolites, anti-tumor antibiotics, topoisomerase inhibitors, or mitotic inhibitors.[1] These may act through various molecular mechanisms; however, they share essentially the same goal of preventing the replication and growth of cancer cells. They are pharmacologically designed to act primarily on rapidly dividing cells present within cancerous tissue. However, it is well known that these agents, due to their predesigned toxicity towards fast dividing cells of the body, are associated with an array of adverse effects including immunosuppression, anemia, gastrointestinal distress, and hair loss.[2] Much attention has therefore focused on targeted drug delivery,[3] whereby specific delivery of chemotherapeutics to the tumor site is achieved. By physically localizing

drugs to only the region of interest, exposure to healthy tissue is minimized, resulting in decreased side effects. It is anticipated that this additional physical targeting, coupled with the already existing pharmacological targeting can result in improvements in the safety profile of chemotherapeutics. As the goal of the clinician in administering chemotherapy is to eradicate or reduce the size of cancerous tumors, these improvements in safety offer opportunities for more aggressive treatment, thereby increasing the odds of positive, clinical response.

As described in Chapter 2, much of the work in the field of nanomedicine is focused on achieving targeted drug delivery. One such approach involves the conjugation of chemotherapeutics to water soluble polymers.[4, 5] The primary way in which these polymer-drug conjugates achieve site-specific delivery is via the "enhanced permeability and retention (EPR) effect" where increased uptake of macromolecules by solid tumors can occur due to a combination of increased vascular permeability and poor lymphatic drainage present within the tumor microenvironment.[6, 7] Even with this advantage, clinical translation of polymer-drug conjugates has remained elusive due in part to marginal efficacy as a result of insufficient tumor accumulation.[8]

As previously described in Chapter 2, one additional option to achieve enhanced delivery is via active targeting. This approach relies on the inclusion of cancer-specific targeting moieties, which are designed to enhance cancer cell binding and internalization.[9] For example, it was previously demonstrated that the attachment of cyclic Arg-Gly-Asp (RGD) peptides to the side chains of *N*-(2-hydroxypropyl)methacrylamide (HPMA) copolymers can facilitate binding to $\alpha_v\beta_3$ cell adhesion integrins of angiogenic blood vessels in the neovasculature of solid tumors. In

this way, tumor accumulation and retention can be increased several fold as compared to their non-targeted counterparts.[10, 11]

The utilization of such active targeting strategies, while effective, does not address the issue of tumor heterogeneity.[12] Although it is well understood that a tumor is not a collective mass of cells with a single phenotype, tumors are often characterized as "positive" or "negative" for a particular cancer cell marker or target. In reality, however, tumors are composed of multiple cell populations whose dynamic nature is supported by both genetic instability and epigenetic diversity.[13, 14] Therefore, only a subset of cells within a tumor may be susceptible to a particular targeted therapy. While initial treatment often yields progress in terms of tumor reduction, selection occurs resulting in tumor adaptation, resistance and recurrence.[15]

In Chapter 4, a strategy was described which sought to in part overcome these limitations by increasing tumor accumulation and the efficiency of active targeting.[16-18] This is achieved using a combination of gold nanorod-induced tumor hyperthermia and heat shock targeted HPMA copolymer-drug conjugates. Following exposure to hyperthermia, increases in cellular stress induce the expression of heat shock proteins (HSPs), which act as molecular chaperones to help stabilize cellular protein structures and inhibit protein aggregation.[19] In particular, it was demonstrated that glucose regulated protein 78 kDa (GRP78), a member of the HSP70 family of proteins, is induced following heat shock. While much of this expression occurs within the cell, significant expression also occurs on the cell surface, where GRP78 plays a role in the transduction of cell proliferation signals.[16, 20] This induced cell surface expression is therefore utilized as a specific cancer target. Such a strategy is advantageous in that it

does not rely on the inherent baseline expression of any particular cell receptor, but is directed instead towards this induced target.

In this strategy, delivery of tumor hyperthermia is performed via gold nanorod (GNR) mediated plasmonic photothermal therapy (PPTT). Gold nanorods, having a well-defined size and shape exhibit a localized surface plasmon resonance (SPR) peak in the near infrared range.[21] When excited via a laser light source of a similar wavelength, hyperthermia can be induced in an efficient and extremely localized fashion. This tool can therefore be used to induce the expression of cell surface HSPs, which serve as targets for delivery. It was demonstrated that hyperthermia induced via this method can increase the tumor accumulation and penetration of macromolecules via localized increases in blood flow and vascular permeability.[17, 18]

This chapter is focused on the evaluation of heat shock protein (GRP78) targeted HPMA copolymer-drug conjugates in combination with hyperthermia in a prostate cancer model. Polymer-drug conjugates containing the following chemotherapeutics were evaluated: aminohexylgeldanamycin (AHGDM), an HSP90 inhibitor; docetaxel, a microtubule stabilizer; and cisplatin, a DNA crosslinker. These agents were selected for evaluation in this strategy due to our previous experience with targeted HPMA copolymer-conjugates (see Chapter 4 and Appendix A), as well as reports of enhanced activity in combination with hyperthermia.[22-24] The targeting peptide WDLAWMFRLPVG, previously selected by phage display,[25] was conjugated to the side chains of the copolymers to facilitate binding to cell surface expressed GRP78. The relative binding affinity towards GRP78 for each conjugate was evaluated in a competitive binding assay. *In vitro* cytotoxicity was then assessed in combination with

hyperthermia to determine if this strategy resulted in antagonistic, additive, or synergistic effects. Finally, utilizing GNR-mediated PPTT to deliver localized hyperthermia, this combination strategy was evaluated for efficacy and general tolerability *in vivo* in human prostate cancer bearing mice.

5.2 Materials and methods

5.2.1 Materials

Geldanamycin (NSC 122750) was supplied by the National Cancer Institute Developmental Therapeutics Program (NCI DTP). Docetaxel was provided by AK Scientific (Mountain View, CA). Potassium tetrachloroplatinate (Cl_4K_2Pt) was obtained from Alfa Aesar (Ward Hill, MA). The GRP78 targeting peptide WDLAWMFRLPVG and the corresponding scrambled peptide RWLWVADPFLMG were synthesized via Fmoc chemistry using a Protein Technologies (Tucson, AZ) PS3 solid phase peptide synthesizer and identities verified by amino acid analysis and ESI/MS. For competitive binding studies, a rabbit anti-GRP78/BiP antibody (Enzo Life Sciences #ADI-SPA-826F) was radiolabeled with ^{125}I using a modified Iodogen method as previously described.[26] Na-^{125}I was obtained from American Radiolabeled Chemicals, Inc. (St. Louis, MO) and Iodogen reagent (1,3,4,6-tetrachloro-3α,6α-diphenylglycoluril) was obtained from Thermo Fisher Scientific (Rockford, IL).

5.2.2 Comonomer synthesis and characterization

The comonomers *N*-(2-hydroxypropyl)methacrylamide (HPMA)[27]; *N*-methacryloylglycylglycyl-2-thiazolidine-2-thione (MA-GG-TT)[28]; *N*-methacryloyl-

glycylphenylalanylleucylglycine (MA-GFLG-OH)[29]; and *N*-methacryloyl-tyrosinamide (MA-Tyr-$CONH_2$)[30] were synthesized and characterized according to previously described methods. Conjugation of the anticancer agents docetaxel and AHGDM to produce the drug comonomers MA-GFLG-DOC and MA-GFLG-AHGDM were carried out as previously described.[31, 32] The precursor comonomer *N*-methacryloyl-glycylphenylalanylleucylglycl-*N*-Boc-1,2-diaminoethane (MA-GFLG-NH-Et-NH-Boc) was synthesized by coupling MA-GFLG-OH to *N*-Boc-1,2-diaminoethane. Briefly, 1 mol eq. of MA-GFLG-OH and 3 mol eq. of N-Boc-1,2,-diaminoethane were dissolved in anhydrous DMF. The solution was cooled to 4°C and 3 mol eq. of DIPC and DIPEA were then added dropwise. The solution was stirred overnight followed by additional stirring at room temperature for 1 hr. DMF was then removed and the resulting residue re-dissolved in diethyl ether and washed repeatedly with sodium phosphate buffer at pH 6.0. The final product was obtained after removal of diethyl ether and identity verified by ESI/MS.

5.2.3 Synthesis and characterization of HPMA copolymer-drug conjugates

HPMA copolymers were synthesized via free radical copolymerization of comonomers in methanol acidified with glacial acetic acid using 2,2'-Azobis[2-(2-imidazolin-2-yl)propane]dihydrochloride (VA-044) as the initiator. Polymerization was performed in a sealed ampule under N_2 gas and the temperature was maintained at 50°C for 24 hrs. The concentrations of monomers and VA-044 during polymerization were maintained at 17.5% and 0.5% (w/v) to control molecular weight. Post polymerization, the polymers were precipitated and washed repeatedly in diethyl ether. Heat shock

targeted conjugates were obtained by aminolysis of 2-thiazolidine-2-thione containing precursor copolymers with WDLAWMFRLPVG peptide, and non-targeted conjugates were obtained by aminolysis with RWLWVADPFLMG (scrambled) peptide in anhydrous DMSO/DIPEA (Figure 5.1). For DOC conjugates, following aminolysis, reaction mixtures were diluted in 50 mM pH 6.0 sodium citrate buffer to prevent premature release of DOC via hydrolysis. For AHGDM conjugates, following aminolysis, reaction mixtures were diluted in DI water. Conjugates were then dialyzed against distilled water using 3.5 kDa molecular weight cut-off (MWCO) regenerated cellulose dialysis membranes (Spectrum Laboratories, Inc., Rancho Dominguez, CA), lyophilized, and stored at -20°C.

Cisplatin conjugates were obtained from MA-GFLG-NH-Et-NH-Boc containing copolymers, which were prepared following peptide aminolysis (Figure 5.1). Following aminolysis, boc deprotection was performed in a cleavage cocktail which consisted of trifluoroacetic acid:ethanedithiol:triisopropylsilane:water [92.5:2.5:2.5:2.5 v/v]. Following deprotection, copolymers were again dialyzed and lyophilized. Complexation of cisplatin to the resulting diamine side chains was then performed in distilled water using 5 mol equivalents of Cl_4K_2Pt. The resulting conjugates were again dialyzed against distilled water and lyophilized, followed by storage at -20°C.

Weight average molecular weight (M_w) and polydispersity (M_w / M_n) were determined by size exclusion chromatography (SEC) on a Superose 12 column (10 mm x 30 cm) (GE Healthcare, Piscataway, NJ) using a Fast Protein Liquid Chromatography (FPLC) system (GE Healthcare). Samples were monitored for UV, differential refractive index (dRI), multi-angle laser light scattering (MALLS) and dynamic light

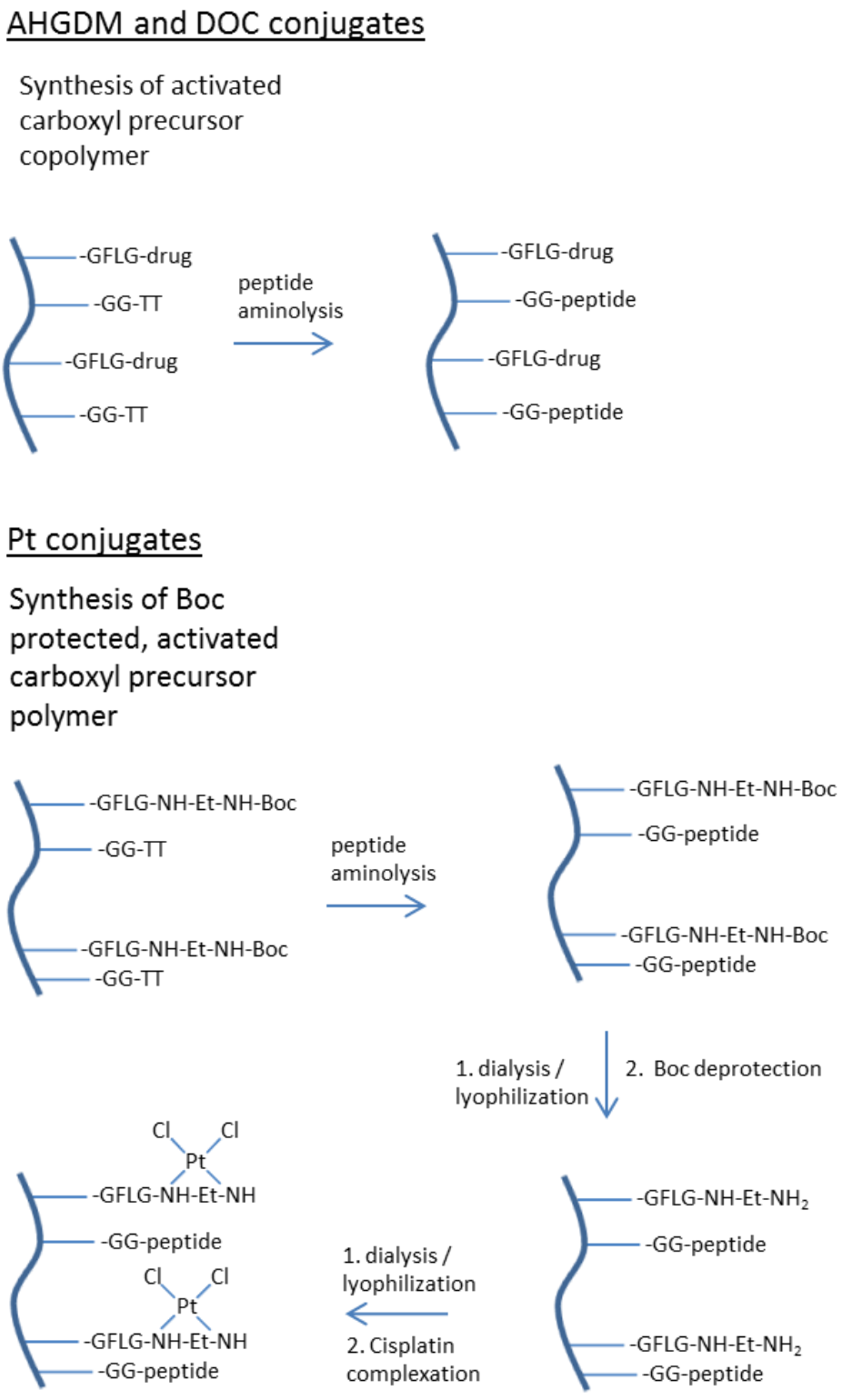

Figure 5.1. Schematics of HPMA copolymer-drug conjugate synthesis.

scattering (DLS) detection using a DAWN HELEO II light scattering instrument (Wyatt Technologies, Santa Barbara, CA). SEC coupled with dRI detection was used to confirm the absence of small molecular weight impurities. MALLS was used to determine molecular weight and polydispersity. For AHGDM conjugates, drug content was determined by UV spectrophotometry at 332 nm. For DOC conjugates, drug content was measured following enzymatic release of DOC by papain followed by quantification of free DOC by HPLC as previously described.[31] For cisplatin conjugates, Pt content was quantified by inductively coupled plasma mass spectrometry (ICP-MS) analysis (University of Utah Core Research Facilities, Salt Lake City, UT). Targeting peptide content for heat shock targeted and non-targeted (scrambled peptide) conjugates was quantified by amino acid analysis (University of Utah Core Research Facilities).

5.2.4 Cell culture

The DU145 human prostate cancer cell line was obtained from ATCC (Manassas, VA) and cultured at 37°C in a humidified atmosphere of 5% CO_2 in Eagle's Minimum Essential Medium (ATCC #30-2003) supplemented with 10% fetal bovine serum (FBS) (Thermo Scientific HyClone, Logan, UT). Cells were maintained in a logarithmic growth phase during all studies.

5.2.5 Competitive binding affinity to cell surface expressed GRP78

The comparative binding affinities of the GRP78 targeting peptide WDLAWMFRLPVG and copolymer-drug conjugates bearing the same to cell surface

expressed GRP78 on the surface of DU145 cells were assessed using a competitive binding assay. Cells were harvested, washed with PBS, and re-suspended in binding PBS (pH 7.4 + 1.0 % bovine serum albumin). Suspended cells were added to 1.2 μm pore size 96-well Multiscreen HV filter plates (Millipore, Billerica, MA) at 100,000 cells per well. They were co-incubated at 4°C with ^{125}I-anti-GRP78 antibody and increasing peptide equivalent concentrations of copolymer conjugates or free WDLAWMFRLPVG peptide between 0 and 500 μM. After 2 hrs, incubation was discontinued and media removed by vacuum filtration using a multiscreen vacuum manifold (Millipore). Retained cells were washed five times with PBS pH 7.4 + 1.0 % BSA. Filters were collected and radioactivity determined using a Cobra Auto-Gamma-counter (Canberra Industries, Inc., Meriden, CT). Each experiment was performed in triplicate, with three samples per experiment. Binding percentages relative to cells incubated with ^{125}I-anti-GRP78 antibody alone were calculated and non-linear regression analysis and determination of IC_{50} values carried out using GraphPad Prism (GraphPad Software, Inc., La Jolla, CA). Incubation with nontargeted copolymer conjugates (scrambled peptide) was also performed at equivalent peptide concentrations to serve as negative controls.

5.2.6 Single agent *in vitro* cytotoxicity

The ability of the HPMA copolymer-drug conjugates to inhibit the growth of DU145 human prostate cancer cells was evaluated *in vitro* using a 2-(2-methoxy-4-nitrophenyl)-3-(4-nitrophenyl)-5-(2,4-disulfophenyl)-2H-tetrazoliummonosodium salt (WST-8) cell viability assay (Dojindo Molecular Technologies, Inc., Rockville, MD).

Media containing 0.5% DMSO was used throughout to prevent precipitation of free drugs. This concentration was previously determined to not affect cell viability over the time course of the experiments. DU145 cells (3000 per well) were plated in 96-well plates for 24 hrs. Media was then removed and replaced with media containing treatments. Cells were exposed to treatments for 12 hrs. For each treatment case, drug concentrations were varied to include data points ranging from non-toxic to highly toxic. Following drug treatment, media was removed, cells washed with PBS, growth media replaced, and cells were allowed to grow for an additional 60 hrs (72 hrs total experiment duration). Media was then removed and cell viability quantified by WST-8 assay (modified MTT assay) using a SpectraMax M2 microplate UV spectrophotometer (Molecular Devices, Sunnyvale, CA). Each experiment was performed in triplicate, with each experiment comprising assessment of viability at eight different drug concentrations with three samples analyzed per concentration. Relative viability was calculated by normalization of UV absorbance against untreated cells. Relative viability as a function of log drug concentration was plotted and nonlinear least-squares regression analysis and calculation of IC_{50} values were performed using GraphPad Prism.

5.2.7 *In vitro* cytotoxicity of hyperthermia

The cytotoxic effect of hyperthermia treatment alone was evaluated *in vitro* against DU145 using a method analogous to that used to determine single agent cytotoxicity. DU145 cells (3000 per well) were plated in 96-well plates for 24 hrs. Cells were then exposed to either 40, 43, or 46°C for various durations spanning 15 min

to 48 hrs. Cells incubated continuously at 37°C served as controls. Temperatures other than 43°C were investigated for informational purposes only and were not used in subsequent combination index value calculations. Following hyperthermia treatment, cells were further incubated such that the total experiment duration was 72 hrs, followed by cell viability assessment as previously described. Each experiment was performed in triplicate, with six samples analyzed per treatment case.

5.2.8 *In vitro* combination treatment and combination index analyses

The cytotoxic effects of the combination treatment of moderate hyperthermia and heat shock targeted conjugates were evaluated *in vitro* (Figure 5.2). DU145 cells (3000 per well) were plated in 96-well plates for 24 hrs. Media was then removed and replaced with media containing treatments. Subsequently cells were immediately exposed to moderate hyperthermia (43°C, 30 min incubation) or control (37°C, 30 min incubation). Following hyperthermia treatment, cells were incubated for an additional 11.5 hrs (12 hrs total drug exposure). Following combination treatment, cells were washed and allowed to grow for an additional 60 hrs. Cell viability was then assessed as previously described.

Thermal enhancement was defined as IC_{50} of control (37°C) / IC_{50} when combined with hyperthermia (43°C). Drug effect was defined as (1- [% relative viability / 100]). Combination index analysis was performed using CalcuSyn combination index software version 2.1 (Biosoft, Inc., Cambridge, UK) based on the Choe-Tolalay method.[33] Each experiment was performed in triplicate, comprising assessment of viability for each combination treatment at eight different drug

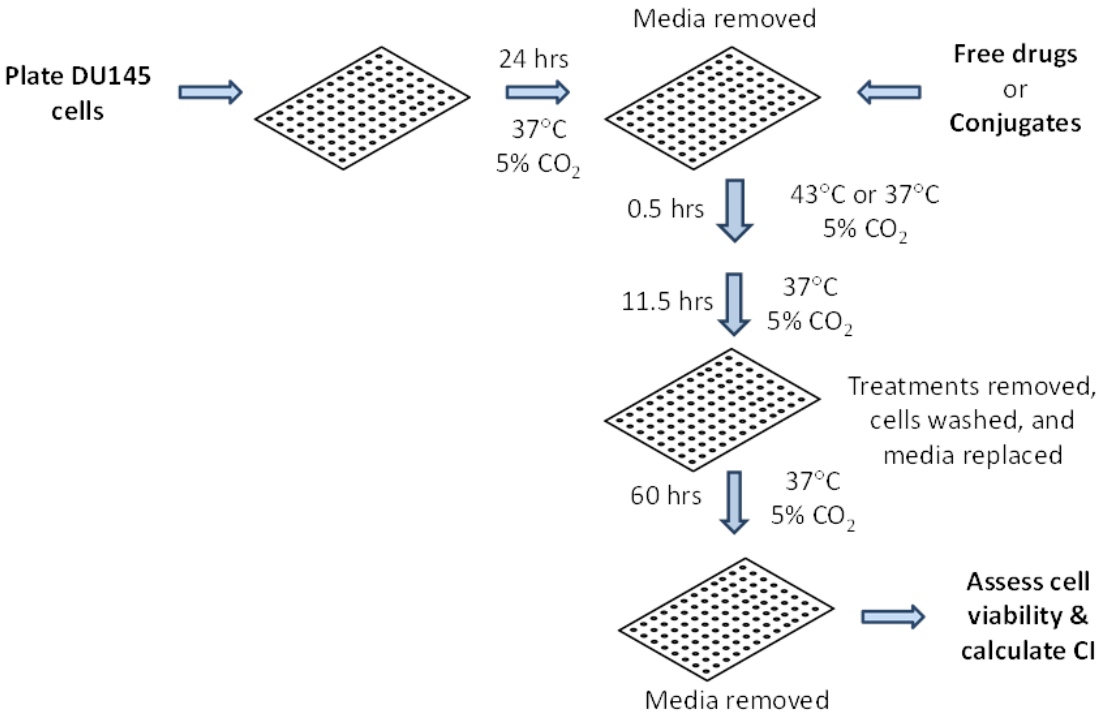

Figure 5.2. Method utilized for determination of *in vitro* combination index values of drug treatments in combination with hyperthermia.

concentrations with three samples analyzed per concentration. Combination index was then plotted as a function of drug effect for each treatment case. This form of graphical representation was chosen over others commonly used for combination index analysis (i.e., isobolograms),[34] due to the use of a fixed hyperthermia dose and a variable drug dose (to obtain a range of effects), as compared to variations in drug ratios commonly investigated in these type of studies.

5.2.9 *In vivo* efficacy

Efficacy of the combination treatment of tumor hyperthermia and heat shock targeted HPMA copolymer-docetaxel conjugates was evaluated in 8-week-old athymic (nu/nu) mice. Mice were obtained from Charles River Laboratories (Davis, CA) and used in accordance with the Institutional Animal Care and Use Committee (IACUC) of the University of Utah. Under anesthesia, mice were subcutaneously injected with 10^7 DU145 cells on both the right and left flank of each animal. When the tumors had reached approximately 7 mm in diameter (2-3 weeks), the animals were administered PEGylated gold nanorods, synthesized and characterized as previously described,[16] (9.6 mg/kg) via tail vein injection. After 48 hrs, animals were then treated with a single intravenous dose of either saline, free docetaxel (formulated in polysorbate 80:EtOH:saline [20:13:67, v/v/v]), nontargeted (scrambled peptide) conjugate, or heat shock targeted HPMA copolymer-docetaxel conjugate at 10 mg/kg (DOC equivalent). Immediately following injection, tumors on the right flank received tumor hyperthermia via PPTT as previously described.[16] Briefly, animals were anesthetized and tumors were swabbed with 50% propylene glycol to enhance laser penetration.[17] Tumors on

the right flank only were then radiated for 10 min using an 808 nm laser and intra-tumoral temperature monitored via a 33 gauge needle thermocouple. Tumor temperature was maintained between 42 and 43°C via minor adjustments in laser output power. Tumors on the left of each animal served as internal controls. Animals were then monitored twice a week for changes in tumor volume and animal weight. Eight animals were evaluated per treatment group. Tumor dimensions (length and width) were measured and tumor volume estimated as length × width × $\pi/6$. Normalized tumor volume (mean ± SEM) and changes in animal weight (mean ± SEM) were then plotted as a function of time.

5.2.10 Statistical analysis

Differences in relative binding affinity, IC_{50} values, combination index values, normalized tumor volumes, and changes in animal weight were determined by one-way ANOVA. Where differences were detected, Tukey's test was used to test for significance between groups. The default significance level was set at α=0.05 for all statistical tests.

5.3 Results and discussion

5.3.1 Synthesis and characterization

A representative chemical structure of the HPMA copolymer-drug conjugates utilized in this study is given in Figure 5.3, and physicochemical characteristics are given in Table 5.1. All conjugates were synthesized to have a size above the renal threshold for HPMA copolymers (approximately 45 kDa),[35] thereby evading rapid renal

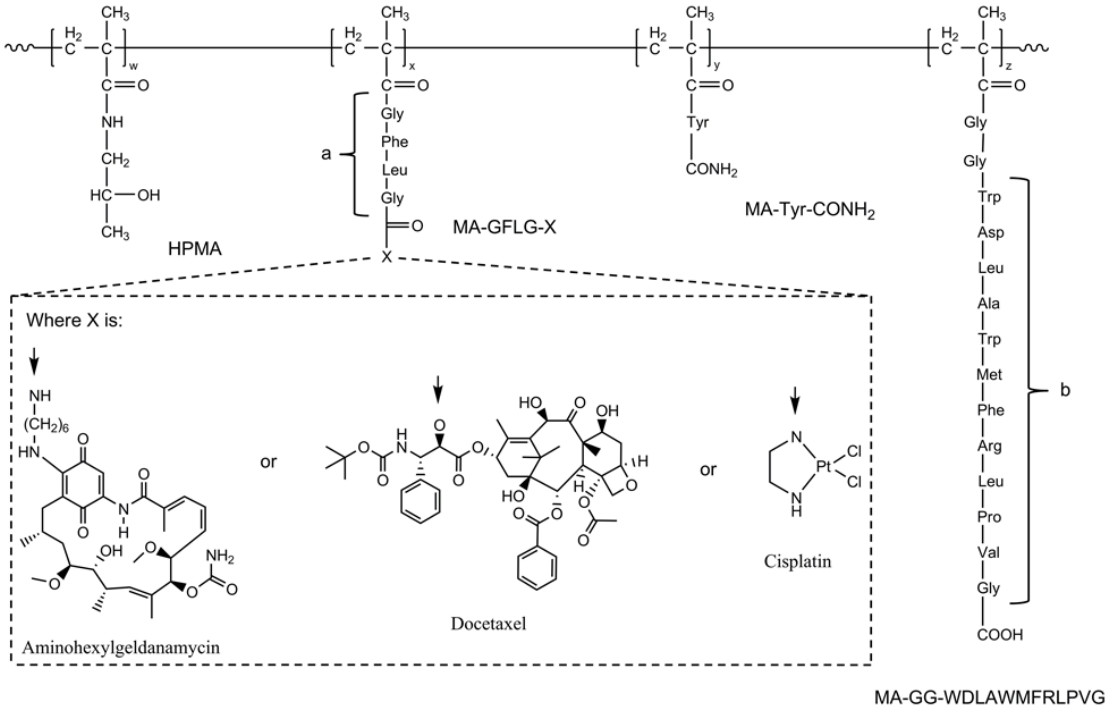

Figure 5.3. Representative chemical structure of HPMA copolymer-drug conjugates. The chemotherapeutic agent aminohexylgeldanamycin (AHGDM), docetaxel (DOC), or cisplatin was conjugated to the copolymer side chain via the enzymatically degradable GFLG linker (a), and the glucose regulated protein 78 kDa (GRP78) targeting peptide WDLAWMFRLPVG (b) was conjugated via a GG linker.

Table 5.1. Characteristics of HPMA copolymer-drug conjugates

Polymer	Description	----- *Feed composition - (mol%)* -----				M_w[a] (kDa)	M_w/M_n[a]	Drug content[b] mol% (wt%)	Targeting peptide content[c] mol% (wt%)
		HPMA	MA-GFLG-X*	MA-GG-TT	MA-Tyr-$CONH_2$				
p-AHGDM	Non-targeted AHGDM conjugate	88	5	5	2	76	1.4	4.8 (12.7)	2.9 (17.6)
p-AHGDM-HSP	HSP targeted AHGDM conjugate	88	5	5	2	71	1.4	4.9 (12.9)	2.8 (17.0)
p-DOC	Non-targeted DOC conjugate	90.5	2.5	5	2	78	1.4	1.9 (6.2)	2.8 (16.7)
p-DOC-HSP	HSP targeted DOC conjugate	90.5	2.5	5	2	81	1.4	2.0 (6.6)	2.6 (15.4)
p-Pt	Non-targeted Pt conjugate	87	6	5	2	89	1.5	5.4 (4.1)	3.4 (19.7)
p-Pt-HSP	HSP targeted Pt conjugates	87	6	5	2	86	1.5	6.0 (4.5)	3.3 (18.8)

* where X is AHGDM, DOC, or HN-Et-HN-Boc (precursor for Pt conjugates)

[a] as measured by SEC/MALLS

[b] Determined by UV spectroscopy for AHGDM, enzymatic release/HPLC for DOC, and ICP/MS for Pt.

[c] Determined by amino acid analysis. Scrambled peptide used for nontargeted conjugates.

filtration, and resulting in longer blood circulation times. This was of particular importance in our *in vivo* studies, as our combination strategy relies on two phenomena to increase tumor accumulation. First, tumor hyperthermia, induced immediately following intravenous administration of the conjugates, can increase both tumor blood flow and vascular permeability, thereby resulting in increased accumulation. Second, tumor hyperthermia can induce the expression of the cell surface heat shock protein GRP78. However, this expression does not occur immediately following exposure to hyperthermia, but requires between 8 and 12 hrs before maximum expression is observed.[16] Therefore, the utility of this heat shock targeting strategy requires that the conjugates still be available in circulation during this period of maximum expression. The conjugates were hence synthesized with molecular weights such that they exhibited these required long circulation times.

In this chapter, HPMA copolymer-drug conjugates (AHGDM, DOC, or Pt) modified with the GRP78 targeting peptide WDLAWMFRLPVG in combination with tumor hyperthermia were studied. For each drug that was evaluated (AHGDM, DOC, or Pt), precursor polymers bearing activated carboxyl groups (2-thiazoline-2-thione), were first synthesized. Heat shock protein (GRP78) targeting conjugates were obtained following aminolysis with the GRP78 targeting peptide WDLAWMFRLPVG. While some possibility of reaction between the guanidine groups present in the targeting peptides and 2-thiazoline-2-thione activated carboxyl groups exists, no evidence of this was observed. Such a reaction would tend to produce higher molecular weight copolymers, and no such shift in molecular weight was observed during SEC analysis (see Appendix D). In Chapter 4, the GRP78 targeting peptide WIFPWIQL was used.

However, the hydrophobic nature of this peptide limits the amount of drug loading that can be achieved while maintaining aqueous solubility. Conjugates bearing the WIFPWIQL peptide also demonstrated significant nonspecific uptake in the liver, spleen, and kidneys.[16] The more hydrophilic alternative peptide (WDLAWMFRLPVG) was therefore used in this study. A brief comparison of the biodistribution of HPMA copolymers utilizing these different peptides is also given in Appendix C. Nontargeted conjugates were prepared using a scrambled peptide (RWLWVADPFLMG). In this way, differences in behavior could be attributed to differences in binding affinity for GRP78, and not differences in copolymer physicochemical properties. The total amount of targeting peptide in each conjugate ranged from 2.6 – 3.4 mol% (Table 5.1), which is consistent with levels previously shown to facilitate sufficient active targeting[11, 36] (see also Appendix A).

The amount of each drug that was incorporated into the copolymers was based on previous observations of what level could be achieved while maintaining sufficient aqueous solubility. While the percent conversion (mol% of drug incorporation based on feed amount) was high and ranged from 90 – 98% for AHGDM and Pt conjugates, lower conversions for DOC conjugates of 76 – 80% were observed (Table 5.1). Since DOC is conjugated to the copolymer via ester linkages as compared to amide linkages for AHGDM and Pt conjugates, some hydrolysis of the ester bonds likely occurred post polymerization, most notably during attachment of the targeting peptides.

5.3.2 Competitive binding affinity to cell surface expressed GRP78

The relative binding affinities of each of the heat shock targeted conjugates towards cell surface expressed GRP78 was evaluated *in vitro* by a competitive binding

assay. DU145 cells were co-incubated with a fixed concentration of ^{125}I-radiolabeled anti-GRP78 antibody and increasing concentrations of WDLAWMFRLPVG peptide, heat shock targeted conjugates, or controls (nontargeted conjugates). All heat shock targeted conjugates demonstrated some degree of binding towards GRP78, and all non-targeted conjugates demonstrated no evidence of competitive binding (Figure 5.4). For AHGDM and DOC conjugates, the binding affinities (on a molar peptide basis) for targeted conjugates were 1600 ± 200 μM and 1080 ± 70 μM respectively. These values were significantly different from that of free WDLAWMFRLPVG peptide (96 ± 14 μM), signifying a decrease in the ability of the peptide to bind following conjugation. This anticipated result, however, is consistent with previous reports of HPMA copolymers-peptide conjugates, demonstrating effectiveness in increasing tumor accumulation[11] (see also Appendix A). Pt conjugates, however, demonstrated a significant shift in binding affinity to 230 ± 40 mM. While this can possibly be explained due to conformational changes in the copolymer due to the presence of the cisplatin analogue, it most likely results directly from the synthetic strategy. Due to the highly reactive nature of the cisplain analogue to nucleophilic substitution, it is required that the complexation of Cl_4K_2Pt with -HN-Et-HN_2 side groups occur as the last synthetic step. However, during this step, it is possible that some complexation to Arg side chains of the heat shock targeting peptide WDLAWMFRLPVG occurs, thereby interfering with its ability to effectively bind cell surface GRP78. This lack of effective binding could also be responsible to the lack of synergism observed for heat shock targeted Pt conjugates in combination studies (see Section 5.3.5).

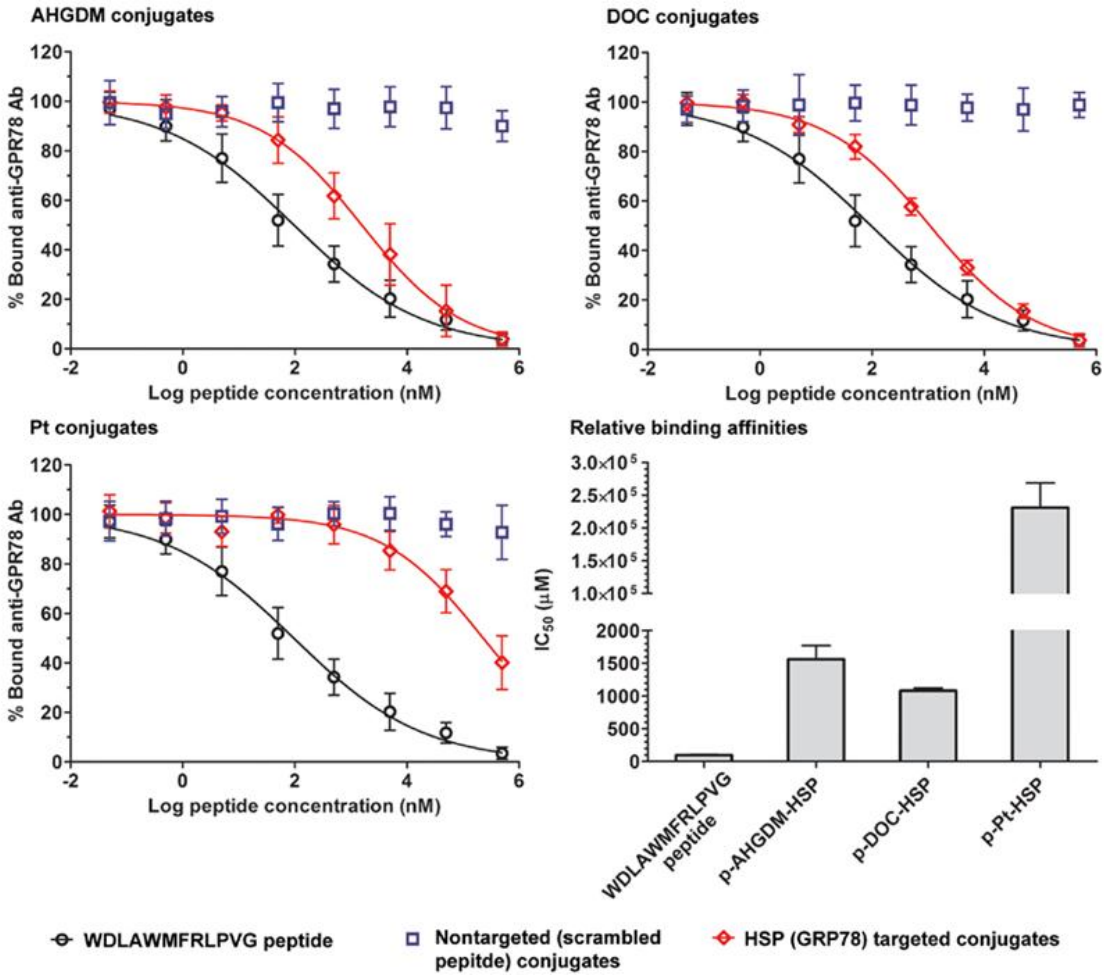

Figure 5.4. Binding affinity of HPMA copolymer-drug conjugates to GRP78 expressed on the surface of DU145 human prostate cancer cells. Strong binding affinity was observed for HSP targeted conjugates bearing AHGDM and docetaxel, and weak affinity was observed for the HSP targeted conjugate bearing cisplatin. For all conjugates, binding affinity was reduced as compared to native WDLAWMFRLPVG peptide. No evidence of binding was observed for nontargeted conjugates. Data expressed as mean ± SD of three experiments.

5.3.3 Single agent *in vitro* cytotoxicity

The ability of each HPMA copolymer-drug conjugate to inhibit the growth of DU145 human prostate cancer cells was evaluated *in vitro*. In an effort to mimic a realistic *in vivo* exposure time, the cells were exposed to each treatment case (conjugates, free drugs, or controls) for 12 hrs. This relatively short exposure time also provides an opportunity to allow differences in the kinetics or binding and uptake for different conjugates (i.e., nontargeted vs. targeted) to affect cytotoxicity.

These experiments yielded two primary observations. First, DOC treatments (free drugs and conjugates) were highly potent in inhibiting cell growth, with IC_{50} values ranging from 2.47 to 15.7 nM (Table 5.2, Figure 5.5). In comparison, AHGDM and Pt treatments were less potent with IC_{50} values ranging from 1.81 to 2.76 μM and 4.4 to 44 μM respectively. The increased potency of DOC treatments, including that observed for the HSP targeted conjugate (1.8 nM), was a primary factor in choosing DOC therapy for *in vivo* evaluation. These observed values were consistent with previous reports for similar conjugates[32, 37] (see also Appendix A). Second, statistically significant increased cytotoxicity was observed for HSP targeted AHGDM and DOC conjugates in comparison with their nontargeted counterparts. For AHGDM conjugates, HSP targeting resulted in a reduced IC_{50} of 1.85 as compared to 2.76 for the non-targeted conjugate ($p<0.001$) (Table 5.2 and Figure 5.5). For DOC conjugates, HSP targeting resulted in a reduced IC_{50} of 1.86 as compared to 13.1 for the nontargeted conjugate ($p<0.001$). These observations can be explained by the inherent cell surface expression of GRP78 on the surface of DU145 cells, which facilitates binding and internalization of HSP targeted conjugates, resulting in increased cytotoxicity. For the

Table 5.2. ***In vitro*** **cytotoxicity IC_{50} values of HPMA copolymer-drug conjugates in combination with hyperthermia.**

IC_{50}	AHGDM (μM)		DOC (nM)		Pt (μM)	
	Control (37°C)	Hyperthermia (43°C)	Control (37°C)	Hyperthermia (43°C)	Control (37°C)	Hyperthermia (43°C)
Free drugs	1.81 ± 0.05	1.39 ± 0.06	2.47 ± 0.08	1.86 ± 0.06	4.4 ± 0.2	3.2 ± 0.1
Nontargeted conjugates	2.76 ± 0.05	2.52 ± 0.08	15.7 ± 0.6	13.1 ± 0.5	44 ± 2	42 ± 2
Heat shock targeted conjugates	1.85 ± 0.05	0.83 ± 0.03	9.4 ± 0.3	2.4 ± 0.1	43 ± 2	37 ± 2

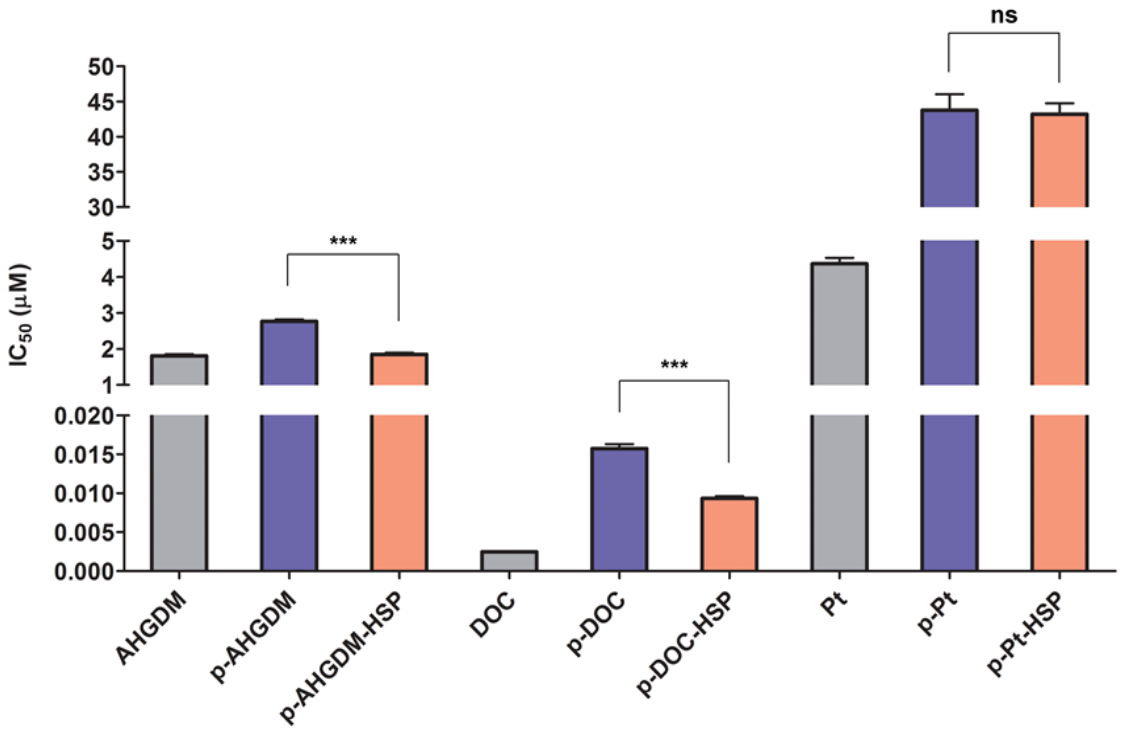

Figure 5.5. Cytotoxicity of single-agents towards DU145 human prostate cancer cells. Growth inhibition IC_{50} values of free drugs (grey), nontargeted conjugates (blue), and HSP targeted conjugates (red). DOC conjugates were significantly more potent than AHGDM or Pt conjugates, with IC_{50} values in the nanomolar range. HSP targeted AHGDM and DOC conjugates were also statistically significantly more potent than their nontargeted counterparts. Data expressed as mean ± SD or 3 experiments.

*** indicates statistically significant differences ($p<0.001$).

HSP targeted Pt conjugate, no difference in potency was observed as compared to the nontargeted conjugate. Again, this is possibly due to the loss of binding affinity of the HSP targeting peptide following cisplatin conjugation, as previously discussed.

5.3.4 *In vitro* cytotoxicity of hyperthermia

To ascertain the combined *in vitro* effects of the conjugates under investigation in combination with hyperthermia, it was first necessary to understand the effect hyperthermia alone has on cell viability. DU145 cells were exposed to hyperthermia (simple incubation) at varying temperatures (40°C, 43°C, and 46°C). Exposure time ranged from 15 min to 48 hrs. Following exposure to hyperthermia, cells were incubated at 37°C for a total of 72 hrs after initiation of hyperthermia, followed by assessment of cell viability. As anticipated, higher temperatures and increased exposure times were associated with decreased cell viability (Figure 5.6). In terms of potency, the exposure times required to decrease cell viability to 50% (relative to unexposed cells) were 41 min, 2.7 hrs, and 18.2 hrs for 46°C, 43°C, and 40°C respectively (Figure 5.6). It is important to note that for subsequent combination studies, this data indicates that exposure to hyperthermia (43°C, 30 min incubation) contributes only a 7.5% decrease in relative viability. The data obtained during the experiment for 43°C incubation were subsequently used for combination index analysis in combination studies.

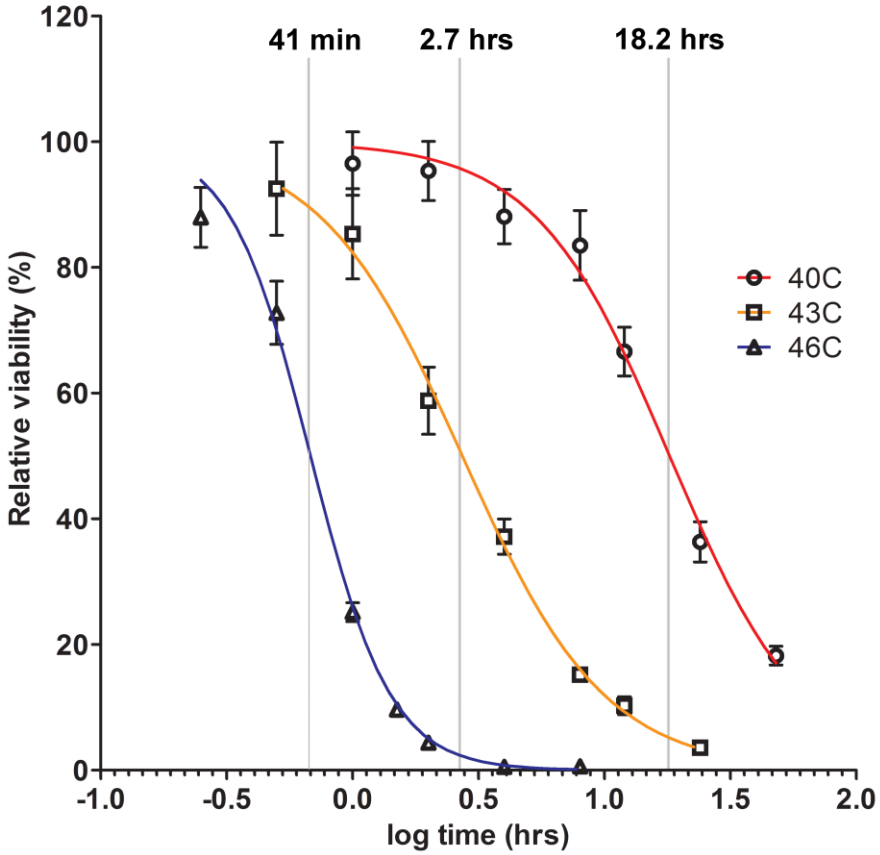

Figure 5.6. Cytotoxicity of hyperthermia towards DU145 human prostate cancer cells. Increases in temperature and exposure time were associated with increased cytotoxicity. Exposure times of 18.2 hrs, 2.7 hrs, and 42 min were needed to reduce viability to 50% at temperatures of 40°C, 43°C, and 46°C respectively.

5.3.5 *In vitro* combination treatment and combination index analyses

In Chapter 4, it was demonstrated that hyperthermia (43°C, 30 min incubation) induces an approximate 4-fold increase in the cell surface expression of GRP78 in DU145 cells, and that this increased expression results in increased cellular uptake kinetics of HSP targeted HPMA copolymers.[16] It is therefore anticipated that this increased cellular uptake rate will translate into increased cytotoxicity of HSP targeted HPMA copolymer-drug conjugates. In this experiment, DU145 cells were exposed to a combination of hyperthermia (43°C, 30 min incubation) and 12 hrs incubation with HSP targeted conjugates, nontargeted conjugates, or free drug controls. This timing was selected to be analogous to the exposure that occurs *in vivo* utilizing a combination strategy, where tumor cells are exposed to a brief period of simultaneous drug treatment and hyperthermia followed by a longer period of exposure to drug treatment alone. Cell viability was then assessed 72 hrs following initiation of combination treatment. When two therapies are used in combination, their overall effect can be antagonistic, additive, or synergistic. Antagonism, which is normally the least desired, is when the overall effect of the combination treatment is *less than* the sum of the effects of the therapies when used individually. Antagonism can often occur when two therapies are competing for a particular target, or when overlap occurs in the biochemical effects of the agents. When a combination treatment is additive, the overall effect is *equal to* the sum of the effects of the individual therapies. Synergism, which is usually most desired, occurs when the overall effect of the combination treatment is *greater than* the sum of the effects of the individual therapies. This can occur when the effects of one therapy potentiates the effects of another. In cancer chemotherapy, this most often occurs when

drugs of different mechanisms of action are combined, and where the effects of one drug upregulate or otherwise sensitize cells to treatment with the second drug. Various methods exist for determining whether a combination treatment is antagonistic, additive, or synergistic.[38] The most commonly employed, however, is that described by Chou and Talalay[33] and is based on the following equation:

$$CI\ (combination\ index) = \frac{D_1}{D_{x1}} + \frac{D_2}{D_{x2}} \qquad \text{(Equation 1)}$$

where D_1 and D_2 are the doses of treatment 1 and 2 that give X effect, and D_{x1} and D_{x2} are the doses of treatment 1 and 2 that would give the same effect as the combination. For a combination treatment of two therapies, this method requires evaluation of the effects of each therapy when used individually, as well as in combination. The result is calculation of a combination index (CI) parameter. When CI is between 1 and ∞ (CI > 1), the combination treatment is antagonistic. When CI = 1, the combination treatment is additive, and when CI is between 0 and 1 (CI < 1), the treatment is synergistic. (Note that the absolute scales of antagonism and synergism are not equivalent.) In this study, combination index (CI) analysis was performed to determine if the combined effects of drug treatment and hyperthermia were antagonistic, additive, or synergistic. The combination index was evaluated as a function of effect, defined as (1- [% relative viability / 100]).

All free drug controls (AHGDM, DOC, and cisplatin) were nearly additive (CI = 1) in combination with hyperthermia over the range of effects observed (Figure 5.7). At first glance, these observations appear to contrast other reports suggesting synergism of

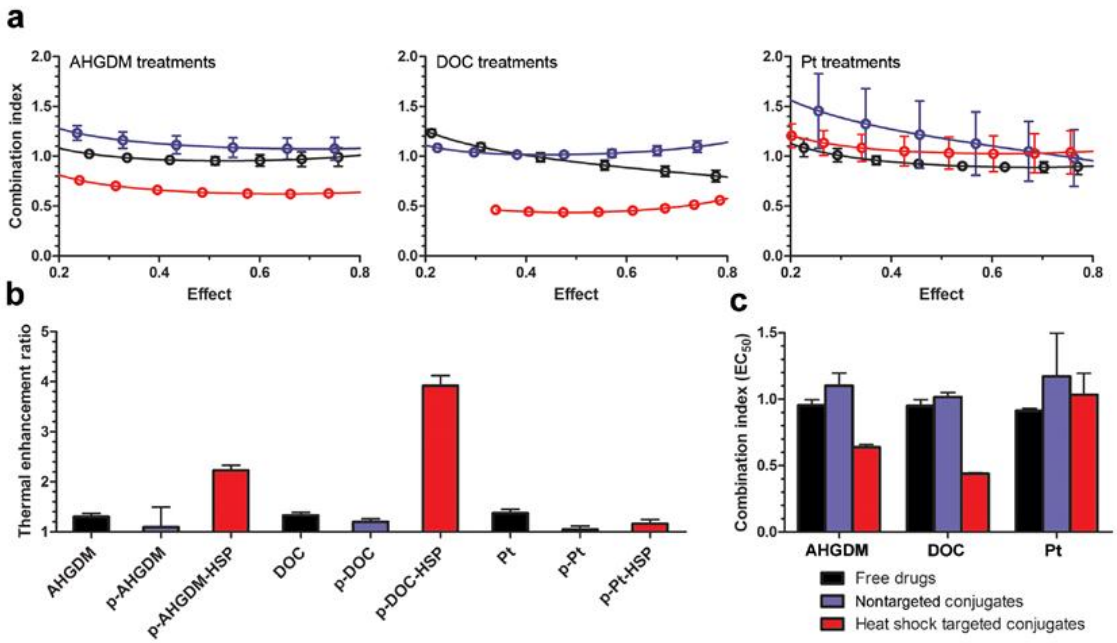

Figure 5.7. ***In vitro*** **combination of hyperthermia and drug therapy. a)** Combination index values as a function of drug effect against DU145 cells. Treatments consisted of free drug (black), nontargeted (scrambled peptide) conjugates (blue), and HSP targeted conjugates (red). HSP targeted AHGDM and DOC conjugates demonstrated significant synergism in combination with hyperthermia. **b)** Thermal enhancement ratios (IC_{50} northermia / IC_{50} hyperthermia) for each treatment case. **c)** Direct comparison of combination index values between treatments at 50% drug effect. All data expressed as mean ± SD of three experiments.

these compounds with hyperthermia.[22, 23] However, the combined effects and resulting combination index values are highly dependent on the sequence and timing of the combination therapy, and these experiments were performed to be analogous to potential *in vivo* exposure. These results are therefore not directly comparable with other studies and are best interpreted in a relative manner between the treatment groups in this study. All nontargeted conjugates were also additive in their combined effects with hyperthermia, with the slight exception of the nontargeted Pt conjugate (p-Pt), which was antagonistic at low effect levels. However, this sole observation was highly variable, and was not statistically significant. In combination with hyperthermia, both HSP targeted AHGDM and DOC conjugates demonstrated marked synergism with combination index values of approximately 0.65 and 0.45 respectively over a range of effect levels. The HSP targeted Pt conjugate demonstrated additive combined effects with hyperthermia, possibly due to its lack of binding affinity for GRP78 as previously discussed. For HSP targeted AHGDM and DOC conjugates, however, these results clearly demonstrate the potential for increased cellular delivery utilizing this heat shock targeted approach. These levels of synergism were not observed for the non-targeted AHGDM and DOC conjugates, which were prepared by addition of the scrambled peptide to same precursor polymer, suggesting this effect is primarily due to the HSP targeted conjugates' interaction with cell surface expressed GRP78.

To quantify the increase in cytotoxicity observed for treatments in combination with hyperthermia as compared to treatment alone, the thermal enhancement ratio of each treatment case was evaluated (Figure 5.7). The thermal enhancement ratio was defined as the IC_{50} observed for the treatment alone (no hyperthermia) divided by the

IC_{50} observed for the treatment in combination with hyperthermia. These results support those from combination index analysis, with HSP targeted AHGDM and DOC conjugates exhibiting increased potency with thermal enhancement ratios of 2.2 and 3.9 respectively. These combined results demonstrate the ability of cell surface expressed GRP78 to facilitate increased delivery of HSP targeted HPMA copolymer-drug conjugates, resulting in an increase in overall cytotoxicity. The HSP targeted DOC conjugate was selected for further *in vivo* evaluation due to its combined high potency, significant thermal enhancement, and observed synergism in combination with hyperthermia.

5.3.6 *In vivo* efficacy

In Chapter 4, it was demonstrated that tumor hyperthermia, delivered via GNR mediated PPTT, and heat shock targeting can increase the tumor accumulation and retention of HPMA copolymer-peptide conjugates. Building upon these results and the *in vitro* results demonstrating synergism of HSP targeted DOC conjugates in combination with hyperthermia, *in vivo* efficacy was evaluated. Docetaxel therapy in combination with tumor hyperthermia, induced via GNR mediated PPTT, was evaluated in DU145 human prostate cancer bearing nu/nu mice. Each animal bore two subcutaneous tumors (left and right flank). Tumors were approximately 7 mm in diameter at the time of treatment. Mice were injected intravenously with a single bolus dose of either free DOC, nontargeted (scrambled peptide) DOC conjugates, or HSP targeted DOC conjugates at 10 mg/kg DOC. Injection of saline solutions served as negative controls. Immediately following administration, tumor hyperthermia was

performed via GNR mediated PPTT to the right tumor only as previously described,[16] and tumor temperature was maintained between 42°C and 43°C for 10 min. Tumors on the left served as northermia controls. Mice were then monitored twice a week for changes in tumor volume and total body weight. No statistically significant differences in animal weights between treatment groups were observed throughout the course of the study (Figure 5.8). This was anticipated, as therapy was given well below the maximum tolerated dose of docetaxel.[31] All treatments demonstrated some level of tumor reduction as compared to saline (Figure 5.8), and are discussed in rank order of efficacy beginning with the least efficacious. Tumors treated with saline and hyperthermia showed minor tumor regression, with an average normalized tumor volume over 30 days of 393% as compared to 624% for saline alone (without hyperthermia). While *in vitro* experiments evaluating the effect of hyperthermia on cytotoxicity suggested minimal damage at this exposure level, the tumor regression observed indicates that some amount of tissue damage to the tumor occurred during hyperthermia treatment, most likely due to variations in the temperature distribution during heating. The cellular damage by histology is in agreement with previous work using similar treatments.[18] Treatments with free DOC and the non-targeted DOC conjugate were equally efficacious, with an observed overall growth of 321%. Combined treatment of free DOC or nontargeted DOC conjugates with hyperthermia were comparable to treatment with the HSP targeted DOC conjugate alone (no hyperthermia), with overall growths of 229%, 165%, and 198% observed respectively. The only treatment group which maintained tumor reduction over the entire study period was hyperthermia in combination with HSP targeted DOC therapy, wherein

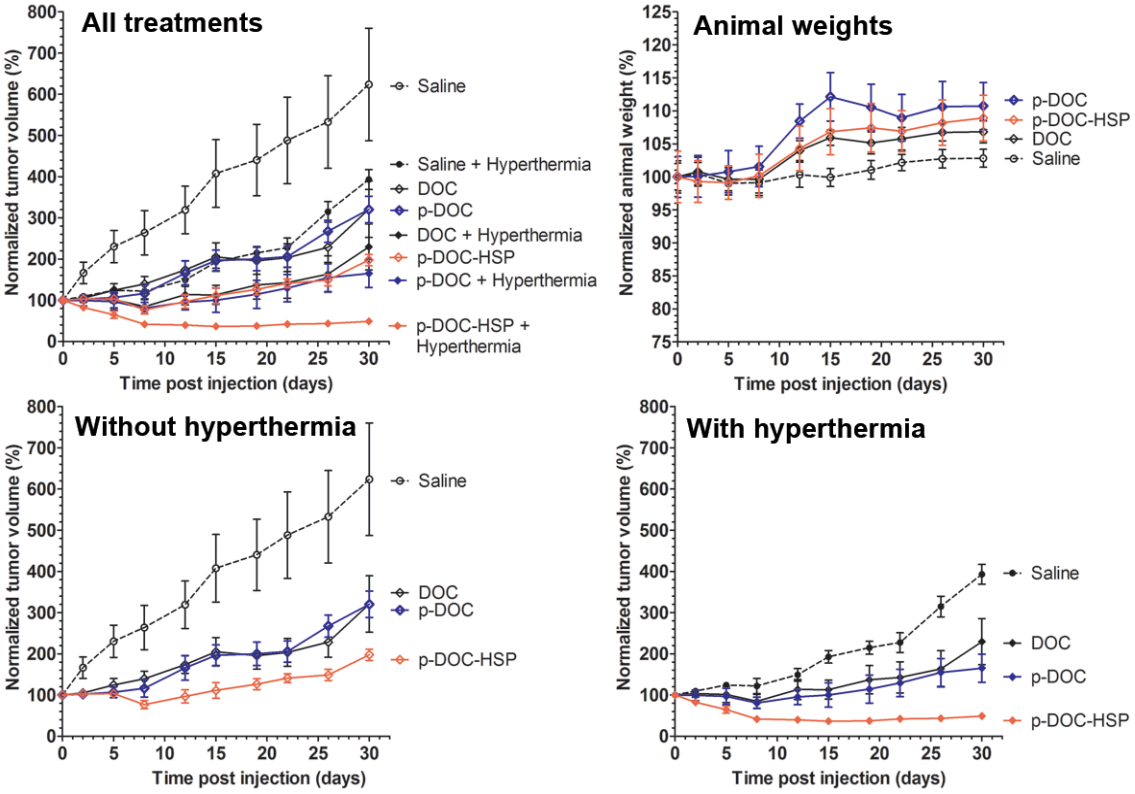

Figure 5.8. ***In vivo*** **efficacy of tumor hyperthermia and heat shock targeted HPMA copolymer-docetaxel therapy.** A combination of tumor hyperthermia, delivered via PPTT, and HSP targeted docetaxel therapy (p-DOC-HSP) results in maintained tumor regression over a period of 30 days following a single intravenous dose at 10 mg/kg DOC eq. No differences in animal weights were observed between treatment groups over the same time period. Data represented as mean ± SEM, with N=8 animals per treatment group.

tumor volume was maintained at 49% of initial volume after 30 days. These results demonstrate the efficacy of combination therapy and strongly support the proposed heat shock targeting rationale.

5.4 Conclusion

In this chapter, it was demonstrated that tumor hyperthermia can be utilized as a tool to increase the active targeting of heat shock targeted HPMA copolymer-drug conjugates. The combined effects of hyperthermia and HSP targeted AHGDM and DOC conjugates were found to be synergistic in inducing cytotoxicity to DU145 human prostate cancer cells *in vitro*. It was further demonstrated that a combination of tumor hyperthermia, delivered via GNR mediated PPTT, can increase the efficacy of HSP targeted HPMA copolymer-DOC conjugates in human prostate cancer bearing mice. These results demonstrate the potential for tumor hyperthermia to increase the delivery of targeted macromolecular chemotherapeutics.

5.5 References

1. V. Malhotra and M.C. Perry. Classical chemotherapy: mechanisms, toxicities and the therapeutic window. Cancer Biol Ther. 2:S2-4 (2003).

2. R.R. Love, H. Leventhal, D.V. Easterling, and D.R. Nerenz. Side effects and emotional distress during cancer chemotherapy. Cancer. 63:604-612 (1989).

3. T. Lammers, F. Kiessling, W.E. Hennink, and G. Storm. Drug targeting to tumors: principles, pitfalls and (pre-) clinical progress. J Control Release. 161:175-187 (2012).

4. R. Duncan. Polymer therapeutics as nanomedicines: new perspectives. Curr Opin Biotechnol. 22:492-501 (2011).

5. N. Larson and H. Ghandehari. Polymeric conjugates for drug delivery. Chem Mater. 24:840-853 (2012).

6. Y. Matsumura and H. Maeda. A new concept for macromolecular therapeutics in cancer chemotherapy: mechanism of tumoritropic accumulation of proteins and the antitumor agent smancs. Cancer Res. 46:6387-6392 (1986).

7. H. Maeda. Tumor-selective delivery of macromolecular drugs via the EPR effect: background and future prospects. Bioconjug Chem. 21:797-802 (2010).

8. R. Duncan and R. Gaspar. Nanomedicine(s) under the microscope. Mol Pharm. 8:2101-2141 (2011).

9. J.D. Byrne, T. Betancourt, and L. Brannon-Peppas. Active targeting schemes for nanoparticle systems in cancer therapeutics. Adv Drug Deliv Rev. 60:1615-1626 (2008).

10. D.B. Pike and H. Ghandehari. HPMA copolymer-cyclic RGD conjugates for tumor targeting. Adv Drug Deliv Rev. 62:167-183 (2010).

11. M.P. Borgman, O. Aras, S. Geyser-Stoops, E.A. Sausville, and H. Ghandehari. Biodistribution of HPMA copolymer-aminohexylgeldanamycin-RGDfK conjugates for prostate cancer drug delivery. Mol Pharm. 6:1836-1847 (2009).

12. T.A. Denison and Y.H. Bae. Tumor heterogeneity and its implication for drug delivery. J Control Release. 164:187-191 (2012).

13. J.M. Adams and A. Strasser. Is tumor growth sustained by rare cancer stem cells or dominant clones? Cancer Res. 68:4018-4021 (2008).

14. M. Shackleton, E. Quintana, E.R. Fearon, and S.J. Morrison. Heterogeneity in cancer: cancer stem cells versus clonal evolution. Cell. 138:822-829 (2009).

15. E.A. Hopper-Borge, R.E. Nasto, V. Ratushny, L.M. Weiner, E.A. Golemis, and I. Astsaturov. Mechanisms of tumor resistance to EGFR-targeted therapies. Expert Opin Ther Targets. 13:339-362 (2009).

16. A.J. Gormley, N. Larson, S. Sadekar, R. Robinson, A. Ray, and H. Ghandehari. Guided delivery of polymer therapeutics using plasmonic photothermal therapy. Nano Today. 7:158-167 (2012).

17. A.J. Gormley, K. Greish, A. Ray, R. Robinson, J.A. Gustafson, and H. Ghandehari. Gold nanorod mediated plasmonic photothermal therapy: a tool to enhance macromolecular delivery. Int J Pharm. 415:315-318 (2011).

18. A.J. Gormley, N. Larson, A. Banisadr, R. Robinson, N. Frazier, A. Ray, and H. Ghandehari. Plasmonic photothermal therapy increases the tumor mass penetration of HPMA copolymers. J Control Release (2013, In press).

19. K. Richter, M. Haslbeck, and J. Buchner. The heat shock response: life on the verge of death. Mol Cell. 40:253-266 (2010).

20. M. Ni, Y. Zhang, and A.S. Lee. Beyond the endoplasmic reticulum: atypical GRP78 in cell viability, signalling and therapeutic targeting. Biochem J. 434:181-188 (2011).

21. S. Link and M.A. El-Sayed. Shape and size dependence of radiative, non-radiative and photothermal properties of gold nanocrystals. Int Rev Phys Chem. 19:409-453 (2000).

22. S. Ohno, Z.H. Siddik, Y. Kido, L.A. Zwelling, and J.M. Bull. Thermal enhancement of drug uptake and DNA adducts as a possible mechanism for the effect of sequencing hyperthermia on cisplatin-induced cytotoxicity in L1210 cells. Cancer Chemother Pharmacol. 34:302-306 (1994).

23. Y.G. Shellman, W.R. Howe, L.A. Miller, N.B. Goldstein, T.R. Pacheco, R.L. Mahajan, S.M. LaRue, and D.A. Norris. Hyperthermia induces endoplasmic reticulum-mediated apoptosis in melanoma and non-melanoma skin cancer cells. J Invest Dermatol. 128:949-956 (2008).

24. E. Dovern, I.H. de Hingh, V.J. Verwaal, W.J. van Driel, and S.W. Nienhuijs. Hyperthermic intraperitoneal chemotherapy added to the treatment of ovarian cancer. A review of achieved results and complications. Eur J Gynaecol Oncol. 31:256-261 (2010).

25. M.A. Arap, J. Lahdenranta, P.J. Mintz, A. Hajitou, A.S. Sarkis, W. Arap, and R. Pasqualini. Cell surface expression of the stress response chaperone GRP78 enables tumor targeting by circulating ligands. Cancer Cell. 6:275-284 (2004).

26. J.M. Walker. The protein protocols handbook, Humana Press, Towota, N.J., 1996.

27. J. Strohalm and J. Kopecek. Poly N-(2-hydroxypropyl) methacrylamide: 4. Heterogenous polymerization. Angew Makromol Chem. 70:109-118 (1978).

28. P. Rejmanova, J. Labsky, and J. Kopecek. Aminolyses of monomeric and polymeric p-nitrophenyl esters of methacryloylated amino acids. Makromol Chem. 178:2159-2168 (1977).

29. K. Ulbrich, V. Subr, J. Strohalm, D. Plocova, M. Jelinkova, and B. Rihova. Polymeric drugs based on conjugates of synthetic and natural macromolecules.

I. Synthesis and physico-chemical characterisation. J Control Release. 64:63-79 (2000).

30. J.H. Lee, P. Kopeckova, J. Kopecek, and J.D. Andrade. Surface properties of copolymers of alkyl methacrylates with methoxy (polyethylene oxide) methacrylates and their application as protein-resistant coatings. Biomaterials. 11:455-464 (1990).

31. A. Ray, N. Larson, D.B. Pike, M. Gruner, S. Naik, H. Bauer, A. Malugin, K. Greish, and H. Ghandehari. Comparison of active and passive targeting of docetaxel for prostate cancer therapy by HPMA copolymer-RGDfK conjugates. Mol Pharm. 8:1090-1099 (2011).

32. Y. Kasuya, Z.R. Lu, P. Kopeckova, S.E. Tabibi, and J. Kopecek. Influence of the structure of drug moieties on the in vitro efficacy of HPMA copolymer-geldanamycin derivative conjugates. Pharm Res. 19:115-123 (2002).

33. T.C. Chou and P. Talalay. Quantitative analysis of dose-effect relationships: the combined effects of multiple drugs or enzyme inhibitors. Adv Enzyme Regul. 22:27-55 (1984).

34. R.J. Tallarida. An overview of drug combination analysis with isobolograms. J Pharmacol Exp Ther. 319:1-7 (2006).

35. L.W. Seymour, R. Duncan, J. Strohalm, and J. Kopecek. Effect of molecular weight (Mw) of N-(2-hydroxypropyl)methacrylamide copolymers on body distribution and rate of excretion after subcutaneous, intraperitoneal, and intravenous administration to rats. J Biomed Mater Res. 21:1341-1358 (1987).

36. K. Greish, A. Ray, H. Bauer, N. Larson, A. Malugin, D. Pike, M. Haider, and H. Ghandehari. Anticancer and antiangiogenic activity of HPMA copolymer-aminohexylgeldanamycin-RGDfK conjugates for prostate cancer therapy. J Control Release. 151:263-270 (2011).

37. E. Gianasi, M. Wasil, E.G. Evagorou, A. Keddle, G. Wilson, and R. Duncan. HPMA copolymer platinates as novel antitumour agents: in vitro properties, pharmacokinetics and antitumour activity in vivo. Eur J Cancer. 35:994-1002 (1999).

38. T.C. Chou. Drug combination studies and their synergy quantification using the Chou-Talalay method. Cancer Res. 70:440-446 (2010).

CHAPTER 6

CONCLUSIONS AND FUTURE DIRECTIONS

6.1 Conclusions

Anticancer chemotherapy is often restricted by the inherent adverse effects of the agents being administrated, resulting in dose limiting toxicities. For the drug delivery scientist, the overall goal is to deliver a maximal dose to the tumor tissue, while minimizing delivery to normal, healthy tissues. This can be achieved using nanoscale sized drug carriers, such as polymer-drug conjugates, which have been shown to accumulate preferentially in tumor tissues via the enhanced permeability and retention (EPR) effect. In addition, active targeting strategies, by modification of drug carriers with targeting moieties can be used to potentially enhance delivery. For example, previous work[1] has investigated HPMA copolymer-drug conjugates bearing cyclic RGD peptide as drug carriers targeting $\alpha_v\beta_3$ integrins expressed on the surface of angiogenic blood vessels (see also Appendix A). The work performed in this thesis also employed active targeting strategies using small peptides as targeting moieties attached to HPMA copolymers. The goal, however, in addition to evaluating the fundamentals of active targeting, was to demonstrate induction of the cell receptor itself. This was achieved by exposure to hyperthermia, which triggers the heat shock protein response. Induced expression was then utilized to enhance cellular delivery.

The research presented herein relied heavily on recent studies demonstrating the utility of gold nanorod (GNR) mediated plasmonic photothermal therapy (PPTT) in generating localized tumor hyperthermia.[2, 3] In these studies, GNR mediated PPTT further demonstrated the ability to increase the passive delivery of macromolecules via changes in blood flow and vascular permeability.[3] It was therefore natural to utilize this tool in a heat shock targeting approach to yield an overall therapy which increased both the passive and active targeting of macromolecules.

It was first necessary to demonstrate that HPMA copolymer-drug conjugates could be synthesized that target cell surface expressed GRP78, the inducible target of concern. In Chapter 3, HPMA copolymer-AHGDM drug conjugates bearing the GRP78 targeting peptide WIFPWIQL were synthesized and characterized. Stability of the conjugates was assessed in various biological media. Very minor release was observed in all conditions. Next, the ability of WIFPWIQL peptide to maintain its affinity to bind cell surface expressed GRP78 after being conjugated to the HPMA copolymer backbone was evaluated in a competitive binding assay. A reduction in binding affinity was observed, which was consistent with previous work utilizing targeting peptides.[1, 4] The ability of the conjugates to inhibit the growth of human prostate cancer cell lines was then evaluated. Conjugates targeting GRP78 demonstrated increased cytotoxicity as compared to untargeted conjugates. These studies demonstrated that HPMA copolymer-drug conjugates bearing the WIFPWIQL peptide could target cell surface expressed GRP78 and enhance cytotoxicity in human prostate cancer cells.

We hypothesized that tumor hyperthermia, delivered via GNR mediated PPTT, could increase the cell surface expression of GRP78, thereby enhancing active binding and uptake of GRP78 targeted conjugates and increase cellular delivery. The focus of Chapter 4 was to perform proof of concept studies to test this hypothesis. First, it was demonstrated that additional GRP78 expression occurred on the cell surface of DU145 cells following *in vitro* hyperthermia (43°C, 30 min incubation). Next, the cellular uptake kinetics of FITC labeled conjugates targeting GRP78, during the period of hyperthermia induced GRP78 expression, was evaluated. It was observed that GRP78 targeted conjugates were taken up at a significantly increased rate, as compared to untargeted conjugates, suggesting GRP78 mediated binding and uptake. Next, the effect of this induced expression on the cytotoxicity of AHGDM bearing conjugates was evaluated. GRP78 targeted conjugates demonstrated increased toxicity following hyperthermia as compared to both untargeted conjugates and free drug controls, suggesting GRP78 mediated delivery. Based on these positive *in vitro* results, analogous experiments were performed *in vivo* to further evaluate this targeting strategy. Following tumor hyperthermia, delivered via GNR mediated PPTT (42°C-43°C tumor temperature, 10 min duration), increased expression of GRP78 in tumor tissue was observed by immunohistochemistry as compared to untreated tumors. Finally, the tumor accumulation and biodistribution of ^{125}I radiolabeled GRP78 targeted HPMA copolymers were evaluated as a function of time following hyperthermia. Modest increases in exposure were observed for tumors receiving either GRP78 targeted conjugates alone or tumor hyperthermia alone and significant tumor exposure was observed when the combination of the two was used. These results clearly

demonstrate the ability of this combination therapy to increase the tumor delivery of GRP78 targeted HPMA copolymers. However, significant non-specific uptake of the targeted conjugates was observed in the kidneys, liver, and spleen. It was hypothesized that this may be the result of the hydrophobic nature of the conjugates, due to presence of the hydrophobic targeting peptide WIFPWIQL. Further studies, therefore, utilized a less hydrophobic GRP78 targeting peptide, namely WDLAWMFRLPVG in an attempt to reduce this non-specific uptake.

In Chapter 5, the goal was to demonstrate efficacy of this combination strategy *in vivo*. Conjugates bearing the anticancer agents aminohexylgeldanamycin (AHGDM), docetaxel (DOC), or cisplatin were synthesized using the less hydrophobic GRP78 targeting peptide WDLAWMFRLPVG and their binding to GRP78 was evaluated. They were then assessed *in vitro* for their ability to synergistically induce cytotoxicity in combination with hyperthermia. Targeted docetaxel and AHGDM conjugates demonstrated specific binding to cell surface expressed GRP78, high potency, and synergistic effects in combination with hyperthermia. In DU145 tumor bearing mice, a single treatment of tumor hyperthermia, induced via GNR mediated PPTT, and intravenous administration of GRP78 targeted HPMA copolymer-docetaxel at 10 mg/kg resulted in maintained tumor regression for a period of 30 days. These results were the first demonstration of *in vivo* efficacy using tumor hyperthermia to increase the delivery of HPMA copolymer-drug conjugates.

In conclusion, this thesis investigated the use of tumor hyperthermia to increase the active delivery of targeted HPMA copolymer-drug conjugates. Data was collected to support initial idea conception, followed by more in depth proof of concept studies,

which demonstrated the validity of this therapy. Finally, *in vivo* efficacy of the therapy was demonstrated in a human prostate cancer animal model. Overall, these results demonstrate the potential for tumor hyperthermia to be used as a tool to increase the delivery of heat shock targeted macromolecular chemotherapeutics.

6.2 Future directions

From a wider perspective, this thesis focused on establishing, as a concept, the use of a combination of tumor hyperthermia and heat shock protein targeting to increase the delivery of chemotherapeutic drugs. While the data presented herein focused on the goal of achieving increases in tumor delivery, a complete mechanistic understanding of the primary phenomena at play remains to be explored.

For example, it was demonstrated that GRP78 is expressed on the cell surface of DU145 cells following hyperthermia. These experiments, however, only provided a snapshot of a very dynamic process. The kinetics of receptor uptake, trafficking, and recycling were not investigated. It is essential that such investigations be made, as these dynamic processes are critical for the cellular delivery of macromolecules.[5, 6] Detail of these processes may yield additional information that can be used to further optimize delivery.

In this thesis, all of the conjugates investigated in combination with hyperthermia were synthesized to have molecular weights above renal threshold. This was done to take full advantage of the EPR effect, and ensure that the conjugates were maintained in systemic circulation during the period of elevated heat shock protein expression. These drug carriers are not biodegradable, and thus will most likely suffer

from poor elimination following administration. The applicability of targeting cell surface expressed HSPs following hyperthermia, however, is not entirely dependent on these drug carriers. Other biodegradable polymeric systems such as poly(glutamic acid) or backbone degradable HPMA copolymers (see Section 2.24) could potentially be used and achieve similar effects. This issue could also be addressed in an alternate manner. Previously, it was demonstrated that actively targeted low molecular weight HPMA copolymer-drug conjugates also accumulate in tumors[1] (see also Appendix A). It would therefore be interesting to see if lower molecular weight conjugates could show similar increases in delivery in combination with hyperthermia, as these conjugates have the benefit of eventual renal clearance post administration.

In addition, it is unclear whether the advances in delivery observed in this thesis can be achieved using other hyperthermia modalities. As previously discussed (see Section 2.5.3), techniques such as high intensity focused ultrasound (HIFU) are being increasing utilized in the clinic for the localized delivery of hyperthermia. Differences in spatial temperature distribution and resulting effects on blood flow and vascular permeability between these different hyperthermia modalities should be investigated.

This thesis also dealt specifically with induction of the heat shock protein GRP78 as a target. However, it is entirely unclear if this is the best target for such a strategy, since other inducible heat shock proteins[7] were not investigated. For the therapy to be fully optimized, some form of screening experiments should be performed to, in effect, look at the cell surface receptor expression following hyperthermia to see if other proteins are more strongly induced or could offer additional advantages in achieving cellular delivery.

The overall goal of this research is the development of clinically beneficial anticancer therapies. For this to occur, a number of challenges should be addressed. First, the nonspecific uptake of nanomedicines in healthy organs must be minimized. This can potentially be achieved through careful optimization of size and other physicochemical characteristics, such as hydrophilicity and surface charge. However, this can prove challenging for multifunctional drug carriers, such as actively targeted polymer-drug conjugates. Second, clinical application of this research necessitates the ability to apply hyperthermia in a localized, specific, and relatively non-invasive manner. Hyperthermia was applied in this thesis using GNR mediated PPTT. However, this technology is still in its infancy, and questions and concerns remain regarding its clinical applicability and the potential chronic toxicity of GNRs. The application of hyperthermia via HIFU should therefore be investigated. If HIFU results in similar increases in delivery, this method would be more preferred for clinical translation, due to its non-invasive nature and clinical acceptance.[8]

The use of high temperature localized hyperthermia to induce thermoablative cytotoxicity in tumors using various approaches is also an area of current research.[9] In this thesis, the focus was to demonstrate that moderate hyperthermia can increase the delivery of targeted chemotherapeutics. However, chances of a better clinical response could possibly be achieved by using a combination of these approaches. For example, the delivery of chemotherapeutics could be enhanced by moderate hyperthermia, followed by subsequent high temperature hyperthermia. This strategy would fully utilize the benefits of each approach and could possibly lead to more efficacious therapy.

These investigations would allow for a more complete mechanistic understanding of this combination therapy and build upon the conclusions of this work. It is anticipated that this therapy, when fully optimized, can have a significant impact in the field of polymer therapeutics, and assist in the clinical translation of nanomedicines, with the ultimate goal of finding more effective and less toxic cancer therapies.

6.3 References

1. D.B. Pike and H. Ghandehari. HPMA copolymer-cyclic RGD conjugates for tumor targeting. Adv Drug Deliv Rev. 62:167-183 (2010).

2. A.J. Gormley, A. Malugin, A. Ray, R. Robinson, and H. Ghandehari. Biological evaluation of RGDfK-gold nanorod conjugates for prostate cancer treatment. J Drug Target. 19:915-924 (2011).

3. A.J. Gormley, K. Greish, A. Ray, R. Robinson, J.A. Gustafson, and H. Ghandehari. Gold nanorod mediated plasmonic photothermal therapy: A tool to enhance macromolecular delivery. Int J Pharm. 415:315-318 (2011).

4. M.P. Borgman, A. Ray, R.B. Kolhatkar, E.A. Sausville, A.M. Burger, and H. Ghandehari. Targetable HPMA copolymer-aminohexylgeldanamycin conjugates for prostate cancer therapy. Pharm Res. 26:1407-1418 (2009).

5. L.M. Bareford and P.W. Swaan. Endocytic mechanisms for targeted drug delivery. Adv Drug Deliv Rev. 59:748-758 (2007).

6. R. Duncan. Designing polymer conjugates as lysosomotropic nanomedicines. Biochem Soc Trans. 35:56-60 (2007).

7. G. Multhoff, C. Botzler, M. Wiesnet, E. Muller, T. Meier, W. Wilmanns, and R.D. Issels. A stress-inducible 72-kDa heat-shock protein (HSP72) is expressed on the surface of human tumor cells, but not on normal cells. Int J Cancer. 61:272-279 (1995).

8. S. Crouzet, F.J. Murat, G. Pasticier, P. Cassier, J.Y. Chapelon, and A. Gelet. High intensity focused ultrasound (HIFU) for prostate cancer: current clinical status, outcomes and future perspectives. Int J Hyperthermia. 26:796-803 (2010).

9. R.W. Habash, R. Bansal, D. Krewski, and H.T. Alhafid. Thermal therapy, Part III: ablation techniques. Crit Rev Biomed Eng. 35:37-121 (2007).

APPENDIX A

COMPARISON OF ACTIVE AND PASSIVE TARGETING OF DOCETAXEL FOR PROSTATE CANCER THERAPY BY HPMA COPOLYMER-RGDFK CONJUGATES[≠]

A.1 Introduction

Prostate cancer is the leading cause of cancer among men in the United States and the second leading cause of death with 217,730 new cases and an estimated 32,050 deaths in 2010.[2] In the last decade, much progress in the treatment of prostate cancer has been reported. However, routine treatment regimens have frequently changed due to poor prognosis of advanced disease. Despite standard treatment, the current survival from the time of diagnosis in patients with metastatic disease of 3.5 years is unacceptable.[3] These results demand the exploration of new alternatives which overcome drawbacks of current treatment modalities.

Docetaxel (Taxotere®) is a semisynthetic natural product which was approved by the FDA in 2004 for metastatic and androgen dependent prostate cancer. Clinical trial results strongly suggest the use of docetaxel as a first line of treatment for prostate cancer.[4, 5] Docetaxel binds to β-tubulin, thereby stabilizing microtubules and inducing cell-cycle arrest resulting in apoptosis.[6] It is up to five times more potent than

[≠] Co-authored (equal contribution) manuscript with A. Ray.[1]

paclitaxel in vitro with regard to tubulin promotion and inhibition of depolymerization.[7] There is incomplete cross resistance between paclitaxel and docetaxel and they act synergistically with several drugs including cisplatin and carboplatin in cancer.[8] Docetaxel is reported to have both anti-angiogenic and antitumor efficacy.[9] However, treatment with this drug is associated with gastrointestinal toxicity[10] and can result in aggravated risk of acute and subacute pulmonary damage.[11] Another major problem associated with administration of docetaxel is its poor aqueous solubility, requiring formulation with the nonionic surfactant polysorbate 80 (Tween® 80). Administration of docetaxel is associated with the occurrence of unpredictable acute hypersensitivity reactions and cumulative fluid retention.[12] These adverse effects have been attributed, in part, to the presence of polysorbate 80 and have consequently initiated research focused on the development of a less-toxic, better-tolerated polysorbate 80-free formulation.

Considerable progress has been made over the past 2-3 decades in the development of polymeric carriers for targeted drug delivery to solid tumors.[13, 14] Due to their macromolecular nature, polymeric systems accumulate passively in target tissues such as the reticuloendothelial system (RES) (through nonspecific uptake by macrophages) or tumors by a process called the **E**nhanced **P**ermeability and **R**etention (EPR) effect.[15, 16] The mechanism of the EPR effect has been summarized according to the following cascade of events: i) tumor angiogenesis results in hypervasculature, providing increased blood flow to the tumor, ii) tumor vasculature becomes highly permeable for macromolecules and plasma proteins due to factors such as tumor vascular permeability factor, bradykinin, and tumor necrosis factor, iii) a less effective

functioning of lymphatic drainage observed in tumors results in long-term retention of macromolecular drugs. These factors result in larger carriers having decreased renal clearance, thereby taking longer to be eliminated from the body.[17]

HPMA copolymers are well characterized, water-soluble, biocompatible, non-immunogenic and non-toxic synthetic polymeric drug carriers.[13, 18, 19] The *in vivo* disposition of macromolecules depends to a significant extent on their physicochemical properties. It has been shown that liver and kidney based clearance are the major factors affecting the biodistribution of macromolecules[20] and such clearance is a function of molecular weight. Studies have shown that HPMA copolymers and other polymeric macromolecules of molecular weights less than approximately 45kDa (hydrodynamic diameter < 5~6 nm) are rapidly filtered by the kidney.[17, 21-23] Most macromolecules that passively target tumors via the EPR effect have sizes larger than 7 nm, in order to overcome the glomerular renal threshold, thereby resulting in prolonged plasma half-life. Despite significant progress made in the field of macromolecular drug delivery, one challenge encountered in the development of such therapy is the fate of large macromolecules post treatment.

Another challenge often overlooked while using the EPR effect as a rationale for drug delivery of macromolecules is the elevated interstitial fluid pressure (IVF) which reduces convective transport in the core of the tumor.[24, 25] It is reported that the imbalance of the pro and anti-angiogenic factors lead to formation of chaotic new blood vessels in tumors.[26-28] This leads to uneven blood distribution, leaving unevenly perfused or unperfused regions inside the tumor.[29-32] These factors lead to interstitial hypertension in the core of the tumor.[33-35] Interstitial pressure and impaired blood

supply reduces the effective transport of anticancer agents in solid tumors.[26] Active targeting can possibly overcome these limitations for drug penetration.[36]

The tripeptide sequence, Arg-Gly-Asp (RGD) has been identified as a high affinity $\alpha_v\beta_3$ selective ligand by phage display.[37] The conformationally restrained cyclic RGDfK binds to $\alpha_v\beta_3$ up to 200-fold more avidly than linear peptides.[38] RGD peptides have been conjugated to humanized antibodies[39], liposomes[40-42], and poly(ethylene glycol)[43] to improve the biodistribution and increase tumor accumulation. The RGD (Arg-Gly-Asp) peptides have been used to target tumor angiogenesis.[44, 45] They have been used for the targeted delivery of chemotherapeutic agents, gene therapy[46] and oncolytic adenovirus.[47] They have also been reported to be tumor penetrating and its co-administration enhances the efficacy of anticancer drugs.[48] Compared to non-targeted systems, previous investigations have identified actively targeted HPMA copolymer–cyclo-RGD conjugates that increase tumor accumulation[49-53]. This accumulation takes place through specific interaction of RGD motifs present in the copolymer side chains with $\alpha_v\beta_3$ integrins overexpressed on both angiogenic blood vessels[38] and a variety of tumor cells including prostate cancer.[54] Enhanced accumulation was also demonstrated by active targeting in various human prostate cancer xenografts.[49, 52] Further, these targeted conjugates have also shown to inhibit HUVEC cell migration thereby delaying neoangiogenesis.[55] To enhance efficacy and reduce toxicity of docetaxel and to compare and contrast the effects of active vs passive targeting, studies presented in this Appendix aim at producing HPMA copolymer-docetaxel-cyclic RGD conjugates for targeted delivery to prostate tumors.

A.2 Methods

A.2.1 Chemicals

All chemicals obtained commercially were of analytical grade and used without further purification. Docetaxel was obtained from AK Scientific (Mountain View, CA). RGDfK (MW 604.5) was obtained from New England Peptide Inc. (Boston, MA) at > 95% purity and used as supplied. Methacryloyl chloride, glycyl-glycine, and p-nitrophenol, were obtained from Sigma-Aldrich (St. Louis, MO). Glycyl-phenylalanine and leucyl-glycine were obtained from Bachem Americas, Inc (Torrance, CA). *N*-(2-hydroxypropyl)methacrylamide (HPMA)[56], N-methacryloylglycylglycyl-p-nitrophenyl ester (MA-GG-ONp)[57], N-methacryloylglycylphenylalanylleucylglycine (MA-GFLG-OH)[58], N-methacryloylglycylphenylalanyl-leucylglycine- p nitrophenyl ester (MA-GFLG-ONp)[58], and N-methacryloyl-tyrosinamide (MA-Tyr)[59] were synthesized and characterized according to previously described methods.

A.2.2 Synthesis and characterization of comonomers

A.2.2.1 *N*-Methacryloylglycylphenylalanylleucylglycyl-docetaxel (MA-GFLG-Docetaxel). Docetaxel, (0.335g, 4.1 mmol), 4-(dimethylamino-) pyridine (DMAP, 0.049g, 4.0 mmol) and MA-GFLG-OH (0.188 g, 4.0 mmol) were dried under vacuum. The reaction mixture was dissolved under nitrogen in anhydrous N, N-dimethylformamide (DMF, 5 ml), cooled with an ice bath (salt/ice) at < 0°C and diisopropylcarbodiimide (DIPC, 76 µl, 4.89 mmol) was added drop wise. The reaction mixture was subsequently stirred for an hour before the ice bath was removed and the mixture was allowed to warm up to room temperature, stirred overnight and progress

monitored by thin layer chromatography (TLC, eluent dichloromethane (DCM): methanol (MeOH) (95:5)) for the disappearance of the starting material and the formation of MA-GFLG-Docetaxel, and further characterized by mass spectroscopy (m/z M^{+}+Na = 1272.62). DMF was removed under vacuum using rotavapor. The product was purified by silica gel chromatography and eluted using ethylacetate (EtOAc): MeOH (95:5)). The product identity was confirmed by Thermo Finnegan LTQ FT high resolution mass spectrometry (m/z M^{+1} for $C_{66}H_{84}N_5O_{19}^{+}$, calculated 1250.57605 (100%), 1251.57941 (71.4%), found m/z 1250.57487 (100%), 1251.57827 (71.4%)).

A.2.2.2 *N*-methacryloylglycylglycyl-RGDfK. MA-GG-ONp (0.20g, 0.623 mmol) and RGDfK (0.376 g, 0.623 mmol) were mixed in a round bottom flask, kept in a vacuum desiccator for 1 hr followed by addition of anhydrous dimethylsulfoxide (DMSO, 5 mL) and stirred for 18 hrs at room temperature. DIPEA (200 µL) was then added to the reaction mixture and further stirred for 4 hrs. The progress of the reaction was monitored by mass spectrometry for the disappearance of RGDfK (m/z M^{-1} 603.2). The reaction mixture was concentrated under high vacuum, followed by addition of H_2O (25 mL). This mixture was partitioned in diethyl ether (3 x 25 mL). The organic layer was removed and the aqueous layer lyophilized to obtain a white solid. Product formation was confirmed by Thermo Finnegan LTQ FT high resolution mass spectrometry (for $C_{35}H_{50}N_{10}O_{11}$, calculated m/z 786.36605 (100%), 787.36941 (37.9%), 788.37276 (7%), found m/z 786.38951 (100%), 787.39328 (37.9%), 788.39627 (7%)).

A.2.3. Synthesis and characterization of HPMA copolymer conjugates

HPMA copolymers were synthesized via free radical copolymerization of comonomers in 10% v/v anhydrous DMSO in acetone using N, N′- azobisisobutyronitrile (AIBN) as the initiator (Figure A.1).[56] The feed composition of comonomers for all copolymers is given in Table A.1. The weight composition of the comonomers to solvent was kept at 12.5: 87.5 (w/w). The comonomer mixtures were sealed in an ampoule under nitrogen and stirred at 50°C for 24 hrs. Solvent was removed by rotary evaporation, copolymer precursor was dissolved in methanol and precipitated and washed in diethyl ether. Copolymer precipitates were dissolved in deionized water and purified using dialysis tube molecular weight cut off (MWCO, 3500, SpectraPor®) to remove small molecular weight impurities. Samples were characterized for weight average molecular weight (M_w), number average molecular weight (M_n) and polydispersity (M_w/M_n) by size exclusion chromatography (SEC) on a Superose 6 column (10 mm x 30 cm) (GE Healthcare, Piscataway, NJ) using a Fast Protein Liquid Chromatography (FPLC) system (GE Healthcare). The peaks that eluted off the column were monitored via both ultra-violet absorbance (UV), differential refractive index (RI), and quasi-elastic light scattering (QELS) using a DAWN HELEOS II light scattering instrument (Wyatt Technologies, Santa Barbara, CA) with imbedded QELS and an OptiLab rEX differential refractometer (Wyatt Technologies). The Superose 6 column was previously calibrated with fractions of known molecular weight HPMA homopolymers. The hydrodynamic radii were determined by QELS and calculated from the Stokes-Einstein relation. All data were collected and analyzed using Wyatt Technology Corporation Astra 5.3.4.13 light scattering software (Wyatt Technologies).

A.2.4 Docetaxel and RGDfK content determination in conjugates

Drug contents of the synthesized copolymers were determined by enzymatic release[60] of free docetaxel and quantification by HPLC. Briefly, 5.0 mg of the

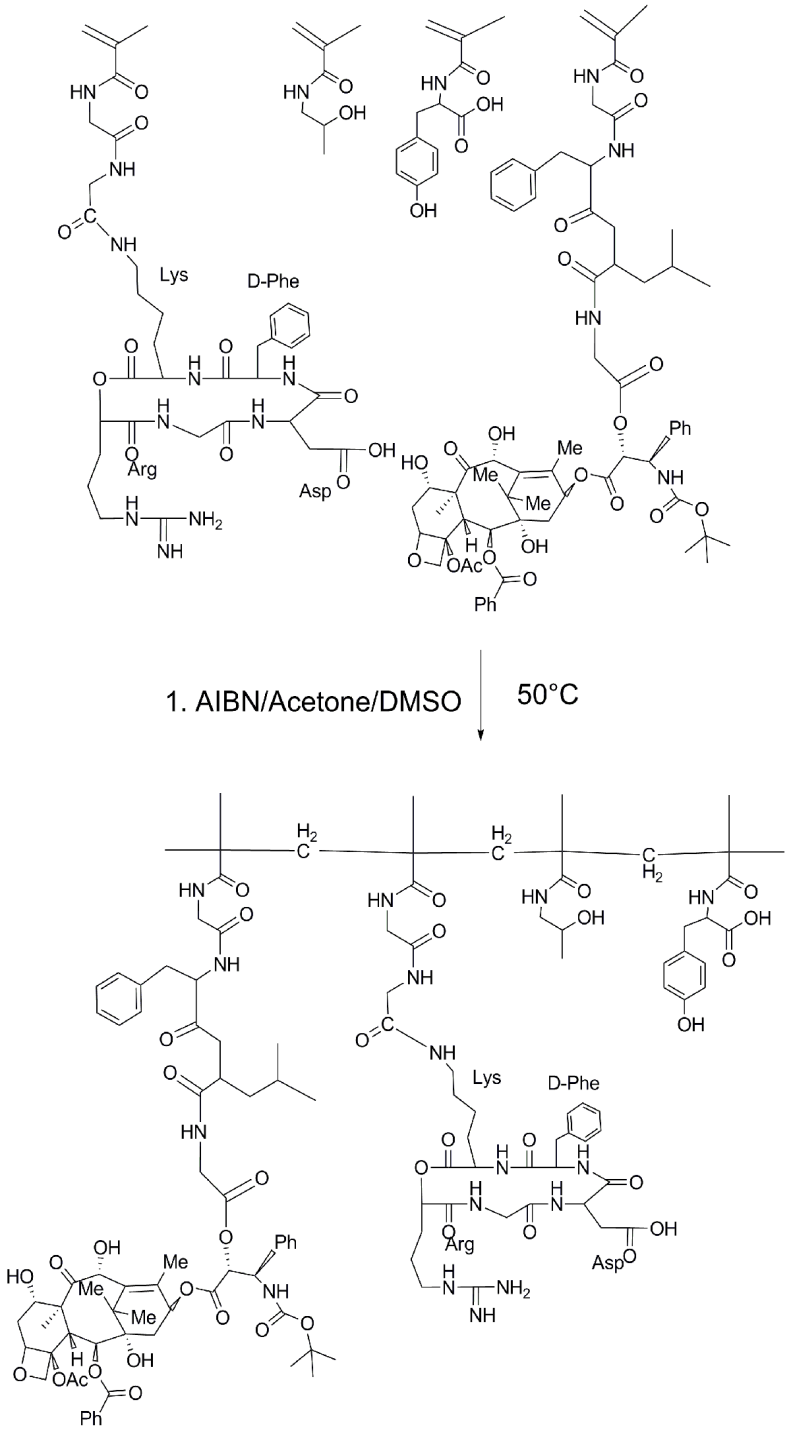

Figure A.1. Schematic synthesis and resulting structure of HPMA copolymer-RGDfK-docetaxel (P2) conjugates.

[a] Select copolymers contained the monocyclized RGDfK peptide targeteing moiety to target docetaxel to $\alpha_v\beta_3$ integrins.

Table A.1. Characteristics of HPMA copolymer conjugates

Polymer no.	Structure	Comonomer Feed Composition (mol %)					Est. M_w (kD)[a]	M_w/M_n[a]	Hydrody-namic diameter (nm)	DOC[b]	RGDfK[c]
		HPMA	MA-GFLG-DOC	MA-GG-RGDfK	MA-Tyr	3-MPA	(SEC)		(QELS)	wt %	wt %
P1	P-(GFLG-DOC)	95.5	2.5	-	2	4	32.6	2.9	3.0	6.8	-
P2	P-(GFLG-DOC-RGDfK)	92.5	2.5	3	2	4	26.9	1.9	3.0	6.84	5.061
P3	P-(GFLG-DOC)	95.5	2.5	-	2	1	87.1	4.9	7.6	7.15	

[a] Estimated by size exclusion chromatography (SEC), [b] Determined by HPLC

[c] Determined by amino acid analysis

conjugate was dissolved in 200 µl DMSO. Ten µl of this solution were incubated in 20 µl buffer A consisting of 0.1 M citrate phosphate buffer containing 2 mM EDTA at pH 6.0, 0.6 mM papain and 100 µl of buffer B consisting of 0.1 M citrate phosphate buffer containing 2 mM EDTA at pH 6.0 and 10 mM of glutathione. The mixture was incubated at 37°C for 24 hrs. The condition for complete release of the drug was optimized by varying the concentration of papain (0.1 mM to 1.0 mM) over time (data not shown). An aliquot (50µl) of the reaction mixture was removed and diluted in 450 µl water: acetonitrile (65:35) and evaluated for docetaxel content by HPLC and compared to calibration standards prepared using serial dilutions of docetaxel in the mobile phase. Mobile phase consisted of deionized water (Milli-Q system, Millipore, Billerica, MA, USA) and HPLC grade acetonitrile (ACN) using the following gradient: 0 min, 35% ACN; 15 min, 65% ACN; 25 min, 75% ACN; 30 min 95% ACN; 39 min, 100% ACN; 40 min 65% ACN. HPLC analyses were performed with an Agilent Series 1100 HPLC (Agilent Technologies, Wilmington, DE, USA) equipped with an Alltima C18 5 µm 150 x 4.6 mm column and a photo diode array detector scanning at 200 – 500 nm. A flow rate of 1.0 mL/min was maintained and the sample injection volume was 20 µl. A post time of 5 min was used to allow column equilibration between samples. UV absorbance at 230 nm was used for quantification of docetaxel. RGDfK content was determined by amino acid analysis (University of Utah Core Research Facilities, Salt Lake City, UT).

A.2.5 *In vitro* stability of the conjugates

The rate of release of docetaxel from the polymer-drug conjugates was evaluated in phosphate buffer saline (PBS) at pH 7.4 and in cell culture media. Two mg of each of the three copolymers P1, P2 and P3 (Table A.1) were incubated in 1 ml PBS (0.1 M phosphate buffer in 0.05 M of NaCl at pH 7.4) and 1 ml cell culture media (recommended media for DU145 from ATCC supplemented with 10% (v/v) fetal bovine serum (FBS) (HyClone, Logan, UT)), 100 U/ml penicillin, and 100 mg/ml streptomycin (Sigma). The samples were incubated at 37°C and a 100 µl aliquot was removed at times 0 min, 1 hr, 2 hrs, 6 hrs, 12 hrs, and 24 hrs. The aliquots were immediately cooled to 4°C in ice and then free docetaxel was extracted with dichloromethane (DCM, 3 x 100 µl). The organic extract was concentrated under nitrogen (N_2) and then reconstituted in HPLC grade ACN: deionized water ((Milli-Q system) (1:1). The release of the free drug was analyzed by HPLC and compared to calibration standards prepared using serial dilutions of docetaxel in the mobile phase. The mobile phase consisted of deionized water ((Milli-Q system) and HPLC grade ACN using the following gradient: 0 min, 50% ACN; 10 min, 50% ACN; 10.01 min, 95% ACN; 13 min 95% ACN; 13.01 min, 50% ACN; 15 min 65% ACN. HPLC analyses were performed with an Agilent Series 1100 HPLC (Agilent Technologies, Wilimington, DE, USA) equipped with an Alltima C18 5 µm 150 x 4.6 mm column and a photo diode array detector scanning at 200 – 500 nm. A flow rate of 1.0 mL/min was maintained and the sample injection volume was 20 µl. A post time of 2 min was used to allow column equilibration between samples. UV absorbance at 230 nm was used for quantification of docetaxel.

A.2.6 Cell lines

Human umbilical vein endothelial cells (HUVEC) and human prostate cancer DU145 and PC3 cell lines were obtained from American Type Culture Collection (ATCC) (Manassas, VA). DU145 and PC3 cells were maintained in the recommended media from ATCC supplemented with 10% (v/v) FBS, 100 U/ml penicillin, and 100 mg/ml streptomycin (Sigma). HUVECs were cultured in endothelial cell growth media-2 (EGM-2) (Lonza Inc., Allendale, NJ). Cells were incubated at 37°C in a humidified atmosphere of 5% CO_2 (v/v) and kept in logarithmic phase of growth throughout all experiments.

A.2.7 *In vitro* cell growth inhibition

Cell number and growth kinetics were assessed by utilizing a water-soluble tetrazolium salt, WST-8 [2-(2-methoxy-4-nitrophenyl)-3-(4-nitrophenyl)-5-(2,4-disulfophenyl)-2H-tetrazolium, monosodium salt], as a component of Cell Counting Kit-8 from Dojindo Molecular Technologies, Inc. (Sunnyvale, CA). Cells were seeded in 100 μl of cultured media at a density of 1×10^4 (DU145) or 1.5×10^4 (PC-3 and HUVEC) cells per cm^2 into a 96-well microtiter plate. They were subsequently allowed to adhere for 24 hrs before medium was replaced with fresh medium containing various concentrations of conjugates, free drug, or controls. Due to the poor water solubility of free docetaxel, stock solutions of conjugates, free drug, and controls were prepared in DMSO and subsequently diluted, resulting in a final concentration of 0.5 % (v/v) DMSO in complete growth medium. No significant toxicities were observed for any cell line when exposed to 0.5% DMSO concentrations for the duration of the

experiment. The cytotoxicity of free drug and HPMA copolymer-docetaxel conjugates was evaluated in two different experimental setups: i) continuous incubation with drugs for 72 h (DU145, PC-3); ii) short-term incubation or "pulse-chase" experiments where cells were incubated with drugs for 2 hrs only, washed with PBS and then incubated for an additional 70h (DU145). In pulse-chase experiments all compounds were added to cells either immediately after dilution in cell growth medium or after 16 h of pre-incubation in the same medium at 37^{o}C. Following treatment with drugs, cells were washed once with PBS and WST-8 was added. The absorbance of colored product at 450 nm, reference at 630 nm, was measured using a SpectraMax M2 microplate reader (Molecular Devices, Sunnyvale, CA). The number of viable cells exposed to the drugs was expressed as a percentage of untreated (control) cells, concentration–response curves were graphed, and IC_{50} values were determined by nonlinear regression analysis using GraphPad Prism v. 5.03 (GraphPad Software Inc., La Jolla, CA).

A.2.8 Comparative cell receptor binding assay

The comparative affinities of free RGDfK and HPMA copolymer conjugates were assessed using a competitive binding assay to $\alpha_v\beta_3$ receptors present on HUVEC and DU145 cells. HUVEC and DU145 cells were harvested, washed with PBS, and re-suspended in binding buffer (20 mmol/L tromethamine, pH 7.4, 150 mmol/L NaCl, 2 mmol/L $CaCl_2$, 1 mmol/L $MgCl_2$, 0.1% bovine serum albumin). Cell suspensions were added to 1.2 μm pore size 96-well Multiscreen HV filter plates (Millipore, Billerica, MA) at 100,000 cells per well. They were then co-incubated at 4°C with 0.5 ng ^{125}I-echistatin (Perkin Elmer, Waltham, MA) and increasing RGDfK peptide equivalent

concentrations of copolymer conjugates or free RGDfK peptide between 0 and 500 μM. Following 20 min incubation, media was removed from cells using a Multiscreen vacuum manifold (Millipore) and cells were washed three times with binding buffer. Filters were collected and radioactivity determined using a Cobra Auto-Gamma-counter (Canberra Industries, Inc., Meriden, CT). Each experiment was performed in triplicate, with n=4 per replicate. Binding percentage relative to control wells containing only ^{125}I-echistatin was calculated and non-linear regression analysis and determination of IC_{50} values was carried out using GraphPad Prism.

A.2.9 *In vivo* efficacy of HPMA copolymer-drug conjugates

Six-week-old athymic (nu/nu) mice were obtained from Charles River Laboratories (Davis, CA, USA) and used in accordance with the Institutional Animal Care and Use Committee (IACUC) of the University of Utah. Mice were anesthetized using 4% isoflurane mixed with oxygen followed by subcutaneous injection of 1×10^7 DU145 cells per flank (n=5 mice per treatment group). When the mean tumor size had reached approximately 50 mm^3, the mice were treated with a single dose of conjugates, free docetaxel, or control (saline injection) via tail vein injection. Conjugates were prepared in saline and free docetaxel required formulation in polysorbate 80: EtOH: saline (20:13: 67, v/v/v) to ensure solubility. The animals were routinely monitored and tumor growth was measured twice weekly and tumor volume was calculated as length $\cdot$ width$^2 \cdot \pi/6$. Tumor volumes at each time point were normalized by the initial volume and are reported as mean normalized tumor volume (%) ± standard error of the mean.

Animal weights were also measured at each time point and normalized to initial animal weight reported as mean ± standard deviation.

A.2.10 Statistical analysis

Differences in growth inhibition IC_{50} values were determined by one-way ANOVA. Where differences were detected, Scheffe's post-hoc analysis was used to test for significance between groups. *In vivo* data were analyzed by repeated measure ANOVA. Where differences were detected, Scheffe's post-hoc analysis was used to test for significance between groups. GraphPad Prism v. 5.03 and SPSS v 17 (Chicago, IL) was used for statistical analysis. The significance level was set at α=0.05 for all statistical tests.

A.3 Results and discussion

A.3.1 Physicochemical characteristics of polymeric conjugates

The characteristics of the HPMA copolymer conjugates are listed in Table A.1. The sizes of the copolymer conjugates, i.e., P1 (HPMA copolymer-GFLG-Docetaxel (low molecular weight)), P2 (HPMA copolymer-GFLG-Docetaxel-GG-RGDfK) and P3 (HPMA copolymer-GFLG-Docetaxel (high molecular weight)) were controlled by changing the ratio of the total comonomers to 3-mercaptoprotionic acid (3-MPA), which acts as a chain transfer reagent in the presence of a free radical initiator.[61] Docetaxel was attached to the HPMA copolymer backbone via a lysosomally degradable oligopeptide linker glycylphenylalanylleucylglycine and targeting peptide RGDfK was attached by the non-degradable dipeptide glycylglycine. The P1 and P2

conjugates (with and without $\alpha_v\beta_3$ integrin targeting peptide RGDfK) had a 4% molar equivalent of 3-MPA, while the high molecular weight conjugate had a 1% molar equivalent of 3-MPA. SEC and HPLC profiles of the conjugates indicate the absence of small molecular weight impurities or free docetaxel. Drug content of each polymer was measured by releasing docetaxel enzymatically using papain followed by HPLC analysis and was found to be 6.8 wt%, 6.84 wt% and 7.15 wt% for P1, P2 and P3 respectively. The molecular weights of the copolymers as estimated by SEC on a Superose 6 column were 32.6 kDa, 26.9 kDa and 87.1 kDa. The hydrodynamic diameter of the conjugates as measured by quasi elastic light scattering (QELS) were 3.0 nm, 3.0 nm and 7.6 nm for P1, P2, and P3 respectively. RGDfK content of P2 was estimated by amino acid analysis and was found to be 5.061 wt% of the polymer.

A.3.2 *In vitro* stability of polymer-drug conjugates

The in vitro stability of conjugates was investigated at physiological pH as well as in cell culture media at pH 7.4. The three conjugates P1, P2 and P3 released 14.8 ± 2.6%, 18.6 ± 4.8% and 10.8 ± 2.3% in PBS pH 7.4 and 23.4 ± 3.3, 23.2 ± 2.4 and 24.1 ± 2.7 in cell culture media in the first 24 hrs (Figure A.2). The higher release of the conjugates in the media is likely due to the presence of serum esterases which cleave the ester bond between the conjugate and the drug. All copolymer systems under study had less than 20% release of docetaxel in PBS at pH 7.4 and less than 25% release in cell culture media in 24 hrs, indicating adequate stability for in vivo accumulation of a portion of intact conjugates in solid tumors.

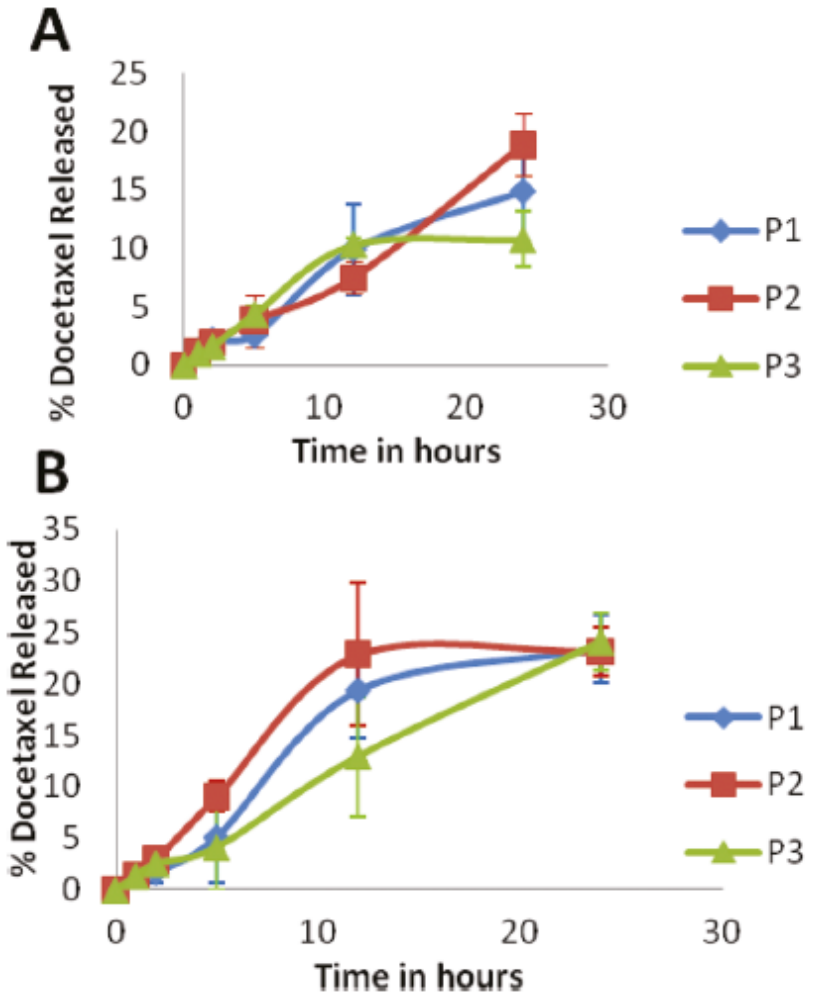

Figure A.2. Stability of polymer-drug conjugates. Stability of polymer-drug conjugates in PBS, pH 7.4 (A) and cell culture medium (B) at 37°C. Diamond represents P1, the untargeted low molecular weight conjugates; the square represents P2, the RGDfK targeted low molecular weight conjugates; and the triangle represents P3, the high molecular weight conjugate. The values of three independent measurements are presented as mean ± SD.

A.3.3 *In vitro* cell growth inhibition

All conjugates inhibited proliferation of prostate cancer cell lines and HUVECs at nanomolar concentrations (Figure A.3A-C). Analysis of growth inhibition curves revealed that the conjugates were 1.4- to 2.7-fold less toxic than free docetaxel when cells were incubated for continuous 72 hrs (Table A.2). HUVECs were more sensitive to docetaxel compared to prostate cancer cell lines as almost half of the drug concentrations were required to achieve the same magnitude of cell growth inhibition. Besides distinct difference between cytotoxic potential of free and conjugated form of docetaxel the difference between IC_{50} values for polymeric conjugates was found statistically insignificant ($p > 0.05$) for all cell lines tested.

Considering different routes of cellular entry and the necessity of lysosomal degradation of a linker between the polymer backbone and a drug, macromolecular therapeutics usually show 50-200 fold difference in toxicity compared to a free drug.[18] The difference observed between IC_{50} values of free and conjugated forms of docetaxel was expected but was significantly smaller compared to the difference for other macromolecular therapeutics. It is possible that the hydrolysis of the ester bond and fast drug release from the conjugates are responsible for high toxicity of the conjugates. The same issue could play an important role in the efficacy of the conjugates in vivo as ester bonds could be cleaved by abundant esterases in the bloodstream.[61] In an attempt to mimic *in vivo* physiological conditions, DU145 cells in this study were exposed to the polymer-drug conjugates for 2 hrs, a time period relevant to the plasma half-life of typical HPMA copolymer-drug conjugates.[49] In these sets of experiments DU145 cells were exposed to the drugs for 2 hrs only and subsequently were washed with phosphate buffered saline and incubation continued in fresh growth medium without drugs until the

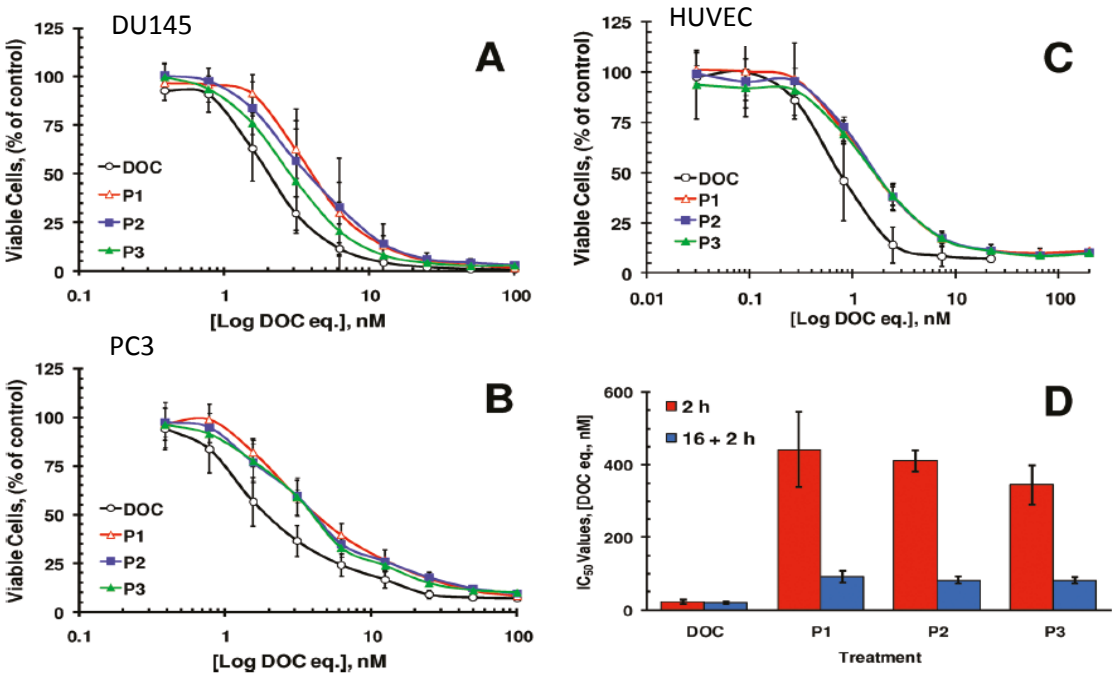

Figure A.3. Toxicity of docetaxel conjugates toward cultured cells. DU145 (A), PC-3 (B) prostate cancer cells and HUVECs (C) were exposed to the compounds for a continuous 72 hrs. In pulse-chase experiments (D) DU145 cells were incubated with the compounds for 2 hrs only, washed with PBS and incubated in fresh growth medium for an additional 70 hrs. The legend for this plot indicates how long compounds were in contact with cell growth medium. All compounds were added to cells either immediately after dilution in cell growth medium (2 hrs) or after 16 hrs of preincubation in the same medium at 37°C (16 ± 2 hrs). The values of three to four independent experiments are presented as mean ± SD.

Table A.2. Calculated IC_{50} values (nM) after continuous 72 hrs incubation of cells with drugs.

	DU145	PC-3	HUVEC
DOC	2.1+/-0.5	1.8+/-0.4	0.8+/-0.1
P1	4.4+/-1.1*	4.4+/-0.7*	2.7+/-0.9*
P2	3.0+/-0.4*	4.3+/-0.4*	2.3+/-0.4*
P3	3.3+/-0.8*	3.9+/-0.7*	1.9+/-0.5*

* $p < 0.05$ vs DOC.

number of cells was estimated. Therefore, this experimental set up allowed testing the influence of two important variables in these drug delivery systems: drug release rate and the presence of RGDfK targeting moiety. These experiments revealed a 15- to 20-fold difference between IC_{50} values of free and conjugated docetaxel when they were added to DU145 cells immediately after dilution in growth medium (Figure A.3D). This difference is most likely due to the difference in the mechanisms of cellular internalization between two forms of the drug, because the stability studies performed with polymer-drug conjugates revealed that less than 3% docetaxel was released from polymer-drug conjugates in the presence of cell culture media within 2 hrs (Figure A.2). This suggested that the conjugates were not completely hydrolyzed within the first two hours. Prolonged 16 hrs pre-incubation of the conjugates in growth medium before the initiation of pulse-chase experiments significantly changed the observed difference between the two forms of doxorubicin (Figure A.3D). After preincubation only 4- to 5-fold difference between IC_{50} values of free and conjugated docetaxel was observed most likely due to the release of the drugs from the conjugates. As in the experiments with 72 hrs continuous incubation, no statistically significant difference between IC_{50} values for the polymeric conjugates was found. Thus, given the two variables evaluated in this experiment, the release rate of free docetaxel proved to be the determinant variable that influenced the cytotoxicity of the tested constructs in vitro. High toxicity of the drug masked the binding advantage of the RGDfK moiety *in vitro*.

A.3.4 Competitive binding studies

Competitive binding studies demonstrated binding of the targeted HPMA copolymer-Docetaxel-RGDfK conjugate (P2) to HUVEC and DU145 cell lines with IC_{50} values of 0.5 ± 0.2 μM and 2.6 ± 0.3 μM respectively (Figure A.4). RGDfK peptide alone showed similar comparative binding affinities of 0.3 ± 0.1 μM and 1.5 ±

0.3 μM at equivalent peptide concentrations in HUVEC and DU145 cell lines. Untargeted conjugate (P1) was also evaluated in both cell lines and showed no evidence of active binding (Figure A.4). These results demonstrate the ability of the targeted conjugate P2 (Table A.1) to bind to $\alpha_v\beta_3$ integrins of HUVECs and DU145 cells. In both cases, conjugation of RGDfK to the HPMA copolymer backbone resulted in a small decrease in its binding affinity as compared to free RGDfK probably due to steric hindrance of the macromolecular system (Figure A.4).

A.3.5 *In vivo* antitumor efficacy of the conjugates

One focus of this study was to evaluate whether the efficacy of macromolecules with sizes below renal threshold can be enhanced by active targeting. To this end, we have chosen the cyclic integrin targeting peptide RGDfK as it has shown the ability to substantially increase tumor accumulation of HPMA copolymers in prostate tumors.[52] Docetaxel was chosen as it is the preferred drug of choice for patients with metastatic hormone refractive prostate cancer.[10] Efficacy of the conjugates was evaluated in nu/nu mice bearing DU145 prostate tumor xenografts. A single dose of each conjugate, free docetaxel, or control was administered. Physiological saline was used as a negative control and free docetaxel as positive control. The dose selection for both free drug and polymeric conjugates was 20 mg/kg and 40 mg/kg docetaxel equivalent, which corresponds to 60 mg/m^2 and 120 mg/m^2 in humans weighing 65 kg, as per calculation factors shown in the literature.[62, 63] This dose was based on several phase II/III clinical trials[5, 64-72] using docetaxel as a single agent as well as in combination chemotherapy, where doses varied between 30 mg/m^2 to 75 mg/m^2 given over several cycles.

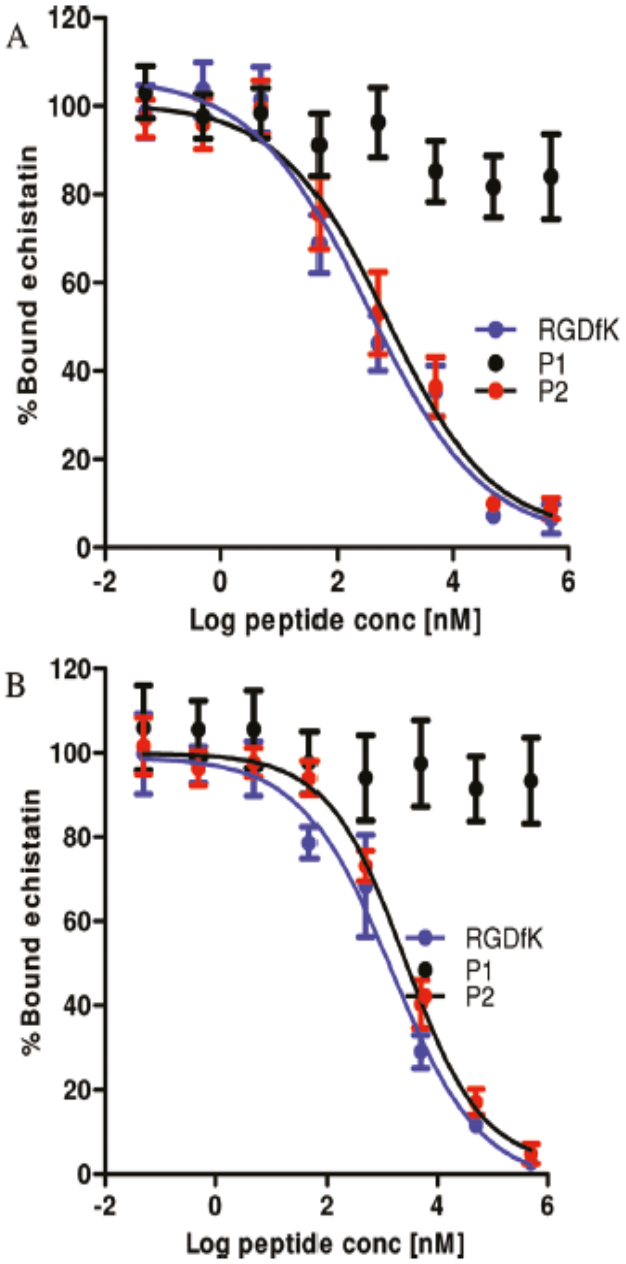

Figure A.4. Competitive binding of copolymer conjugates. Competitive binding of HPMA copolymer conjugates and free RGDfK peptide binding of HPMA copolymer conjugates with and without RGDfK was compared to free peptide on (A) HUVEC and (B) human prostate cancer DU145 cells. Results are expressed as means of triplicate ± SD. For sample characteristics see Table A.1.

Animals injected with free docetaxel at both 20 mg/kg and 40 mg/kg showed signs of hyper- acute toxicity as they were rendered immobile for the first 30 min post injection. The lethargy shown by animals injected with free docetaxel was most likely a result of toxicity associated with the drug as well as the polysorbate 80 required to dissolve the drug for i.v. injection. None of the animals in the control group or those treated with conjugates showed any signs of acute toxicity. Mice weights were followed up through the duration of the study as an overall measurement of the safety of administered compounds. The normalized weights of animals showed no statistical difference between all groups for the duration of study (Figure A.5A). Animals injected with free docetaxel showed statistically significant 2.6 and 2.9 fold reduction in mean tumor size as compared to saline at concentrations of 20 mg/kg ($P < 0.01$) and 40 mg/kg ($P < 0.001$). Although, conjugate P1 (untargeted, low molecular weight HPMA-docetaxel) at 20 mg/kg demonstrated a 0.9-fold difference in mean tumor size as compared to saline, this difference was not statistically significant ($P > 0.1$). However, treatment animals with P1 at 40 mg/kg resulted in a 2.3-fold reduction in mean tumor size as compared to saline ($P < 0.05$).

Conjugate P2 (RGDfK targeted, low molecular weight HPMA copolymer-docetaxel) and conjugate P3 (untargeted, high molecular weight HPMA copolymer-docetaxel) at injected doses of 20 mg/kg (Figure A.5B) and 40 mg/kg (Figure A.5C) showed reduction in mean tumor size as compared to saline ($P < 0.001$) of 3.3, 3.2, 3.5 and 3.4-fold respectively. While animals injected with both conjugates P2 and P3 demonstrated reduction in tumor size greater than the group injected with free docetaxel, only results with P2 at both 20 mg/kg and 40 mg/kg were statistically

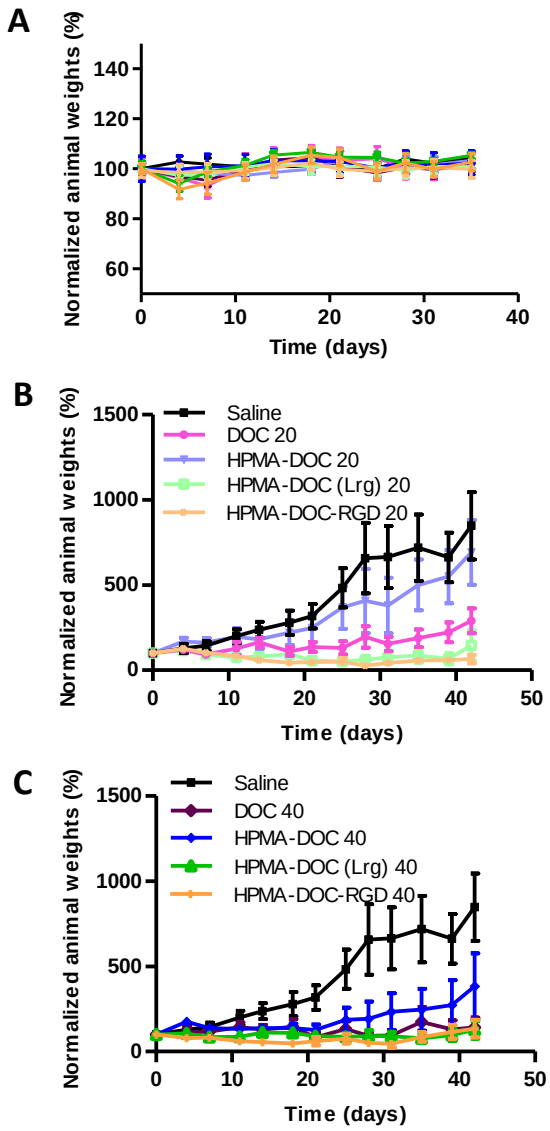

Figure A.5. *In vivo* efficacy. (A) Normalized animal weights as a function of time. Data are expressed as mean ± SEM (n = 5 per treatment group). (B) Efficacy of free drug and targeted/nontargeted polymer-drug conjugates P1, P2 and P3 at drug equivalent concentration of 20 mg/kg in nu/nu mice bearing DU145 tumor xenografts. (C) Efficacy of free drug and targeted/nontargeted polymer-drug conjugates P1, P2 and P3 at drug equivalent concentration of 40 mg/kg in nu/nu mice bearing DU145 tumor xenografts. Tumor volumes were normalized by their respective volume on day 0 (approx 50 mm^3). Data are expressed as mean ± SEM (n = 10 tumors per treatment group). For sample characteristics see Table A.1.

significant. The efficacy of P1 at 20 mg/kg was statistically inferior to P2 at 20 mg/kg and 40 mg/kg ($P < 0.01$) and P3 at doses of 20 mg/kg and 40 mg/kg ($P < 0.05$) with a mean difference in tumor size of 2.5, 2.4, 2.3 and 2.2 fold. P1 at 40 mg/kg had no statistical difference in mean tumor size with P2 and P3 at 20 mg/kg and 40 mg/kg. P2 and P3 had no statistical difference at doses of 20 mg/kg or 40 mg/kg.

The lack of efficacy for P1 at 20 mg/kg in spite of efficacy observed in free docetaxel can be explained below: i) low molecular weight P1 with a hydrodynamic diameter of 3.0 nm was small enough to be rapidly eliminated by glomerular filtration, thereby minimizing the persistence time of the conjugate in blood circulation which is necessary to achieve tumor accumulation due to the EPR effect, and /or ii) the release of docetaxel from the conjugate was not fast enough for it to be effective prior to its elimination. Therefore, free docetaxel at this concentration was more effective than the untargeted low molecular weight conjugate. The efficacy of P1 was evident at 40 mg/kg because sufficient docetaxel could be released from the conjugate prior to elimination. The only advantage shown by animals injected with P1 was the lack of adverse hyperacute reaction in response to injection that was observed for free docetaxel administration, possibly due to the aqueous solubility acquired by polymer conjugation.

At 20 mg/kg, P2 showed the largest difference in tumor size with saline. Conjugate P2, like P1 had a hydrodynamic diameter of 3.0 nm which was well below the glomerular renal threshold. The activity observed in these conjugates most probably is a consequence of active targeting as they had $\alpha_v\beta_3$ integrin targeting peptide RGDfK linked to the polymer side chains, thereby allowing them to anchor on to the

neovasculature of angiogenic blood vessels. The RGD peptides have also been reported to be tumor penetrating and its coadministration enhances the efficacy of anticancer drugs.[48] RGDfK in conjugate P2 may have also contributed to a greater efficacy. Conjugate P3, on the other hand, had a hydrodynamic diameter of 7.6 nm which was above the glomerular renal threshold. This increases the plasma half-life and improves efficacy by passive targeting via the EPR effect. Administration of P3 at concentrations of 20 mg/kg had a reduction in mean tumor size difference as compared to saline ($P < 0.001$) and P1 ($P < 0.05$). Again, the difference in activity at 20 mg/kg of P3 when compared to free docetaxel was not statistically significant for the study period of 42 days.

Further, when comparisons were made between active targeting (P2) and passive targeting via the EPR effect (P3) at drug equivalent concentrations of 20 mg/kg, though the mean difference in tumor size between the groups was not significant, the mean tumor size reduction was greater in case of actively targeted P2 conjugates. However at 40 mg/kg, which corresponds to 120 mg/m^2 in humans and is more than 1.5 times the highest concentration administered in clinical trials of docetaxel for treatment of prostate cancer, free drug and all three conjugates P1, P2 and P3 induced statistically significant tumor size reduction as compared to saline. The efficacy of P1 was evident at 40 mg/kg because sufficient docetaxel was released from the conjugate prior to elimination. Administrations of all three conjugates, unlike free docetaxel, demonstrated no visible signs of toxicity, and were freely soluble in saline.

The post hoc analysis of the variance of the mean size of the tumor over entire study period of 42 days classified the conjugates and controls into three categories, i.e.

those with high activity, those with moderate activity and those with no activity. Each compound falls under one or two categories. According to this analysis saline falls in the low activity category, P1 at 20 mg/kg falls under the low and moderate activity categories, P1 at 40 mg/kg, free docetaxel at both 20 mg/kg and 40 mg/kg doses fall under moderate and high activity categories while P2 and P3 at both 20 mg/kg and 40 mg/kg fall under the high activity category.

To summarize, administrations of all three conjugates, unlike free docetaxel, demonstrated no visible signs of toxicity, and were freely soluble in saline. Actively targeted conjugate P2 demonstrated the highest tumor size reduction for the duration of the study as compared to free docetaxel, small nontargeted conjugate P1 and passively targeted (via EPR) high molecular weight conjugate P3. All three conjugates were soluble in aqueous media and did not show any visible signs of hyper-acute toxicity in animals. Further, while P3 does not have a biodegradable polymer backbone which would result in accumulation of the macromolecule post treatment, P2 has the advantage of a small size (3.0 nm) which can allow the dose fraction that does not reach the tumor to be eliminated.

A.4 Conclusion

HPMA copolymer-docetaxel conjugates with sizes of 3.0 nm and 7.6 nm, which correspond to dimensions below and above the glomerular renal threshold, as well as $\alpha_v\beta_3$ integrin targeting conjugate HPMA copolymer-docetaxel-RGDfK of hydrodynamic diameter 3.0 nm, were successfully synthesized to evaluate the effect of active targeting with passive targeting. All the conjugates inhibited proliferation of

human prostate cancer DU145 and PC3 cells as well as HUVEC at nanomolar concentrations. Cytotoxicity experiments by pulse-chase method where the incubation time with free drug and conjugates was limited to 2 hrs resulted in a 15- to 20-fold difference in activity of conjugates as compared to free docetaxel. This suggests that the conjugates were not completely hydrolyzed within the first two hours. Animals showed no visible signs of toxicity when injected with conjugates. HPMA copolymer-docetaxel conjugates of hydrodynamic diameter 7.6 nm and HPMA copolymer-docetaxel-RGDfK of hydrodynamic diameter 3.0 nm demonstrated the greatest tumor reduction capability with statistically significant tumor regression compared to saline. Overall, the results demonstrate that $\alpha_v\beta_3$ integrin targeted, low molecular weight conjugates with improved water solubility, reduced toxicity and ease of elimination post treatment *in vivo* are promising candidates for prostate cancer therapy.

A.5 References

1. A. Ray[*], N. Larson[*], D.B. Pike, M. Gruner, S. Naik, H. Bauer, A. Malugin, K. Greish, and H. Ghandehari. ([*]first co-authors). Comparison of active and passive targeting of docetaxel for prostate cancer therapy by HPMA copolymer-RGDfK conjugates. Mol Pharm. 8:1090-1099 (2011).

2. A. Jemal, R. Siegel, E. Ward, Y. Hao, J. Xu, and M.J. Thun. Cancer statistics, 2009. CA Cancer J Clin. 59:225-249 (2009).

3. D. Mazhar and J. Waxman. Early chemotherapy in prostate cancer. Nat Clin Pract Urol. 5:486-493 (2008).

4. D.P. Petrylak, C.M. Tangen, M.H. Hussain, P.N. Lara, Jr., J.A. Jones, M.E. Taplin, P.A. Burch, D. Berry, C. Moinpour, M. Kohli, M.C. Benson, E.J. Small, D. Raghavan, and E.D. Crawford. Docetaxel and estramustine compared with mitoxantrone and prednisone for advanced refractory prostate cancer. N Engl J Med. 351:1513-1520 (2004).

5. I.F. Tannock, R. de Wit, W.R. Berry, J. Horti, A. Pluzanska, K.N. Chi, S. Oudard, C. Theodore, N.D. James, I. Turesson, M.A. Rosenthal, and M.A. Eisenberger. Docetaxel plus prednisone or mitoxantrone plus prednisone for advanced prostate cancer. N Engl J Med. 351:1502-1512 (2004).

6. A. Montero, F. Fossella, G. Hortobagyi, and V. Valero. Docetaxel for treatment of solid tumours: a systematic review of clinical data. Lancet Oncol. 6:229-239 (2005).

7. I. Ringel and S.B. Horwitz. Studies with RP 56976 (taxotere): a semisynthetic analogue of taxol. J Natl Cancer Inst. 83:288-291 (1991).

8. N. Katsumata. Docetaxel: an alternative taxane in ovarian cancer. Br J Cancer. 89 Suppl 3:S9-S15 (2003).

9. K.A. Hotchkiss, A.W. Ashton, R. Mahmood, R.G. Russell, J.A. Sparano, and E.L. Schwartz. Inhibition of endothelial cell function in vitro and angiogenesis in vivo by docetaxel (Taxotere): association with impaired repositioning of the microtubule organizing center. Mol Cancer Ther. 1:1191-1200 (2002).

10. S. Mike, C. Harrison, B. Coles, J. Staffurth, T.J. Wilt, and M.D. Mason. Chemotherapy for hormone-refractory prostate cancer. Cochrane Database Syst Rev:CD005247 (2006).

11. K. Leimgruber, R. Negro, S. Baier, B. Moser, G. Resch, S. Sansone, M. Adami, P. Zanon, C. Graiff, E. Egarter-Vigl, and C.J. Wiedermann. Fatal interstitial pneumonitis associated with docetaxel administration in a patient with hormone-refractory prostate cancer. Tumori. 92:542-544 (2006).

12. F.K. Engels, R.A. Mathot, and J. Verweij. Alternative drug formulations of docetaxel: a review. Anticancer Drugs. 18:95-103 (2007).

13. J. Kopecek, P. Kopeckova, T. Minko, and Z. Lu. HPMA copolymer-anticancer drug conjugates: design, activity, and mechanism of action. Eur J Pharm Biopharm. 50:61-81 (2000).

14. R. Duncan. The dawning era of polymer therapeutics. Nat Rev Drug Discov. 2:347-360 (2003).

15. Y. Matsumura and H. Maeda. A new concept for macromolecular therapeutics in cancer chemotherapy: mechanism of tumoritropic accumulation of proteins and the antitumor agent smancs. Cancer Res. 46:6387-6392 (1986).

16. H. Maeda, J. Wu, T. Sawa, Y. Matsumura, and K. Hori. Tumor vascular permeability and the EPR effect in macromolecular therapeutics: a review. J Control Release. 65:271-284 (2000).

17. Y. Noguchi, J. Wu, R. Duncan, J. Strohalm, K. Ulbrich, T. Akaike, and H. Maeda. Early Phase Tumor Accumulation of Macromolecules: A Great Difference in Clearance Rate between Tumor and Normal Tissues. Cancer Science. 89:307-314 (1998).

18. J. Kopecek and P. Kopeckova. HPMA copolymers: origins, early developments, present, and future. Adv Drug Deliv Rev. 62:122-149 (2010).

19. B. Rihova, M. Bilej, V. Vetvicka, K. Ulbrich, J. Strohalm, J. Kopecek, and R. Duncan. Biocompatibility of N-(2-hydroxypropyl) methacrylamide copolymers containing adriamycin. Immunogenicity, and effect on haematopoietic stem cells in bone marrow in vivo and mouse splenocytes and human peripheral blood lymphocytes in vitro. Biomaterials. 10:335-342 (1989).

20. M. Nishikawa, Y. Takakura, and M. Hashida. Pharmacokinatic evaluation of polymeric carriers. Adv Drug Deliv Rev. 21:135-155 (1996).

21. Y. Takakura, T. Fujita, M. Hashida, and H. Sezaki. Disposition characteristics of macromolecules in tumor-bearing mice. Pharmaceutical Research. 7:339-346 (1990).

22. Y. Takakura and M. Hashida. Macromolecular carrier systems for targeted drug delivery: pharmacokinetic considerations on biodistribution. Pharmaceutical Research. 13:820-831 (1996).

23. Y. Takakura, R.I. Mahato, M. Nishikawa, and M. Hashida. Control of pharmacokinetic profiles of drug-macromolecule conjugates. Adv Drug Deliv Rev. 19:377-399 (1996).

24. Y. Boucher, L.T. Baxter, and R.K. Jain. Interstitial pressure gradients in tissue-isolated and subcutaneous tumors: implications for therapy. Cancer Res. 50:4478-4484 (1990).

25. R.K. Jain. Transport of molecules in the tumor interstitium: a review. Cancer Res. 47:3039-3051 (1987).

26. R.K. Jain. Normalization of tumor vasculature: an emerging concept in antiangiogenic therapy. Science. 307:58-62 (2005).

27. P. Carmeliet and R.K. Jain. Angiogenesis in cancer and other diseases. Nature. 407:249-257 (2000).

28. G.D. Yancopoulos, S. Davis, N.W. Gale, J.S. Rudge, S.J. Wiegand, and J. Holash. Vascular-specific growth factors and blood vessel formation. Nature. 407:242-248 (2000).

29. M. Leunig, F. Yuan, M.D. Menger, Y. Boucher, A.E. Goetz, K. Messmer, and R.K. Jain. Angiogenesis, microvascular architecture, microhemodynamics, and interstitial fluid pressure during early growth of human adenocarcinoma LS174T in SCID mice. Cancer Res. 52:6553-6560 (1992).

30. F. Yuan, H.A. Salehi, Y. Boucher, U.S. Vasthare, R.F. Tuma, and R.K. Jain. Vascular permeability and microcirculation of gliomas and mammary carcinomas transplanted in rat and mouse cranial windows. Cancer Res. 54:4564-4568 (1994).

31. W.S. Kamoun, S.S. Chae, D.A. Lacorre, J.A. Tyrrell, M. Mitre, M.A. Gillissen, D. Fukumura, R.K. Jain, and L.L. Munn. Simultaneous measurement of RBC velocity, flux, hematocrit and shear rate in vascular networks. Nat Methods. 7:655-660.

32. B. Endrich, H.S. Reinhold, J.F. Gross, and M. Intaglietta. Tissue perfusion inhomogeneity during early tumor growth in rats. J Natl Cancer Inst. 62:387-395 (1979).

33. Y. Boucher and R.K. Jain. Microvascular pressure is the principal driving force for interstitial hypertension in solid tumors: implications for vascular collapse. Cancer Res. 52:5110-5114 (1992).

34. Y. Boucher, M. Leunig, and R.K. Jain. Tumor angiogenesis and interstitial hypertension. Cancer Res. 56:4264-4266 (1996).

35. R.K. Jain and T. Stylianopoulos. Delivering nanomedicine to solid tumors. Nat Rev Clin Oncol. 7:653-664 (2010).

36. A. Nori and J. Kopecek. Intracellular targeting of polymer-bound drugs for cancer chemotherapy. Advance Drug Delivery Reviews,. 57:609-636 (2005).

37. R. Pasqualini, E. Koivunen, and E. Ruoslahti. Alpha v integrins as receptors for tumor targeting by circulating ligands. Nat Biotechnol. 15:542-546 (1997).

38. E. Koivunen, B. Wang, and E. Ruoslahti. Phage libraries displaying cyclic peptides with different ring sizes: ligand specificities of the RGD-directed integrins. Biotechnology (N Y). 13:265-270 (1995).

39. A.J. Schraa, R.J. Kok, H.E. Moorlag, E.J. Bos, J.H. Proost, D.K.F. Meijer, L. de Leij, and G. Molema. Targeting of RGD-modified proteins to tumor vasculature: A pharmacokinetic and cellular distribution study. International Journal of Cancer. 102:469-475 (2002).

40. P.K. Dubey, V. Mishra, S. Jain, S. Mahor, and S.P. Vyas. Liposomes modified with cyclic RGD peptide for tumor targeting. J Drug Target. 12:257-264 (2004).

41. G.A. Koning, M.M. Fretz, U. Woroniecka, G. Storm, and G.C. Krijger. Targeting liposomes to tumor endothelial cells for neutron capture therapy. Appl Radiat Isot. 61:963-967 (2004).

42. R.M. Schiffelers, G.A. Koning, T.L. ten Hagen, M.H. Fens, A.J. Schraa, A.P. Janssen, R.J. Kok, G. Molema, and G. Storm. Anti-tumor efficacy of tumor vasculature-targeted liposomal doxorubicin. J Control Release. 91:115-122 (2003).

43. X. Chen, R. Park, A.H. Shahinian, J.R. Bading, and P.S. Conti. Pharmacokinetics and tumor retention of 125I-labeled RGD peptide are improved by PEGylation. Nucl Med Biol. 31:11-19 (2004).

44. A. Meyer, J. Auernheimer, A. Modlinger, and H. Kessler. Targeting RGD recognizing integrins: drug development, biomaterial research, tumor imaging and targeting. Curr Pharm Des. 12:2723-2747 (2006).

45. E. Ruoslahti. Specialization of tumour vasculature. Nat Rev Cancer. 2:83-90 (2002).

46. A. Hajitou. Targeted systemic gene therapy and molecular imaging of cancer contribution of the vascular-targeted AAVP vector. Adv Genet. 69:65-82 (2010).

47. H. Jiang, C. Gomez-Manzano, F.F. Lang, R. Alemany, and J. Fueyo. Oncolytic adenovirus: preclinical and clinical studies in patients with human malignant gliomas. Curr Gene Ther. 9:422-427 (2009).

48. K.N. Sugahara, T. Teesalu, P.P. Karmali, V.R. Kotamraju, L. Agemy, D.R. Greenwald, and E. Ruoslahti. Coadministration of a tumor-penetrating peptide enhances the efficacy of cancer drugs. Science. 328:1031-1035 (2010).

49. M.P. Borgman, O. Aras, S. Geyser-Stoops, E.A. Sausville, and H. Ghandehari. Biodistribution of HPMA copolymer-aminohexylgeldanamycin-RGDfK conjugates for prostate cancer drug delivery. Mol Pharm. 6:1836-1847 (2009).

50. M.P. Borgman, A. Ray, R.B. Kolhatkar, E.A. Sausville, A.M. Burger, and H. Ghandehari. Targetable HPMA Copolymer-Aminohexylgeldanamycin Conjugates for Prostate Cancer Therapy. Pharm Res. 6:1407-1418 (2009).

51. A. Mitra, T. Coleman, M. Borgman, A. Nan, H. Ghandehari, and B.R. Line. Polymeric conjugates of mono- and bi-cyclic alphaVbeta3 binding peptides for tumor targeting. J Control Release. 114:175-183 (2006).

52. D.B. Pike and H. Ghandehari. HPMA copolymer-cyclic RGD conjugates for tumor targeting. Adv Drug Deliv Rev. 62:167-183 (2010).

53. B. Zarabi, M.P. Borgman, J. Zhuo, R. Gullapalli, and H. Ghandehari. Noninvasive Monitoring of HPMA Copolymer-RGDfK Conjugates by Magnetic Resonance Imaging. Pharm Res. 26:1121-1129 (2009).

54. J.D. Hood and D.A. Cheresh. Role of integrins in cell invasion and migration. Nat Rev Cancer. 2:91-100 (2002).

55. K. Greish, A. Ray, H. Bauer, N. Larson, A. Malugin, D. Pike, M. Haider, and H. Ghandehari. Anticancer and antiangiogenic activity of HPMA copolymer-aminohexylgeldanamycin-RGDfK conjugates for prostate cancer therapy. J Control Release. PMID 21223983: (2011).

56. J. Strohalm and J. Kopecek. Poly *N*-(2-hydroxypropyl) methacrylamide: 4. Heterogenous polymerization. Angew Makromol Chem. 70:109-118 (1978).

57. P. Rejmanova, J. Labsky, and J. Kopecek. Aminolyses of monomeric and polymeric p-nitrophenyl esters of methacryloylated amino acids. Makromol Chem. 178:2159-2168 (1977).

58. K. Ulbrich, V. Subr, J. Strohalm, D. Plocova, M. Jelinkova, and B. Rihova. Polymeric drugs based on conjugates of synthetic and natural macromolecules. I. Synthesis and physico-chemical characterisation. J Control Release. 64:63-79 (2000).

59. J.H. Lee, P. Kopeckova, J. Kopecek, and J.D. Andrade. Surface properties of copolymers of alkyl methacrylates with methoxy (polyethylene oxide) methacrylates and their application as protein-resistant coatings. Biomaterials. 11:455-464 (1990).

60. K. Ulbrich, E.I. Zacharieva, B. Obereigner, and J. Kopecek. Polymers containing enzymatically degradable bonds V. Hydrophilic polymers degradable by papain. Biomaterials. 1:199-204 (1980).

61. T. Baltes, F. Garret-Flaudy, and R. Freitag. Investigation of the LCST of polyacrylamides as a function of molecular parameters and the solvent composition. Journal of Polymer Science Part A: Polymer Chemistry. 37:2977-2989 (1999).

62. E.J. Freireich, E.A. Gehan, D.P. Rall, L.H. Schmidt, and H.E. Skipper. Quantitative comparison of toxicity of anticancer agents in mouse, rat, hamster, dog, monkey, and man. Cancer Chemother Rep. 50:219-244 (1966).

63. S. Reagan-Shaw, M. Nihal, and N. Ahmad. Dose translation from animal to human studies revisited. FASEB J. 22:659-661 (2008).

64. J. Picus and M. Schultz. Docetaxel (Taxotere) as monotherapy in the treatment of hormone-refractory prostate cancer: preliminary results. Semin Oncol. 26:14-18 (1999).

65. D. Friedland, J. Cohen, R. Miller, Jr., M. Voloshin, R. Gluckman, B. Lembersky, B. Zidar, M. Keating, N. Reilly, and B. Dimitt. A phase II trial of docetaxel (Taxotere) in hormone-refractory prostate cancer: correlation of antitumor effect to phosphorylation of Bcl-2. Semin Oncol. 26:19-23 (1999).

66. W. Berry, S. Dakhil, M.A. Gregurich, and L. Asmar. Phase II trial of single-agent weekly docetaxel in hormone-refractory, symptomatic, metastatic carcinoma of the prostate. Semin Oncol. 28:8-15 (2001).

67. T.M. Beer, W.C. Pierce, B.A. Lowe, and W.D. Henner. Phase II study of weekly docetaxel in symptomatic androgen-independent prostate cancer. Ann Oncol. 12:1273-1279 (2001).

68. G. Gravis, F. Bladou, N. Salem, G. Macquart-Moulin, G. Serment, J. Camerlo, D. Genre, V.J. Bardou, D. Maraninchi, and P. Viens. Weekly administration of docetaxel for symptomatic metastatic hormone-refractory prostate carcinoma. Cancer. 98:1627-1634 (2003).

69. D.P. Petrylak. Docetaxel for the treatment of hormone-refractory prostate cancer. Rev Urol. 5 Suppl 2:S14-21 (2003).

70. D.P. Petrylak, D.P. Ankerst, C.S. Jiang, C.M. Tangen, M.H. Hussain, P.N. Lara, Jr., J.A. Jones, M.E. Taplin, P.A. Burch, M. Kohli, M.C. Benson, E.J. Small, D. Raghavan, and E.D. Crawford. Evaluation of prostate-specific antigen declines for surrogacy in patients treated on SWOG 99-16. J Natl Cancer Inst. 98:516-521 (2006).

71. V.J. Sinibaldi, M.A. Carducci, S. Moore-Cooper, M. Laufer, M. Zahurak, and M.A. Eisenberger. Phase II evaluation of docetaxel plus one-day oral estramustine phosphate in the treatment of patients with androgen independent prostate carcinoma. Cancer. 94:1457-1465 (2002).

72. D.M. Savarese, S. Halabi, V. Hars, W.L. Akerley, M.E. Taplin, P.A. Godley, A. Hussain, E.J. Small, and N.J. Vogelzang. Phase II study of docetaxel, estramustine, and low-dose hydrocortisone in men with hormone-refractory prostate cancer: a final report of CALGB 9780. J Clin Oncol. 19:2509-2516 (2001).

APPENDIX B

SYNTHESIS AND EVALUATION OF POLY(STYRENE-*CO*-MALEIC ACID) MICELLAR NANOCARRIERS FOR THE DELIVERY OF TANESPIMYCIN

B.1 Introduction

Heat shock protein 90 (Hsp90) is a 90 kDa chaperone protein that facilitates the cellular response to stress by regulating the folding and activity of many client proteins, which include critical growth-stimulating proteins involved in the malignant transformation of various cancers.[1] Hsp90 expression is elevated during cellular stress conditions such as heat, pH, and glucose deprivation[2] and in a variety of cancers including melanoma, leukemia, colon, lung, breast, and prostate.[3]

Geldanamycin (GDM), a benzoquinone ansamycin derived from *Streptomyces hygrocopicus*, is a naturally occurring inhibitor of Hsp90 and has been studied extensively as an anticancer agent.[4] GDM binds to the N-terminal ATP-binding site of Hsp90 and induces degradation of its client proteins.[5] This ability of GDM to alter multiple oncogenic pathways makes GDM an attractive therapeutic compound. However, the clinical use of GDM has been limited by multiple factors. It exhibits high hepatotoxicity at therapeutic doses in animal models,[6] is poorly soluble in water, and is metabolically unstable.[3] A GDM derivative 17-*N*-allylamino-17-demethoxy-

geldanamycin (tanespimycin, 17-AAG) has been widely investigated as an alternative to GDM, and has shown less toxicity and comparable activity compared to GDM in mouse models.[7, 8] This drug was the first-in-class Hsp90 inhibitor to enter clinical trials.[9] Although the therapeutic index for tanespimycin is increased as compared to GDM, dose limiting toxicity is still due to hepatic and gastrointestinal symptoms.[10] Delivery of tanespimycin is difficult due a poor aqueous solubility of 0.02 – 0.05 mg/mL,[11] requiring the use of surfactants such as Cremophor® EL, which are known to induce histamine release, resulting hypersensitivity reactions and anaphylaxis,[12] and are further associated with hyperlipidaemia, abnormal lipoprotein patters, aggregation of erythrocytes, and peripheral neuropathy.[13]

Polymeric carriers can increase the solubility of poorly water soluble drugs and can accumulate in tumor tissues via the "enhanced permeability and retention" (EPR) effect,[14, 15] thereby increasing the therapeutic index for a given chemotherapeutic agent. Polymeric micelles are characterized by a hydrophilic shell which interacts with an external aqueous environment and a hydrophobic core which acts as a depot for hydrophobic drugs. Polymeric micelles were first reported as potential carriers for use in cancer treatment in the early 1980s[16] and the field has matured to include a number of candidates currently under clinical investigation.[17]

The use of poly(styrene-*co*-maleic acid) (SMA) micelles as drug carriers is currently under investigation.[18, 19] SMA has been proven to be biologically safe and is used clinically in SMANCS, a conjugate of half-butyl SMA bound to the antitumor protein neocarzinostatin.[20] Previous studies have demonstrated immunopotentiating activity associated with SMA moieties, in contrast to immunosupression that is typically

induced by conventional chemotherapeutics.[21, 22] The styrenic core of SMA micelles has been characterized by a high glass transition temperature[23] and a large microviscosity,[24] which may help facilitate higher stability and more controlled release rates of drugs from the micelle core. In addition, the hydrophilic surface of SMA micelles is comprised of carboxyl terminated maleic acid groups, allowing easy surface modification or conjugation with targeting moieties.

Previous work has described the use of HPMA copolymers as drug carriers for geldanamycin derivatives[25, 26, 27]. In these systems, geldanamycin derivatives were covalently bound to the polymer backbone via the lysosomally degradable Gly-Phe-Leu-Gly linker,[28] resulting in highly stable conjugates with drug release occurring via lysosomal degradation following endocytosis. The use of such systems however requires chemical modification of geldanamycin to facilitate conjugation, and such modifications result in a decrease in the activity of geldanamycin. Self-assembled drug delivery systems do not suffer from this limitation as the drug is most often bound to the carrier through non-covalent hydrophobic interactions.

In the study presented in this Appendix, SMA was used to prepare polymeric micelles containing the Hsp90 inhibitor tanespimycin. The micelles were characterized for drug loading efficiency, drug content, size, and zeta potential. The release rate of tanespimycin from the micelles and the ability of the micelles to inhibit the growth of DU145 human prostate cancer cells *in vitro* were evaluated. An *in vivo* preliminary single dose study evaluating the efficacy of the micelles was performed in nu/nu mice bearing DU145 human prostate cancer xenografts.

B.2 Materials and Methods

B.2.1 Materials

Geldanamycin (NSC 122750) was kindly supplied by the National Cancer Institute Developmental Therapeutics Program (NCI DTP). Allylamine was supplied by Alfa Aesar (Ward Hill, MA, USA). Cumene terminated poly(styrene-*co*-maleic anhydride) was obtained from Sigma-Aldrich Corp. (St. Louis, MO, USA) and supplied with a 1.3:1 mole ratio of styrene:maleic anhydride, an average M_n of approximately 1600 as determined by GPC, and an acid number of 465-495 mg KOH/g. *N*-(3-Dimethylaminopropyl)-*N'*ethylcarbodiimide hydrochloride (EDAC) was obtained from Sigma-Aldrich Corp. Bovine serum albumin fraction V (BSA) was obtained from MP Biomedicals (Solon, OH, USA). Polyoxyl castor oil (Cremophor® EL) was obtained from BASF Corp. (Florham Park, NJ, USA). Poly (ethylene glycol) 400 was obtained from Dow Chemical Corp. (Petaluma, CA, USA).

B.2.2 Cell lines and culture

The human prostate cancer cell line DU145 (ATCC, Rockville, MD, USA) was maintained in Eagle's minimum essential medium (ATCC) supplemented with 10% heat inactivated fetal bovine serum. Cell lines were cultured at 37°C in a humidified atmosphere of 5% CO_2. For all procedures, cells were harvested using TrypLE^{TM} Express (Invitrogen, Carlsbad, CA) and cell lines were maintained in a logarithmic growth phase during all studies.

B.2.3 Synthesis of tanespimycin

Two-hundred mg (0.357 mmol) of GDM were dissolved in 10 mL anhydrous dimethylformamide (DMF) at ambient temperature. Eighty μL (1.07 mmol) of allylamine were added and the solution was kept under nitrogen, protected from exposure to light, and allowed to stir overnight at ambient temperature. The color of the solution changed from bright yellow-orange to dark purple and completion of the reaction was monitored by TLC on silica gel with chloroform:MeOH [9:1] as mobile phase by the disappearance of GDM. DMF was removed by rotary evaporator, and the resulting crude product was recrystallized from H_2O:EtOH [4:1]. The precipitate was analyzed by electrospray ionization mass spectrometry (ESI-MS).

B.2.4 Preparation of SMA-tanespimycin

Preparation of SMA micelles was similar to the method previously reported with modifications[29] (Figure B.1). First, poly(styrene-*co*-maleic anhydride) was hydrolyzed under aqueous alkaline conditions. Deionized water was adjusted to pH 14 with 4N NaOH and heated to 70°C. Poly(styrene-*co*-maleic anhydride) was added under stirring and the solution was maintained at pH 14 and 70°C. The resulting hydrolyzed SMA solution was adjusted to pH 7.0 with 1N HCl, diluted to a final concentration of 50 mg/mL, and allowed to cool to ambient temperature. Twelve mL (600 mg SMA) were removed and diluted to approximately 60 mL with deionized water. 200 mg of tanespimycin was dissolved in minimal DMSO, and added drop wise while stirring, resulting in a cloudy solution. The solution was then adjusted to a pH of 5.0 and 600 mg EDAC in 5 mL deionized water was added drop wise at pH 5.0 and allowed to stir

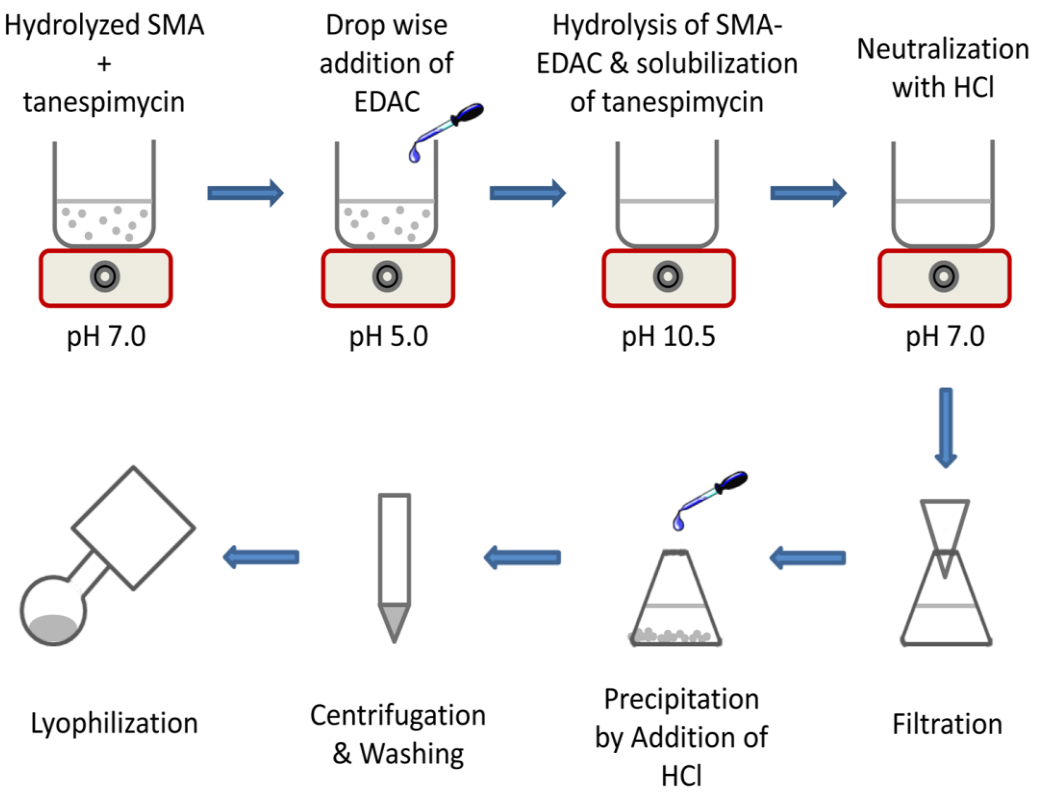

Figure B.1: Preparation of SMA-tanespimycin micelles. SMA-tanespimycin micelles were prepared by first suspending tanespimycin in an aqueous solution of hydrolyzed SMA containing EDAC. The solution was then adjusted to alkaline conditions which resulted in encapsulation of tanespimycin by SMA micelles. The resulting solution was neutralized and SMA-tanespimycin micelles isolated.

for 30 minutes. Next, the solution was adjusted to pH 10.5 by the addition of 1N NaOH, the pH was subsequently adjusted to 7.0 with 1N HCl, and the resulting solution was filtered to remove undissolved tanespimycin. 1N HCl was then added dropwise to the filtrate to precipitate the micelles. The precipitated micelles were then centrifuged and purified by washing repeatedly with cold 0.01 N HCl in deionized water. Residual water/HCl was removed by lyophilization to obtain the final SMA-tanespimycin product.

B.2.5 Loading efficiency of SMA-tanespimycin

For the purpose of this study, loading efficiency is defined as the total weight of the drug in the final SMA-tanespimycin product divided by the initial weight of the drug introduced for micellar preparation. A standard curve was prepared by serial dilution of tanespimycin in DMSO and quantification of the drug was by UV spectrometry at 335 nm. Loading efficiency and drug content were then obtained by dissolving SMA-tanespimycin in DMSO and measuring absorbance at 335 nm in comparison with the standard curve.

To ensure that the drug was unmodified during micelle preparation, SMA-tanespimycin was further analyzed by reversed phase high-performance liquid chromatography (RP-HPLC). Analysis was performed with an Agilent 1100 LC system equipped with an Alltech Alltima C18 5μm 150 x 4.6 mm column and a photo diode array detector scanning at 200 – 500 nm. The mobile phase consisted of deionized water and acetonitrile (ACN), at the following gradient: analysis time 0 min, 35% ACN; 15 min, 65% ACN; 25 min, 75% ACN; 30 min 95% ACN; 39 min, 100% ACN; 40

min, 65% ACN. A post time of 5 min was used to allow column equilibration between samples. The flow rate was maintained at 1.0 mL/min throughout and the sample injection volume was 20 μL. Samples of tanespimycin and SMA-tanespimycin were prepared in deionized water:ACN [65:35] and injected for analysis. The λ_{max} of tanespimycin at 335 nm was used for final quantitative analysis.

B.2.6 Size and zeta potential of SMA-tanespimycin

SMA-tanespimycin was prepared in 50 mM sodium phosphate buffer pH 7.4 at a concentration of 1.0 mg/mL for analysis. All measurements were performed at 25°C. A Malvern Zeta Sizer ZEN3600 (Malvern Instruments Inc., Westborough, MA) was used to determine mean Z-average size, size distribution and zeta-potential. All measurements were performed on three separately prepared samples.

.

B.2.7 Drug release from SMA-tanespimycin

The release of tanespimycin from the micellar preparations was evaluated using a dialysis method and compared to the release in a standard vehicle formulation of EtOH:Cremophor EL®:PEG 400 [2:1:1] (EtOH:CrEL:PEG).[30] SMA-tanespimycin was prepared at a concentration of 2.5 mg/mL (0.625 mg/mL tanespimycin) and drug-EtOH:CrEL:PEG was prepared by dissolving tanespimycin in EtOH:CrEL:PEG followed by a 10X dilution to yield a final concentration of 0.625 mg/mL. Samples were prepared in a 50 mM sodium phosphate buffer pH 7.4 or phosphate buffered saline (PBS) pH 7.4 with 40 mg/mL BSA. Four mL of each sample were placed in a dialysis tube with a molecular weight cutoff of 3500 Da and dialyzed against 5 L of either 50

mM sodium phosphate buffer pH 7.4 or PBS pH 7.4. Media outside the dialysis membrane was changed periodically to ensure a constant sink condition. At each predetermined time point, 200 μL of the sample inside the dialysis membrane was removed and analyzed spectrophotometrically at 335 nm. Quantification of percent release was performed by comparison of sample absorbance with calibration curves prepared for SMA-tanespimycin and tanespimycin-EtOH-CrEL:PEG for each test condition. All experiments were performed in triplicate. Percent release is reported as mean ± standard deviation.

B.2.8 *In vitro* growth inhibition against human prostate cancer cells

The ability of the SMA-tanespimycin to inhibit the growth of DU145 human prostate cancer cells was evaluated using a 2-(2-methoxy-4-nitrophenyl)-3-(4-nitrophenyl)-5-(2,4-disulfophenyl)-2H-tetrazolium,monosodium salt (WST-8) cell viability assay. 3,000 DU145 cells per well were plated in 96-well plates for 24 hrs. Cell culture medium was then removed and cells were treated with SMA-tanespimycin, tanespimycin dissolved in EtOH:CrEL:PEG, or controls for 72 hrs. Following treatment, medium was removed and wells were washed with 200 μL PBS. 100 μL of 10% (v/v) WST-8 reagent in complete growth medium was added to each well, cells were incubated at 37°C / 5% CO_2 for 120 min and absorbance at 450 nm minus 630 nm was determined by UV spectrophotometry. Relative viability was calculated by normalization of the absorbance of untreated cells. All experiments were performed in triplicate, with n=3 wells per replicate. Nonlinear least-squares regression analysis and calculation of IC_{50} was performed using GraphPad Prism.

B.2.9 Cell growth inhibition studies

Six-week-old athymic *(nu/nu)* mice were obtained from Charles River Laboratories (Davis, CA, USA) and used in accordance with the Institutional Animal Care and Use Committee (IACUC) of the University of Utah. Mice were anesthetized using 4% isoflurane mixed with oxygen followed by subcutaneous injection of 1×10^7 DU145 cells per flank (n=5 mice per treatment group). When the mean tumor size had reached approximately 50 mm^3 (about 10 days after tumor inoculation), the mice were treated with a single injection of either saline (control), free tanespimycin dissolved in DMSO, or SMA-tanespimycin at a dose of 10 mg/kg drug equivalent. The animals were routinely monitored and tumor growth was measured twice weekly and tumor volume was calculated as $\text{length} \cdot \text{width}^2 \cdot \pi/6$. Tumor volumes at each time point were normalized by the initial tumor volume and are reported as mean ± standard error of the mean. Animal weights were also measured at each time point and normalized to initial weight reported as mean ± standard deviation.

B.2.10 Statistical analysis

For release studies, tumor regression, and animal weight data, differences between data sets were determined by two-way repeated measures ANOVA using GraphPad Prism. Where differences were detected, a Bonferroni posttest was used to test for significance between groups. The significance level was set to $\alpha=0.05$ for all statistical tests.

B.3 Results and discussion

B.3.1 Synthesis and preparation of SMA-tanespimycin

The development of polymeric micelles in drug delivery has primarily focused on the use of amphiphilic block copolymers with poly(ethylene glycol) (PEG) as the hydrophilic segment and a polyester or a poly(amino acid) derivative as the hydrophobic segment.[31] The loading of hydrophobic drugs and the assembly of such copolymers into micellar structures is commonly performed using methods such as: 1) basic equilibration, 2) dialysis, 3) oil/water emulsion, 4) solution casting, or 5) freeze drying.[32] The present study describes polymeric micelles prepared by varying the pH of an aqueous solution containing poly(styrene-*co*-maleic acid) copolymers and tanespimycin, as a hydrophobic drug.

Tanespimycin was synthesized from GDM, and the resulting purple solid was collected and identified as tanespimycin by ESI-MS. SMA-tanespimycin was prepared by varying the pH of an aqueous solution of hydrolyzed SMA (Figure B.1).

B.3.2 Characterization of SMA-tanespimycin

The preparation of polymeric micelles as drug carriers often employ methods that result in either low loading efficiency or low drug loading capacity.[33] Using the aforementioned process, hydrolyzed SMA incorporated tanespimycin with a loading efficiency of 93% (Table B.1), a significant improvement over previous studies describing polymeric micellar formulations of tanespimycin.[34, 35] The ability of SMA based micelles to achieve high drug loading has previously been demonstrated for the hydrophobic drugs zinc protoporphyrin[18] and doxorubicin.[29] In the current study, a high

Table B.1: Characteristics of SMA-tanespimycin micelles

Property	*Mean*	*SD*
Amount of tanespimycin introduced for micelle preparation (mg)	150.0	-
Drug loading efficiency (%)[a]	93.1	-
Drug loading (% wt/wt)	25.6	-
Mean micelle diameter (nm)[b,c]	74	7
Polydispersity index	0.31	0.08
Zeta potential[c,d] (mV)	-35	3

[a] Drug loading efficiency calculated as mg tanespimycin solubilized by SMA micelles / mg tanespimycin introduced for micelle preparation

[b] Z-average size as measured by dynamic light scattering (DLS)

[c] As measured in 50 mM phosphate buffer at pH 7.4

drug loading of 25.6 % tanespimycin by weight was observed for SMA-tanespimycin as determined by UV spectrophotometry (Table B.1). The micelles were highly soluble, with a drug equivalent aqueous solubility of > 5.0 mg/mL as measured in pH 7.4 PBS buffer, whereas free tanespimycin was soluble only at 0.021 mg/mL. To ensure that tanespimycin remained unmodified during micelle preparation, SMA-tanespimycin in comparison with free tanespimycin was analyzed by RP-HPLC. Both tanespimycin and SMA-tanespimycin showed a prominent peak at 15.2 min, and both peaks exhibited UV spectra characteristic of tanespimycin (data not shown). Drug loading of tanespimycin as determined by RP-HPLC was 25.2 % by weight and in agreement with drug loading determined by UV spectrophotometry.

Size is a critical parameter for macromolecular drug delivery systems designed to escape renal filtration. It has been proposed that carriers with sizes greater than 10 nm accumulate in the tumor tissues via the EPR effect. SMA-tanespimycin micelles had a mean diameter of 74 ± 7 nm and a poly dispersity index of 0.31 ± 0.08 as measured by dynamic light scattering (Figure B.2). The micelles had a zeta potential of -35 ± 3 mV as measured in a 50 mM phosphate buffer at pH 7.4. SMA micelles were characterized by carboxyl terminated maleic acid surface groups which impart a negative charge to the micelles.

The high loading efficiency and possibility to tune the loading ratio of tanespimycin into SMA micelles represents significant advantages for industrial scale up, in contrast to many other micellar systems.

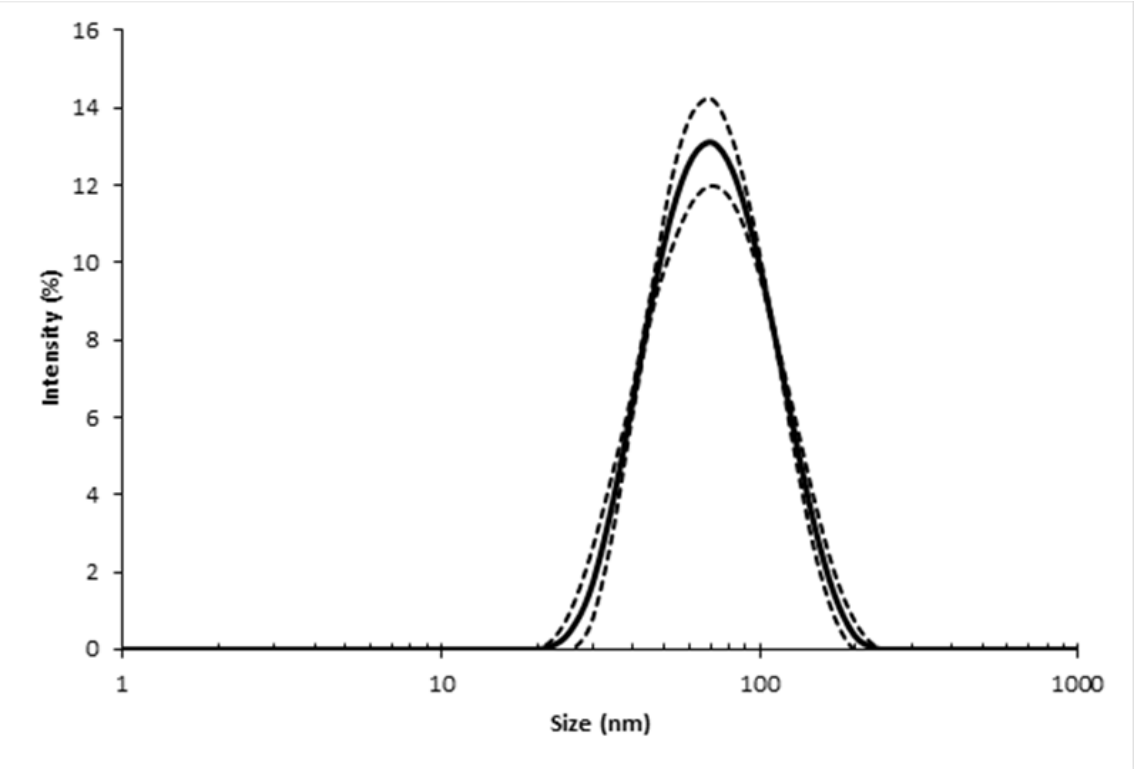

Figure B.2. Size distribution of SMA-tanespimycin micelles. The size distribution of SMA-tanespimycin micelles was determined using a Malvern Zeta Sizer at a concentration of 1.0 mg/mL at pH 7.4. Data are expressed as mean (solid line) ± SD (dashed line) (N=3).

B.3.3 Release of tanespimycin from SMA-tanespimycin micelles

The incorporation of tanespimycin into SMA micelles can increase tumor uptake and alter biodistribution, resulting in an increase in the therapeutic index of the drug. For this to occur, it is essential that tanespimycin is retained by the carrier for a period of time to allow drug accumulation in tumor tissue via the EPR effect. However, release from the carrier is also essential to allow tanespimycin to elicit its pharmacologic effect. Release rate is therefore a critical parameter in anticancer macromolecular drug delivery, and an ideal anticancer carrier should be able to retain its cargo for approximately 6 hrs while tumor accumulation occurs,[36] followed by complete drug release. To address this issue, the *in vitro* release rate of tanespimycin from SMA-tanespimycin micelles was evaluated using a dialysis method and compared to the release of tanespimycin formulated in EtOH:CrEL:PEG. Release was assessed in a pH 7.4 buffer where 51% and 95% tanespimycin was released from SMA-tanespimycin micelles in 2 and 8 hrs respectively. Release from tanespimycin formulated in EtOH:CrEL:PEG was not significantly different, with 60% and 99% released in 2 and 8 hrs respectively. To better ascertain release of tanespimycin from the blood plasma compartment *in vivo*, a second test condition was evaluated wherein BSA was included inside the dialysis bag at a physiologically relevant concentration of 40 mg/mL. Release of tanespimycin from SMA-tanespimycin micelles in the presence of BSA was reduced at all time-points greater than 1 hour ($p<0.001$) as compared to release from pH 7.4 buffer alone (Figure B.3). Release of tanespimycin from SMA-tanespimycin micelles was also significantly reduced as compared to tanespimycin formulated in EtOH:CrEL:PEG at all times greater than 1 hr ($p<0.001$), with only 62%

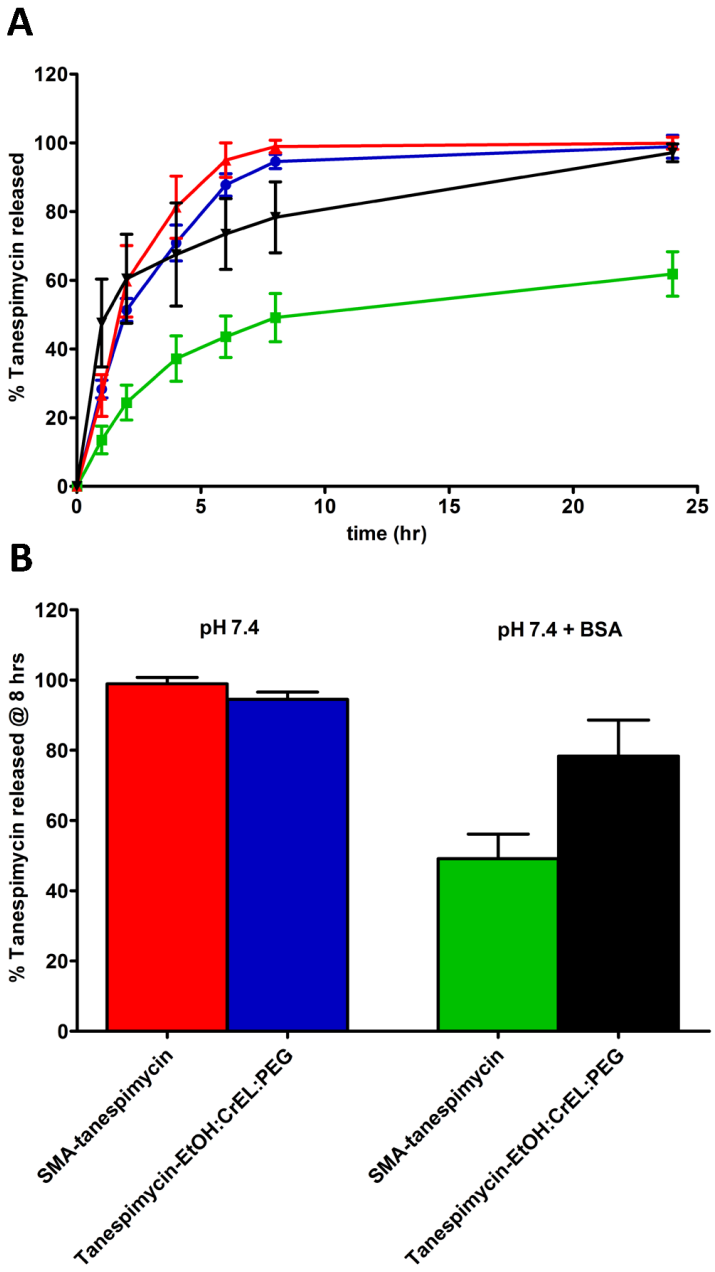

Figure B.3: Release of tanespimycin from SMA-tanespimycin. Release of tanespimycin from SMA micelles was evaluated using a dialysis method and compared to tanespimycin formulated in EtOH:CrEL:PEG as control. Panel A: Release of tanespimycin from SMA-tanespimycin (red) and tanespimycin-EtOH:CrEL:PEG (blue) in a pH 7.4 buffer and release of tanespimycin from SMA-tanespimycin (green) and tanespimycin-EtOH:CrEL:PEG (black) in a pH 7.4 buffer containing 40 mg/mL BSA. Panel B: Release of tanespimycin at 8 hrs. Data expressed as mean ± SD (N=3).

* Difference detected at $p<0.05$ significance level.

release observed in 24 hrs (Figure B.3). This reduction in release rate can be explained by the well characterized noncovalent binding of SMA to serum albumin[37], and it is thus anticipated that serum albumin can serve as a secondary carrier for SMA-tanespimycin micelles *in vivo*.

B.3.4 Cytotoxicity of SMA-tanespimycin micelles *in vitro*

The ability of SMA-tanespimycin micelles to inhibit the growth of DU145 human prostate cancer cells was evaluated *in vitro* using a WST-8 cell viability assay. Incorporation of tanespimycin into SMA-tanespimycin micelles resulted in a decrease in its ability to inhibit the growth of DU145 cells with an IC_{50} of 230 ± 10 nM as compared to an IC_{50} of 15.0 ± 0.3 nM for tanespimycin solubilized in EtOH:CrEL:PEG (Figure B.4). For controls, SMA and EtOH:CrEL:PEG solutions were subjected to the same dilution protocol and evaluated for growth inhibition ability and showed no cytotoxicity over an equivalent concentration range. During the 72 hrs incubation time of these studies, the release of tanespimycin from SMA-tanespimycin micelles was most likely minimized because of the lack of a perpetual sink condition. Although SMA-tanespimycin micelles were less toxic as compared to free tanespimycin, they remained cytotoxic in the nanomolar concentration range. This reduction in cytotoxicity of SMA-tanespimycin micelles as compared to free tanespimycin can be explained by a number of possible factors. The micelles first need to be taken up by cells via endocytosis, whereas tanespimycin can passively diffuse across cellular membranes. Uptake of the micelles could further be reduced due to the interactions of the negatively charged carboxylic acid rich surface of the micelles with negatively

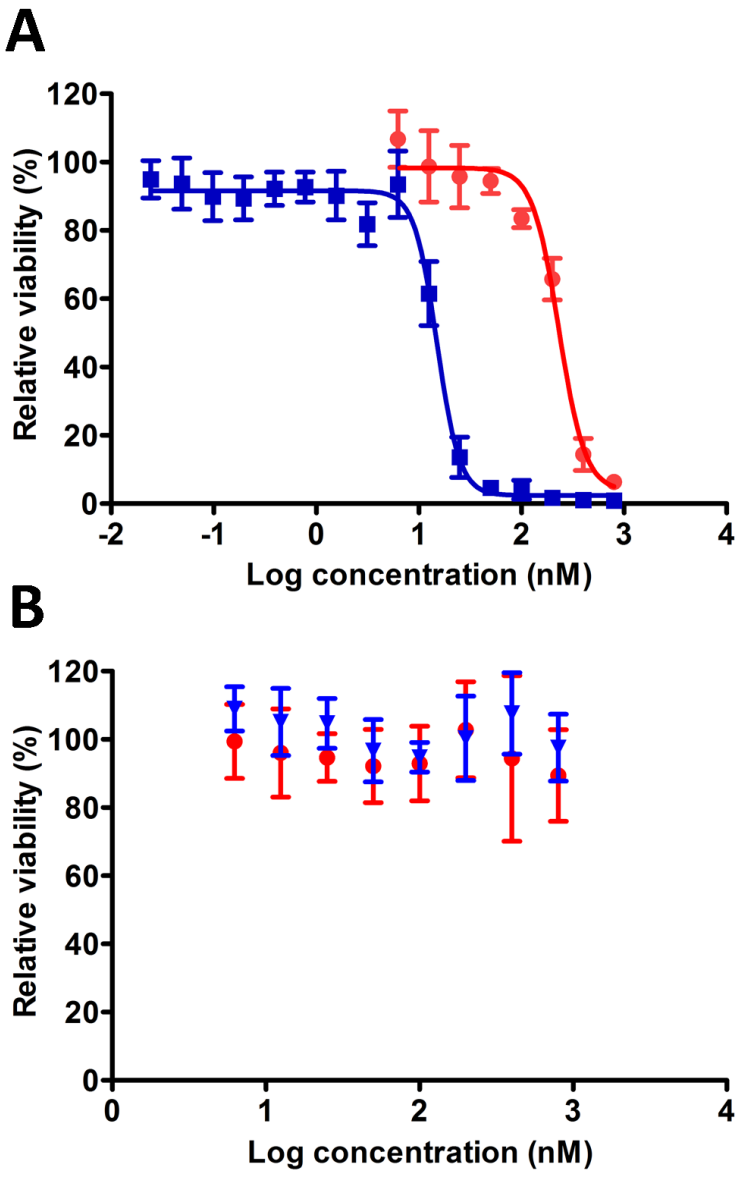

Figure B.4. Cell growth inhibition of SMA-tanespimycin micelles. DU145 human prostate cancer cells were treated for 72 hrs with increasing drug equivalent concentrations of tanespimycin formulated in EtOH:CrEL:PEG (blue), SMA-tanespimycin micelles (red) [Panel A], EtOH:CreEL:PEG vehicle alone (blue) or hydrolyzed SMA (red) [Panel B]. Following treatment, cell viability was assessed by WST-8 assay. Nonlinear regression and IC_{50} values were determined by analysis using GraphPad Prism.

charged membranes. Tanespimycin must also be released from the micelle core in order for it to elicit its pharmacological effect, which occurs over a prolonged time interval, further reducing overall cytotoxic exposure. The reduced toxicity of SMA-tanespimycin micelles can potentially be advantageous in an *in vivo* scenario by minimizing systemic exposure of tanespimycin while allowing time for accumulation in tumor tissues to occur.

B.3.5 *In vivo* efficacy of SMA-tanespimycin micelles

The delivery of tanespimycin via SMA-tanespimycin micelles results in an increase in the therapeutic index for tanespimycin. Toward this aim, a preliminary *in vivo* efficacy study was performed in athymic nu/nu mice bearing subcutaneous DU145 human prostate cancer xenografts. As accumulation in tumor tissues via the EPR effect was anticipated for SMA-tanespimycin micelles, a subtherapeutic dose of 10 mg/kg tanespimycin equivalent was used. A single dose of SMA-tanespimycin micelles, free tanespimycin, or saline were injected via tail-vein injection and animals were monitored twice weekly for changes in tumor volume as an indicator of efficacy (Figure B.5). Body weight was also recorded as an indicator of general toxicity (Figure B.5). At a single dose of 10 mg/kg tanespimycin equivalent, SMA-tanepsimycin micelles resulted in a reduction in normalized mean tumor volume that was maintained throughout the duration of the study (23 days), whereas normalized mean tumor volume in saline injected animals increased 450%. Relative to saline injected animals, SMA-tanespimycin resulted in a statistically significant decrease in normalized mean tumor volume at all time points following treatment ($p<0.05$). A single dose of free

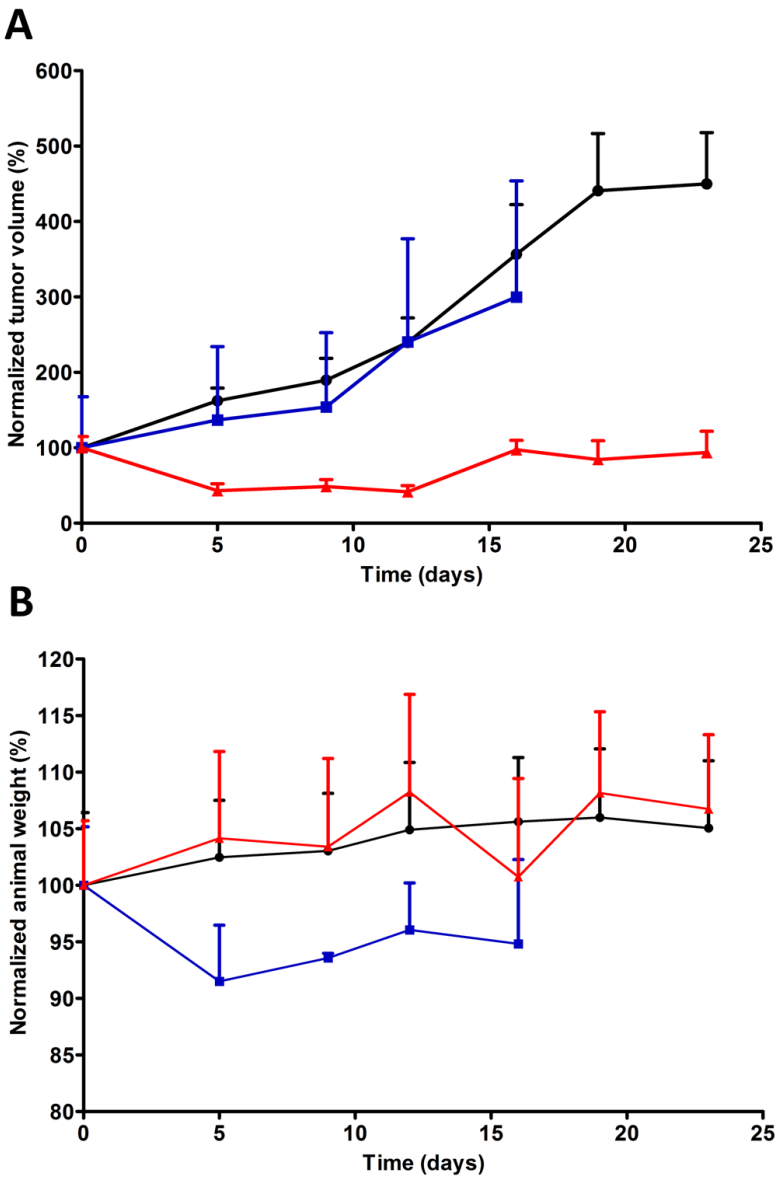

Figure B.5: *In vivo* efficacy of SMA-tanespimycin micelles. Athymic nu/nu mice bearing DU145 tumor xenografts were treated IV with a single dose of 10 mg/kg tanespimycin (blue) or 10 mg/kg tanespimycin equivalent SMA-tanespimycin micelles (red) and compared with a saline injection control group (black). Panel A: Normalized tumor volume was measured as a function of time for each treatment group. Panel B: Normalized animal weight was assessed as a measure of general toxicity. Data are expressed as mean ± SEM (N=5 per treatment group).

* Difference detected at $p<0.05$ significance level.

tanespimycin showed no evidence of efficacy at 10 mg/kg, and normalized mean tumor volume was not different from saline injected animals at all time points. Animals in the free tanespimycin group were euthanized on day 16 as one animal showed excessive tumor burden. SMA-tanespimycin micelles in comparison with free tanespimycin showed a significant reduction in normalized mean tumor volume on day 16 ($p<0.05$). These results coupled with the *in vitro* cytotoxicity results suggest that SMA-tanespimycin micelles have the ability to accumulate in tumor tissues and inhibit tumor growth *in vivo*.

Animal weights were measured twice a week as an indicator of general toxicity during the efficacy study. Relative to saline injected animals, animals treated with SMA-tanespimycin micelles showed no difference in normalized mean animal weight during the study. An 11% reduction in normalized mean animal weight was observed for free tanespimycin as compared to saline injected animals at day 5 ($p<0.05$); differences detected at subsequent time points were not statistically significant. However, it is unclear whether the solvent used to solubilize tanespimycin has contributed to the overt tanespimycin toxicity in this study, or the manifested toxicity was totally due to the free drug. These results demonstrate that SMA-tanespimycin micelles were well tolerated.

This efficacy study was preliminary in its nature as parameters such as maximum tolerated dose and dosing schedule were not optimized. However, the results of the study demonstrate that SMA-tanespimycin micelles were well tolerated and effective in reducing DU145 tumor growth, and suggest that the therapeutic index of tanespimycin is increased by encapsulation in SMA micelles.

Overall, the data from this study demonstrate that delivery of tanespimycin using SMA micelles has several distinct advantages. First, the aqueous solubility of tanespimycin is increased by encapsulation into SMA micelles, and because these interactions are noncovalent, the potent activity of tanespimycin is maintained. Second, the preparation of SMA-tanespimycin micelles is simple, straightforward, and efficient in loading tanespimycin, thus allowing cost efficient scale up at later stages of development. Third, the macromolecular nature of SMA-tanespimycin micelles allows accumulation into tumor tissues, resulting in an increase in the therapeutic index of tanespimycin. These features combine to suggest that SMA-tanespimycin micelles have the potential to increase the efficacy and safety profile of tanespimycin.

B.4 Conclusion

SMA-tanespimycin micelles were prepared in a simple manner with a high loading drug efficiency of 93%. The micelles incorporated 25.6% tanespimycin by weight and exhibited properties that allow for increased blood circulation and tumor accumulation *in vivo*. Tanespimycin was released from the micelles in a controlled manner and showed potent activity against DU145 human prostate cancer cells *in vitro*. The micelles also were well tolerated and exhibited potent anti-cancer in nu/nu mice bearing subcutaneous DU145 human prostate cancer tumor xenografts, with a significant increase in efficacy as measured by tumor regression as compared to free tanespimycin at an equivalent single dose of 10 mg/kg. These data suggest that the therapeutic index of tanespimycin is increased by incorporation into SMA micelles.

B.5 References

1. S. Sharp and P. Workman. Inhibitors of the HSP90 molecular chaperone: current status. Adv Cancer Res. 95:323-348 (2006).

2. J. Buchner. Hsp90 & Co. - a holding for folding. Trends Biochem Sci. 24:136-141 (1999).

3. Y. Fukuyo, C.R. Hunt, and N. Horikoshi. Geldanamycin and its anti-cancer activities. Cancer Lett. 290:24-35 (2010).

4. J.R. Porter, J. Ge, J. Lee, E. Normant, and K. West. Ansamycin inhibitors of Hsp90: nature's prototype for anti-chaperone therapy. Curr Top Med Chem. 9:1386-1418 (2009).

5. L. Whitesell and S.L. Lindquist. HSP90 and the chaperoning of cancer. Nat Rev Cancer. 5:761-772 (2005).

6. J.G. Supko, R.L. Hickman, M.R. Grever, and L. Malspeis. Preclinical pharmacologic evaulation of geldanamycin as an antitumor agent. Cancer Chemother Pharmacol. 36:305-315 (1994).

7. L.R. Kelland, S.Y. Sharp, P.M. Rogers, T.G. Myers, and P. Workman. DT-Diaphorase expression and tumor cell sensitivity to 17-allylamino, 17-demethoxygeldanamycin, an inhibitor of heat shock protein 90. J Natl Cancer Inst. 91:1940-1949 (1999).

8. A.M. Burger, H.H. Fiebig, S.F. Stinson, and E.A. Sausville. 17-(Allylamino)-17-demethoxygeldanamycin activity in human melanoma models. Anticancer Drugs. 15:377-387 (2004).

9. U. Banerji, A. O'Donnell, M. Scurr, S. Pacey, S. Stapleton, Y. Asad, L. Simmons, A. Maloney, F. Raynaud, M. Campbell, M. Walton, S. Lakhani, S. Kaye, P. Workman, and I. Judson. Phase I pharmacokinetic and pharmacodynamic study of 17-allylamino, 17-demethoxygeldanamycin in patients with advanced malignancies. J Clin Oncol. 23:4152-4161 (2005).

10. E.A. Sausville, J.E. Tomaszewski, and P. Ivy. Clinical development of 17-allylamino, 17-demethoxygeldanamycin. Curr Cancer Drug Targets. 3:377-383 (2003).

11. J. Ge, E. Normant, J.R. Porter, J.A. Ali, M.S. Dembski, Y. Gao, A.T. Georges, L. Grenier, R.H. Pak, J. Patterson, J.R. Sydor, T.T. Tibbitts, J.K. Tong, J. Adams, and V.J. Palombella. Design, synthesis, and biological evaluation of hydroquinone derivatives of 17-amino-17-demethoxygeldanamycin as potent, water-soluble inhibitors of Hsp90. J Med Chem. 49:4606-4615 (2006).

12. E.K. Rowinsky and R.C. Donehower. Paclitaxel (taxol). N Engl J Med. 332:1004-1014 (1995).

13. H. Gelderblom, J. Verweij, K. Nooter, and A. Sparreboom. Cremophor EL: the drawbacks and advantages of vehicle selection for drug formulation. Eur J Cancer. 37:1590-1598 (2001).

14. Y. Matsumura, T. Oda, and H. Maeda. [General mechanism of intratumor accumulation of macromolecules: advantage of macromolecular therapeutics]. Gan To Kagaku Ryoho. 14:821-829 (1987).

15. K. Greish, J. Fang, T. Inutsuka, A. Nagamitsu, and H. Maeda. Macromolecular therapeutics: advantages and prospects with special emphasis on solid tumour targeting. Clin Pharmacokinet. 42:1089-1105 (2003).

16. L. Gros, H. Ringsdorf, and H. Schupp. Polymeric antitumor agents on a molecular and on a cellular level? Angewandte Chemie International Edition in English. 20:305-325 (1981).

17. E. Blanco, C.W. Kessinger, B.D. Sumer, and J. Gao. Multifunctional micellar nanomedicine for cancer therapy. Exp Biol Med. 234:123-131 (2009).

18. A.K. Iyer, K. Greish, J. Fang, R. Murakami, and H. Maeda. High-loading nanosized micelles of copoly(styrene-maleic acid)-zinc protoporphyrin for targeted delivery of a potent heme oxygenase inhibitor. Biomaterials. 28:1871-1881 (2007).

19. J. Daruwalla, M. Nikfarjam, K. Greish, C. Malcontenti-Wilson, V. Muralidharan, C. Christophi, and H. Maeda. In vitro and in vivo evaluation of tumor targeting styrene-maleic acid copolymer-pirarubicin micelles: Survival improvement and inhibition of liver metastases. Cancer Sci. 101:1866-1874 (2010).

20. H. Maeda. SMANCS and polymer-conjugated macromolecular drugs: advantages in cancer chemotherapy. Adv Drug Deliv Rev. 46:169-185 (2001).

21. F. Suzuki, T. Munakata, and H. Maeda. Interferon induction by SMANCS: a polymer-conjugated derivative of neocarzinostatin. Anticancer Res. 8:97-103 (1988).

22. F. Suzuki, R.B. Pollard, S. Uchimura, T. Munakata, and H. Maeda. Role of natural killer cells and macrophages in the nonspecific resistance to tumors in mice stimulated with SMANCS, a polymer-conjugated derivative of neocarzinostatin. Cancer Res. 50:3897-3904 (1990).

23. V.B. Rodriguez, S.M. Henry, A.S. Hoffman, P.S. Stayton, X. Li, and S.H. Pun. Encapsulation and stabilization of indocyanine green within poly(styrene-alt-maleic anhydride) block-poly(styrene) micelles for near-infrared imaging. J Biomed Opt. 13:014025 (2008).

24. J. Claracq, S.F.C.R. Santos, J. Duhamel, C. Dumousseaux, and J.-M. Corpart. Rigid interior of styrene-maleic anhydride copolymer aggregates probed by fluorescence spectroscopy. Langmuir. 18:3829-3835 (2002).

25. M.P. Borgman, O. Aras, S. Geyser-Stoops, E.A. Sausville, and H. Ghandehari. Biodistribution of HPMA copolymer-aminohexylgeldanamycin-RGDfK conjugates for prostate cancer drug delivery. Mol Pharm. 6:1836-1847 (2009).

26. N. Larson, A. Ray, A. Malugin, D.B. Pike, and H. Ghandehari. HPMA copolymer-aminohexylgeldanamycin conjugates targeting cell surface expressed GRP78 in prostate cancer. Pharm Res. 27:2683-2693 (2010).

27. Y. Kasuya, Z.R. Lu, P. Kopeckova, S.E. Tabibi, and J. Kopecek. Influence of the structure of drug moieties on the in vitro efficacy of HPMA copolymer-geldanamycin derivative conjugates. Pharm Res. 19:115-123 (2002).

28. V. Subr, J. Kopecek, J. Pohl, M. Baudys, and V. Kostka. Cleavage of oligopeptide side-chains in N-(2-hydroxypropyl)meth-acrylamide copolymers by mixtures of lysosomal enzymes. Journal of Controlled Release. 8:133-140 (1988).

29. K. Greish, T. Sawa, J. Fang, T. Akaike, and H. Maeda. SMA-doxorubicin, a new polymeric micellar drug for effective targeting to solid tumours. J Control Release. 97:219-230 (2004).

30. Z. Zhong and P.J. Licari. Pharmaceutical solution formulations containing 17-AAG. US Patent Application. 20050256097: (2005).

31. S.R. Croy and G.S. Kwon. Polymeric micelles for drug delivery. Curr Pharm Des. 12:4669-4684 (2006).

32. G. Gaucher, M.H. Dufresne, V.P. Sant, N. Kang, D. Maysinger, and J.C. Leroux. Block copolymer micelles: preparation, characterization and application in drug delivery. J Control Release. 109:169-188 (2005).

33. K. Park. Nanotechnology: What it can do for drug delivery. J Control Release. 120:1-3 (2007).

34. M.P. Xiong, J.A. Yáñez, G.S. Kwon, N.M. Davies, and M.L. Forrest. A cremophor-free formulation for tanespimycin (17-AAG) using PEO-<I>b</I>-

PDLLA micelles: Characterization and pharmacokinetics in rats. Journal of Pharmaceutical Sciences. 98:1577-1586 (2009).

35. H.-C. Shin, A.W.G. Alani, D.A. Rao, N.C. Rockich, and G.S. Kwon. Multi-drug loaded polymeric micelles for simultaneous delivery of poorly soluble anticancer drugs. Journal of Controlled Release. 140:294-300 (2009).

36. K. Greish. Enhanced permeability and retention of macromolecular drugs in solid tumors: a royal gate for targeted anticancer nanomedicines. J Drug Target. 15:457-464 (2007).

37. A. Kobayashi, T. Oda, and H. Maeda. Protein binding of macromolecular anticancer agent SMANCS: characterization of poly(styrene-co-maleic acid) derivatives as an albumin binding ligand. Journal of Bioactive and Compatible Polymers. 3:319-333 (1988).

APPENDIX C

COMPARATIVE BIODISTRIBUTION OF HPMA COPOLYMERS BEARING GRP78 TARGETING PEPTIDES: A PRELIMINARY STUDY

C.1 Materials and methods

^{125}Iodine labeled HPMA copolymers bearing the GRP78 targeting peptide WDLAWMFRLPVG were prepared using materials and methods analogous to those used to synthesize and characterize HPMA copolymers bearing the WIFPWIQL peptide (See Section 4.2.1). Biodistribution in major organs was then assessed in athymic nu/nu mice bearing DU145 tumor xenografts as previously described (see Section 4.2.7). Briefly, mice (n=3 per treatment group) were intravenously administered a single bolus dose of 50 mg/kg ^{125}I radiolabeled conjugates. No tumor hyperthermia was induced in this study, as the primary objective was to evaluate major organ uptake. Biodistribution was assessed 4 hrs post injection, as this was when the highest levels of nonspecific uptake were observed for WIFPWIQL bearing conjugates (see Figure 4.5). Mice were euthanized, blood immediately collected, followed by blood perfusion with saline. Tumors and major organs were then collected and analyzed by gamma counting. Percent injected dose per gram of blood/tissue (% ID / g) was calculated.

C.2 Results and Discussion

HPMA copolymers bearing WDLAWMFRLPVG were synthesized and characterized to be as similar to WIFPWIQL conjugated copolymers as possible (See Figure 4.2b). The same batch of precursor polymer that was used to prepare WIFPWIQL bearing copolymers was used to ensure similarities in molecular weight and molecular weight distribution. Weight average molecular weight and polydispersity for the WDLAWMFRLPVG conjugated copolymer were 75.6 kDa and 1.6 respectively, as determined by SEC. The amount of targeting peptide conjugated was also maintained at a similar level (20% by weight) as WIFPWIQL copolymers.

Significant reduced concentrations of WDLAWMFRLPVG copolymers in the spleen, kidneys, and liver were observed as compared to WIFPWIQL copolymers four hours after administration (Figure C.1). No differences in delivery to the tumor or other major organs were observed. These results suggest that the physicochemical properties of the peptides altered the characteristics of the copolymers, resulting in differences in biodistribution. Based on this result, subsequent studies discussed in Chapter 5 utilized the WDLAWMFRLPVG peptide to target cell surface expressed GRP78. It must be noted that the influence of the physicochemical properties of the peptides and their polymeric conjugates under study, on biodistribution and tumor localization, will need to be examined in more detail.

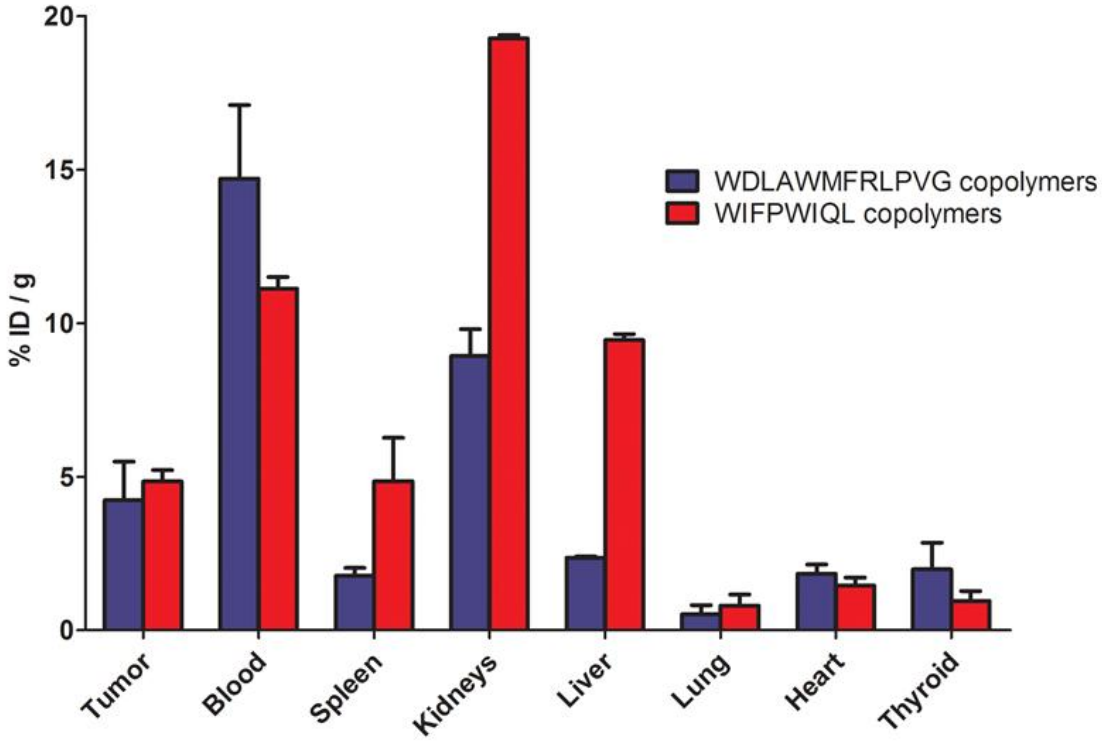

Figure C.1. Biodistribution of WDLAWMFRLPVG and WIFPWIQL copolymers. Four hours after administration, significant reductions in delivery to the spleen, kidneys, and liver were observed for WDLAWMFRLPVG containing copolymers as compared to WIFPWIQL counterparts.

APPENDIX D

SIZE EXCLUSION CHROMATOGRAMS OF SELECTED HPMA COPOLYMER-DRUG CONJUGATES

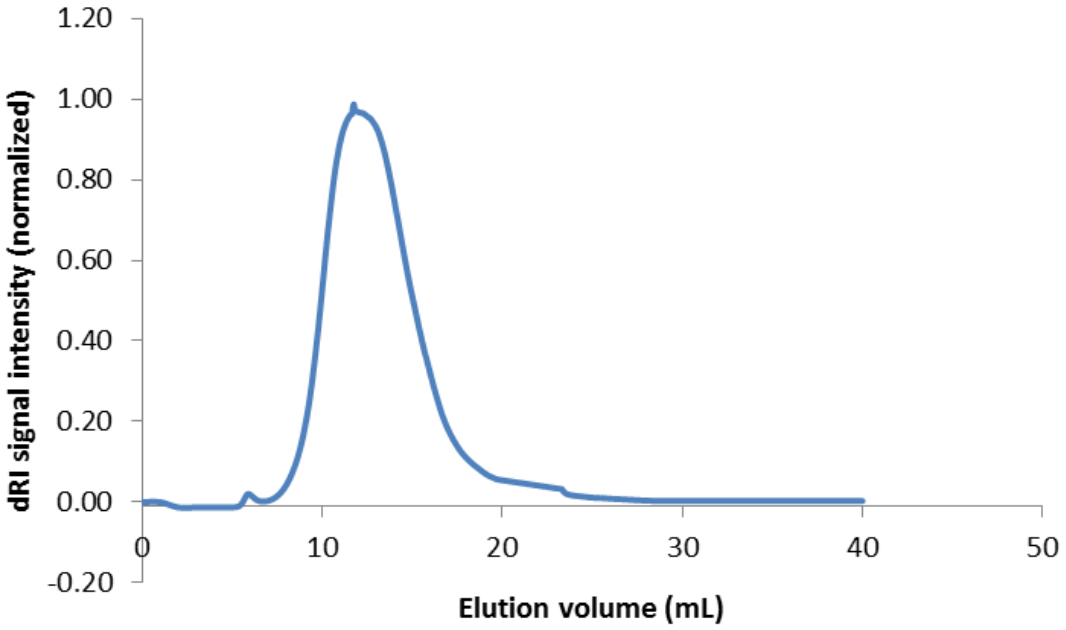

Figure D.1. Size exclusion chromatogram of p-AHGDM. See Table 5.1 for physicochemical characteristics.

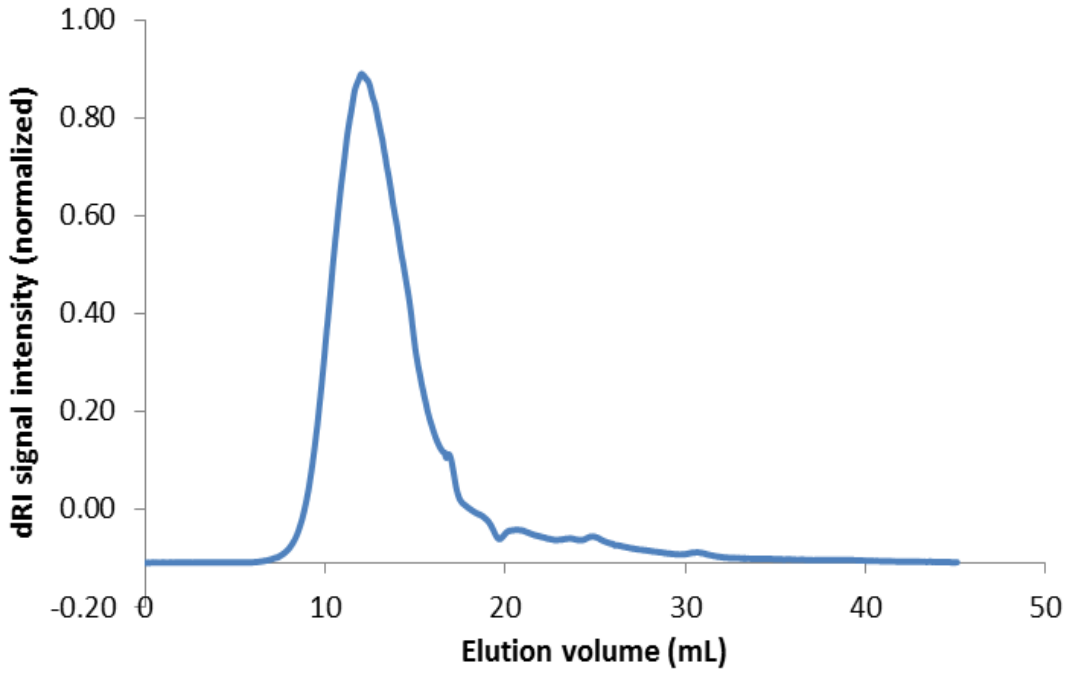

Figure D.2. Size exclusion chromatogram of p-AHGDM-HSP. See Table 5.1 for physicochemical characteristics.

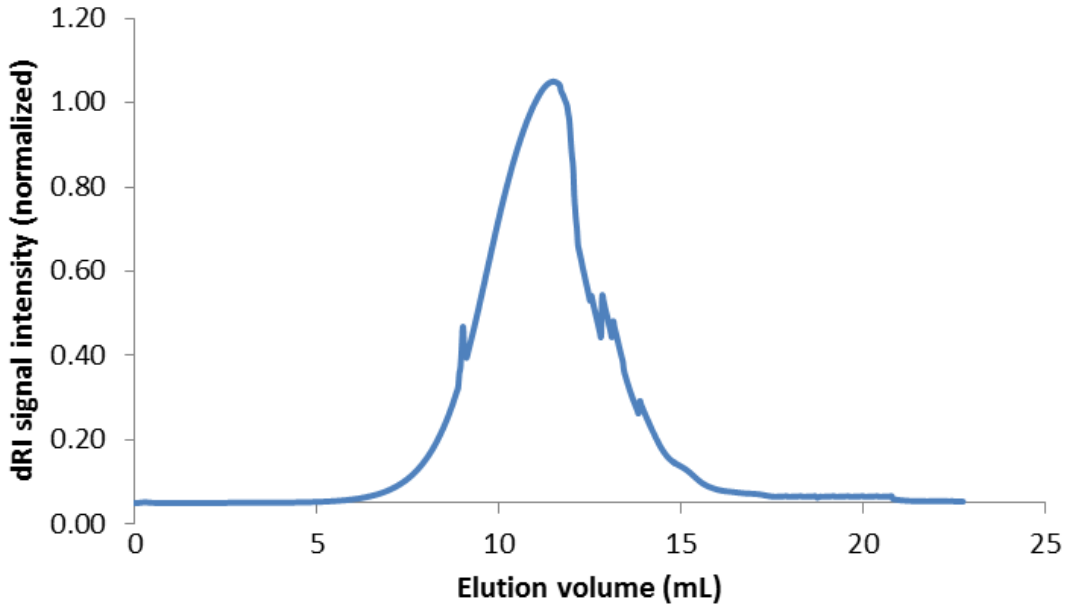

Figure D.3. Size exclusion chromatogram of p-DOC. See Table 5.1 for physicochemical characteristics.

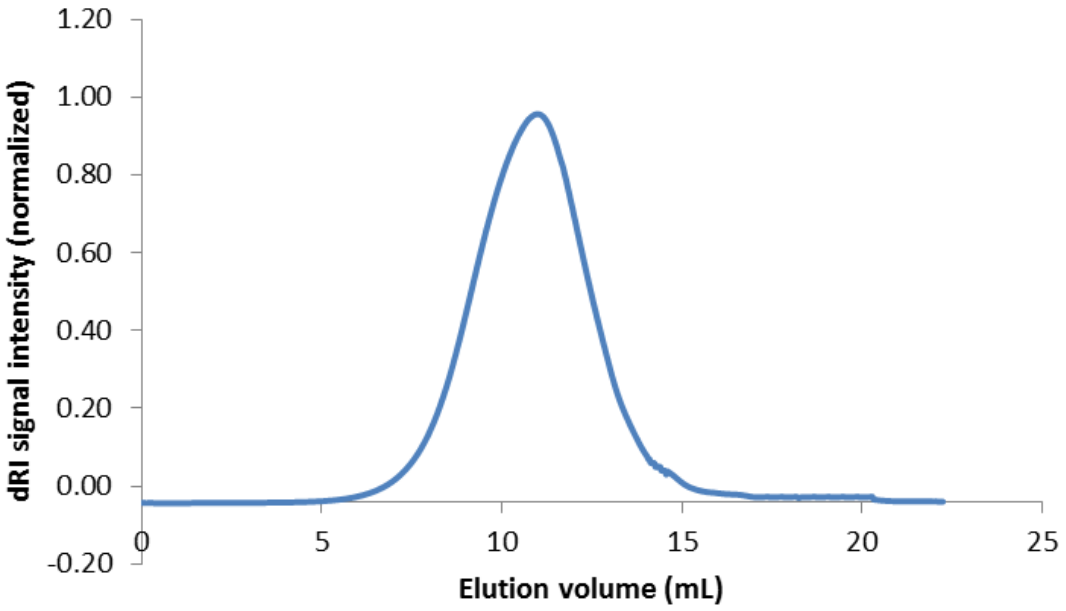

Figure D.4. Size exclusion chromatogram of p-DOC-HSP. See Table 5.1 for physicochemical characteristics.

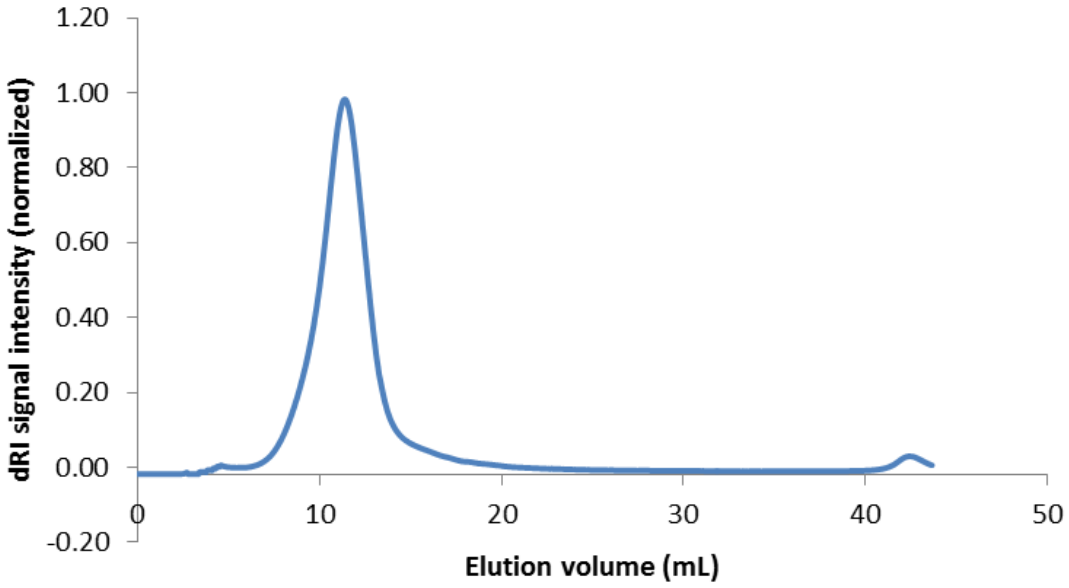

Figure D.5. Size exclusion chromatogram of p-Pt. See Table 5.1 for physicochemical characteristics.

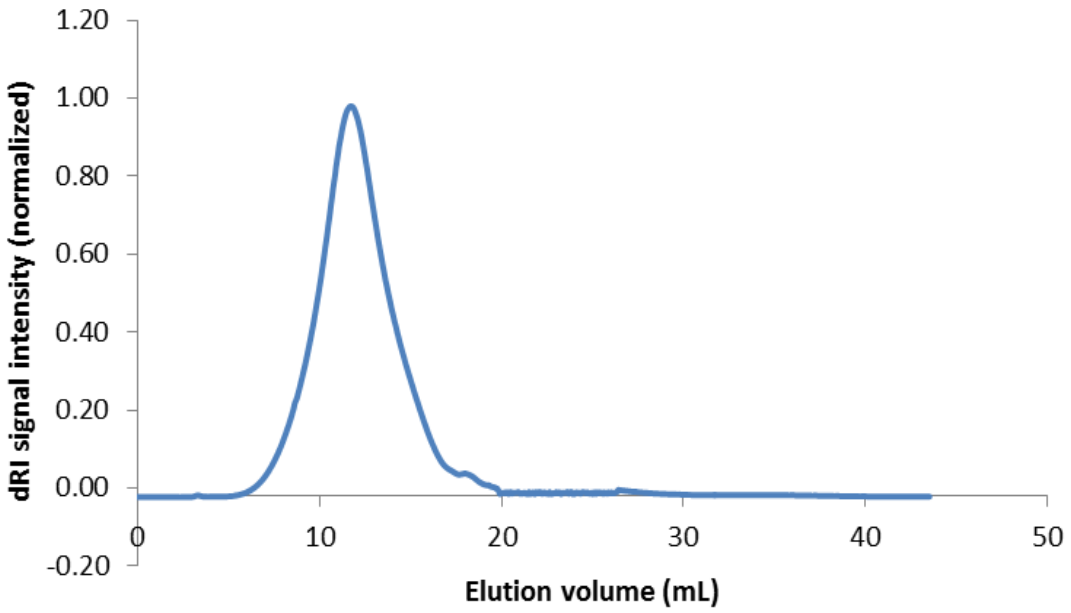

Figure D.6. Size exclusion chromatogram of p-Pt-HSP. See Table 5.1 for physicochemical characteristics.